

**INAUGURAL-DISSERTATION**

zur

Erlangung der Doktorwürde

der Gesamtfakultät für Mathematik, Ingenieur- und

Naturwissenschaften

der Ruprecht-Karls-Universität Heidelberg

vorgelegt von

**Janeta Marahrens (M.Sc.)**

Aus Melle-Westerhausen

Hamburg, 09.12.2021



Tin isotope analysis of tin ore deposits

in Europe and Central Asia

in view of the tin provenance in

archaeological metal objects

**Gutachter:** Prof. Dr. Ernst Pernicka

Prof. Dr. Axel K. Schmitt

**Tag der mündlichen Prüfung:** 27.01.2022







## Contents

LIST OF FIGURES.....	III
LIST OF TABLES .....	VII
LIST OF ABBREVIATIONS .....	IX
ABSTRACT .....	XI
KURZFASSUNG.....	XIII
ACKNOWLEDGEMENT .....	XV
1. INTRODUCTION.....	1
2. TIN .....	7
2.1 Mineralogy and chemistry.....	7
2.2 Ore formation and deposit types .....	10
2.2.1 Geodynamic settings of mineral deposits.....	11
2.2.2 Classification scheme .....	12
3. STUDY AREA AND SAMPLING CAMPAIGNS .....	19
4. GEOLOGICAL SETTING .....	24
4.1 Introduction and Palaeogeography .....	24
4.2 Southwest England.....	28
4.3 Saxonian-Bohemian province .....	31
4.4 Ireland .....	34
4.5 Iberian Peninsula.....	36
4.6 France.....	41
4.7 Italy .....	44
4.8 Serbia.....	46
4.9 Egypt .....	49
4.10 Central Asia.....	51
4.10.1 Kazakhstan .....	52
4.10.2 Uzbekistan and Tajikistan (Zeravshan valley) .....	53
4.10.3 Kyrgyzstan .....	54
4.10.4 Afghanistan .....	54
5. METHODOLOGY .....	56
5.1 Materials and reagents.....	56
5.2 Sample preparation and purification .....	57
5.3 MC-ICP-MS/Stable isotopy of Sn.....	58
6. RESULTS .....	62
6.1 Petrography of the tin ores .....	62
6.2 Tin isotope compositions .....	66
6.2.1 Primary cassiterite .....	68

6.2.2 Secondary cassiterite .....	82
6.2.3 Cassiterite versus stannite.....	84
6.2.4 Types of mineralization.....	87
6.2.5 Comparison with previous studies.....	89
7.    SYNTHESIS AND CONCLUSIONS .....	91
7.1 What do the results mean?.....	91
7.1.1 Primary cassiterite .....	91
7.1.2 Secondary cassiterite .....	99
7.1.3 Stannite.....	100
7.1.4 Types of mineralization.....	101
7.2 Possible causes of fractionation in tin ores.....	104
7.3 Further studies .....	106
7.4 Significance for archaeology .....	107
8.    OUTLOOK.....	114
REFERENCES .....	117
APPENDIX: TIN ISOTOPE DATA .....	137

## LIST OF FIGURES

<b>Figure 2.1:</b> Natural isotope abundances of Sn and Sb.....	7
<b>Figure 3.1:</b> Sample locations: a) SW England, b) Saxonian-Bohemian province, c) Brittany, d) Massif Central, e) Iberian Peninsula, f) Monte Valerio, g) Sardinia, h) Serbia, i) Egypt, j) Uzbekistan, k) Kyrgyzstan, l) Tajikistan, m) Afghanistan. The map was generated with QGIS 2.18.16.....	19
<b>Figure 3.2:</b> Sampling campaign to the mineralogical collection of the Technical Institute in the University of Lisbon (a and b) in 2016, c: Cassiterite sampling during a field trip to several tin mining areas in Portugal in 2016, d and e: cassiterite panning from an altered material. ....	21
<b>Figure 3.3:</b> Sampling campaign to Galicia in 2017: a-c: cassiterite collection from the Natural History Museum in Santiago de Compostela; d: samples from old miners in a small village; e: Minas de Barxa, Ourense; f: Mina Monte Neme, La Coruña. ....	22
<b>Figure 4.1:</b> a) Late Carboniferous plate-tectonic reconstruction, b) Plates and terranes which are of relevance for this work (Ruban et al. 2007). ....	25
<b>Figure 4.2:</b> The west European units of the Variscan fold belt, where Palaeozoic rocks crop out (Ballèvre et al. 2009). The different colours should highlight the potential correlations within the Variscan fold belt. ....	26
<b>Figure 4.3:</b> The metallogenic tin and tungsten province of the European Variscan belt (Chicharro et al. 2016).....	27
<b>Figure 4.4:</b> Simplified geological map of the Cornubian batholith showing the major granite intrusions (modified after Manning 1998; Haustein 2009). The map was generated with QGIS 2.18.16.....	30
<b>Figure 4.5:</b> Simplified geological map of the Saxonian-Bohemian province showing the major granite intrusions (modified after Žak et al. 2014; Zahng et al. 2017; Štemprok and Blecha 2015). AG: Altenberg granite, ATC: Altenberg-Teplice caldera, BG: Bergen granite, EG: Ehrenfriedersdorf granite, ENP: Eibenstock-Nejdek pluton, FLG: Fláje granite, FP: Fichtelgebirge (Smrčiny) pluton, KG: Kirchberg granite, KVP: Karlovy Vary pluton, NG: Niederbobritzsch granite, PG: Pobershau granite, SG: Satzung granite, ZG: Zinnwald granite (Fusán et al. 1967; Cháb et al. 2007; Romer et al. 2007; Žák et al. 2014; Štemprok and Blecha 2015). The map was generated with QGIS 2.18.16. ....	33
<b>Figure 4.6:</b> Map showing the simplified geology of Ireland (Anderson et al. 2018). ALG: Antrim Lava Group, CC: Carlingford Complex, LNG: Lough Neagh Group, MMC: Mourne Mountains Complex, SGC: Slieve Gullion Complex. ....	35

<b>Figure 4.7:</b> Geological map of the Iberian Peninsula with the different zones of the Iberian massif (Arenas et al. 2016) .....	37
<b>Figure 4.8:</b> Zonation of the Variscan orogen (Martínez Catalan 2012). Important abbreviations: CIZ: Central Iberian Zone, CZ: Cantabrian Zone, GTMZ: Galicia-Tras-os-Montes Zone, LC: Lizard Complex, MGCZ: Mid-German Crystalline Zone, MT: Moldanubian thrust, MZ: Moldanubian Zone, OMZ: Ossa-Morena Zone, RHZ: Rheno-Hercynian Zone, S: Sardinia, SASZ: South Armorican shear Zone, SISZ: Southern Iberian shear Zone, SPZ: South Portuguese Zone, STZ: Saxo-Thuringian Zone, WALZ: West Asturian-Leonese Zone. ....	42
<b>Figure 4.9:</b> Late Variscan intrusives of Sardinia and the associated ore deposits. The Monte Linas pluton is marked with the black rectangle. Tin ore deposits: 4) Canale Serci, 8) Perda Niedda, 9) Perdu Cara (Naitza el al. 2017). ....	45
<b>Figure 4.10:</b> Tectonic map of the Dinarides of northern Serbia, including the Alps and the Carpathians (Schefer et al. 2011). ....	48
<b>Figure 4.11:</b> Arabian-Nubian Shield including the post-collisional rare-metal granitic plutons (ANS; Sami et al. 2017).....	50
<b>Figure 4.12:</b> a: Geological sketch map of the Central Asian orogenic belt and b: of the South Tianshan orogen and adjacent region (Gao et al. 2009). ....	52
<b>Figure 5.1:</b> Plot showing the error per mass unit for the Sn isotope ratios analysed with the JMC reference material (Brügmann 2018).....	61
<b>Figure 6.1:</b> Polished resin block images of the different mineralization types of selected samples from SW England and the Saxonian-Bohemian province. a) and b) show a tin ore sample (MA-080521) and cassiterite in a quartz vein (MA-080520) from the Botallack Mine, SWE; c) primary ore, Drakewells Mine, Hingston Down granite (MA-156057); d) and e) show cassiterite in greisen (FG-080683) from the Zinnwald (eastern Erzgebirge) and f) is cassiterite in a quartz vein (FG-011501) from Ehrenfriedersdorf, Erzgebirge West.....	64
<b>Figure 6.2:</b> $\delta^{124}\text{Sn}/^{120}\text{Sn}$ vs. an arbitrary number of all primary and secondary cassiterite and stannite samples from Europe and Central Asia (the 2SD error bars are covered by the symbols). ....	66
<b>Figure 6.3:</b> Frequency distribution of all cassiterite and stannite samples from Europe and Central Asia.....	67
<b>Figure 6.4:</b> a and b: $\delta^{124}\text{Sn}/^{120}\text{Sn}$ vs. an arbitrary number for the isotope ratios of primary cassiterite of the individual mines in SW England and the Saxonian-Bohemian province; c and d: Frequency distribution of SW England and the Saxonian-Bohemian province for primary cassiterite. The averages are calculated based on single mines or mining areas (the 2SD error bars are covered by the symbols). ....	68

<b>Figure 6.5:</b> Land's End granite (LEG), Erzgebirge East (EE) and Erzgebirge West (EW). The grey crosses show other mines or mining areas with only one sample per area. The dotted lines show the average values for the plotted areas and the light grey field is the 2SD for all plotted data (the 2SD error bars are covered by the symbols). .....	71
<b>Figure 6.6:</b> a and b: Isotope composition in different mining areas of primary and secondary cassiterites; c and d: Frequency distribution of primary cassiterite from Portugal and Spain. The average values are calculated on the basis of single mines ore mining areas (the 2SD error bars are covered by the symbols).....	72
<b>Figure 6.7:</b> The tin mines of the Viseu mining district in Portugal (the 2SD error bars are covered by the symbols). .....	73
<b>Figure 6.8:</b> a and b: Isotope composition in different mining areas of primary and secondary cassiterites; c and d: Frequency distribution of primary cassiterite from France and Italy . The average values are calculated on the basis of single mines ore mining areas (the 2SD error bars are covered by the symbols). .....	77
<b>Figure 6.9:</b> $\delta^{124}\text{Sn}/^{120}\text{Sn}$ values versus an arbitrary number for Tajikistan (blue), Uzbekistan (orange), Kyrgyzstan (green), Kazakhstan (aquamarine) and Afghanistan (violet) ); (the 2SD error bars are covered by the symbols). .....	79
<b>Figure 6.10:</b> $\delta^{124/120}\text{Sn}$ values versus an arbitrary number for Egypt (the 2SD error bars are covered by the symbols). .....	80
<b>Figure 6.11:</b> Frequency distribution for primary of Central Asia and Egypt. The average values are calculated on the basis of single mines or mining areas.....	80
<b>Figure 6.12:</b> $\delta^{124}\text{Sn}/^{120}\text{Sn}$ values versus an arbitrary number for the primary (grey crosses) and secondary (colored symbols) cassiterites from Europe and Egypt. The ellipses show the extension of the primary cassiterites for each region. The dotted line represents the average of all primary and secondary cassiterites from the presented areas of Europe and Egypt, the grey range shows the 2SD (the 2SD error bars are covered by the symbols). .....	82
<b>Figure 6.13:</b> Primary cassiterite vs. primary stannite of SWE, SBP and Tajikistan. The blue dashed line represents the average for the cassiterite with 2SD (blue area) and the orange dashed line is the average of the stannite with 2SD (orange area); (the 2SD error bars are covered by the symbols). 85	
<b>Figure 6.14:</b> Primary vs. secondary stannite from Mushiston, Tajikistan (the 2SD error bars are covered by the symbols).....	86
<b>Figure 6.15:</b> Differentiation of the various mineralization types (greisen, quartz vein and pegmatite). The blue framed pegmatites are from the Kunar region in Afghanistan. With decreasing crystallisation	

temperature the isotopic composition becomes heavier, with increasing temperature the composition becomes lighter (the 2SD error bars are covered by the symbols).....	88
<b>Figure 6.16:</b> Comparison of duplicate measurements of samples from the ERC project and Haustein et al. (2010). .....	90
<b>Figure 7.1:</b> Averages of the granites respectively tin mining areas in SW England and the Saxonian-Bohemian province (the 2SD error bars are covered by the symbols). .....	94
<b>Figure 7.2:</b> Averages of the granites respectively tin mining areas in Portugal (green) and Spain (purple; the 2SD error bars are covered by the symbols). .....	96
<b>Figure 7.3:</b> Pegmatites from Afghanistan vs. primary and secondary cassiterite from Central Asia (the 2SD error bars are covered by the symbols). .....	102
<b>Figure 7.4:</b> Schematic illustration of the stratigraphy of the mineralization of pegmatite, greisen and quartz veins. ....	103

## LIST OF TABLES

<b>Table 2.1:</b> Sn contents in cassiterite and stannite (Dill 2010) .....	8
<b>Table 5.1:</b> Instrument settings for the Thermo Scientific Neptune multi-collector ICP-MS (Balliani et al. 2013, marked by *; Brügmann et al. 2017b) .....	59
<b>Table 6.1:</b> Mean values of the $^{124}\text{Sn}/^{120}\text{Sn}$ [%] isotope ratios of primary cassiterite from SW England. The data sets are given with 2SD. Individual analytical results are given in the appendix (Table A1). .....	69
<b>Table 6.2:</b> Mean values of the $^{124}\text{Sn}/^{120}\text{Sn}$ [%] isotope ratios of primary cassiterite from the Saxonian-Bohemian province. The data sets are given with 2SD. Individual analytical results are given in the appendix (Table A2).....	70
<b>Table 6.3:</b> Mean values of the $^{124}\text{Sn}/^{120}\text{Sn}$ [%] isotope ratios of primary cassiterite from Portugal. The data sets are given with 2SD. Individual analytical results are given in the appendix (Table A3). .....	75
<b>Table 6.4:</b> Mean values of the $^{124}\text{Sn}/^{120}\text{Sn}$ [%] isotope ratios of primary cassiterite from Spain. The data sets are given with 2SD. Individual analytical results are given in the appendix (Table A4)..	76
<b>Table 6.5:</b> Mean values of the $^{124}\text{Sn}/^{120}\text{Sn}$ [%] isotope ratios of primary cassiterite from France and Italy. The data sets are given with 2SD. Individual analytical results are given in the appendix (Table A5).....	78
<b>Table 6.6:</b> Mean values of the $^{124}\text{Sn}/^{120}\text{Sn}$ [%] isotope ratios of primary cassiterite from Egypt and Central Asia. The data sets are given with 2SD. Individual analytical results are given in the appendix (Table A6). .....	81
<b>Table 6.7:</b> Mean values of the $^{124}\text{Sn}/^{120}\text{Sn}$ [%] isotope ratios of secondary cassiterite from Europe and Egypt. The data sets are given with 2SD. The primary cassiterites presented here are only from the mining areas where we have primary as well as secondary material. The overall averages of primary cassiterites of the different tin mining areas or granites are presented in chapter 6.2.1. Individual analytical results are given in the appendix (Table A7).....	83
<b>Table 6.8:</b> Mean values of the $^{124}\text{Sn}/^{120}\text{Sn}$ [%] isotope ratios of the stannite samples. The data sets are given with 2SD. Individual analytical results are given in the appendix (Table A7). The Ave cassiterite is calculated only for the tin ore areas presented here with the corresponding stannite samples.....	86
<b>Table 7.1:</b> Summary of the cassiterite and stannite $\delta^{124}\text{Sn}/^{120}\text{Sn}$ [%] averages of all investigate areas. The results are described in chapter 6.2 in detail. All individual data are given in the appendix (Table A1-A9; *Secondary stannite of Tajikistan, Central Asia). .....	92

<b>Table A1:</b> $^{124}\text{Sn}/^{120}\text{Sn}$ and $^{122}\text{Sn}/^{116}\text{Sn}$ isotope ratios of every individual analyses of the primary cassiterites from SW England. The data sets are given with 2SD.....	137
<b>Table A2:</b> $^{124}\text{Sn}/^{120}\text{Sn}$ and $^{122}\text{Sn}/^{116}\text{Sn}$ isotope ratios of every individual analyses of the primary cassiterites from the Saxonian-Bohemian province. The data sets are given with 2SD.....	138
<b>Table A3:</b> $^{124}\text{Sn}/^{120}\text{Sn}$ and $^{122}\text{Sn}/^{116}\text{Sn}$ isotope ratios of every individual analyses of the primary cassiterites from Portugal with 2SD.....	139
<b>Table A4:</b> $^{124}\text{Sn}/^{120}\text{Sn}$ and $^{122}\text{Sn}/^{116}\text{Sn}$ isotope ratios of every individual analyses of the primary cassiterites from Spain. The data sets are given with 2SD.....	141
<b>Table A5:</b> $^{124}\text{Sn}/^{120}\text{Sn}$ and $^{122}\text{Sn}/^{116}\text{Sn}$ isotope ratios of every individual analyses of the primary cassiterites from France and Italy. The data sets are given with 2SD.....	142
<b>Table A6:</b> $^{124}\text{Sn}/^{120}\text{Sn}$ and $^{122}\text{Sn}/^{116}\text{Sn}$ isotope ratios of every individual analyses of the primary cassiterites from Central Asia and Egypt. The data sets are given with 2SD.....	143
<b>Table A7:</b> $^{124}\text{Sn}/^{120}\text{Sn}$ and $^{122}\text{Sn}/^{116}\text{Sn}$ isotope ratios of every individual analyses of the secondary cassiterites. The data sets are given with 2SD.....	145
<b>Table A8:</b> $^{124}\text{Sn}/^{120}\text{Sn}$ and $^{122}\text{Sn}/^{116}\text{Sn}$ isotope ratios of every individual analyses of the primary and secondary (Tajikistan) stannites. The data sets are given with 2SD. ....	146
<b>Table A9:</b> $^{122}\text{Sn}/^{116}\text{Sn}$ and $^{117}\text{Sn}/^{119}\text{Sn}$ isotope ratios of every individual analyses of cassiterite which where analysed by Haustein et al. (2010) and the ERC project. The data sets are given with 2SD. ....	147

## LIST OF ABBREVIATIONS

ABCD	Alpine-Balkan-Carpathian-Dinaride
AD	Abu Dabbab
AG	Altenberg granite
ALG	Antrim Lava Group
AMU	Atomic mass units
ANS	Arabian-Nubian Shield
ATC	Altenberg-Teplice caldera
BG	Bergen granite
BM	Bodmin Moor
CAOB	Central Asian orogenic belt
CB	Castelo Branco
CC	Carlingford Complex
CEZA	Curt-Engelhorn-Zentrum Archäometrie
CH	Cligga Head
CIZ	Central Iberian Zone
CZ	Cantrabian Zone
EE	Erzgebirge East
EG	Ehrenfriedersdorf granite
ENP	Eibenstock-Nejdek pluton
EW	Erzgebirge West
FLG	Fláje granite
FMZ	French Massif Central
FP	Fichtelgebirge (Smrčiny) pluton
GTMZ	Galicia-Tras-Os-Montes Zone
IG	Igla
KG	Kirchberg granite
KVP	Karlovy Vary pluton
KW	Kaiserwald
LAC	Leptyno-Amphibolitic Complex
LEG	Land's End granite
LGU	Lower Gneiss Unit
LI	Lizard Complex
LNG	Lough Neagh Group
Ma	Million ages
MCCZ	Mid-German Crystalline Zone
MC-ICP-MS	Multi-collector inductive-coupled plasma mass spectrometer

## X

ME	Middle Erzgebirge
MMC	Mourne Mountains Complex
MT	Moldanubian thrust
MZ	Moldanubian Zone
NG	Niederbobritzsch granite
NU	Nuweibi
OMZ	Ossa-Morena Zone
PAU	Parautochthon Unit
PG	Pobershau granite
PL	Portalegre
REE	Rare Earth Elements
RHZ	Rheno-Hercynian Zone
S	Sardinia
SAG	St. Agnes Granite
SASZ	South Armorian shear Zone
SAUG	St. Austell Granite
SBP	Saxonian-Bohemian province
SG	Satzung granite
SGC	Slieve Gullion Complex
SISZ	South Iberian shear Zone
SPZ	South Portuguese Zone
STZ	Saxo-Thuringian Zone
SWE	Soutwest England
TEMB	Tethyan Eurasian metallogenic belt
UGU	Upper Gneiss Unit
VC	Viano do Castelo
VI	Viseu
VL	Vogtland
WALZ	West Asturian-Leonese Zone
ZG	Zinnwald granite

## ABSTRACT

The aim of this work is to establish an overview of the tin isotope ratios of cassiterite and stannite from various mineralized regions in Europe, the Mediterranean and Central Asia in order to assess the possibility to geochemically discriminate tin ore deposits, which could have been exploited in ancient times. The motivation for this study was to eventually relate the tin found in ancient bronze objects to specific tin ore deposits and thus to clarify the origin and distribution of the tin bronze technology in the Bronze Age of the so-called Old World. For this purpose, we determined 413 primary and secondary cassiterite and stannite samples from the major tin provinces in SW England and Ireland, the Saxonian-Bohemian province, the Iberian Peninsula, France, Italy, Serbia, Egypt and Central Asia. The tin isotope compositions were analysed in solution with a multi-collector inductive-coupled plasma mass spectrometer (MC-ICP-MS) in the Curt-Engelhorn-Zentrum Archäometrie in Mannheim. The samples mainly derive from granitic pegmatites and hydrothermal vein mineralizations of tin ore deposits associated with granite complexes in the Variscan and Asian fold belts.

Overall, the isotope ratios in primary and secondary cassiterites are highly variable and range from  $\delta^{124}\text{Sn}/^{120}\text{Sn}$  -0.82 to 0.85 ‰. This variation is observed in the tin ore samples from SW England which have an average  $\delta^{124}\text{Sn}/^{120}\text{Sn}$  of  $0.10 \pm 0.59$  ‰ (2SD). Among the tin provinces of the Variscan fold belt in Europe those of SW England and the Saxonian-Bohemian province ( $\delta^{124}\text{Sn}/^{120}\text{Sn} = 0.12$  ‰  $\pm 0.37$ ) show the largest variations but the ranges of isotope ratios in both regions overlap to a large extent. Despite the large overlap, cassiterite from Spain ( $\delta^{124}\text{Sn}/^{120}\text{Sn} = -0.07$  ‰  $\pm 0.35$ ) and France ( $\delta^{124}\text{Sn}/^{120}\text{Sn} = -0.005$  ‰  $\pm 0.31$ ) tend to have on average lighter isotopic compositions than SW England, the Saxonian-Bohemian province or Portugal ( $\delta^{124}\text{Sn}/^{120}\text{Sn} = 0.07$  ‰  $\pm 0.40$ ). However, the stannite samples from SW England and the Saxonian-Bohemian province have significantly lighter isotope ratios than the associated cassiterites. The tin ores from Central Asia exhibit the largest total variation of 1.94 ‰ ranging from -1.27 to 0.67 ‰ for  $\delta^{124}\text{Sn}/^{120}\text{Sn}$ . This extent of fractionation is observed in cassiterites from Afghanistan and Uzbekistan. Afghanistan with its pegmatitic cassiterite has the lightest isotopic composition of all investigated areas with  $-0.38 \pm 0.84$  ‰ for

$\delta^{124}\text{Sn}/^{120}\text{Sn}$  and, therefore, stands out as an identifiable source. Similar to the European stannites, the Asian stannites also have significantly lighter isotope compositions.

Because of the large overlap and the highly variable isotope composition of cassiterites from all tin provinces a clearcut discrimination based on tin isotope ratios is difficult. But on a more detailed scale within each tin province it is possible to distinguish several mining or granite areas by their Sn isotope composition. However, it is also difficult to distinguish between different mineralization types.

## KURZFASSUNG

Ziel dieser Arbeit ist es einen Überblick über die Zinnisotopenverhältnisse von Kassiterit und Stannit aus verschiedenen vererzten Regionen in Europa, dem Mittelmeerraum und Zentralasien zu bekommen, um die Möglichkeit einer geochemischen Unterscheidung von Zinnerzlagerstätten zu bewerten, die in der Antike hätten ausgebeutet werden können. Die Motivation für diese Studie bestand darin, das in antiken Bronzegegenständen gefundene Zinn schließlich in Beziehung zu bestimmten Zinnerzlagerstätten zu setzen und so den Ursprung und die Verbreitung der Zinnbronzetechnologie in der Bronzezeit der sogenannten Alten Welt zu klären. Zu diesem Zweck untersuchten wir 413 primäre und sekundäre Kassiterit- und Stannitproben aus den wichtigsten Zinnprovinzen in SW-England und Irland, der sächsisch-böhmischem Provinz, der Iberischen Halbinsel, Frankreich, Italien, Serbien, Ägypten und Zentralasien. Die Zinnisotopenzusammensetzungen wurden in Lösung mit einem Multi-Kollektor-Massenspektrometer mit induktiv gekoppeltem Plasma (MC-ICP-MS) im Curt-Engelhorn-Zentrum für Archäometrie in Mannheim analysiert. Die Proben stammen hauptsächlich aus granitischen Pegmatiten und hydrothermalen Adermineralisierungen von Zinnerzlagerstätten, die mit Granitkomplexen im variskischen und asiatischen Faltengürtel in Verbindung stehen.

Insgesamt sind die Isotopenverhältnisse in primären und sekundären Kassiteriten sehr variabel und reichen von  $\delta^{124}\text{Sn}/^{120}\text{Sn} = -0,82$  bis  $0,85\text{ ‰}$ . Diese Variation wird in den Zinnerzproben aus SW England beobachtet, die einen Durchschnitt  $\delta^{124}\text{Sn}/^{120}\text{Sn}$  von  $0,10 \pm 0,59\text{ ‰}$  (2SD) aufweisen. Von den Zinnprovinzen des variszischen Faltengürtels in Europa weisen die Provinzen SW England und die sächsisch-böhmischem Provinz ( $\delta^{124}\text{Sn}/^{120}\text{Sn} = 0,12\text{ ‰} \pm 0,37$ ) die größten Unterschiede auf, aber die Bereiche der Isotopenverhältnisse in beiden Regionen überschneiden sich weitgehend. Trotz der großen Überlappung haben Kassiterite aus Spanien ( $\delta^{124}\text{Sn}/^{120}\text{Sn} = -0,07\text{ ‰} \pm 0,35$ ) und Frankreich ( $\delta^{124}\text{Sn}/^{120}\text{Sn} = -0,005\text{ ‰} \pm 0,31$ ) im Durchschnitt eine leichtere Isotopenzusammensetzung als SW England, die sächsisch-böhmischem Provinz oder Portugal ( $\delta^{124}\text{Sn}/^{120}\text{Sn} = 0,07\text{ ‰} \pm 0,40$ ). Die Stannit-Proben aus SW England und der sächsisch-böhmischem Provinz weisen jedoch deutlich leichtere Isotopenverhältnisse auf als die zugehörigen Kassiterite. Die Zinnerze aus Zentralasien weisen mit

1,94 ‰ die größte Gesamtvariation auf, die von -1,27 bis 0,67 ‰ für  $\delta^{124}\text{Sn}/^{120}\text{Sn}$  reicht. Dieses Ausmaß der Fraktionierung ist bei Kassiteriten aus Afghanistan und Usbekistan zu beobachten. Afghanistan mit seinem pegmatitischen Kassiterit hat von allen untersuchten Gebieten die leichteste Isotopenzusammensetzung mit  $-0,38 \pm 0,84$  ‰ für  $\delta^{124}\text{Sn}/^{120}\text{Sn}$  und sticht daher als identifizierbare Quelle hervor. Neben den europäischen Stanniten weisen auch die asiatischen Stannite deutlich leichtere Isotopenzusammensetzungen auf.

Aufgrund der großen Überlappung und der sehr variablen Isotopenzusammensetzung der Kassiterite aus allen Zinnprovinzen ist eine eindeutige Unterscheidung anhand der Zinnisotopenverhältnisse schwierig. Auf einer detaillierteren Ebene innerhalb jeder Zinnprovinz ist es jedoch möglich, mehrere Bergbau- oder Granitgebiete anhand ihrer Sn-Isotopenzusammensetzung zu unterscheiden. Es ist jedoch auch schwierig, zwischen verschiedenen Mineralisierungstypen zu unterscheiden.

## ACKNOWLEDGEMENT

This work has received support from the Advanced Grant no. 323861 of the European Research Council (ERC) awarded to Prof. E. Pernicka. It is part of the research project *Bronze Age Tin – Tin isotopes and the sources of Bronze Age tin in the Old World*.







## 1. INTRODUCTION

The plate tectonic during the Late Palaeozoic was dominated by the supercontinents Gondwana and Laurussia from whose fusion the Variscan belt originated (Ballèvre et al. 2009). Together with Pangea they dominated the global plate-tectonic during this time (Ruban et al. 2007). Gondwana comprised several present-day plates including Arabia, Africa, most of Antarctica and Australia, India, Madagascar and South America (Cocks 2001, Stampfli et al. 2001, Cocks and Torsvik 2002). The supercontinent Laurussia consisted of Avalonia (SW England), Baltica (Serbia) and Laurentia (North-America and Greenland; McKerrow et al. 2000). The various mineralized regions in Europe, the Mediterranean and Central Asia which were investigated for this thesis are part of the European Variscan belt and the Central Asian orogenic belt.

The European Variscan belt was formed in the Late Palaeozoic between 480 and 250 Ma (Matte 2001) and comprises a large Sn-W metallogenic province with quartz-cassiterite and quartz-wolframite ores which are associated with Variscan S-Type granites. The tin- and tungsten mineralizations occur mostly as greisen, stockwork or vein types and the relationship of the Sn-W mineralizations to magmatism is largely accepted (Lehmann 1990). The granitic pegmatites are high temperature ( $> 600^{\circ}\text{C}$ ) crystallisation products with a complex ore mineralogy whereas the mineralization in the vein systems precipitated from hydrothermal fluids at temperatures  $< 400^{\circ}\text{C}$  (Chesley et al. 1993). Besides the Iberian Peninsula the largest tin provinces in Europe are located in SW England and the Saxonian-Bohemian province. Both regions belong to the northern part of the Variscan Mountains and similar processes such as the collision during the Variscan orogeny resulted in the granite-related metallogeny (Sn-W-Cu-As-Zn-Pb) and therefore in the tin deposits in these provinces (Štemprok 1995). The common feature of the deposits is the association with late Variscan granites and their pegmatitic/pneumatolitic and hydrothermal origins (Lehmann 1990; Scrivener et

al. 1994). This also applies to the Iberian Massif, the Armorican Massif (France) and the southern Variscan belt (Italy).

The Central Asian orogenic belt (CAOB) rises from 1000 to about 280 Ma (Coleman 1989; Khain et al. 2003; Kröner et al. 2007; Rytsk et al. 2007) by accretion of island arcs, ophiolites, islands and other crustal parts (Windley et al. 2007). The CAOB is characterised by a huge spread of Palaeozoic and Mesozoic granitic intrusions. The granitoid rocks have diverse compositions from calcalkaline to peralkaline (Jahn et al. 2000a) and most of them are between 500 to 100 Ma (Kovalenko et al. 1996; Jahn et al. 2000 a, b; 2004). The Palaeozoic basis of Central Asia is built up of multiple blocks and terranes which are separated by huge sutures (Garner 2013), which are remains of Neoproterozoic to Mesozoic sedimentary basins, island arcs and terranes (Yakubchuk et al. 2002; Seltmann and Porter 2005; Porter 2006). The tin mineralization in most of the tin ore provinces throughout Central Asia is closely related with silver mineralization represented by quartz-carbonate-sulfide vein and stockwork zones (Borisenko et al. 2006).

The Arabian-Nubian Shield (ANS) in the Mediterranean is located at the northern part of the East African Orogen and is built up of Neoproterozoic juvenile arcs, voluminous granitoid intrusions and Neoproterozoic crust (Hamimi et al. 2014). The rare-metal granitoids in Egypt are classified as metaluminous alkali granites, peraluminous (Li-albite) granites and metasomatized mica-bearing granites (Helba et al. 1997; Abdalla et al. 2009). Cassiterite occurs in form of disseminated cassiterite, stockwork greisen veins and bodies, beryl, cassiterite and wolframite quartz veins and placer deposits (Abdalla et al. 2008).

A detailed description of all geological settings and their tin provinces relevant for this work is given in chapter 4.

To trace the sources of tin and the distribution of the bronze technology in the third and second millennium BC is the central question of the multi-disciplinary “Bronze Age Tin” research project funded by an Advanced Grant of the European Research Council (ERC). The methodological approach is based on the use of isotope ratios of tin as a possible fingerprint of ores and metal

artefacts in order to determine the origin of tin in the artefacts. With modern inductively coupled plasma ionisation (MC-ICP-MS) the fractionation effects caused by chemical and physical processes, which can change the isotope abundance pattern of an element, may be resolved. Since the 1990s, tin isotopy has been used to study the degree of fractionation that can be caused by geological and metallurgical processes. Most studies on this topic followed an archaeological approach to use the tin isotopic composition as a tool to track bronze and tin metal artefacts to their tin ore sources (Gale 1997; Yi et al. 1999; Clayton et al. 2002; Haustein et al. 2010; Balliani et al. 2013; Yamazaki et al. 2013).

Already in the 1960s a possible fractionation of tin isotopes in nature was investigated, but even with the inclusion of extraterrestrial samples no variations in the isotope composition of tin could be found (De Laeter and Jeffery 1965, 1967). Devillers et al. (1983) and Rosman et al. (1984) provided accurate measurements of the tin isotope composition. A deviation from a tin standard was then measured on an industrial tin, but this was due to an effect in the tin refining process rather than to natural processes (Rossmann and McNaughthon 1987). Four years later, it was made possible to detect small isotopic fractionation in a cassiterite sample by using a multi-collector thermion mass spectrometer (MC-TIMS; McNaughton and Rossmann 1991). Gale (1997) was the first to apply the tin isotopy to an archaeological question by studying the possibility of metal recycling in the Bronze Age. He assumed that the tin isotopy of remelted bronze must be different from that of primary metal, but this interesting hypothesis could not be confirmed. However, his work was the prelude to a series of investigations of the tin isotopy for possible archaeometric applications, such as Begemann et al. (1999).

The introduction of the new ICP-mass spectrometer technology with magnetic sector field and multiple collectors (Walder and Freedman 1992; Walder and Furuta 1993; Halliday et al. 1995) represented a major advance in isotope analysis technology because the atomic masses of a number of elements could be determined more precisely than before (Lee and Halliday 1995). For the precise determination of tin isotope ratios a highly sensitive method is required, which became possible with

the development of MC-ICP-MS. This method for tin isotope measurements was first used by Yi et al. (1999), which not only solved the problem of the relatively high initial excitation energy of tin, but also achieved a much higher sample throughput per time unit. Gale (1997) and Yi et al. (1999) were the first who corrected the fractionation of tin, which is caused by the ICP excitation in the mass spectrometer, by the addition of antimony to the measurement solutions. The precision of measurement was 0.32 ‰ (double standard deviation (2SD) for n=10) for  $^{124}\text{Sn}/^{117}\text{Sn}$ . Investigations of tin isotope ratios of cassiterites and tin artefacts followed (Gillis et al. 2001; Nowell et al. 2002; Clayton et al. 2002). This method has since been used for all subsequent tin isotope measurements using an ICP mass spectrometer. Compared to Yi et al. (1999), Clayton et al. (2002) reached a precision of 0.23 ‰ (2SD for n=14) for  $\delta^{122}\text{Sn}/^{116}\text{Sn}$ , which represents a significant improvement in the quality of the measured values. They also investigated various possibilities for the correction of isotope fractionation induced by plasma excitation and it turns out that the antimony doping of the test sample (Yi et al. 1999) in combination with an exponential correction function is the most effective solution (Clayton et al. 2002). Gillis and Clayton (2008) have come to the conclusion that systematic investigation of ores and artefacts are important for the evaluation of the tin isotope potential for archaeological questions. Haustein et al. (2010) have extended the number of analyses of tin ore samples for SW England and the Saxonian-Bohemian province. Most of the past studies tried to trace bronze artefacts and tin metal to their geological tin ore sources (Begemann et al. 1999; Gale 1997; Yi et al. 1999; Clayton et al. 2002; Haustein et al. 2010; Balliana et al. 2013; Yamazaki et al. 2013, 2014).

Due to a lack of an internationally certified reference material for stable tin isotope compositions, it is difficult to compare isotope data even from recent studies. Because it was not possible to retrieve the isotope data of commercially available standard solutions Brügmann et al. (2017b) provided new data on international reference materials made of bronze (BAM 211, IARM-91D) and also tin standard solutions were analysed and compared with previous published data.

In addition, a method for dissolving tin minerals like cassiterite ( $\text{SnO}_2$ ) and stannite ( $(\text{Cu}_2(\text{Fe},\text{Zn})\text{SnS}_4)$ ) had to be developed (Clayton et al. 2002; Haustein et al. 2010; Yamazaki et al. 2013; Berger et al. 2018). For dissolving tin minerals (cassiterite and stannite) they must be converted into acid dissolvable tin metal by reduction at high temperatures. One technique is the conversion of  $\text{SnO}_2$  into acid-soluble tin metal by reduction with graphite at high temperatures of 1100-1200 °C (McNaughton and Rosman 1991; Clayton et al. 2002; Nowell et al. 2002). Dissolving cassiterite with Hl also proved successful (Yamazaki et al. 2013). Brügmann et al. (2017b) discovered that both procedures add substantial analytical uncertainties due to low reproducibility. A new approach was proposed by Haustein et al (2010), i.e., to reduce cassiterite and stannite with KCN to tin metal at a temperature of 800 °C. Brügmann et al. 2017b successfully repeated this procedure with cassiterite and proposed a temperature of 1000 °C. They also found out that for the decomposition of stannite a different approach has to be taken. The addition of copper powder to stannite reduced the sulfide mineral at 1100 °C to tin bronze. The latest studies all used the TRU-Spec resin for the separation of Sn from the matrix after the dissolution of cassiterite (Haustein et al. 2010; Balliana et al. 2013; Yamazaki et al. 2013, 2014; Mason et al. 2016). The studies reported contradictory results regarding the influence of chromatographic separation on the isotopic composition of the sample. A significant fractionation induced by the column chemistry was observed by Yamazaki et al. (2013). This fractionation has on average -0.6 ‰ for  $\delta^{124}\text{Sn}/^{120}\text{Sn}$  relative to a non-purified Sn standard solution. They make the incorporation of organic material from the TRU resin into the tin solution responsible for this isotope shift, which has led to an anomalous fractionation behaviour during the ICP-MS measurement. The studies of Haustein et al. (2010) and Balliana et al. (2013) did not report such a fractionation effect using the TRU resin and Brügmann et al. (2017b) found a very small isotopic shift of  $\leq 0.005\text{‰}/\text{amu}$  by the comparison of the isotope compositions of purified and non-purified solutions, which is statistically not relevant. The whole procedure of dissolving tin minerals is described in chapter 5.2 in detail.

Because cassiterite and stannite are the main carriers of tin (Černý et al. 2005), the isotopic composition of Sn could be used as a petrological tracer for observing the evolution of magmatic-hydrothermal fluid systems which contain tin. Therefore, the tin isotope ratios could be used for differentiating ore deposits or provinces by their specific fingerprint. Begemann et al. (1999) had the idea of tracing tin from artefacts using its own isotopic fingerprint for its origin. Gillis et al. (2001), Nowell et al. (2002) and Clayton et al. (2002) were the first to compare the tin isotope ratios of tin ores (cassiterite) and ancient tin objects of various origins. However, there is no uniform picture of the applicability of the tin isotope to archaeological issues. For example, the investigations do not show whether individual deposits are isotopically homogeneous and can be distinguished from other deposits, nor are clear relationships made between ores and artefacts, which is particularly due to the low number of examined ores. The most recent studies of Haustein et al. (2010), Balliana et al. (2013), Yamazaki et al. (2014), Mason et al. (2016), Brügmann et al. (2017a, b) and Berger et al. (2018, 2019) observed reproducibly determined variations of tin isotope abundances in cassiterite or bronze artefacts, but only one study provided a comprehensive data set on tin ore provinces (Haustein et al. 2010). The isotopic variation measured in these materials indicates that high-temperature geological processes fractionate tin isotopes (Yao et al. 2018).

In this study, we determined the isotopic composition of tin in cassiterite and stannite of 413 samples from pegmatitic and hydrothermal mineralization as well as samples from placer deposits of the major granite plutons and tin mining areas in Europe and Central Asia. This contribution presents a new data set of SW England, Ireland, the Saxonian-Bohemian province, the Iberian Peninsula, France, Italy, Serbia, Egypt, Kazakhstan, Uzbekistan, Tajikistan, Kyrgyzstan and Afghanistan.

In summary it can be said that the previous approaches have not resulted in a uniform picture concerning the tin isotopy in relation to archaeological questions. This work is intended to provide a comprehensive catalogue of tin isotope data of all major tin ore deposits in Europe, Egypt and Central Asia which were important or could be of importance in the Bronze Age. Furthermore, the causes of fractionation in the tin ores are still largely unknown.

## 2. TIN

### 2.1 Mineralogy and chemistry

With 10 isotopes ( $^{112}\text{Sn}$ - $^{124}\text{Sn}$ ) tin has the largest number of naturally occurring isotopes of all elements and therefore has the largest mass range of 12 amu (Fig. 2.1; Yao et al. 2018). This mass difference offers potential for mass fractionation in nature. The relative abundance of the isotopes can be changed during chemical and/or physical processes during ore formation and metallurgical processes as well as by corrosion.

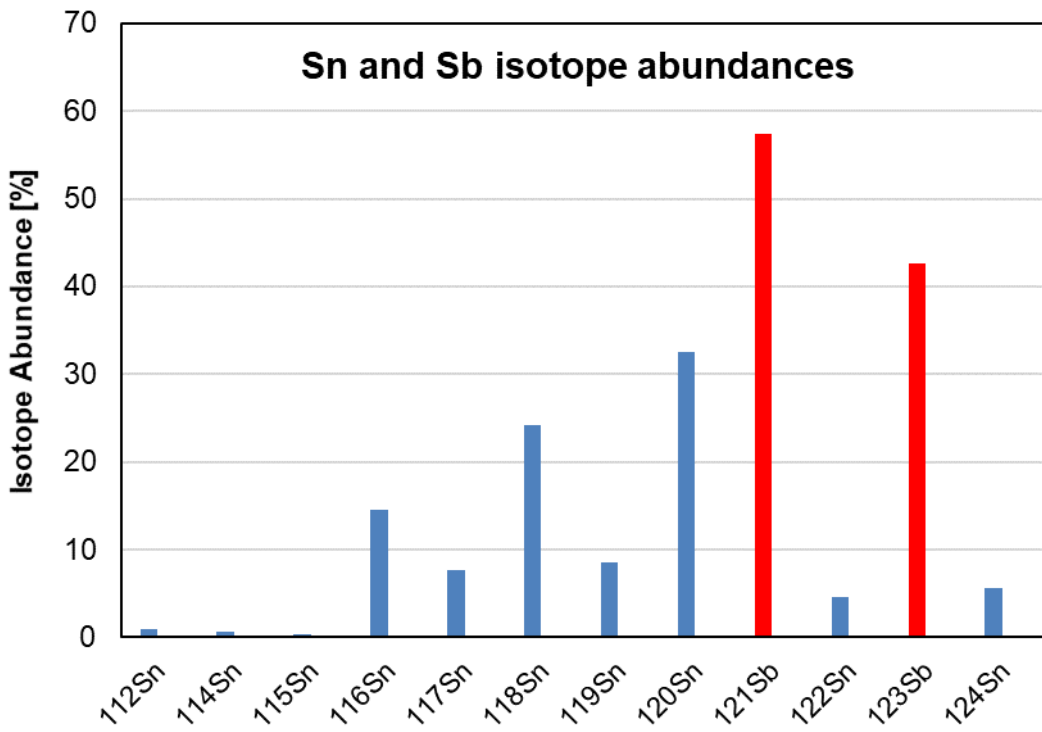


**Figure 2.1:** Natural isotope abundances of Sn and Sb.

However, it should be noted that, in contrast to lead for example, the tin isotope ratios are not influenced by the radioactive decay of other elements, so any observed isotopic variations can only be attributed to chemical processes during the ore formation. Haustein (2009) concluded that the

isotope differences to be expected in tin can only be small compared to lead. In numerous metal systems redox reactions are known to fractionate isotopes (e.g., Cu, Fe). Polyakov et al. (2005) showed that within the temperature range of tin mineralization (300-700°C), the oxidation state of tin has a large influence on the fractionation.

Tin is a metal that acts as a volatile, siderophile and chalcophile element and can occur in the Sn<sup>0</sup>, Sn<sup>2+</sup>, or Sn<sup>4+</sup> valence states (Yao et al. 2018), which can make it soluble by complexation with various ligands (Robb 2005). Sn<sup>4+</sup> with its ion radius of 0.71 Å is similar to those of Fe<sup>3+</sup> (0.64 Å), Ti<sup>4+</sup> (0.68 Å), Nb<sup>5+</sup> (0.68 Å), Ta<sup>5+</sup> (0.69 Å) and Sc<sup>3+</sup> (0.81 Å), which gives many possibilities for substitution of these elements in the rock-forming Fe-bearing minerals (Dill 2010). On average 1.7 ppm tin is present in the Earth's crust (Rudnick and Gao 2003). It occurs in α Sn (grey) and β Sn (white) modification. The metal has a silvery to grey colour. The most common tin mineral is cassiterite (SnO<sub>2</sub>), a tetragonal dioxide with Sn contents about 78.8 wt% in stoichiometric cassiterite. Besides cassiterite the second most important tin mineral is stannite (Cu<sub>2</sub>FeSnS<sub>4</sub>) with 27.8 wt% Sn (Dill 2010).

**Table 2.1:** Sn contents in cassiterite and stannite (Dill 2010).

		Max. wt% Sn	Density (g/cm <sup>3</sup> )
Cassiterite	SnO <sub>2</sub>	78.8	6.8-7.1
Stannite	Cu <sub>2</sub> FeSnS <sub>4</sub>	27.8	4.4

Tin minerals can contain significant concentrations of Fe up to 6 wt% and other elements like Nb, Ta, Zr, Mn, As, Ge, Sc, Zr, Ga, Be, Hf, In, W, Mn and V (Pohl 2011).

The crystal morphology of cassiterite varies as a function of temperature and can therefore be used in the field for a first and approximate classification of the tin mineralization according to its formation temperature. Mostly bipyramidal and short crystals without prisms are found in pegmatites, greisen and high-temperature veins, whereas in lower-temperature hydrothermal deposits the cassiterite crystals appear bipyramidal with well developed elongated faces of the prism

(Pohl 2011). This type is called “needle tin” or “Cornish tin”. In low-temperature hydrothermal deposits the “wood tin” occurs, which is built up of collomorphic, fibrous aggregates of slim acicular crystals. In contrast to low-temperature deposits the cassiterites from high-temperature deposits develop in stubby prisms with various faces and frequently twinning (Dill 2010).

The Sn-hydroxide complexes  $\text{Sn}(\text{OH})_4$  and  $\text{Sn}(\text{OH})_2$  are stable under alkaline conditions with lower temperatures. The solubility of these complexes is much lower than those of Sn-chloride complexes which are formed at higher temperatures and lower pH (Robb 2005). Tin is incorporated into Fe-enriched biotite if it is present as  $\text{SnO}^{4+}$  complex in a granitic melt without substitution of  $\text{SiO}_2$  (Dill 2010). During the late stages of granite emplacement Sn is released on decomposition of biotite. The cassiterite precipitation remains below 375°C during decreases of T and P. Jackson et al (1982) came to a different conclusion, noting that the formation of the ore-forming fluids in the solidus is usually promoted by immiscibility and causes the movement of volatile substances into apical positions in the roof of the pluton.

The most efficient transporters of tin are chloride and hydrochloride complexes such as  $\text{SnCl}_2$ ,  $\text{SnOHC}\text{l}$  and  $\text{Sn}(\text{OH})_2\text{Cl}_2$  (Wood and Samson 1998). During the precipitation of tin, the transporting acidic fluids can become neutralized by the hydrolysis of feldspars, muscovite + quartz  $\pm$  biotite  $\pm$  chlorite  $\pm$  Fe sulfides. This can happen during greisenisation or during reactions with granitic wall rocks (Dill 2010). The Sn deposition is not greatly affected by changes in temperature or pressure, when it reaches levels of above 400°C and 1-2 kbar (Štemprok 1987; Taylor and Wall 1993), whereas it is more sensitive to fluid acidity and alkali chloride concentration changes. In tin ore deposits the temperature for the cassiterite formation is commonly between 300-500°C (Lehmann 1990).

Most of the tin granites are generally of peraluminous S-type character, highly fractionated and strongly reduced (Pohl 2011), unlike the I-type fractionation suites which are associated with ore systems which carry molybdenum (Lehmann 1990). Suites of granites with high intrusion levels and

high contents of F, Li, Rb, Cs, Nb, Sn and Y are also associated with Sn deposits, which is typical for A-type granites (Shaw and Flood 1992). The granite types can be characterised as:

- I-type granite: characteristic mafic mineral is hornblende; SiO<sub>2</sub> content is highly variable; is formed in great depths under high temperatures by anatexis of magmatic educts (granites, granodiorites, diorites) or during continental collision and subduction of sediments. It is bound to active, convective continental margins of the cordillera type (Clemens 2003).
- S-type granite: typical mafic minerals are muscovite, aluminosilicate, garnet and cordierite; SiO<sub>2</sub> contents are relatively high, the chemical composition is peraluminic; the educts are of sedimentary origin (gneiss, mica slate and other metapelitic rocks); S-type granites are collision-bound (Clemens 2003).
- A-type granite (anhydrous and anorogenic): typical mafic minerals are biotite, alkali amphibole and pyroxene; SiO<sub>2</sub> content is high, composition is often peralkaline; most probable educts are granulites; A-type granites are anorogenic intraplate granites, a product of multiple melt-extraction from the same source rock (Eby 1992).

## 2.2 Ore formation and deposit types

An ore can be described as a solid naturally occurring mineral aggregate of economic interest from which one or more valuable constituents may be recovered by treatment. An alternative definition is a rock that may be, will be, is or has been mined and from which something of value may be extracted. The major component for element concentration to an ore body is the composition and evolution of the parental granitoid. The ore formation is also controlled by the plate tectonic setting, P/T-parameters of melting and water and the intrusive depth (Pohl 2011). The partial pressure of oxygen (redox state) of the melt, assimilation of country rocks and the evolution of the magma by fractionation, cooling and crystallisation including fluid segregation can be of importance too (Pohl

2011). Arndt and Ganino (2012) define an ore deposit as “an accumulation of a useful commodity that is present in high-enough concentration and in sufficient quantity to be extractable at a profit”.

The different types of granitoids can host various ores. The I-type granitoids are the most common intrusive magmatic rocks which are rich of hornblende and have higher concentrations of Ca, Na and Sr in contrast to S-type granites derived from sediments (Pohl 2011). They are SiO<sub>2</sub> rich rocks which often contain muscovite besides biotite. The highly fractionated intrusions (“tin granites”) of the I- and S-type granites are unambiguously linked to tin, tungsten and tantalum ore deposits (Blevin and Chappell 1995). Within A-type granitoids sodium-rich and potassium-rich granites can occur, whereas the potassium-rich granites show intense hydrothermal silicification and tourmalinization which lead to the formation of tin, tungsten, lead, zinc and fluorspar deposits (Pohl 2011). According to Yao et al. (2018), redox reactions are important for the genesis of all primary cassiterite ores, independent of the process and place of mineralization. Under reducing conditions (tin predominantly in the Sn<sup>2+</sup> state), the solubility of tin granitic magmas is several orders of magnitude higher than under oxidizing conditions with tin as Sn<sup>4+</sup> as stable species (Linnen et al. 1995, 1996).

The most efficient metal transport in ore formation is carried out by aqueous fluids like ocean and meteoric water to hydro-carbo-thermal systems (Lehmann et al. 2000). The origin of these ore fluids is seawater, meteoric water, and juvenile water (Hoefs 1997).

### **2.2.1 Geodynamic settings of mineral deposits**

Mineral deposit systems can only form under specific conditions in different tectonic systems because they need specific conjunctions of processes to produce the metal enrichments that result in ore deposits (Groves and Bierlein 2007). Several phanerozoic Sn-W deposits are associated with S-type granites which occur in rather unusual tectonic settings like continent-continent orogens (e.g., Alpine-Himalayas, Appalachian-Caledonian; Kerrich et al. 2005). The tectonic environment for

other Mesozoic to Tertiary deposits is more clearly defined as a backarc setting, for example for the Sn-W deposits of the Tasman orogen in Australia (Solomon and Groves 1994). Tin deposits can also occur in accretionary orogens on continental margins like the deposits in Bolivia, Andes (Groves and Bierlein 2007). The formation of an ore deposit is related to specific tectonic settings:

- Late Permian-Triassic intracontinental rifting along the northern margin of Gondwana,
- Jurassic intraoceanic rifting,
- Subduction-related settings,
- Post-collision continent-continent settings include Pb-Zn, Sb, As, Au-Cu deposits (Janković 1997).

## 2.2.2 Classification scheme

A classification of ore deposits is based on the fact that ores are rocks and they can be attributed to an igneous or sedimentary origin (Robb 2005). This scheme of classification can also reflect the genetic processes which lead to the ore formation, as igneous and sedimentary deposits are often syngenetic and formed contemporaneously with the host rock. Increase of pressure and temperature can substantially modify the original composition of ore deposits, but it is evident that metamorphism itself does not represent an essential process where ore deposits are created (Robb 2005). Hydrothermal processes can be seen as an analogue for metamorphism in ore-forming processes. After Einaudi (2000) mineral deposits can be classified into three types based on these processes: magmatic deposits (e.g., pegmatitic deposits), hydrothermal deposits (veins, greisen) and sedimentary deposits (placers). In placer deposits dense or heavy detrital minerals are deposited during sedimentation (Robb 2005). Groves and Bierlein (2007) declare that mineral deposits represent notable metal concentrations resulting from magmatic, magmatic-hydrothermal or hydrothermal processes in geodynamic environments characterised by high thermal and/or mechanical energy near plate boundaries.

Dill (2010) suggested the “chessboard” classification scheme of mineral deposits. In this scheme mineralogy and geology act as x- and y-coordinates of a classification chart of mineral resources. On the x-axis magmatic and sedimentary lithologies are plotted together with tectonic structures and the y-axis represents 63 commodity groups comprising minerals and elements. This results in the following classification scheme of tin-tungsten deposits:

(1) Magmatic tin-tungsten deposits

- a. Sn-Ta-Nb pematites
- b. Granitic skarn deposits
  - i. Proximal Sn-(W) skarn deposits (Erzgebirge-Cornwall type) (Russia, Tasmania-Australia, Alaska)
  - ii. Distal skarn/replacement deposits (Manto-type) (Australia, China)
- c. Post-granitic endo- and exogranitic greisen vein in S- and A-type granites and breccia pipe deposits
- d. Porphyry-type and subvolcanic deposits
  - i. W-Mo deposits (Bolivia, Argentina, Peru, Japan, Canada)
  - ii. Sn-(Ag-Pb-Zn-Cu) vein type deposits (Bolivia)
- e. Stratiform Sn-W deposits (Australia, South Korea)
- f. Volcanic massive sulfide Pb-Zn-Cu deposits (VMS)
  - i. Iberian type

(2) Structure-related tungsten deposits

- a. Thrustbound Au-W deposits

(3) Sedimentary tin-tungsten deposits

- a. SEDEX/SMS Pb-Zn-Ag-FeS-(Sn) deposits
- b. Sn laterite (residual placer) deposits
- c. Sn placer deposits sensu stricto
  - i. Alluvial-fluvial

## ii. Marine

The Sn-pegmatites (1a), Post-granitic endo- and exogranitic greisen vein type and lode deposits (1c) and sedimentary tin-tungsten deposits (3) are relevant for this work, since all samples for this purpose can be assigned to these groups.

### ***Magmatic and hydrothermal tin deposits***

#### **Granitic pegmatites (high-T)**

The Sn-(Li-Ta-Nb; 1a) pegmatites occur in Brazil, Russia, DR Kongo and Cornwall (Badham 1980). These metalliferous pegmatites have arsenopyrite, loellingite, wolframite with minor cassiterite associated with tourmaline, zinnwaldite, apatite, chlorite, stilbite, stokesite, topaz, triplite and thoreaulite. Pegmatites are a coarse-grained crystalline modification of a magmatic rock. They crystallise from highly fractionated hydrous residual melts of felsic magma bodies which are enriched in volatiles and incompatible trace elements (Pohl 2011). The majority of the pegmatites are related to granites and consist of microcline, albite, orthoclase, mica and quartz. Granitic pegmatites are found as oval and lenticular bodies in the form of dykes. The increasing mobility of more fractionated melts explains the external zonation of different pegmatites around parent intrusions because the increasing fractionation lowers the solidus temperature, density and viscosity of melts (Černý 1991).

Melting that leads to pegmatite formation occurs when incompatible elements such as lithium, REEs, thorium or uranium and at the same time volatile substances such as water, phosphorus, boron or fluorine accumulate in the residual melt during the crystallisation of a pluton. On the one hand, the presence of the highly volatile components considerably lowers the melting point, so that the melt solidifies only at a temperature of about 450 °C. On the other hand, it becomes more liquid, i.e. the

---

viscosity is significantly reduced (London 2005). For this reason, the melt can move along fissures far into the surrounding rocks often for many kilometers. This explains why ordinary pegmatites occur near the parent intrusion, whereas specialized, complex pegmatites and hydrothermal ore deposits are found at greater distances (Pohl 2011).

Most geologists assume that pegmatites crystallise predominantly at temperatures of the water-rich granite solidus, near 650–700 °C (London 2005). However, there are also deviations when P-T estimates made from certain mineral aggregates, isotope data or fluid inclusions are compared with magmatic formation conditions (London 2005).

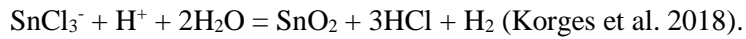
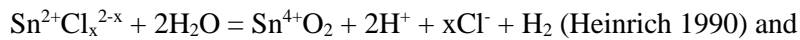
### **Vein type deposits (low-T)**

The greisenization (hydrothermal greisen) represents one type of hydrothermal host rock alteration. In S- and A-type granites a large variety of post-granitic endo- and exogranitic greisen vein type (1c) and lode Sn and W bearing deposits occur (Dill 2010). The term “greisen” was defined by tin miners in the Erzgebirge as an altered lithium-albite granite in which feldspar and biotite are converted to an aggregation of quartz, topaz, muscovite, zinnwaldite and protolithionite (both Li-micas). In addition, tourmaline, rutile, cassiterite, fluorite, wolframite, scheelite and various silicates can be found (Pohl 2011). Greisen bodies enriched in tin and tungsten may represent useful ore (Halter et al. 1996). Greisen is an alteration composition which mainly consists of quartz, muscovite and topaz. It can contain tourmaline and fluorite in low quantities and generally forms close to quartz-cassiterite-wolframite veins (Robb 2005). Greisen mainly develops at the dome zones of highly differentiated (S-types) granites, containing Sn and W mineralizations and significant amounts of other incompatible elements (e.g., F, Li, B). Jackson et al. (1989) proposed a temperature range of the greisenising fluids of 250–500°C based on fluid inclusion data. The genesis of this type of deposit results from the regional hydrothermal circulation triggered by heat from the emplacement and

crystallisation of younger magma pulses (Chesley et al. 1993). An example is along the Czech-German border in the area of the Saxonian-Bohemian province where granite-related Sn-W mineralization occurs within deposits at for example Altenberg, Ehrenfriedersdorf, Pechtesgrün, Zinnwald and Krásno (Mochnacka et al. 1995; Tischendorf et al. 1995; Webster et al. 2004). Other post-granitic endo- and exogranitic Sn-W mineralizations are known from Cornwall. Here the granites show hydraulic fracturing which is caused by the buildup of magmatic-hydrothermal fluids during the final stages of crystallisation in the apical zones of the granites. This results in the formation of greisen bordered vein systems within the granite, adjacent wall rocks as well as lodes which are concentrated along the axis of the batholith and mainly consists of Sn, Cu, W, Fe, Zn and Ag (Jackson et al. 1989; Muller et al. 2006). Tourmaline, muscovite, orthoclase, chlorite, wolframite, arsenopyrite, stannite, cassiterite, topaz, and apatite are formed during these late- to post-granitic processes (Bray and Spooner 1983; Alderton 1993; Williamson et al. 2000).

Hydrothermal mineral deposits (quartz and polymetallic veins) are formed by the precipitation of solid minerals from hydrothermal solutions (Dill 2010). Many factors are important for the genesis of a hydrothermal mineral deposit, like the presence of hot water for dissolving and transporting minerals, the availability of gaps in the rock to allow the solutions to move, and chemical reactions that will result in deposition. One form of this deposit type is the hydrothermal-metasomatic ore deposit, in which the ore is formed by hydrothermal chemical conversion and replacement of the preexisting rock. In ore veins, small local metasomatic processes are ever-present co-products of hydrothermal activities (Pohl 2011). Although the metasomatic ore formation near igneous intrusions is most frequent (skarn- and contact-metasomatic deposits), there are also metasomatic ore deposits with no genetic relation to a magma, for example marine limestone (Pohl 2011). Another type of hydrothermal ore deposits are the ore veins. The mining of ore veins has already been described by fundamental books from Agricola (1556) to Lindgren (1933). Veins develop as tabular bodies of hydrothermal precipitates that penetrate fissures in the rocks. They often form upwards to a field of smaller veins and veinlets. The “stockwork orebodies” are built up of short veins with a three-dimensional orientation (Pohl 2011). These bodies are very closely spaced, which means that the

entire affected rock body can be mined. Brecciated rock bodies can host rich ore and many vein deposits are spatially and genetically associated with fissured rocks (Jebrak 1997). Several fissures like the tin ore veins in Cornwall have zones of intensive micro-fracturing which gives access to fluids from main flow channels (Dominy et al. 1996). The cassiterite precipitation from hydrothermal solutions happens probably by reactions associated with the oxidation of Sn-chloride complexes, like:



This precipitation can occur over a temperature range of 320-550°C, based on fluid inclusion analysis and mineral stability studies (Yao et al. 2018). However, the main phase for precipitation in most ores lies within the range of 350-400°C (Campbell and Panter 1990; Markl and Schumacher 1996; Korges et al. 2018). Cassiterite precipitates from reduced, magma-derived hydrothermal fluids, which needs electron-transfer to produce  $\text{Sn}^{4+}$  (Yao et al. 2018). Tin in the  $\text{Sn}^{4+}$  state is present in cassiterite and stannite (Eibschütz et al. 1967; Greenwood and Whitfield 1968).

### ***Sedimentary tin deposits***

Placer deposits are of importance because they can contain a wide variety of minerals and metals like gold, uraninite, diamonds, cassiterite, ilmenite, rutile and zircon (Robb 2005). They are mechanically formed accumulations of heavy, durable minerals that can occur in transported soil or regolith, in fluvial and in coastal sediments (Pohl 2011). A basic requirement for the concentration of minerals as placer deposits is their mechanical and chemical resistance to weathering and transport as well as their higher density compared to the usual rock-forming minerals (Pohl 2011). Ore-forming processes, which lead to the formation of placer deposits and metal accumulation in connection with chemical sediments and diagenetic fluid flow, are intimately related to the origin, tectonic setting,

and development of the sedimentary host rocks. The shoreline and fluvial placer deposit types (e.g., gold, cassiterite, and diamonds) reflect ore-forming processes that prevail in cratonic environments, where properties such as long-lasting stability and high deposition energies apply to the post-treatment of the sediment load (Robb 2005). Cassiterite aggregates from placer deposits can contain a broad spectrum of inclusions of Ti-Nb-Fe minerals. These mineral inclusions may help to constrain the source rock of the sedimentary aggregates (Dill et al. 2006). Based on the variability of these minerals the following processes for the evolution of placers can be defined: pegmatitic-hydrothermal granitic source rock evolution, formation of paleoplacers, chemical weathering and replacement of preexisting oxides and phosphates, neomorphism, internal sedimentation, and colluvial-fluvial placer deposition (Dill et al. 2006).

### 3. STUDY AREA AND SAMPLING CAMPAIGNS

Although tin deposits vary considerably, they can be classified according to their depth, location relative to the granite contact and type of mineralization (Taylor 1979). Therefore, we examined distinct types of mineralization from several different localities: SW England (SWE) and the Saxonian-Bohemian province (SBP), Ireland, the Iberian Peninsula, France, Italy, Serbia, Egypt and Central Asia (Fig. 3.1). The geology of the sample locations is described in chapter 4.

The data set for this work consists of 413 primary and secondary cassiterite and stannite samples. Due to the fact that most of the ores are from historic mining districts, the majority of the samples are derived from different museum collections, private collectors and auctions.

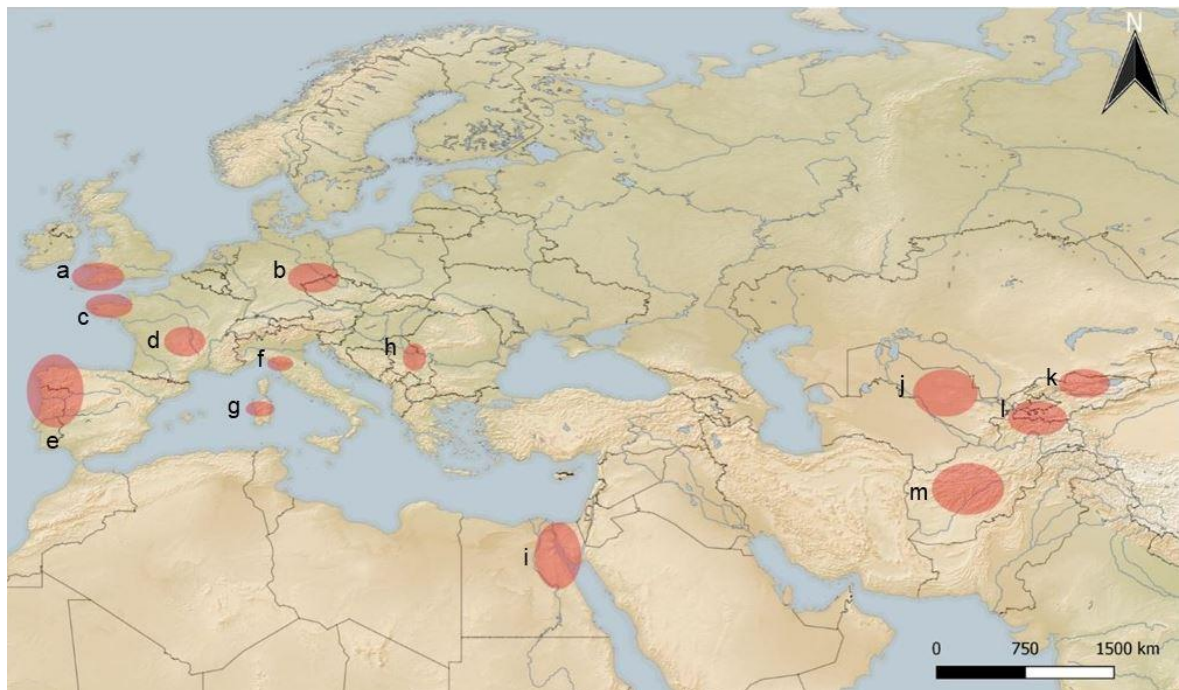


**Figure 3.1:** Sample locations: a) SW England, b) Saxonian-Bohemian province, c) Brittany, d) Massif Central, e) Iberian Peninsula, f) Monte Valerio, g) Sardinia, h) Serbia, i) Egypt, j) Uzbekistan, k) Kyrgyzstan, l) Tajikistan, m) Afghanistan. The map was generated with QGIS 2.18.16.

The 60 tin ore samples from SW England were taken from 30 different locations in Cornwall and Devon from five major granitic complexes (Land's End, Carnmenellis, St. Austell, Dartmoor,

Bodmin Moor) and from two smaller intrusions (St. Agnes, Cligga Head; Fig. 4.4). We determined the tin isotopic composition of ore samples (cassiterite and stannite) of different mineralization types. Thus, the most important magmatic and hydrothermal phases of the Cornubian Batholith are represented. The sample set consists of nine secondary ores (placer tin), four stannites and 47 cassiterite samples of hydrothermal greisen-, quartz-, and polymetallic veins. Six cassiterite samples were measured several times (MA-080518, MA-080869, MA-081297, MA-080881, MA-080510 and MA-080511), in order to estimate the variation of the isotopic composition within a sample (Table A1 Appendix). From Ireland five placer samples from the Mourne Mountains were processed. The Saxonian-Bohemian province is represented by 99 ore samples from deposits in Germany and the Czech Republic from 21 different localities in the Fichtelgebirge, Saxon-Bohemian Erzgebirge, Vogtland, and the Kaiserwald (Fig. 4.5). This dataset consists of 23 secondary and 76 primary ores (cassiterite of greisen and quartz vein type and stannite). Two samples were measured several times (FG-050688 and FG-050690). Haustein et al. (2010) already studied the isotopic composition of cassiterites from SW England and the Saxonian-Bohemian province. This sample material was taken from the mineralogical collection of the TU Bergakademie in Freiberg. We re-analysed several samples (Table A2 Appendix) of the previous study because the modern equipment at our institute provides more precise data. In addition, we extended the data set by analysing new samples from the collection in the Curt-Engelhorn-Zentrum Archäometrie, private collectors and museums, and the geological collection of the Universität Heidelberg.

The 66 cassiterite samples from Portugal were taken from 38 different areas within nine districts (Castelo Branco, Guarda, Portalegre, Porto, Viseu, Bragança, Vila Real, Aveiro, Viana do Castelo). The sample set consists of six secondary ores and 60 primary ores from quartz vein, pegmatite and greisen type mineralizations (Table 6.6). The samples were taken in 2016 from the mineralogical collection of the Technical Institute of the University of Lisbon (Fig. 3.2 a and b). The sample material we took at a field trip to several tin mining areas in Portugal in 2016 was not analysed due to the low tin content (Fig. 3.2 c-e).



**Figure 3.2:** Sampling campaign to the mineralogical collection of the Technical Institute of the University of Lisbon (a and b) in 2016, c: Cassiterite sampling during a field trip to several tin mining areas in Portugal in 2016, d and e: cassiterite panning from an altered material.

From Spain we analysed 49 primary and secondary cassiterite samples from 21 different localities in Salamanca, Ourense, La Coruña, Cáceres, Zamora and Pontevedra in northwestern and western Spain. The sample material consists of 47 primary ore samples from greisen type and quartz veins and two placer samples.

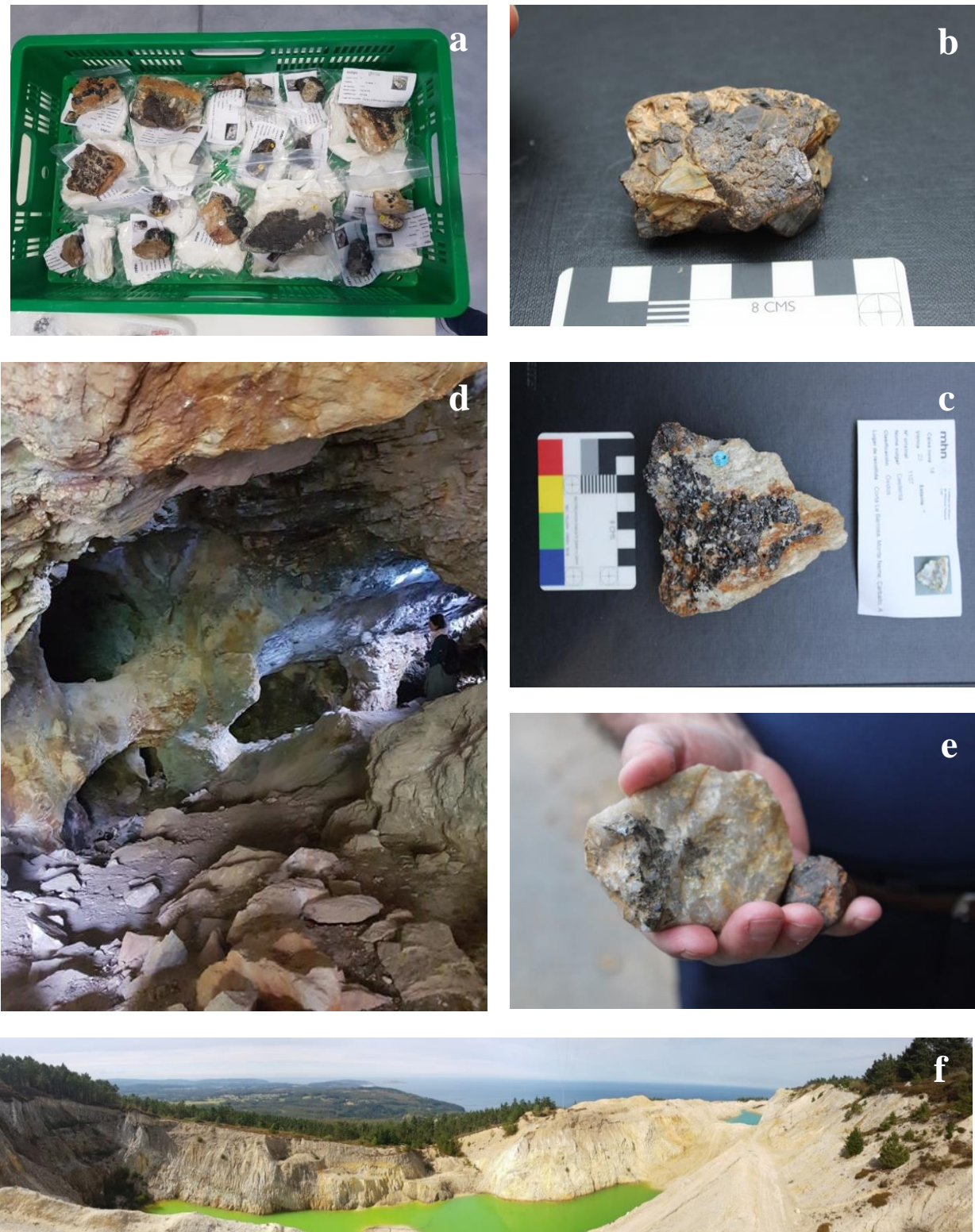


**Figure 3.3:** Sampling campaign to Galicia in 2017: a-c: cassiterite collection from the Natural History Museum in Santiago de Compostela; d: samples from old miners in a small village; e: Minas de Barxa, Ourense; f: Mina Monte Neme, La Coruña.

The samples were obtained from the TU Bergakademie Freiberg and private collectors. During the latest sampling campaign to Galicia, we could sample the cassiterite collection from the Natural History Museum in Santiago de Compostela (Fig. 3.3 a-d) and we visited several tin mines like the Mina Monte Neme (Fig. 3.3 f).

From France our collection encompasses 31 samples from the Massif Central (n=19) and Brittany (n=12) out of 14 different localities like Echassières, Montebras, Vienne and Vaulry in the Massif Central (Table 6.8). The data set consists of two placer samples and 29 primary cassiterite samples from the Bundesanstalt für Geowissenschaften und Rohstoffe in Hanover, the geological collection of the Universität Heidelberg, the CEZA collection and private collectors.

The sample collection of primary cassiterite from Italy, mostly of quartz vein type, consists of 6 samples from Sardinia and two samples from Monte Valerio and southeastern Europe is covered by two different placer samples from Bukulja (Serbia) from the collection of the Curt-Engelhorn-Zentrum Archäometrie.

From Central Asia we determined 80 samples of different tin mining areas around five countries. The data set of Tajikistan consists of 37 tin ore samples of primary material (stannite=10, cassiterite=11) and secondary tin (n=16) from seven different localities. From Uzbekistan we analysed 1 cassiterite sample (Lapas region) and from Kyrgyzstan we have 1 sample out of the Karasa mine. The 39 cassiterite samples from Afghanistan are all of primary ore type of 6 different mining areas or mines (Shar-e Bala-ye Khavat, Alingar/Alishang, Dara-i-Pech, Grangal mine, Paprok mine, Kunar mine). The 2 cassiterite samples from Kazakhstan are from Askaraly and Cherdoyek. In addition, we also analysed 12 samples from Wadi Muweilha, Igla, Nuweibi and Abu Dabbab in Egypt. The sample set consists of 5 placer samples and 7 primary cassiterite samples. All these cassiterite and stannite samples are from the collection of CEZA and several private collections and mineral dealers.

The following chapter describes the geological setting and the palaeogeography of the sample locations.

## 4. GEOLOGICAL SETTING

### 4.1 Introduction and Palaeogeography

The plate tectonic during the Late Palaeozoic was dominated by the supercontinents Gondwana and Gondwanian-derived microplates and Laurussia (Matte 2001). From this fusion the Variscan orogeny respectively the Variscan belt emerged (Fig. 4.1; Ballèvre et al. 2009) and together with Pangea these supercontinents dominated the global plate tectonic during this time (Ruban et al. 2007). Gondwana consisted of several present-day plates including Arabia, Africa, most of Antarctica and Australia, India, Madagascar and South America (Cocks 2001, Stampfli et al. 2001, Cocks and Torsvik 2002) and the sample locations of Egypt belonged to it. The supercontinent Laurussia consisted of Avalonia (SW England), Baltica (Serbia) and Laurentia (Fig. 4.1 and 4.2; McKerrow et al. 2000). The microcontinent Avalonia consists of the northern foreland of the Variscan belt from Ireland to north Germany (Unrug et al. 1999). Gondwana and Laurussia are kept separate by the Rheic Ocean up to the Mid-Carboniferous (325-310 Ma) until they collided during the Variscan orogeny to form the Pangea supercontinent (Fig. 4.1; Stampfli and Borel 2002; Torsvik and Cocks 2004). The Hun microcontinent was separated from Gondwana in the late Silurian and was attached to Laurussia in the Upper Carboniferous (Ruban et al. 2007). It hosted Armorica, Perunica and Austro-Alpine (Ruban et al. 2007) and also parts of Central Asia (Fig. 4.1).

The Armorica microplate comprises most of Western Europe south of the British Isles (Armorican Massif of Brittany) and part of northern Africa (Matte 2001). In Iberia, Armorica corresponds to the Ossa-Morena zone and in France, Armorica includes Central Brittany and the Normandy. In the Bohemian Massif, Armorica is in accordance with the Saxo-Thuringian and the Barrandian microplates. Torsvik (1998) defined Armorica as a small continental plate including France and northern Iberia only, whereas Matte (2001) has presented a new definition, that it was a small continental plate between the Beja-Lizard-Rheno-Hercynian suture and the Galicia-Southern Brittany-Southern Bohemian suture. However, all agree in locating Armorica close to Gondwana in

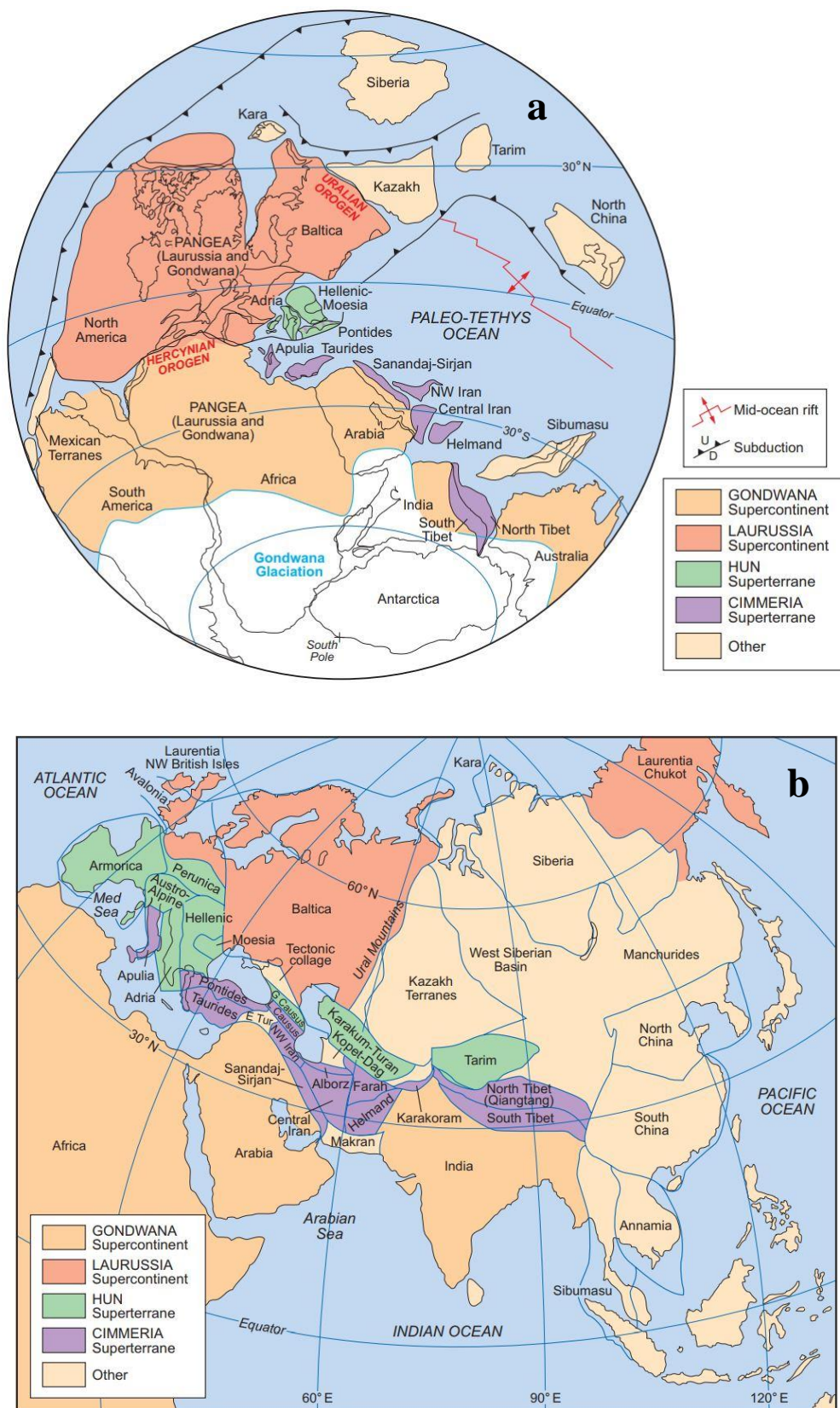


**Figure 4.1:** a: Late Carboniferous plate-tectonic reconstruction, b: Plates and terranes which are of relevance for this work (Ruban et al. 2007).

the Ordovician. It was attached to Avalonia in the early Devonian by the closure of the Rheic ocean (Fig. 4.2; Matte 2001).

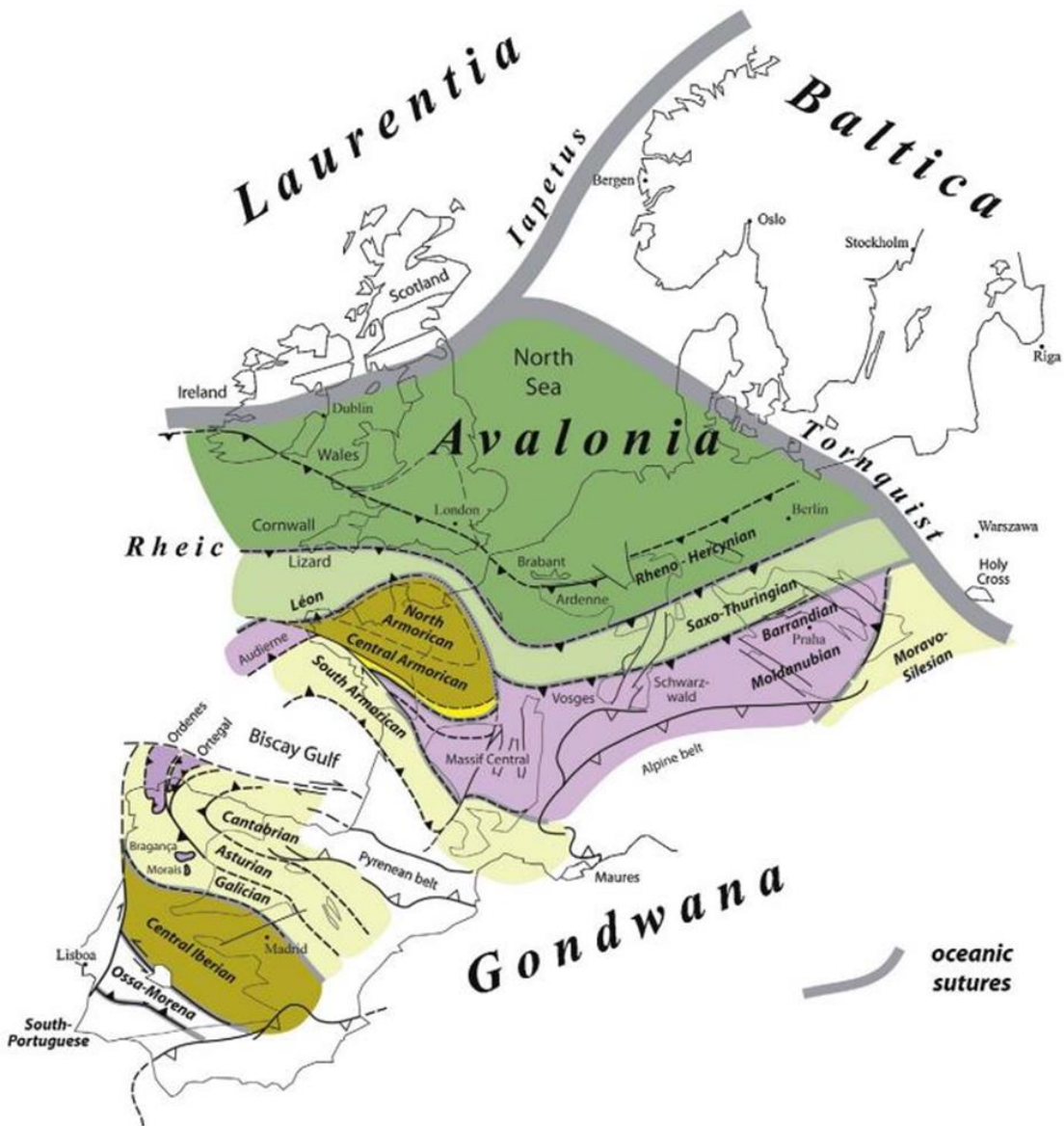


**Figure 4.2:** The west European units of the Variscan fold belt, where Palaeozoic rocks crop out (Ballèvre et al. 2009). The different colours highlight the potential correlations within the Variscan fold belt.

The Sn-rich provinces of the late Variscan granitoids of Europe have been extensively studied (Fig. 4.3; Jackson et al. 1989; Breiter et al. 1999; Štemprök and Blecha 2015; Chicharro et al. 2016)

because the mineral deposits can give insights into the relation between the tectonic setting, the magmatic evolution and the ore genesis in this period. In these areas with evidence of multiple phases of mineralization the tin deposits are accumulated in relatively small areas around geochemically “special” granites (e.g., granites that contain Sn-, W-, Li-, and F- and REE-bearing minerals). This specialisation of the tin ores has been explained by Sn enrichment which is controlled by physicochemical parameters during magmatic differentiation, evolution and emplacement (Chappel and White 2001; Heinrich 1990; Lehmann 1982, 1987, 1993).

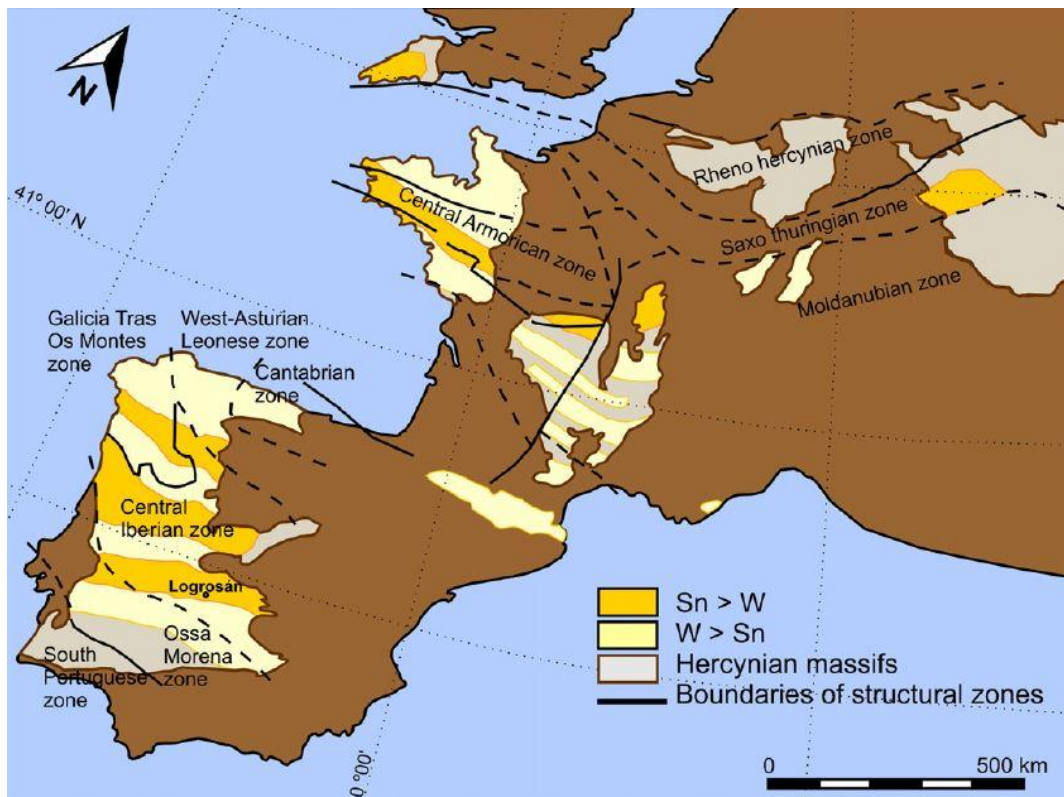


**Figure 4.3:** The metallogenic tin and tungsten province of the European Variscan belt (Chicharro et al. 2016).

The emplacement span of the granite bodies of all investigated areas is between 330-270 Ma during the Variscan orogeny (Carboniferous to Permian). All the areas described below form the Tethyan-Eurasian Metallogenic Belt (TEMB), which stretches from the western Mediterranean over the Alps through the Caucasus, across Central Asia and the Tibetan Plateau to Indonesia (Janković 1977).

## 4.2 Southwest England

The tectonic history of SW England is related to the closure of the Rheic Ocean in the Devonian to Carboniferous (Floyd et al. 1993; Leveridge and Hartley 2006; Shail and Leveridge 2009). The Variscan rocks are part of the European Rhenohercynian Zone (Nance et al. 2010). One of the largest granite bodies in Great Britain is the Cornubian batholith of the southwestern peninsula, which is exposed along a 250 km long, ENE-trending array of five major plutons (Dartmoor, Bodmin Moor, St. Austell, Carnmenellis, Land's End; Fig. 4.4) and numerous smaller satellite bodies (Exley and Stone 1982; Chen et al. 1993; Clark et al. 1993; Floyd et al. 1993; Duchoslav et al. 2017). All these granite bodies host tin mineralizations (Dines 1956; Floyd et al 1993; Chen et al. 1993).

It is assumed that the batholith was emplaced as a reaction of the subduction which was caused by the convergence of Laurasia and Africa (the assembly of Pangea), with similar granites and styles of mineralization as evident elsewhere along the orogenic belt, notably in Spain, Portugal, France, and the Czech Republic (Robb 2005). The early segregation of a voluminous aqueous phase from the magma is responsible for widespread alteration of pluton margins and much of the mineralization in the granite (Jackson et al. 1989).

The plutons of the batholith consist of different granite types, e.g., fine to coarse-grained biotite and biotite-muscovite granites, Li-mica granites to topaz granites formed by fractional crystallisation of crustal magmas (Müller et al. 2006; Duchoslav et al. 2017). The exposed part (more than 90%) is dominated by coarse-grained biotite-muscovite granites (Manning 1986; Štemprok 1995). The Li-mica granites occur as megacrystic and epigranular granites in the Tregonning/Godolphin pluton and in the western part of the St. Austell pluton (Stone and Exley 1985). All granites in the Cornubian batholith, and many similarly mineralized bodies elsewhere along the Variscan belt, are classified as S-type granites (Dabyshire and Shepherd 1985; Stone and Exley 1985; Štemprok 1995). U-Pb dating on monazite indicate emplacement ages of 300-275 Ma (Romer and Kroner 2015), the oldest pluton

---

being Carnmenellis, Bodmin, Isles of Scilly and the youngest ones being Dartmoor, St. Austell and Land's End granite.

In SW England most of the metal-containing deposits are of hydrothermal origin (Scrivener and Shepherd 1998). The tin occurs predominantly in steeply dipping lode veins with lengths of hundreds to thousands of meters (Yao et al. 2018) and consists of quartz-tourmaline-cassiterite (Jackson et al. 1989). Two main processes led to the formation of hydrothermal ore bodies, namely the separation of hydrous saline fluids directly from crystallising granitic magma and the later induction and circulation of external crustal fluids. These processes gave rise to two types of hydrothermal mineralizations (apart from pegmatites and skarns): quartz veins with cassiterite and/or wolframite with gangue material made of quartz, tourmaline, chlorite, fluorite and either siderite and calcite, and bodies of quartz and tourmaline with cassiterite, commonly also with haematite. The homogenization temperature for the veins is 275-400°C (Jackson et al. 1982). Magmatic-hydrothermal fluids are also accountable for the formation of endo- and exogranitic mineralized quartz veins (Robb 2005). Stanniferous sulfide-bearing chloritic lodes are less common and comprise cassiterite-chlorite assemblages with subsequent precipitation of pyrite-chalcopyrite-stannite-sphalerite (Briomley and Holl 1986) at 200-380°C (Jackson et al. 1982). The mineralization was emplaced at 2 to 5 km depth (Smith et al. 1996). A special characteristic of the Cornubian mineralizations is the occurrence of sheeted, greisen-bordered veins which generally represent the sites of favored Sn-W mineralization. These veins consist mainly of quartz and tourmaline with variable cassiterite and wolframite, and a greisen alteration comprising quartz, muscovite, Li-mica, and topaz. The systems capture a well-defined metallogenetic zoning or paragenetic sequence and extend for multiple kilometers out into the surrounding country rock (Robb 2005).

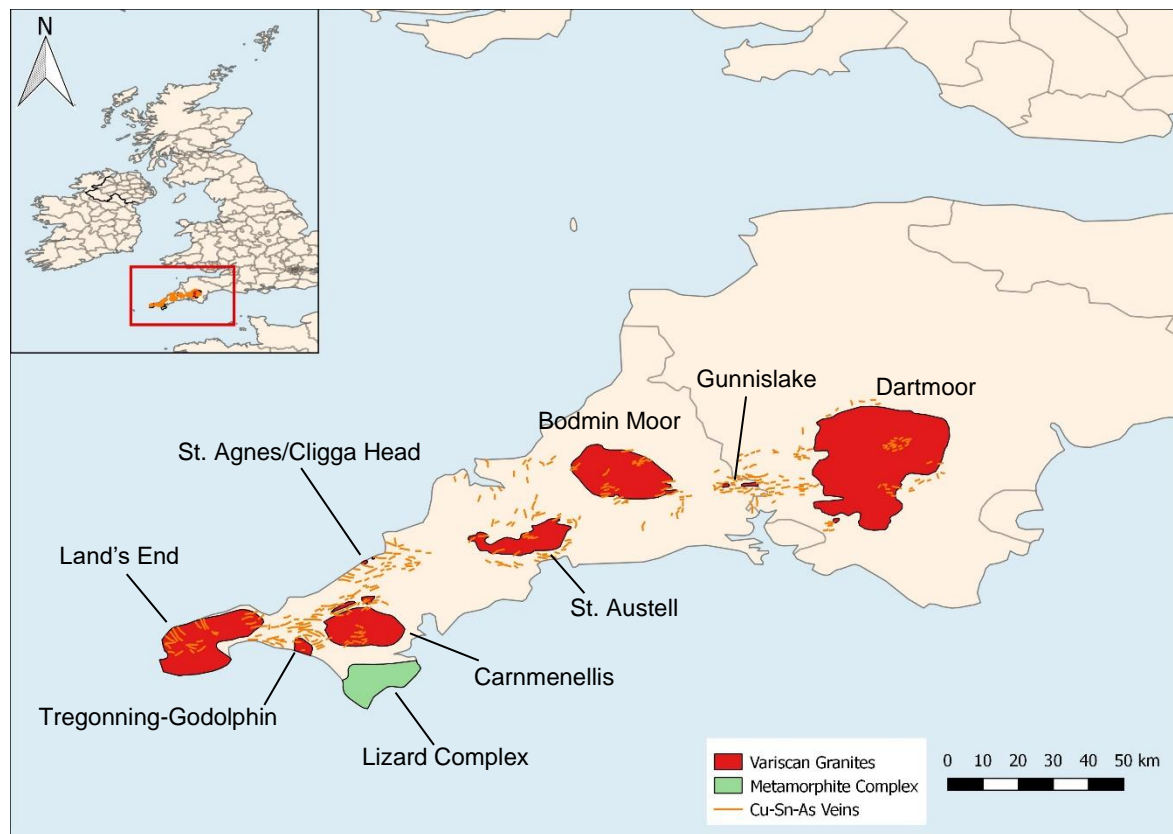


**Figure 4.4:** Simplified geological map of the Cornubian batholith showing the major granite intrusions (modified after Manning 1998; Haustein 2009). The map was generated with QGIS 2.18.16.

The formation of the hydrothermal veins or the hydrothermal overprint of the plutons can be divided into four stages: (i) tourmaline-bearing skarns, followed by (ii) tourmaline-bearing pegmatites, greisen, hydrothermal veins (greisen bordered), (iii) E-W striking polymetallic cassiterite-quartz veins with Cu-Zn-Pb-Fe-As sulfides and (iv) the latest formation of N-S to NW-SE striking Pb-Zn-Ag-U quartz-fluorite-barite-sulfide veins (Chesley et al. 1993; Duchoslav et al. 2017). Sn is also found in skarn and pegmatite type deposits. Placer deposits are associated with all granite plutons and are derived by the erosion of hydrothermal veins and granite bodies.

The mining activity in SW England can be traced back to the Bronze Age, however the climax was reached in the 19th century. The tin mining documentation spans 3500 years, even though the prehistoric evidence only comprises a few finds of slag (Penhallurick 1986; Tylecote et al. 1989), or smaller finds like a cassiterite pebble in Devon (Fox 1957). The remains of tin mining operations

(streaming, open pit, and underground mining) and tin smelting (medieval "blowing" houses, i.e. tin smelting furnaces) are archaeological evidence of tin mining in SW England (Tylecote et al. 1989). Until the 16<sup>th</sup> century, when the underground mining became more important, tin was only exploited by washing of streams or placer deposits (Hatcher 1973). Mainly Sn (2.5 million tons of cumulative metal production) and Cu (2 million tons of cumulative metal production) were mined, but other metals such as Fe, As, Pb, Zn, W, U, and Ag have also been extracted (Alderton 1993). In the early 20<sup>th</sup> century Cornwall's tin mining industry began to collapse, and in 1998 the last working tin mine South Crofty was finally closed (Selwood et al. 1998).

### **4.3 Saxonian-Bohemian province**

The Saxonian-Bohemian province (SBP; Western, Middle, and Eastern Erzgebirge, Kaiserwald, Fichtelgebirge, Vogtland; Fig. 4.5) lies in the northwestern part of the Bohemian massif, which represents the easternmost part of the European Variscan belt, at the contact of the Saxothuringian and Moldanubian Zones (Fig. 4.1 and 4.2; Franke 2001; Žák et al. 2014).

The Erzgebirge is part of the Saxothuringian zone of the mid-European Variscan belt, exposed for a length of 120 km and a width of 45 km. It consists of Precambrian and Early Palaeozoic rocks that were folded at 380 Ma. Several granite bodies of different compositions intruded between 325 and 300 Ma (Förster 1999). The Middle Erzgebirge Pluton (Fig. 4.5) is characterised by small granite outcrops which are largely concealed under the surface (Štemprok and Blecha 2015). According to Hösel et al. (1997) the Western and Middle plutons are interconnected in depth. The cassiterite bearing veins, greisen stringers and stockworks of quartz-muscovite greisens are associated with the granites in the Middle Erzgebirge (Štemprok and Blecha 2015).

The body of the Erzgebirge-Fichtelgebirge batholith (Štemprok 1995) with its three plutons (Western, Middle, Eastern pluton; Fig. 4.5; Štemprok and Blecha 2015) is built up of late Variscan

granites which were emplaced into Early Palaeozoic metamorphic basement (Thomas 1989; Thomas and Klemm 1997). The batholith comprises large masses of early biotitic granodiorite and monzogranite, followed by smaller bodies of topaz-biotite-muscovite syenogranites (Pohl 2011). Three major types of granites have been identified in the Saxonian-Bohemian province: late Variscan Li-mica granites (alkali feldspar granites), two-mica granites and biotite granites (Romer et al. 2007; Zhang et al. 2017). The granites of the Western Erzgebirge consist of Li-mica granites of S-type except for the Kirchberg granite which is an S-type biotite granite intrusion. The Middle Erzgebirge is built up of Li-mica granites of S-type as well (Zhang et al. 2017), whereas the Eastern Pluton of the Erzgebirge consists of A-type Li-mica granites and intermediate to felsic volcanic rocks (Štemprok 1995; Romer et al. 2007), which are part of a large volcano-plutonic caldera structure (Förster et al. 1999). However, the Niederbobritzsch and the Fláje intrusions in the Eastern Pluton (Fig. 4.6) are composed of biotite granite. In the Vogtland and the Fichtelgebirge the granites have been identified as two-mica S-type granites whereas the Kaiserwald consists of biotite granites of S-type compositon (Romer et al. 2007).

In the Saxonian-Bohemian province, just as for SW England described above (Chesley et al. 1993), four stages of mineralization are observed: (i) skarns, (ii) pegmatites and sheeted greisen veins, (iii) Sn-bearing polymetallic veins and (iv) late polymetallic sulphide veins (Tischendorf 1989). The ore deposits consist mostly of tin and tungsten and are related to the granite outcrops and their contacts, in which the types of cassiterite-wolframite greisen, skarn and vein deposits occur (Štemprok 1995; Štemprok and Blecha 2015). Pegmatites are of minor importance. Ores found in the batholith occur in stratiform greisen bodies within endogranitic lithium granites, as greisen veins within older granite, in hydrothermal cassiterite-quartz veins located in siliceous metamorphic country rocks and as small metasomatic replacement bodies in carbonates (Pohl 2011). The major tin deposits of the Erzgebirge (Sadisdorf, Ehrenfriedersdorf, Altenberg, Zinnwald, and Krupka) are associated with the highly fractionated Li-mica granites (Zhang et al. 2017). The granite dome of the Zinnwald (Cínovec) is the apical part of a pluton emplaced in the Late Carboniferous Altenberg-Teplice caldera in the eastern Erzgebirge (Fig. 4.5; Tomek et al. 2019). Cassiterite ore in the Zinnwald is hosted mostly by

greisen formed under lithostatic pressures, with less ore within similar veins that developed under hydrostatic conditions at a depth of 2 to 3 km and at temperatures between 335 to 410°C (Korges et al. 2018; Yao et al. 2018). In the tin deposits of the Erzgebirge the older pegmatitic-pneumatolytic parageneses are clearly distinguishable from the younger hydrothermal sulphide parageneses, unlike Cornwall where transitions can be found as well (Haustein 2009).

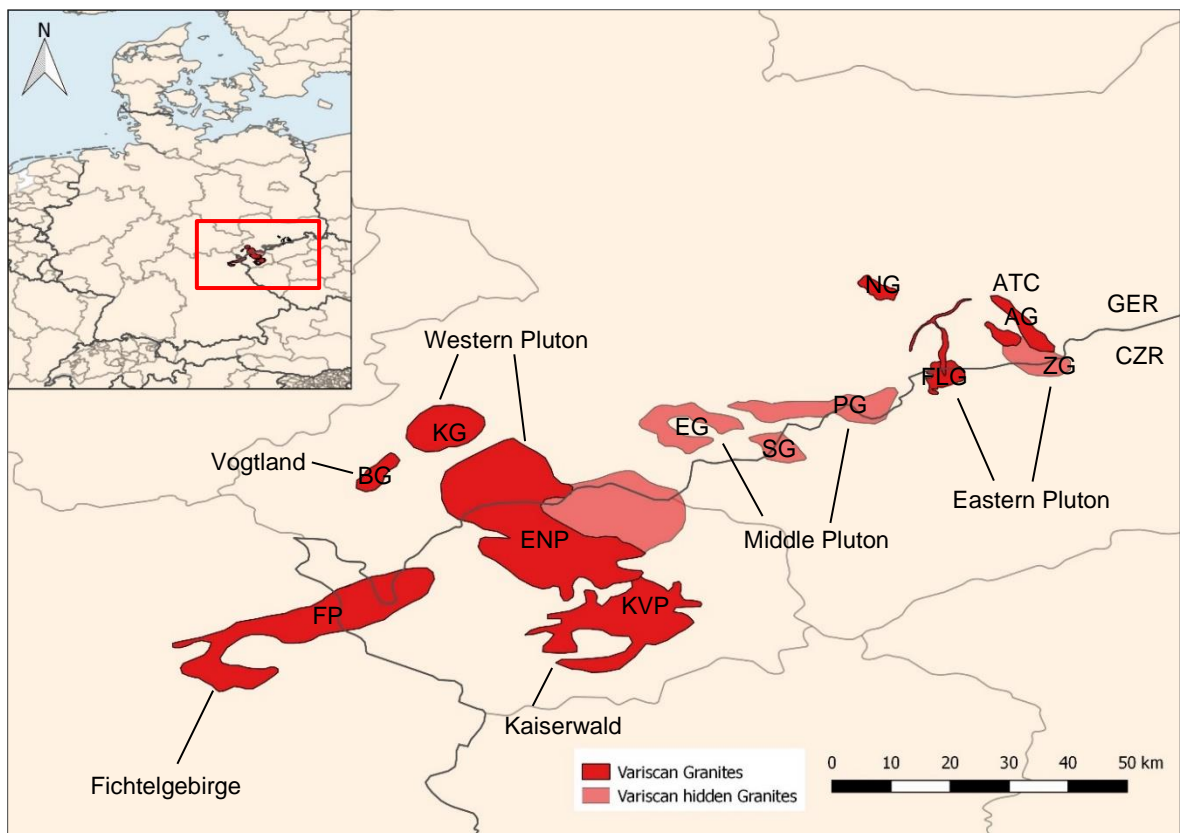


**Figure 4.5:** Simplified geological map of the Saxonian-Bohemian province showing the major granite intrusions (modified after Žák et al. 2014; Zahng et al. 2017; Štemprok and Blecha 2015). AG: Altenberg granite, ATC: Altenberg-Teplice caldera, BG: Bergen granite, EG: Ehrenfriedersdorf granite, ENP: Eibenstock-Nejdek pluton, FLP: Fláje granite, FP: Fichtelgebirge (Smrčiny) pluton, KG: Kirchberg granite, KVP: Karlov Vary pluton, NG: Niederbobritzsch granite, PG: Pobershau granite, SG: Satzung granite, ZG: Zinnwald granite (Fusán et al. 1967; Cháb et al. 2007; Romer et al. 2007; Žák et al. 2014; Štemprok and Blecha 2015). The map was generated with QGIS 2.18.16.

The dating of zircons, monazites and uraninites shows that the intrusion of the latest Variscan granites of the SBP lies in a relatively close interval of 327-290 Ma for all plutons (Breiter et al. 1999; Romer et al. 2007; Förster and Romer 2010; Štemprok and Blecha 2015). The granite

emplACEMENT interval is therefore wider than in SW England (Štemprok 1995). For U-Pb ages of hydrothermal cassiterite Zhang et al. (2017) determined the minimum age of regionally distributed alkali feldspar granite intrusions as a close period of  $330\text{--}326 \pm 3$  Ma.

The evidence for Bronze Age mining is only limited to a few settlements (Bouzek et al. 1989). According to Bartelheim and Niederschlag (1998) there is no evidence for tin extraction for the early Bronze Age in the Erzgebirge and there are no indications for any area in Europe of tin mining in the earliest phase of the Bronze Age so far. Since the 12th century tin mining in Ehrenfriedersdorf and Altenberg has been documented (Powell et al. 2019), and already Agricola (1556) mentioned the mining of placers. The archaeological evidence of prehistoric tin mining is only based on the spatial assignment of sources for placer tin to Early Bronze Age Únětice Culture and the Late Bronze Age Lusatian Culture settlements (Powell et al. 2019), but a current study by Tolksdorf et al. (2019) suggests placer mining at Altenberg in the early second millennium BC.

In the 16<sup>th</sup> century the Erzgebirge became the centre of ore mining in Central Europe. The tin ore mines of Altenberg and Ehrenfriedersdorf were operated until 1991 and a tin production of 300.000 t since historical record is documented for the Saxonian-Bohemian province, whereas the SW England tin province is much richer in tin with a production of 1.500.000 t (Štemprok 1995).

#### **4.4 Ireland**

The tectonic history of Ireland relates to the formation of the Irish and British Caledonides (Anderson et al. 2018). Ireland lies at the continental margin of Baltica, which was affected by this orogenesis.

This early Palaeozoic deformation formed a mountain range from northern America, across Ireland and Scotland up to Scandinavia with a main phase in the Silurian. The north-eastern part of Ireland comprises abundant Mesozoic and Cenozoic sequences (Anderson et al. 2018). The intrusive magmatism which lead to the formation of the Mourne Mountains in NE Ireland occurred through

most of the Palaeocene with a development of two other central igneous complexes between 65 and 57 Ma: Carlingford and Slieve Gullion (Cooper 2004; Cooper and Johnston 2004; Cooper et al. 2012; Anderson et al. 2016). The Mourne Mountains were formed between 57 and 55 Ma. U-Pb (SHRIMP) data yield ages of  $56.5 \pm 1.3$  Ma (Gamble et al. 1999).

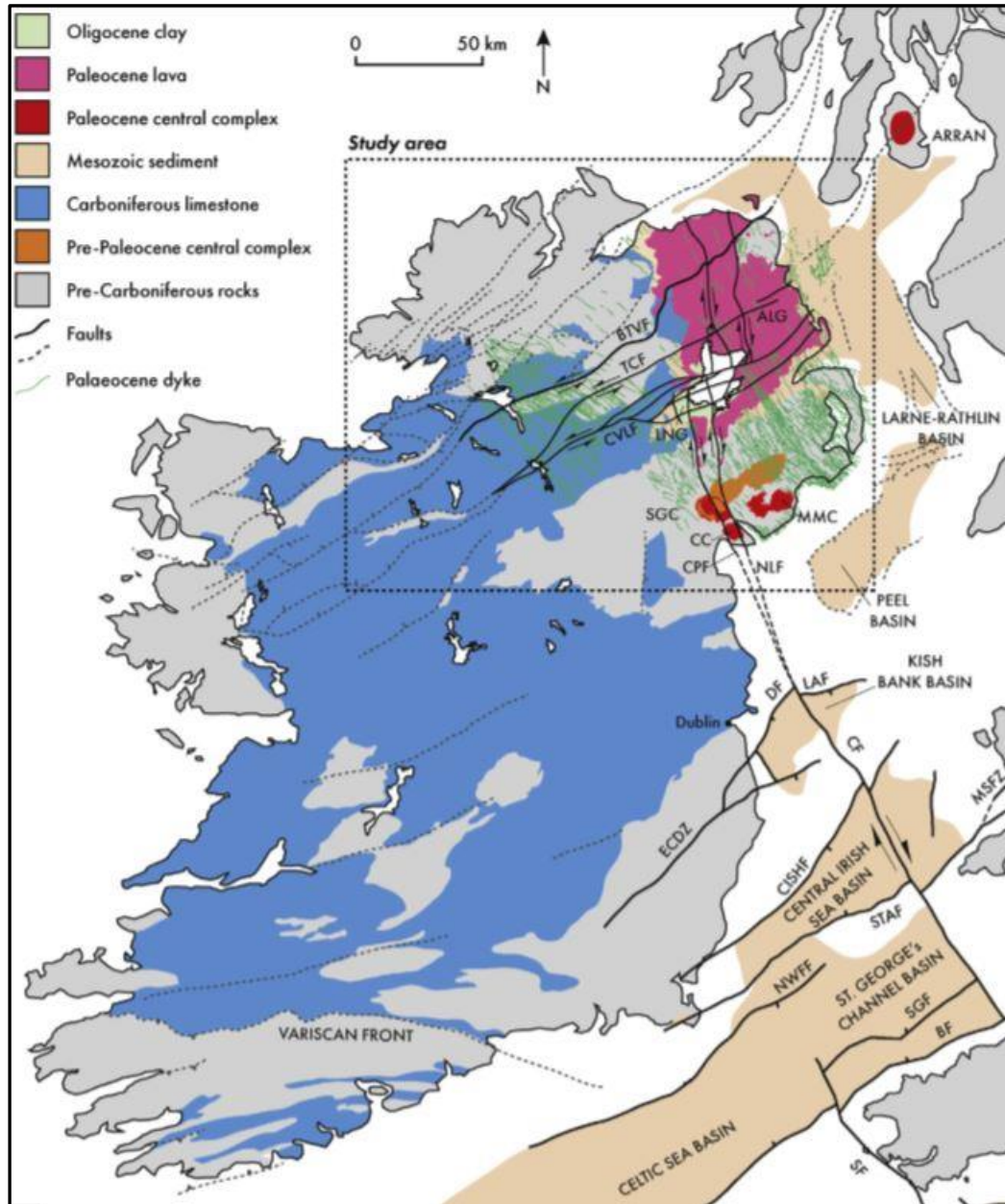


**Figure 4.6:** Map showing the simplified geology of Ireland (Anderson et al. 2018). ALG: Antrim Lava Group, CC: Carlingford Complex, LNG: Lough Neagh Group, MMC: Mourne Mountains Complex, SGC: Slieve Gullion Complex.

#### 4.5 Iberian Peninsula

The Iberian Variscan belt is a large segment of the European Variscan Fold Belt (Sant’Ovaia et al. 2010). Within the Variscan belt of the Iberian Peninsula the Iberian Massif represents the main outcrop (Catalan 2012). Most of the pre- and syn-Variscan outcrops in the Iberian Peninsula lie in the Iberian Massif. During the Variscan orogeny several autochthonous and allochthonous terranes that belonged to Gondwana and Laurussia accreted (García-Arias et al. 2018). Based on lithology, stratigraphy and the Variscan deformation style the Iberian Massif can be divided into six zones (Fig. 4.7 and 4.8; Shaw et al. 2012): The Cantabrian Zone (CZ), West Asturian-Leonese Zone (WALZ), Central Iberian Zone (CIZ), Galicia-Tras-Os-Montes Zone (GTMZ; Farias et al. 1987) and the Ossa-Morena Zone (OMZ), which belonged to Gondwana (Stampfli et al. 2011), and the South Portuguese Zone (SPZ; Julivert et al. 1972) which belonged to Avalonia (Stampfli et al. 2013).

The tectonic evolution of Western Europe resulted from the collision of Laurentia-Baltica and Gondwana through the Late Devonian and most of the Carboniferous (Ribeiro et al. 1990; Martínez Catalán et al. 2007; Martins et al. 2011). Therefore, three main phases of ductile deformation (D1, D2 and D3) have been described for NW of the Iberian Peninsula (Noronha et al. 1979). The D1 and D2 phases of deformation agree with the collision of the Variscan orogeny, while the D3 phase is Namurian-Westphalian in age (Martins et al. 2011).

In the innermost zone of the Iberian Variscan belt (CIZ) these deformation phases (D1, D2, D3) and a later extensional fragile phase (D4) led to the formation of the zone itself (Noronha et al. 1979; Dias et al. 1998; Martins et al. 2011). The Ossa-Morena Zone (OMZ) is a Gondwana zone with strong Cadomian imprint and the South Portuguese Zone (SPZ) consists of an external thrustbelt and foreland basins (Shaw et al. 2012). In the Ossa-Morena Zone two Cambrian magmatic pulses are known, namely an early rift- and a main rift-related event, which are related to the intra-continental rifting of North Gondwana, which probably resulted in the opening of the Rheic Ocean in the Lower Ordovician (Sánchez-García et al. 2014). The South Portuguese Zone is a thin-skinned thrust belt

with basic rocks, which are interpreted as a fragment of oceanic lithosphere, cropping out along the boundary between the South Portuguese and the Ossa-Morena Zone (Martínez Catalán et al. 2008).

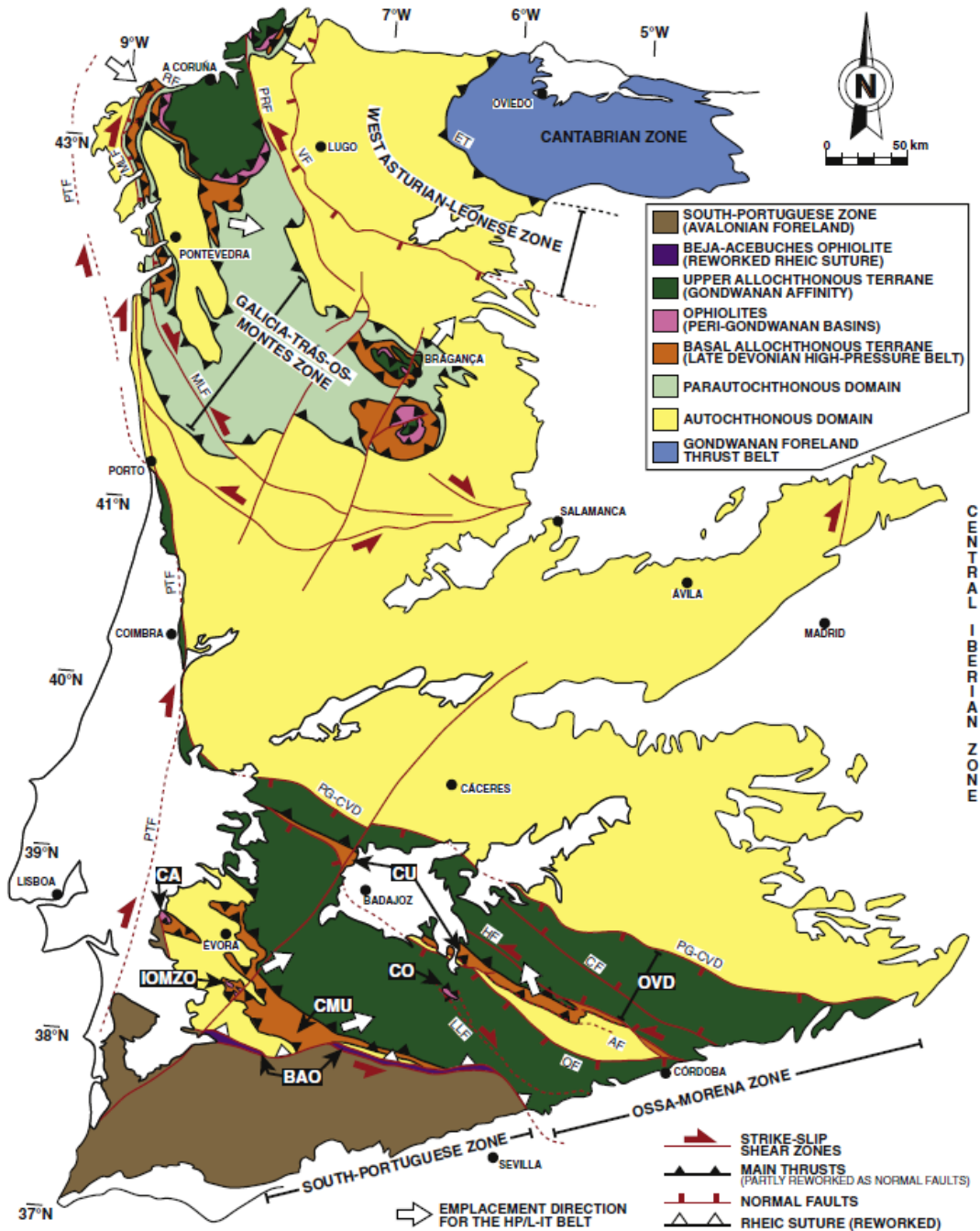


**Figure 4.7:** Geological map of the Iberian Peninsula with the different zones of the Iberian massif (Arenas et al. 2016).

The granite emplacement in Iberia is mainly synorogenic (syn-late and late to post-D3: 320-300 Ma), and late to post-orogenic (post-D3: 299-290 Ma; Dias et al. 2002; Martins et al. 2011). Between 300-

280 Ma a huge granite emplacement produced heat flow anomalies that drove long-lived systems of notable hydrothermal activity through the upper crust (Mateus and Noronha 2010). This caused a reactivation of D3 Variscan shear zones, which formed a complex network of pathways that activated fluid circulation. The fluids may have carried significant amounts of metals like Sn, W, Au, Cu, and Pb (Mateus and Noronha 2001, 2010). The CIZ is also defined by huge volumes of granitic rocks which make up about 60-70 % of the outcropping rocks (Azevedo and Valle Aguado 2006). For the Portuguese part of the CIZ isotopic ages for the syn-D3 granitoids are between 314-307 Ma, for example U-Pb ages of  $314 \pm 5$  Ma on zircon and monazite of the Maceira pluton, Casa Vasco pluton with  $311 \pm 1$  Ma, and the Junqueira pluton with an age of  $307.8 \pm 0.7$  Ma (Valle Aguado et al. 2005; Azevedo and Valle Aguado 2006). Therefore, two groups of ages for the syn-D3 or late to post-D3 interpreted granitoids can be determined: 320-310 Ma and 310-290 Ma (U-Pb ages on zircon and monazite; Ferreira et al. 1987; Azevedo and Valle Aguado 2006).

The CIZ as the inner and most stable part of the Hercynian Massif presents an important metallogenic province (Gumiel and Arribas 1990). The ore deposits in this zone have been classified according to the different tectonic cycles: the pre-Hercynian cycle, in which Hg and Sb mineralizations are related to pre-orogenic volcanism, and the Hercynian cycle in which the remaining metals occur as veins and lodes in extension fractures related to collisional magmatism (Gumiel and Arribas 1990). Most of the tin deposits in the Iberian Massif are associated with granitic rocks of northern and central Portugal and have several stages of mineralization. Cassiterite is commonly found in the oxide-silicate stage, which is early paragenetic and is often followed by a sulphide-rich one (Neiva 2008). The granites in Portugal consist of biotite granites and two-mica (biotite-muscovite) granites and they are related to the D3 deformation phase (Ferreira et al. 1987). The granitic rock areas have many hypothermal quartz veins containing cassiterite and wolframite, which surround and cut granites (Neiva 2008). Most of these deposits can be assigned to Hercynian S-type granites with high amounts of Sn (Neiva 2002). Overall, the veins can be associated with Hercynian muscovite-biotite granites (336-287 Ma), which are enriched in Sn, Rb, Cs, Li and F and usually contain 18 to 100 ppm Sn (Neiva 2008). In contrast to biotite, muscovite comprises a higher amount of total granite tin.

The Cantabrian Zone (CZ), the West Asturian-Leonese Zone (WALZ) in Spain and the Spanish parts of the Central Iberian Zone (CIZ) consist of a Neoproterozoic subduction related basin and a Palaeozoic passive margin (Fig. 4.7 and 4.8; Fernández-Suárez et al. 2000). In the CIZ (Julivert et al. 1972), two different tectonic domains are differentiated based on structural and geochemical criteria: the Domain of Recumbent Folds (Ollo de Sapo) and the SW Schist and Greywacke Domain (Martínez Catalán et al. 2004) or the Domain of vertical folds (northern and southern CIZ; Garcias-Arias et al. 2018).

The Galicia-Tras-Os-Montes Zone (GTMZ; Fig. 4.7) in northwestern Spain is built up of a metasedimentary unit (Schistose Domain) and other units which form allochthonous complexes thrusting over the metasedimentary unit (Gil Ibarguchi and Arenas 1990). The GTMZ is controlled by a thrust system which is linked to the emplacement of tectonic covers during the Variscan Orogeny (Farias et al. 2014). Two deformation events are responsible for the emplacement of these covers: D1, recumbent folds with axial plane cleavage and D2, recumbent folds with axial plane crenulation cleavage or shistosity (Fuertes-Fuente et al. 2000). During the last deformation event (D3) the tectonic evolution becomes a wrench regime which is characterised by folds and shear zones (Fuertes-Fuente et al. 2000). In NW Spain D3 granitoids are widespread and are differentiated into biotite granites of calc-alkaline character and peraluminous two-mica or muscovite granites (Barrera et al. 1989).

The Variscan belt of Europe comprises an important metallogenic province for tin, tungsten, gold and uranium and one can find numerous mineralizations, which are located in the inner part of the Iberian Variscan belt (Murciego et al. 1997). The cassiterite occurs in different types like disseminations in granites, pegmatites, aplites, quartz veins and stockworks, and in alluvial placers. Most of the deposits are found in the surroundings of major lineaments and fault zones (Carvalho 1977), which are located either inside or in the environment of granitic rocks (Murciego et al. 1997). Many Sn-W ores are associated with the Variscan granites and form the Iberian Sn-W metallogenic province (Neiva 1984). The D3 deformational phase commonly related to Sn-W, Au and U

mineralizations in the Iberian Massif (González-Clavijo et al. 1993; López-Moro et al. 2013; Pereira et al. 1993).

The Sn-Ta-Nb Penouta granite in northwestern Spain for example is a leucogranite which is a highly evolved rare-metal post-kinematic granite, which was mined from Roman times until 1985 (Llorens González et al. 2017). The mineralization mainly consists of cassiterite and columbite group minerals. Upward quartz veins and greisen zones containing coarse-grained cassiterite are associated with the wall rock. The Penouta granite is located in the eastern part of Ourense and it is one of the best known Variscan Sn-Ta-Nb deposits from the Iberian Massif. This Sn-Ta-Nb leucogranite intruded the formations of the Viana do Bolo Series and the Ollo de Sapo Formation after the main Variscan deformation phase. It is a fine- to medium-grained leucocratic granite mainly composed of quartz, muscovite, albite and K-feldspar (Llorens González et al. 2017).

Another huge ore deposit in Spain is the Logrosán Sn-(W) deposit, which is associated with an S-type granite and consists of endo- and exogranitic greisen type and quartz-cassiterite veins (Chicharro et al. 2016). The mineralization developed from 308-303 Ma and the emplacement of the Logrosán granite took place at 308 Ma. It yields a U-Pb TIMS age of  $307.88 \pm 0.86$  Ma (Chicharro et al. 2014). The granite is associated with the CIZ of the Iberian Massif and is characterised as an S-type, tin- and phosphorous-rich granite, which intruded into Neoproterozoic metasedimentary rocks (Chicharro et al. 2014). The southwesternmost extension of the Sn-W metallogenic province of the European Variscan belt is represented by this area (Martínez Catalán et al. 1996; Villaseca et al. 2014; Romer and Kroner 2015). The cassiterite from Logrosán is a very pure  $\text{SnO}_2$  phase with traces of Fe, Ti, Nb and Ta (Chicharro et al. 2016).

## 4.6 France

The Massif Central is associated with the north Gondwana margin that is the southern part of the Massif Armorica which emerged from six main tectonic-metamorphic events (Faure et al. 2009). The Massif Central of France (Fig. 4.8) is the largest area where Variscan metamorphic and plutonic rocks are exposed. Based on the petrological characteristics of the French Massif Central (FMC) it can be divided into four Gondwana-derived units: the Upper Gneiss Unit (UGU), the leptyno-amphibolitic complex (LAC), the Lower Gneiss Unit (LGU) and the parautochthon unit (PAU; Burg and Matte 1978; Matte 1986; Ledru et al. 1989; Lotout et al. 2017). The FMC holds a diversity of metallic deposits. Rare-metal and  $W \pm Sn$  type deposits are related to magmatic-hydrothermal processes in the FMC (Cuney et al. 2002). Two  $W \pm Sn$  mineralizing events took place at 323 and 310 Ma (Cuney et al. 2002). An event at around 305 Ma (Bouchot et al. 2000) marks a peak of metalliferous activity within the orogen with a development of ore deposits containing Au, As, Sb, W, Sn or rare-metals. During the final crystallisation of specialised magmas, the  $W \pm Sn$  and rare-metal deposits were emplaced in the upper crust. These granites, which are rich in these magmatophile elements, generated small hydrothermal cells (Bouchot et al. 2005).

The deposits in France show a large variety of mineralization style, including vein, stockwork, and greisen. In the northwestern part of the French Massif Central the  $W \pm Sn$  deposits mostly consist of quartz-tourmaline veins within and along the margins of batholiths and were formed from 321-309 Ma (Bouchot et al. 2005).

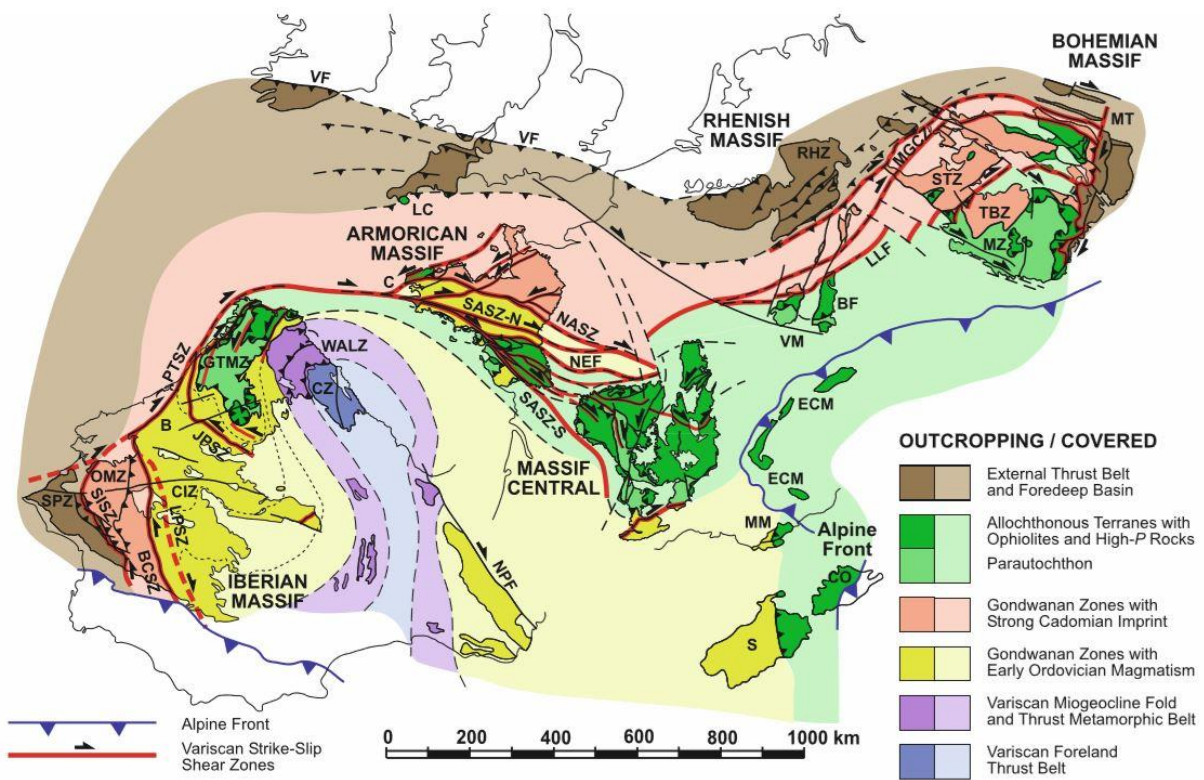


**Figure 4.8:** Zonation of the Variscan orogen (Martínez Catalan 2012). Important abbreviations: CIZ: Central Iberian Zone, CZ: Cantabrian Zone, GTMZ: Galicia-Tras-os-Montes Zone, LC: Lizard Complex, MGCZ: Mid-German Crystalline Zone, MT: Moldanubian thrust, MZ: Moldanubian Zone, OMZ: Ossa-Morena Zone, RHZ: Rheno-Hercynian Zone, S: Sardinia, SASZ: South Armorican shear Zone, SISZ: Southern Iberian shear Zone, SPZ: South Portuguese Zone, STZ: Saxo-Thuringian Zone, WALZ: West Asturian-Leonese Zone.

The W ± Sn deposits of the southwestern FMC consist of quartz-wolframite veins in schist next to large Namurian granite batholiths. U-Pb ages in monazite show ages of  $305 \pm 3$  Ma for the deposit formation (Lafon and Respaut 1986). The paragenetic sequences which were observed in the W ± Sn deposits indicate an early wolframite ± scheelite, cassiterite, and arsenopyrite stage. The ore deposits in the North with 310 Ma are older than those in the South with ages of 305-300 Ma (Bouchot et al. 2005), which indicates a metalliferous peak in this time span.

Most of the mineralizations in the FMC formed during the Neo-Variscan stage, from the Late Carboniferous to the Early Permian (Marignac and Cuney 1999). During this stage numerous hydrothermal deposits were formed, like high-T granite-centered tungsten deposits, which are mainly

associated with cordierite-bearing high-level intrusions of Namurian-Westphalian age, and rare-metal granites and the associated hydrothermal tin mineralizations resulting from fluid-induced low-degree partial melting of the middle crust. All the Sn, W, Au, Sb, most of the U, and a significant part of the Zn-Pb that are now found within the FMC were deposited during the Permo-Carboniferous (Marignac and Cuney 1999). The majority of the deposits are connected to hydrothermal activity, either in granite-centered systems or in fault zones. Marignac and Cuney (1999) postulate four ore forming stages for the FMC with Sn in stage 2 which represents the Namurian to Early Stephanian stage of granite-centered (Sn)-W-bearing quartz-vein systems, overlapping collision-related and extension-related magmatism. The French Massif Central was mined since the gallo-roman times for Au, Ag, Pb and Sn with a peak in the 18th and 19th century (Marignac and Cuney 1999).

A variety of different ore formation types can be found like in Vaulry W-Sn Intrabatholithic quartz veins, in Echassières W peribatholithic quartz veins and in Monatebras Sn-Be-Ta-Li breccia pipe dissemination in granite. The deposits in the FMC of Echassières, Montebras, and Vienne are characterised as rare-metal mineralizations (Ta, Nb, Be, Li) and occur as pegmatitic veins, small granitic stocks or rhyolitic dykes with a paragenesis of cassiterite, lepidolite, and topaz (Vallance et al. 2001). Hydrothermal alterations occur as lepidolite, amblygonite, apatite, and columbo-tantalite. The age of mineralization ( $^{40}\text{Ar}/^{39}\text{Ar}$  dating) is determined as  $309.9 \pm 0.7$  Ma on lepidolite for Montebras (Cuney et al. 1990, 1992, 2002) and  $309 \pm 1$  Ma on muscovite for Vienne (Raimbault et al. 1995; Raimbault 1998). The deposits of Vaulry and Vienne occur as wolframite-quartz stockwork hosted by a late Mississippian leucogranite at its eastern contact with Gueret-type granite (Vaulry), leucogranite enriched in rare metals and crosscut by wolframite  $\pm$  cassiterite quartz veins and greisen (Vienne). The paragenesis is barren quartz, quartz, wolframite, cassiterite, loellingite/arsenopyrite, pyrite, chalcopyrite, and traces of gold in late microfissures (Marignac and Cuney 1999). The hydrothermal alteration occurs as pseudo-greisen, muscovite, and biotite. The age of mineralization ( $^{40}\text{Ar}/^{39}\text{Ar}$  dating) is  $312.0 \pm 1.1$  Ma on muscovite for Vaulry (Vallance et al. 2000, 2001).

Brittany in France is represented by the Armorican Massif which is a part of the western European Variscan belt (Ballèvre et al. 2012). During the Variscan orogeny several magmatic events occurred in the Armorican Massif at around 316-300 Ma (Tartèse and Boulvais 2010). Chauris and Marcoux (1994) characterise the Variscan Armorican Massif as a metallogenic province with different types of mineral deposits. An important source of metals for systems like Sb ( $\pm$  Au) are the mafic and ultramafic bodies in the Armorican Massif (Pochon et al. 2017).

## 4.7 Italy

A fragment of the southern Variscan belt builds the Palaeozoic basement of Sardinia (Fig. 4.9; Carmignani et al. 1994; Rossi et al. 2009). The Corsica-Sardinia batholith, which was formed in the late Carboniferous-Permian along the northern Gondwana margin, can be divided in three magmatic sequences: (i) an early Mg-K calc-alkaline series comprising of monzo-diorites, monzonites, and subordinate ultrapotassic mafic rocks, (ii) a composite peraluminous calc- alkaline sequence composed of granodiorites and monzogranites with subordinate tholeiitic gabbros with an age of 322-285 Ma (Gaggero et al. 2007; Oggiano et al. 2007), and (iii) a sequence of metaluminous calc-alkaline to calcic gabbros and alkaline volcanic complexes ranging in composition from basalt to rhyolite. With the emplacement of alkaline granites and sub-volcanic complexes the magmatic activity ended between 290-260 Ma (Gaggero et al. 2007; Paquette et al. 2003). The Sardinian Palaeozoic basement and other southern European Variscan belts like the French Massif Central show structural, stratigraphical and geochemical similarities because of the formation during the same geodynamic event of Variscan continental collision (Boni et al. 2000).

The calc-alkaline granitoid bodies in Sardinia consist of quartz diorites, monzogranites, granodiorites and leucogranites and show radiometric ages of 307-275 Ma (Del Moro et al. 1975). Because of these ages and the lack of schistosity they were attributed to post-collisional Variscan stages (Late

Carboniferous to Permian). Boni et al. (1999) published ages of 330 Ma by  $^{40}\text{Ar}/^{39}\text{Ar}$  analysis, which were obtained for the granodiorites.

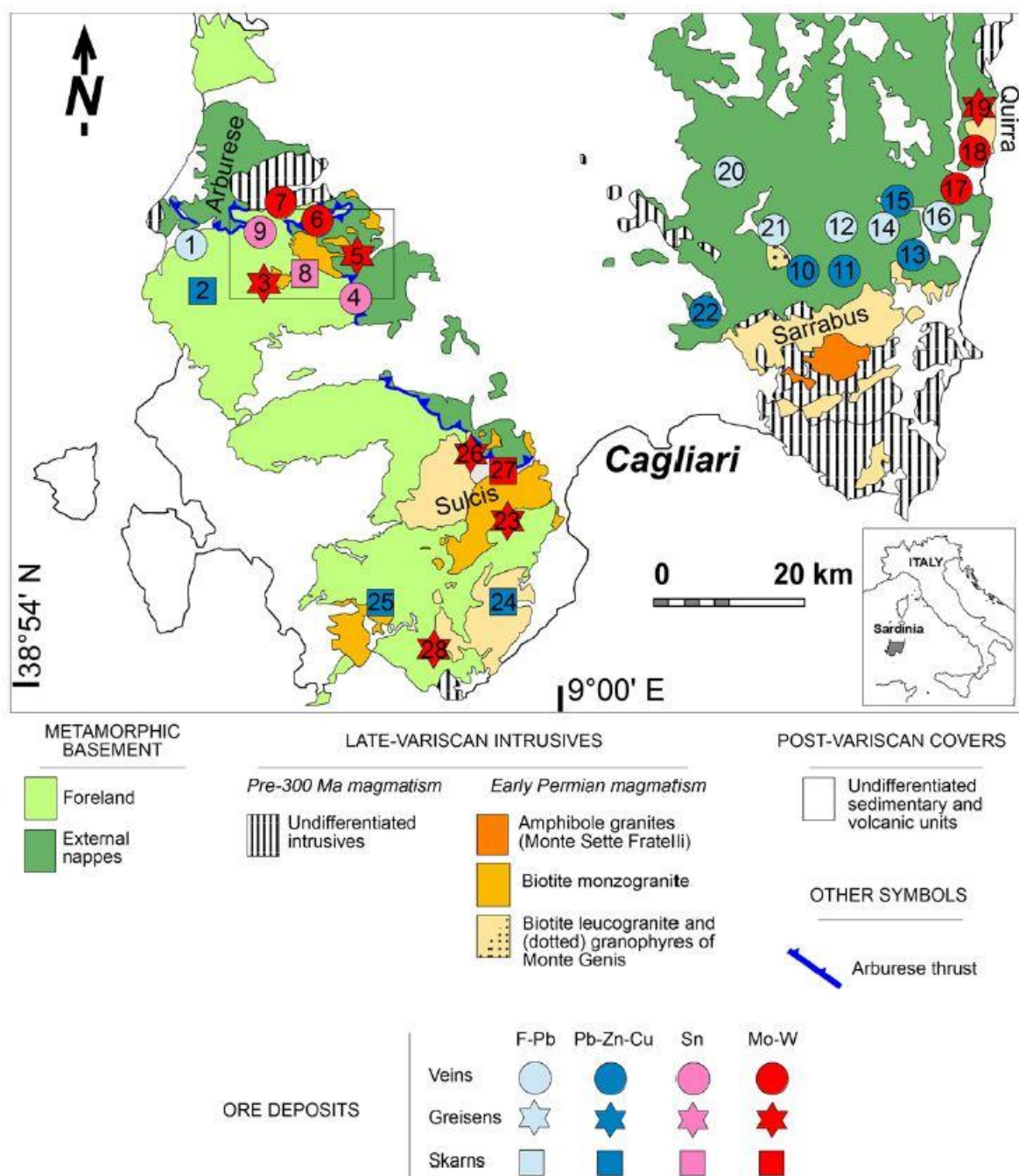


**Figure 4.9:** Late Variscan intrusives of Sardinia and the associated ore deposits. The Monte Linas pluton is marked with the black rectangle. Tin ore deposits: 4) Canale Serci, 8) Perda Niedda, 9) Perdu Cara (Naitza et al. 2017).

The oldest magmatic complexes in Sardinia date at 320-290 Ma and younger magmatic events took place at 290-270 Ma (Casini et al. 2015). The Corsica-Sardinia batholith is formed by the emplacement of a large number of calc-alkaline plutons (Carmignani et al. 1994; Casini et al. 2015). Most of our samples from Sardinia are from the Arbus pluton with an age of  $303.7 \pm 1.1$  Ma (Cuccuru et al. 2016). This pluton is associated with a large hydrothermal vein network. Sn and Mo mineralization can also be found around the Monte Linas pluton (Fig. 4.9), which was emplaced at 290 Ma (Naitza et al. 2017). Different types of Sn- and Mo-bearing ores are associated with this pluton and it is the only area in Sardinia that is associated to Sn mineralization (Naitza et al. 2017) which occur as vein and skarn-type mineralizations. The Sn-bearing ores are represented by Sn-As and Sn-Pb-Zn-Cu veins and skarn Fe-Zn-Sn ores. The low-fO<sub>2</sub> and high-chlorine solutions of the hydrothermal systems of this pluton lead to the mobilisation of Sn and changes in physicochemical conditions result in the deposition of cassiterite (Naitza et al. 2017). The emplacement time for the Monte Linas pluton is given by Re-Os ages of  $289 \pm 1$  Ma on molybdenite (Boni et al. 2003). In Monte Valerio in NE Italy a late Variscan tin province is associated with the granites of the Sardinian batholith.

## 4.8 Serbia

The Alpine-Balkan-Carpathian-Dinaride (ABCD) province is a metallogenic and geodynamic area and belongs to the Alpine-Himalayan orogenic system which resulted from the convergence of the African, Arabian, and Indian plates and their collision with Eurasia during the Cretaceous (Heinrich and Neubauer 2002). Calc-alkaline magmatism is associated with certain segments and extensive regional metamorphism in this system. A discontinuous distribution of ore deposits reflects the segmented geodynamic character of the orogen (Mitchell 1996; Jankovic 1997). The ABCD region comprises a few phases of ore formation which is a result of the complex geodynamic history (Heinrich and Neubauer 2002).

The petrogenesis of the Neogene S-type granites of Mt. Bukulja and Mt. Cer in the Dinarides of northern Serbia (Fig. 4.10; Karamata et al. 1992; Cvetković et al. 2007a; Koroneos et al. 2010) is associated with the Pannonian extension. The Mt. Cer intrusive with a K-Ar age at around 16 Ma for the S-Type two-mica granite (Koroneos et al. 2010) and the two-mica Mt. Bukulja intrusion with an age of 20-17 Ma (Cvetković et al. 2007b) correspond to the granitoides of the Dinarides. The emplacement of these two intrusions took place during the early stages of extension related to the formation of the Pannonian basin (Koroneos et al. 2010; Cvetković et al. 2007b). The early Miocene age and the association with core complex formation plead for S-type granites because of the location at the southern margin of the Pannonian basin. These granites are located in the backarc area of the subduction of the European lithosphere (Csontos 1995; Seghedi et al. 2004). A separate suture zone, the Sava Zone, runs along the eastern edge of the innermost Dinarides and it separates the Dinarides from the Carpatho-Balkan orogen (Schefer et al. 2011).

The Miocene granitoid pluton of Mt. Bukulja in central Serbia is situated in the southern Pannonian/northern Dinarides region (Cvetković et al. 2007a). Two series of granitoitic rocks crop out in the Pannonian-Carpathian-Dinaride area: granitoids in the Dinarides with Late Oligocene age which build the southern continuation of the Periadriatic calc-alkaline magmatism (von Blanckenburg and Davis 1995; Pamić 1993; Pamić and Balen 2001) and granitoids with Miocene age which are supposed to be related to the early extensional phases in the Pannonian-Carpathian basin (Karamata et al. 1990). The Miocene series consists of the Mt. Bukulja and Mt. Cer plutons in Serbia, some granitic bodies further north and the Mt. Pohorje granite in Slovenia (Cvetković et al. 2007a). The largest part of the Mt. Bukulja pluton comprises a medium-grained two-mica granite (Cvetković et al. 2007a), which is frequently cut by pegmatitic and aplitic veins. The western part of the Mt. Bukulja granitic body intrudes in the low-grade Devonian/Carboniferous schists of the Jadar Block (Fig. 4.10; Karamata et al. 1994).

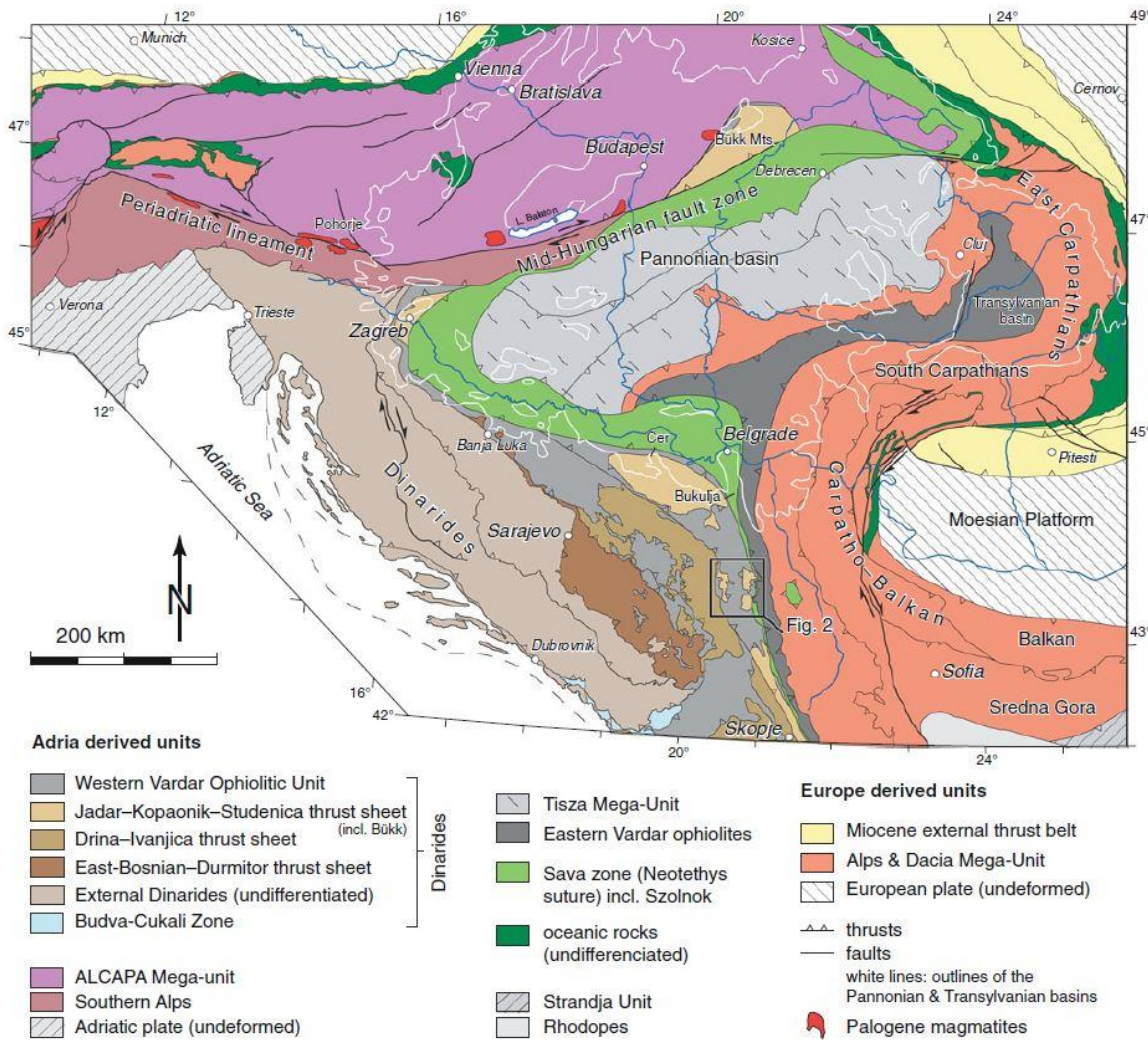


**Figure 4.10:** Tectonic map of the Dinarides of northern Serbia including the Alps and the Carpathians (Schefer et al. 2011).

The Alpine-Balkan-Carpathian-Dinaride (ABCD) belt played an important role in the history of European civilizations, from Greek and Roman civilizations until today because it is one of the world's oldest mining areas (Heinrich and Neubauer 2002). Durman (1997) studied the role of the Balkans tin economy in Europe's Bronze Age and identified several tin mineralization areas and associated placer deposits, and has suspected that they may have contributed to the region's supply of tin. For two sites (Mt Cer and Bukulja, Serbia), the exploitation potential has been confirmed, and these tin placer deposits are the richest, which can be enriched by panning to a percent-level of tin. For the other locations identified by Durman (1997) it is still unknown (Powell et al. 2020).

## 4.9 Egypt

The Arabian-Nubian Shield (ANS) is located at the northern part of the East African Orogen (Fig. 4.11), whose geological evolution took place during the Pan-African orogeny (Vail 1985). It is built up by Neoproterozoic juvenile arcs, depositional basins, voluminous granitoid and gabbroic intrusions and Neoproterozoic crust (Hamimi et al. 2014). Helba et al. (1997) and Abdalla et al. (2009) classified the Egyptian rare-metal granitoids as metaluminous alkali granites, peraluminous (Li-albite) granites and metasomatised mica-bearing granites. The northern part of the Arabian-Nubian Shield is characterised by rare-metal granitoids which intruded between 630 and 590 Ma with a calc-alkaline/peralkaline nature (Küster 2009; Meert 2003; Melcher et al. 2015; Moghazi et al. 2011). The Eastern Desert in Egypt which lies in the northern part of the ANS hosts several cassiterite and rare metal bearing granitoids, like the Igla and Abu Dabbab granites (Fig. 4.11), which are lithium albite associations (Abdalla et al. 2008) and occur as small stocks with dyke-like outcrops.

The Eastern Desert granitoids are classified as syn- to late-orogenic calc-alkaline diorites to granodiorites (670-590 Ma) and post-collisional alkali-feldspar granites (590-530 Ma; Sami et al. 2017), which are identified by the presence of snowball quartz and accessory minerals like columbite-tantalite, cassiterite, wolframite, beryll and traces of zircon crystals. Cassiterite in these granitoids occurs in the form of disseminated cassiterite, stockwork greisen veins and bodies, beryll, cassiterite and wolframite quartz veins and placer deposits (Abdalla et al. 2008).

Because of the occurrence of Ta, Na and Sn ore metals, some of the plutons in the Eastern Desert (e.g., Abu Dabbab and Nuweibi) may be of great metallogenic and economic importance (Melcher et al. 2015). The Central Eastern Desert hosts a variety of rare-metal bearing granitoids which are characterised as calc-alkaline/alkaline to peralkaline A-type and volatile-rich rocks (Sami et al. 2017). The granites host mineralization of metallic elements such as Nb, Ta, Sn, W, U, Th, Zr, REEs and minerals like columbite, tantalite, and cassiterite, which were formed by magmatic processes (Pollard 1995).

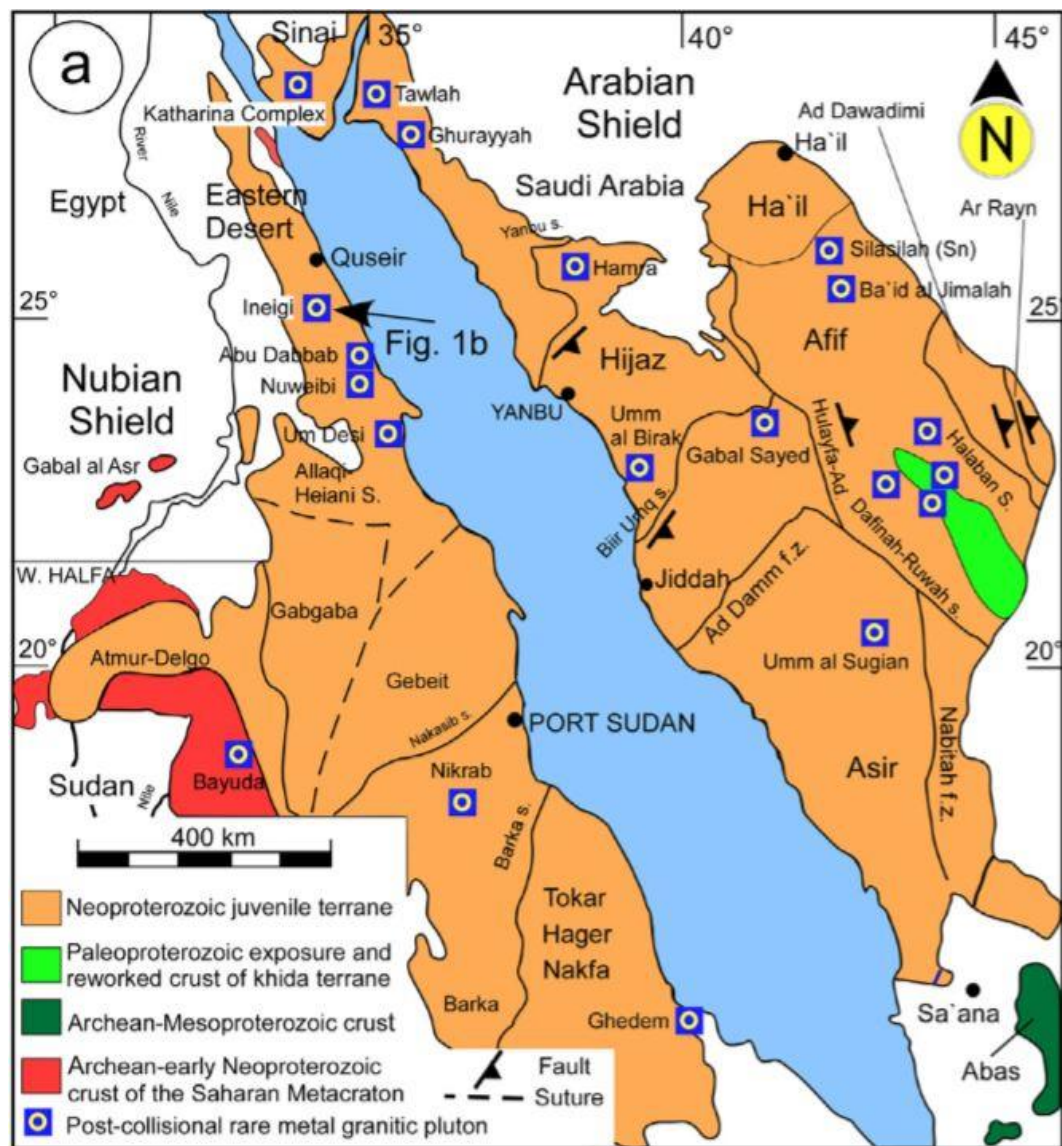


**Figure 4.11:** Arabian-Nubian Shield including the post-collisional rare-metal granitic plutons (ANS; Sami et al. 2017).

## 4.10 Central Asia

The Central Asian orogenic belt (CAOB; or Central Asian orogenic supercollage or the Altaids; Jahn 2004; Windley et al. 2007; Yakubchuck 2004; Wilhem et al. 2012) has experienced a long history of accretionary tectonics from the late Neoproterozoic to the Early Mesozoic (Sakura et al. 2017). The belt stretches from the Ural Mountains (Puchkov 1997) to the Pacific coast (Wilde et al. 2010), over the Siberian craton (Vernikovsky et al. 2004) to the main Altai suture, which extends from the Pacific margin to the southern Tien Shan in western China (Biske and Seltmann 2010) and from Uzbekistan to the Uralian Suture (Fig. 4.12; Alexeiev et al. 2009).

The CAOB emerged from 1000 to about 280 Ma (Coleman 1989; Khain et al. 2003; Kröner et al. 2007; Rytsk et al. 2007) by accretion of island arcs, ophiolites, oceanic islands, microcontinents and other geological structures (Windley et al. 2007). The accretion occurred during the Vendian-Ordovician when Baltica and Siberia were separated by a wide ocean. At the active margins of these two continents a vast accretionary collage was formed by accumulation of island arcs and Precambrian microcontinents (Windley et al. 2007). The Palaeozoic basis of Central Asia is built up of multiple blocks and terranes which are separated by huge sutures (Garner 2013). These are remains of Neoproterozoic to Mesozoic sedimentary basins, island arcs and terranes, which were formed by complex processes of subduction, collision, accretion and overthrusting (Yakubchuck et al. 2002; Seltmann and Porter 2005; Porter 2006). The CAOB is characterised by a huge spread of Palaeozoic and Mesozoic post-accretionary calcalkaline to alkaline to peralkaline granitic intrusions (Jahn et al. 2000a).

Most of the granitoid rocks are between 500-100 Ma in age, discerned with whole-rock Nd isotope signatures as summarized by Kovalenko et al. (1996) and Jahn et al. (2000 a, b, 2004). The granitoids show low Sr isotopic ratios, positive  $\varepsilon_{\text{Nd}}(T)$  values and young Sm-Nd model ages ( $T_{\text{DM}}$ ) of 300-1200 Ma. This is in strong contrast to the granitoids in the European Caledonides and Hercynides of

the same age, where the data show their juvenile character and indicate their origin from source rocks or magmas from the upper mantle (Jahn et al. 2000a).

The tin mineralization in many tin ore provinces in Central Asia is closely related to silver mineralization represented by quartz-carbonate-sulfide vein and stockwork zones (Borisenco et al. 2006).

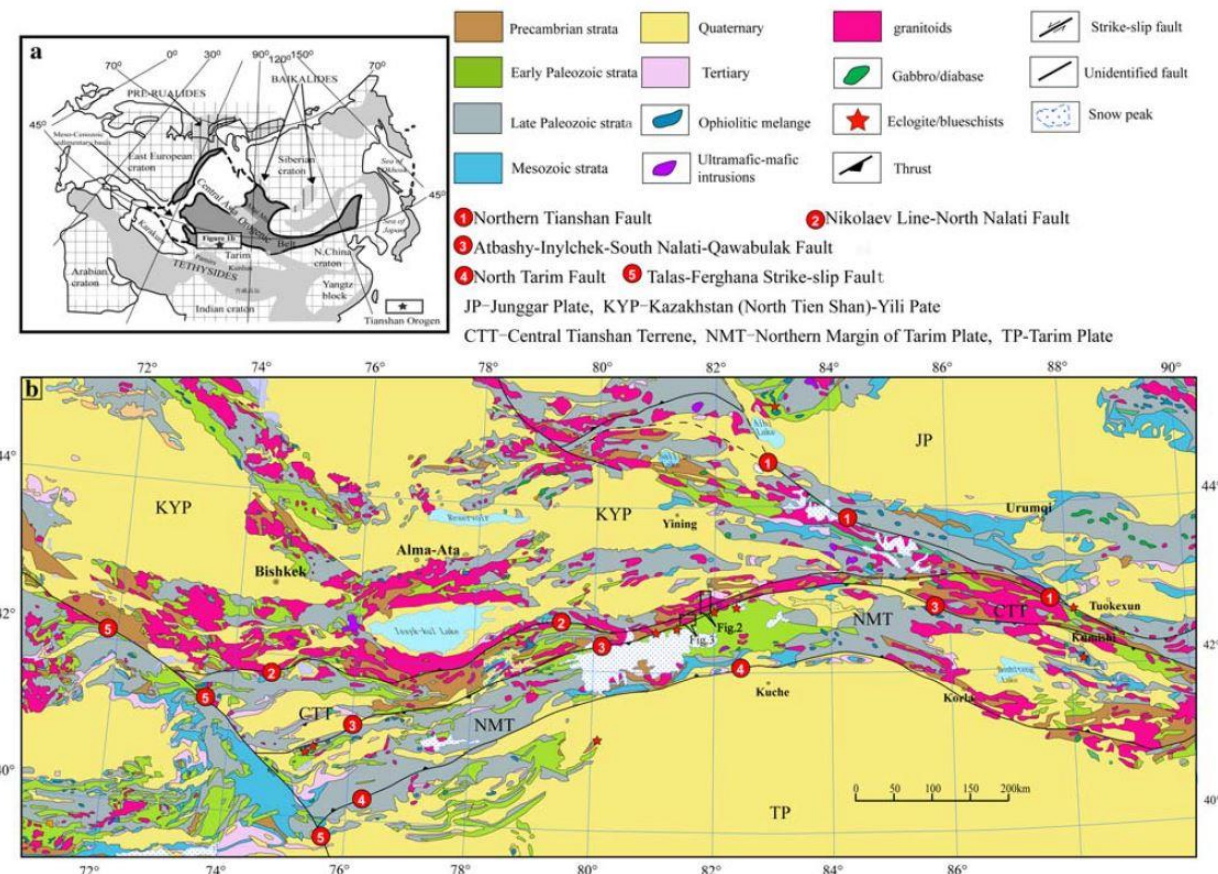


**Figure 4.12:** a) Geological sketch map of the Central Asian orogenic belt and b) of the South Tianshan orogen and adjacent region (Gao et al. 2009).

#### 4.10.1 Kazakhstan

The region of northern, northeastern and central Kazakhstan comprises Precambrian microcontinental blocks and several early to middle Palaeozoic arc terranes, which host major sulfide

ore deposits (Kröner et al. 2007). Two main ideas for the time of formation of the Kazakhstan Continent have emerged: either it was created by middle to late Palaeozoic thrust duplication and bending of several island arcs that originated in the Baltica and Siberia continents (Şengör and Natal' in 1996; Yakubchuck 2004) or the Kazakhstan Continent was formed by merging of island arcs and microcontinents which came from eastern Gondwana and the resulting continent was then bent into an orocline in the Late Palaeozoic (Windley et al. 2007; Abrajevitch et al. 2008; Alexeiev et al. 2010; Biske and Seltmann 2010). The Kazakhstan arc chain passed multiple subductions through the formation of the Central Asian orogenic Belt (Xiao and Santosh 2014). Several microcontinents in Kazakhstan are characterised by a Paleoproterozoic basement with a Neoproterozoic to Early Palaeozoic cover (Windley et al. 2007).

#### **4.10.2 Uzbekistan and Tajikistan (Zeravshan valley)**

The Zeravshan valley in Uzbekistan and Tajikistan forms the southwestern edge of the Central Asian orogenic Belt and hosts numerous tin mines like the Lapas tin mine in Uzbekistan. Tajikistan is rich in mineral resources with more than 400 different mineral deposits (Sun et al. 2017). The main tin ore deposits are found in the Zeravshan-Hisar geological and structural zone, in Central and South Pamir of Tajikistan. The largest tin deposit in this area is Mušhiston, where tin mainly occurs in mushistonite, cassiterite and stannite with a total grade of 0.65 % Sn (Sun et al. 2017). Because of hydrothermal redistribution rich oxidic ores can be found. Besides malachite and cassiterite, mushistonite ( $\text{CuSn}(\text{OH})_6$ ), which is named after the deposit, occurs here (Sun et al. 2017). A belt of tin and tungsten mineralizations, which extends from the north of Buchara (Uzbekistan) above the Zirabulak-Mountains and Samarkand to Central-Tajikistan, hosts the tin deposits of the Zeravshan valley (Garner 2015). The number and density of sites found in the valley of Karnab, Lapas, Changali (Uzbekistan) and Mušhiston (Tajikistan) suggests ancient tin mining (Sverchkov 2009).

#### **4.10.3 Kyrgyzstan**

In eastern Kyrgyzstan the Uchkoshkon tin granites of the Saryjaz ore district are rich in Sn and volatile elements. The characteristics of the Saryjaz granites increase their ore-bearing potential, which is similar to the Sn-bearing granites of Cornwall and the Erzgebirge (Solomovich et al. 2012). The Saryjaz ore district lies in the eastern part of the Koksahl segment of the South Tien Shan collisional belt. This segment is built up of overthickened continental crust, which arises from the subduction of the Tarim continental crust underneath the Kazakh continent (Biske 1996; Chen et al. 1999). The Kokshal segment is characterised by significant Sn-W deposits (Solomovich et al. 2012). In this segment several Sn deposits like the Uchkoshkon Sn deposit and other hydrothermal and skarn Sn deposits are related to the Uchkoshkon granites. This large biotite granite pluton ( $260 \text{ km}^2$ ) intrudes the Kokshal thrust package and the Uchkoshkon tin deposit occurs in the exocontact zone in the Northwest of this pluton (Solomovich et al. 2012). Rb-Sr isochron ages of  $273 \pm 9 \text{ Ma}$  (Solomovich and Trifonov 2002) and U-Pb zircon TIMS ages of  $279 \pm 8 \text{ Ma}$  (Konopelko et al. 2007) points to an Early Permian age for the granite. Some of the geochemical specialities of the Uchkoshkon granite like an increased K/Na ratio and the reduced nature of the parental magma are of advantage for cassiterite solubility in a magmatic aqueous phase (Taylor and Wall 1993). The Uchkoshkon deposit is primarily a Sn-deposit with minor W and Mo. The ore mineralization was formed in two stages: greisen and main stage hydrothermal lode mineralization, where the two occur together, and the main stage lodes, which post-date the greisen veins (Trifonov et al. 1984).

#### **4.10.4 Afghanistan**

The geology of northern Afghanistan is practically unknown because of the mostly Russian and restricted published literature (Brookfield and Hashmat 2001). The North Afghan platform and adjacent areas are built up of a pre-Jurassic basement of pre-Carboniferous to Triassic rocks which

are overlain by Jurassic to recent sedimentary rocks (Brookfield and Hashmat 2001). There are two main mineralization zones in Afghanistan: south of Kandahar to the province of Badachšan and one further west in the Sistān area which extends to the north in the surroundings of Herat. The cassiterite is often associated with other ores like copper, lead, gold and chlorite (Stech and Pigott 1986). The tin ores extend from the Hissar Mountains and the Pamir via the Zeravšan valley and Tian Shan, continue to the northeast to Kyrgyzstan, the Atasu Mountains (Central Kazakhstan) up to the Kalba-Narym Massif and the Altai (Eastern Kazakhstan). Several tin mines with Bronze Age tin extraction are known from these areas (Kuz'mina 1991).

## 5. METHODOLOGY

The isotopic composition of tin was determined with a multi-collector mass spectrometer with inductively coupled plasma (MC-ICP-MS; Neptune Plus, Thermo Fisher Scientific). All the sample dissolution and ion exchange chemistry procedures and measurements were performed at the Curt-Engelhorn-Zentrum Archäometrie in Mannheim, Germany.

### 5.1 Materials and reagents

The digestion and separation procedures were performed at the Curt-Engelhorn-Zentrum Archäometrie in Mannheim in a Class 100 clean laboratory. All necessary acid solutions ( $\text{HNO}_3$ ,  $\text{HCl}$  and  $\text{HF}$ ) were purified by sub-boiling distillation in quartz glass and Teflon stills. The ultrapure water was obtained from a SG-Ultra Clear TWF UV purification system (resistivity  $\leq 18.2 \text{ M}\Omega$ ). The Savillex® pressure vials, which were needed for the sample digestion, were previously cleaned with p.A.  $\text{HCl}$  and afterwards filled with distilled  $\text{HCl}$  and rinsed with ultrapure water. The columns used for Sn separation have a resin reservoir of 0.5 ml and a solution reservoir of 4 ml. For the separation of Sn from the samples the anion-exchanger TRU Resin (TRU-B50-S, particle size: 50-100  $\mu\text{m}$ , Eichrom Technologies, Inc., Lisle, Ireland) was used (Yi et al. 1995; Haustein et al. 2010; Balliani et al. 2013; Yamazaki et al. 2013; Brügmann et al. 2017b) and loaded into the columns with frits of polypropylene. Brügmann et al. (2017b) prepared an in-house standard (PSn) from an ultraclean tin metal (Puratronic, Batch W14222, Johnson Matthey) by desolving it in  $\text{HCl}$ . This tin metal as an in-house standard was used by several studies before (Yi et al. 1999; Gillis et al. 2001; Clayton et al. 2002; Nowell et al. 2002; Gillis and Clayton 2008; Haustein et al. 2010). All Sn isotope ratios presented here are reported in delta notation relative to this in-house standard.

## 5.2 Sample preparation and purification

The cassiterite whole rock and crystal samples, which were not yet present in powder form like the collection of the CEZA, were first crushed and the cassiterite was handpicked from the rest of the material under a microscope. Unidentified pieces were tested with energy-dispersive X-ray fluorescence and the samples were finally ground to powder for further treatment.

In order to measure the isotope composition of cassiterite and stannite by ICP-MS, the samples must be transferred into acid dissolvable metal by reducing it at high temperatures (McNaughton and Rosman 1991; Clayton et al. 2002; Nowell et al 2002; Brügmann et al. 2017b; Berger et al. 2018). The powder samples were reduced with two different methods: with potassium cyanide (KCN) and with cementation (reduction with copper). In the beginning a large number of the samples were reduced with Cu until it turned out that the reduction of cassiterite with KCN and the reduction of stannite with Cu is more effective and reliable (Berger et al. 2018). The reduction experiments were performed in polished graphite plates with small holes, into which the sample material of 10 mg SnO<sub>2</sub> and the Cu respectively KCN were loaded. The graphite plates were put into corundum crucibles, embedded in active carbon and then heated for several hours in a muffle furnace. After reduction, the tin and bronze (Cu-reduced tin) beads were dissolved overnight with HCl and H<sub>2</sub>O<sub>2</sub>. For Sn isotopic analysis the tin metal solution was measured directly after dilution with H<sub>2</sub>O and HNO<sub>3</sub>. The solution of the bronze alloy was run through an exchange chromatography column containing TRU Spec resin in order to isolate Sn from the matrix. Previous studies have also successfully tested this resin (Yi et al. 1995; Haustein et al. 2010; Balliani et al. 2013; Yamazaki et al. 2013; Brügmann et al. 2017b). This procedure minimizes matrix effects and avoids isobaric interferences during isotope measurements (Brügmann et al. 2017b) because the bronze solutions can contain more than 80 wt.% Cu as well as variable concentrations of Fe, Zn, Cd, As, Sb, Te and Pb. The columns were cleaned with 2 M HCl and filled with 0.1 ml of a prefilter and 0.5 ml of TRU-Spec resin. Before use, the resin was rinsed with Milli-Q water to settle down. Prior to the elution,

the resin was cleaned with 0.4 M HNO<sub>3</sub> and H<sub>2</sub>O. For conditioning the resin was rinsed with 3 M HCl. In the next step the sample solution with a total amount of 20 µg of Sn was pipetted onto the column. After eluting the irrelevant Cu fraction with 3 ml of 2 M HCl and 6 ml of 0.25 M HCl, Sn was eluted with 10 ml of 0.4 M HNO<sub>3</sub>. In addition, 10 µl concentrated HF was added to the Sn fraction to avoid precipitation of SnO<sub>2</sub>. Brügmann et al. (2017b) reported a recovery rate for the separation procedure for Sn of 100 ± 4 %, determined with the BAM 211 and IARM-91D reference materials. This recovery also agrees with previous studies of Yi et al. (1995), Haustein et al. (2010), Balliani et al. (2013) and Yamazaki et al. (2013). Subsequently 2.7 ml Sn fraction was transferred to a solution for measuring with a total amount of 9 ml by the addition of 6.21 ml 0.4 M HNO<sub>3</sub> and doping of 0.09 ml Sb for mass bias correction to obtain 60 µg/ml Sn.

### 5.3 MC-ICP-MS/Stable isotopy of Sn

For measuring isotope abundances mass spectromic methods are most effective (Hoefs 1997). A mass spectrometer separates charged atoms and molecules based on their masses according to their movements in magnetic and/or electronic fields. Therefore, the isotopes are diverted from their flight path to different degrees depending on their mass and charge. In principle, a mass spectrometer can be divided into four different parts: the inlet system, the ion source, the mass analyser, and the ion detector (Hoefs 1997). The ion beams emerging from the ion source are separated by their mass/charge (m/e) ratio in the mass analyser.

The tin isotopic measurements were performed with a multi-collector mass spectrometer (Thermo Fisher Scientific, Neptune Plus MC-ICP-MS) with excitation by an inductively-coupled plasma, which is equipped with nine Faraday cups. The arrangement of the faraday cups and other instrument settings are summarized in table 5.1. Tin has ten isotopes covering a mass range of 12 amu between <sup>112</sup>Sn and <sup>124</sup>Sn, but only the seven high-mass stable tin isotopes (<sup>116</sup>Sn, <sup>117</sup>Sn, <sup>118</sup>Sn, <sup>119</sup>Sn, <sup>120</sup>Sn, <sup>122</sup>Sn and <sup>124</sup>Sn) were measured. The isotopes <sup>112</sup>Sn, <sup>114</sup>Sn and <sup>115</sup>Sn were not measured due to their very

low abundances (< 1%), which would require highly concentrated measuring solutions to achieve adequate analytical precision (Brügman et al. 2017b).

Sample introduction into the plasma was achieved by using a 100  $\mu\text{l}\cdot\text{min}^{-1}$  PFA nebulizer plugged into a high-stability spray chamber. Solutions were kept at 60  $\mu\text{g}/\text{ml}$  Sn, which generated a  $\sim$ 10 V signal intensity for  $^{124}\text{Sn}$ . The background intensity for  $^{124}\text{Sn}$  ranged from 0 - 0.5 mV. The instrument interface was fitted with Ni-cones of sample- and skimmer-type. For the mass bias correction, the ratio  $^{121}\text{Sb}/^{123}\text{Sb}$  was used. Therefore, the Specpure Sb solution was added to the sample and the in-house standard solutions just before the measurement.

**Table 5.1:** Instrument settings for the Thermo Scientific Neptune multi-collector ICP-MS (Balliani et al. 2013; Brügmann et al. 2017b).

Instrument settings									
Thermo Scientific Neptune MC-ICP-MS									
RF Power	1150-1250 W				Integration time	8.4 s			
Plasma gas flow rate	15 Lmin $^{-1}$				Number of blocks	3			
Auxiliary gas flow rate	0.7 Lmin $^{-1}$				Number of scans	100			
Nebulizer gas flow rate	0.84–0.90 Lmin $^{-1}$								
Sample/Skimmer cones	Ni								
Sample uptake rate	1 mLmin $^{-1}$								
Configuration of the collector									
Position	L4	L3	L2	L1	C	H1	H2	H3	H4
Mass for Sn	$^{116}\text{Sn}$	$^{117}\text{Sn}$	$^{118}\text{Sn}$	$^{119}\text{Sn}$	$^{120}\text{Sn}$	$^{121}\text{Sb}$	$^{122}\text{Sn}$	$^{123}\text{Sb}$	$^{124}\text{Sn}$
Amplifier $\Omega$	11	11	10	11	11	11	11	11	11

The samples were run in a blank-standard-blank-sample-blank-standard bracketing setup. The ion intensities were background and blank corrected online. The isotope ratio calculation, the elimination of outliers based on a  $2\sigma$ -test, the  $\delta$ -value calculations, and the mass bias correction using the

empirical procedure of Russel et al. (1978) and Baxter et al. (2006) were done offline with Excel spreadsheets.

The Sn isotopic ratios are expressed as delta values in per mill relative to the isotopic composition of the in-house standard and are calculated as:

$$\delta = \frac{R_{X, \text{Probe}} - R_{X, \text{Standard}}}{R_{X, \text{Standard}}} \times 1000 \quad (1).$$

The in-house isotopic standard was prepared from an ultraclean tin metal (Puratronic, Batch W14222, Johnson Matthey). Previous studies have also used this tin metal as a reference material (Yi et al. 1999; Clayton et al. 2002; Nowell et al. 2002; Gillis et al. 2003; Gillis and Clayton 2008; Haustein et al. 2010; Brügmann et al. 2017b; Berger et al. 2018). The two commercially available reference materials of bronze, IARM-91D (Grade: CDA/UNS C93200, Analytical Reference Materials International, Manchester, NH, USA) and BAM 211 (G-SnBz10, Bundesanstalt für Materialprüfung, Berlin, Germany), were analysed for the comparison of the isotopic composition data of the bronze metal with ores by colleagues from ERC project (Brügmann et al. 2017b, Berger et al. 2018).

The combined uncertainty (reproducibility) of the measurements is given by two standard deviations (2SD) and includes the analytical uncertainties, which arise during the measurement and the sample processing. For  $\delta^{124}\text{Sn}/^{120}\text{Sn}$  it is 0.021 ‰ for the reference material BAM 211 and 0.018 ‰ for IARM-91D (Brügmann et al. 2017b). The analytical uncertainty (2SD) of cassiterite and stannite is commonly better than 0.025 ‰ for  $\delta^{124}\text{Sn}/^{120}\text{Sn}$  (Brügmann et al. 2017b).

$^{120}\text{Sn}$  as the most abundant isotope (Fig. 2.1) has been selected for calculating the isotope ratios of  $^{116}\text{Sn}/^{120}\text{Sn}$ ,  $^{117}\text{Sn}/^{120}\text{Sn}$ ,  $^{118}\text{Sn}/^{120}\text{Sn}$ ,  $^{119}\text{Sn}/^{120}\text{Sn}$ ,  $^{122}\text{Sn}/^{120}\text{Sn}$  and  $^{124}\text{Sn}/^{120}\text{Sn}$  (Brügmann et al. 2017b).

The larger the mass difference, the larger the fractionation effect and therefore also the analytical error. Actually, there are many possible ratios to choose from, but it turned out that the isotope ratio of  $^{124}\text{Sn}/^{120}\text{Sn}$  is the most stable one because it shows the smallest errors per mass unit (Fig. 5.1; Brügmann et al. 2017a). In addition, the ratios of  $^{122}\text{Sn}/^{116}\text{Sn}$  and  $^{124}\text{Sn}/^{116}\text{Sn}$  will be presented because

they have been used in previous studies (Haustein et al. 2010; Balliani et al. 2013; Yamazaki et al. 2013).

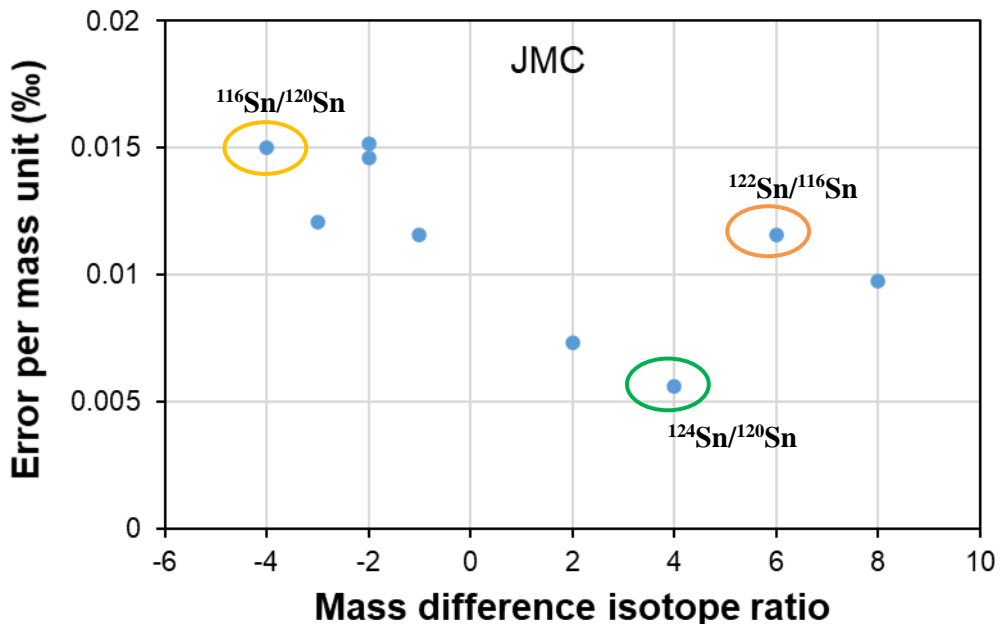


**Figure 5.1:** Plot showing the error per mass unit for the Sn isotope ratios analysed with the JMC reference material (Brügmann 2018).

A total of eight samples from SW England and the Saxonian-Bohemian province which were measured several times (Table A1 and A2 Appendix) provide an impression of the good repeatability of the measurements and of the functionality of the Neptune Plus MC-ICP-MS. The average of the 2SE for  $\delta^{124}\text{Sn}/^{120}\text{Sn}$  of the replicate samples, for example for MA-080518, is 0.01 %. This is similar to or lies in the range of the uncertainty of the standard solutions and reflects the good reproducibility of the analyses.

## 6. RESULTS

### 6.1 Petrography of the tin ores

The description of the petrography is based on a few selected samples from SW England and the Saxonian-Bohemian province which were suitable for the preparation of polished resin blocks. Therefore, representative samples of greisen and quartz veins from these tin ore areas were selected. The pictures (Fig. 6.1) were taken in a reflected light microscope with 2.5- and 10-time magnification. General petrographic and mineralogical informations of cassiterite in various granites from the European Variscan tin ore province are described in previous studies (Jackson et al. 1982; Haapala 1997; Chicharro et al. 2016).

Minerals in thin sections can be identified by the shape, colour and change of colour on rotation, cleavages, and differences in refractive index of two adjacent minerals, twinning, zoning and the interference colours. The cassiterite crystals of the different ore types can show symmetrical to asymmetrical colour and pleochroism variations in the zones from core towards the rims in transmitted light (Jackson et al. 1982; Haapala 1997; Chicharro et al. 2016). However, possible colour variations and pleochroic zonal variations can be determined with electron microprobe analyses or optical investigations with thin sections. The polished resin blocks can only be examined in reflected lights where these variations are hard to observe.

The mineralization types from SW England are described as quartz-wolframite and tourmaline-quartz-cassiterite veins, which are related to high-temperature producing granites and partly associated with different metals (Cu, As, Bi, Ag and Pb). The tectonic setting during the granite formation was a post-Variscan crustal extension in the orogenic foreland, where the emplacement of mantle-derived melts in the lower crust took place (Chen et al. 1993; Le Boutillier et al. 2002; Müller et al. 2006; Romer and Kroner 2016).

The endogranitic quartz veins with greisen (consisting of muscovite, sericite, quartz, and minor tourmaline) can be found throughout SW England (LeBoitilier 2002). They can be composed of tourmaline, muscovite, orthoclase, chlorite, wolframite, arsenopyrite, stannite, cassiterite, topaz, apatite and smaller quantities of Fe, Cu, Mo and Bi sulphides (Alderton 1993; LeBoitilier 2002). The quartz veins in the granites contain more Sn and W than the veins in the surrounding aureole rocks with more Cu, Pb and Zn (Alderton and Harmon 1991).

Greisen is formed by the more or less complete transformation of granite through metasomatic processes (mass transfer processes). This pneumatolytically altered granite is mainly composed of quartz, mica and topaz. The kalifeldspar and biotite are replaced by albite, topaz and quartz, the biotite is converted into Li-mica. Other minerals like apatite, fluorite and ore minerals like cassiterite, wolframite or chalcopyrite can occur (Haustein 2009). The altered granite samples presented here consist of > 70 % quartz, mica (muscovite or lepidolite) and cassiterite (Fig. 6.1). Cassiterite in thin sections (30 µm thickness) shows a light to dark grey colour in relected light and has a faint bireflectance. It has a weak pleochroism and usually forms well-developed euhedral crystals only in directions in which the growth is unobstructed (Craig and Vaughan 1994). The different cassiterite associations show variations in crystal form, colour and composition. The cassiterite in pegmatites shows lighter colours than in other tin ore types and has well-developed colour zoning, which is mainly observed in greisen (Haapala 1997).

The tin ore sample (MA-080521) from the Botallack mine in SW England (Fig. 6.1 a) shows cassiterite (light grey-brown) with many polishing pits and is medium grained with crystals partially several millimeters in size. It also contains quartz and a vein like filling, which could be chalcopyrite. The quartz vein sample (MA-080520) from the Botallack mine (Fig. 6.1 b) has cassiterite (light grey) and euhedral quartz crystals, which are moderate to well rounded. The primary ore sample (MA-156057) from the Hingston Down granite (Fig. 6.1 c) shows a similar composition than the tin ore sample from the Botallack mine.

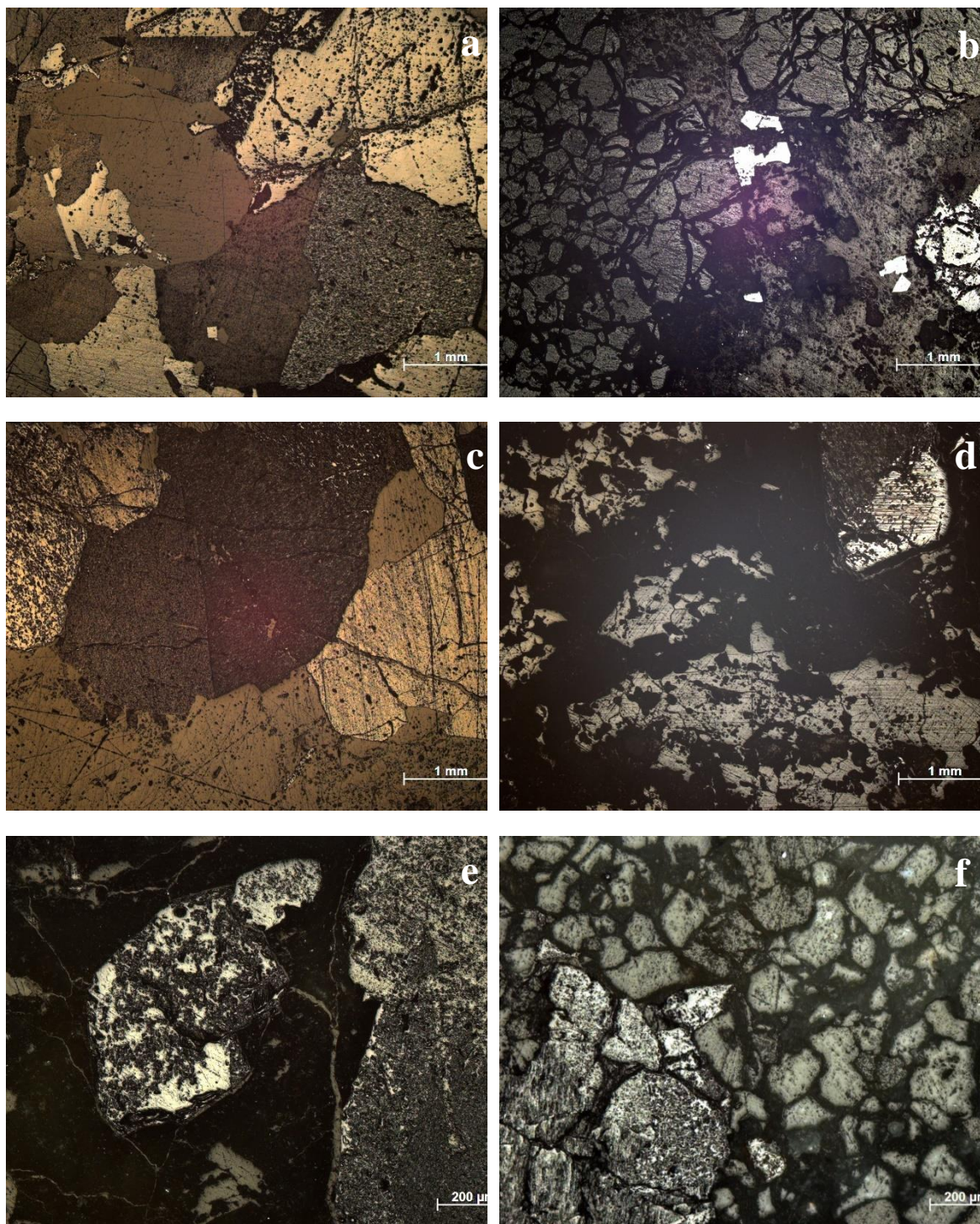


**Figure 6.1:** Polished resin block images of the different mineralization types of selected samples from SW England and the Saxonian-Bohemian province. a) and b) show a tin ore sample (MA-080521) and cassiterite in a quartz vein (MA-080520) from the Botallack Mine, SWE; c) primary ore, Drakewells Mine, Hingston Down granite (MA-156057); d) and e) show cassiterite in greisen (FG-080683) from the Zinnwald (eastern Erzgebirge) and f) is cassiterite in a quartz vein (FG-011501) from Ehrenfriedersdorf, Erzgebirge West.

The greisen sample (FG-080683) from the Zinnwald in the Eastern Erzgebirge (Fig. 6.1 d and e) consists of cassiterite with wolframite. The crystals are coarse-grained, granular and grey in colour. The euhedral cassiterite crystal (top right) also shows polishing pits. The hydrothermal quartz vein sample (FG-011501) from Ehrenfriedersdorf in the Erzgebirge West (Fig. 6.1 f) has moderate to well rounded quartz veins of euhedral shape and cassiterite grains (light grey).

## 6.2 Tin isotope compositions

The database for this work consists of 413 primary and secondary cassiterite and stannite samples and multiple analyses of several samples of tin ore deposits in Europe, Egypt and Central Asia. The single analyses are summarised in tables A1-A8 in the appendix.

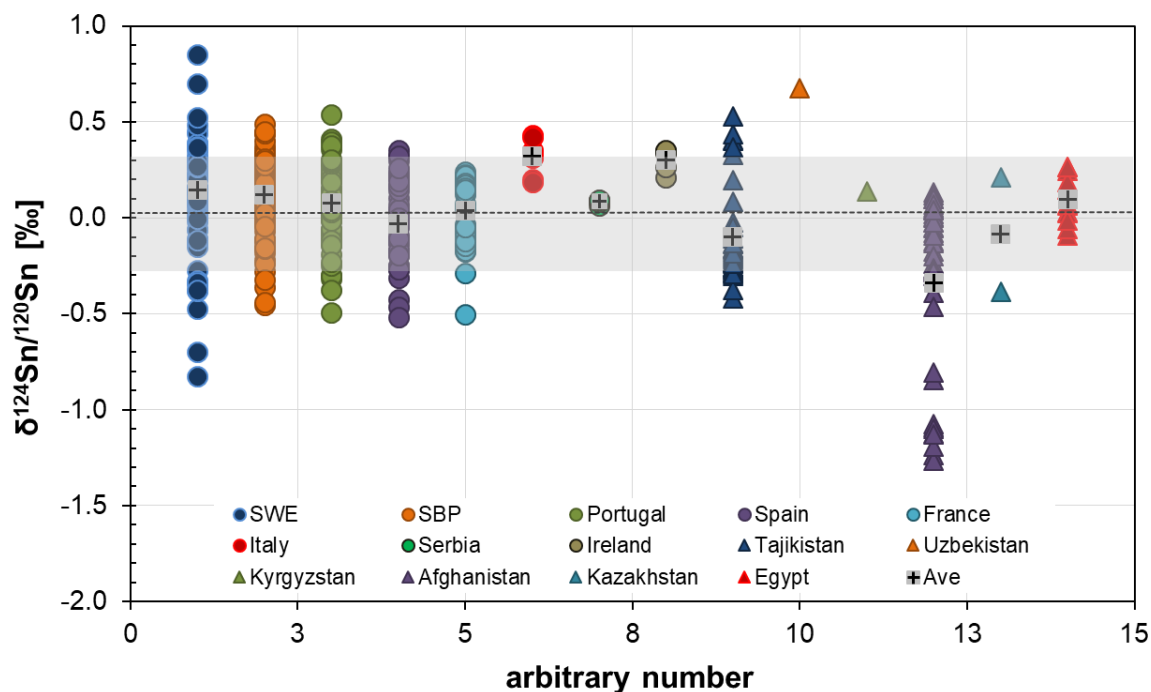


**Figure 6.2:**  $\delta^{124}\text{Sn}/^{120}\text{Sn}$  vs. an arbitrary number of all primary and secondary cassiterite and stannite samples from Europe and Central Asia (the 2SD error bars are covered by the symbols).

Figure 6.2 shows the  $\delta^{124}\text{Sn}/^{120}\text{Sn}$  isotopic compositions of the single analyses of Europe and Central Asia, including cassiterite and stannite samples. Overall, the isotope ratios are highly variable and range from -1.27 ‰ in Afghanistan to 0.85 ‰ in SW England and overlap to a large extent. This variation of  $> 2$  ‰ suggests an enormous fractionation and complex deposit types. The cassiterite and stannite from tin provinces in Europe have on average heavier isotopic compositions with  $0.08 \pm 0.23$  ‰ than those of Central Asia and Egypt with  $-0.13 \pm 0.44$  ‰ for  $\delta^{124}\text{Sn}/^{120}\text{Sn}$ . The tin province of SW England shows the largest variation in Europe (Fig. 6.2), but the isotope ratios of all provinces

overlap to a large extent. The same phenomena can be observed in Central Asia, with Afghanistan showing extreme isotopic compositions. The frequency distribution of all single measurements is shown in figure 6.3. The average of  $0.02 \pm 0.58\text{‰}$  for  $\delta^{124}\text{Sn}/^{120}\text{Sn}$  for Europe and Central Asia is calculated on the basis of all 413 single samples.

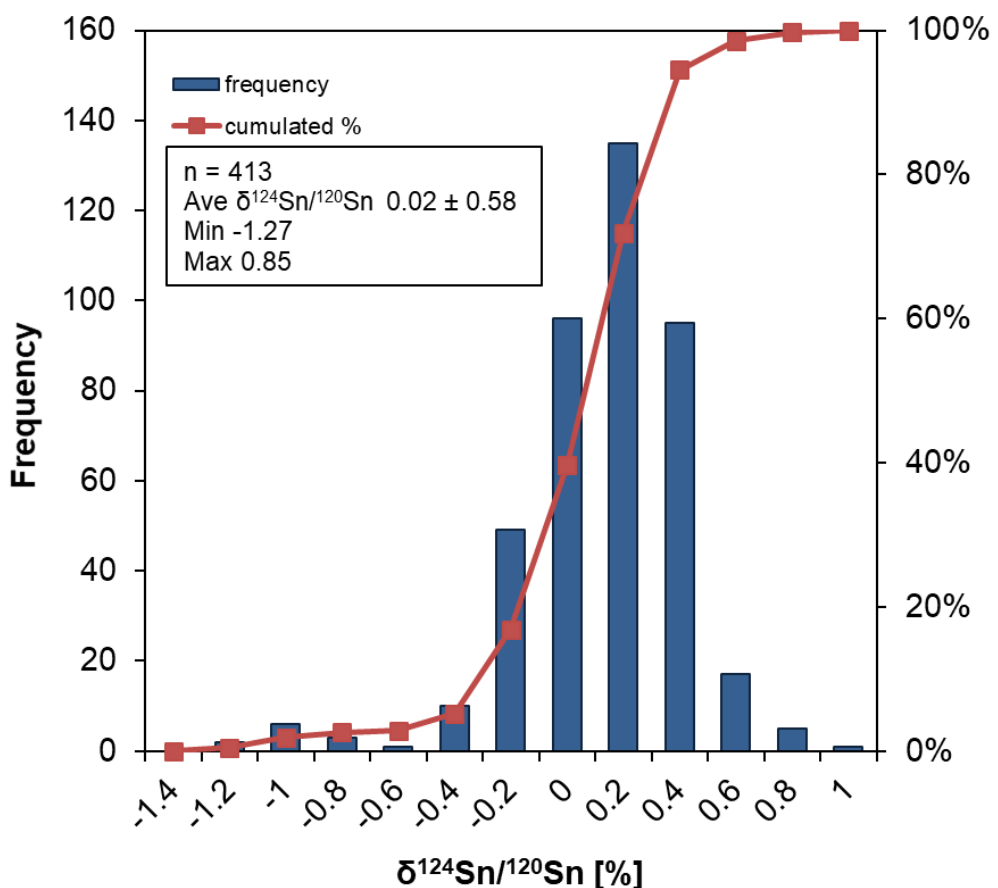


**Figure 6.3:** Frequency distribution of all cassiterite and stannite samples from Europe and Central Asia.

### 6.2.1 Primary cassiterite

#### *SW England and Saxonian-Bohemian province*

We analysed 47 and 73 samples (cassiterite grains, composite powders) from mineralizations in SW England and the Saxonian-Bohemian province, respectively. Multiple samples were measured several times. The minerals were collected from greisen and vein type mineralization.

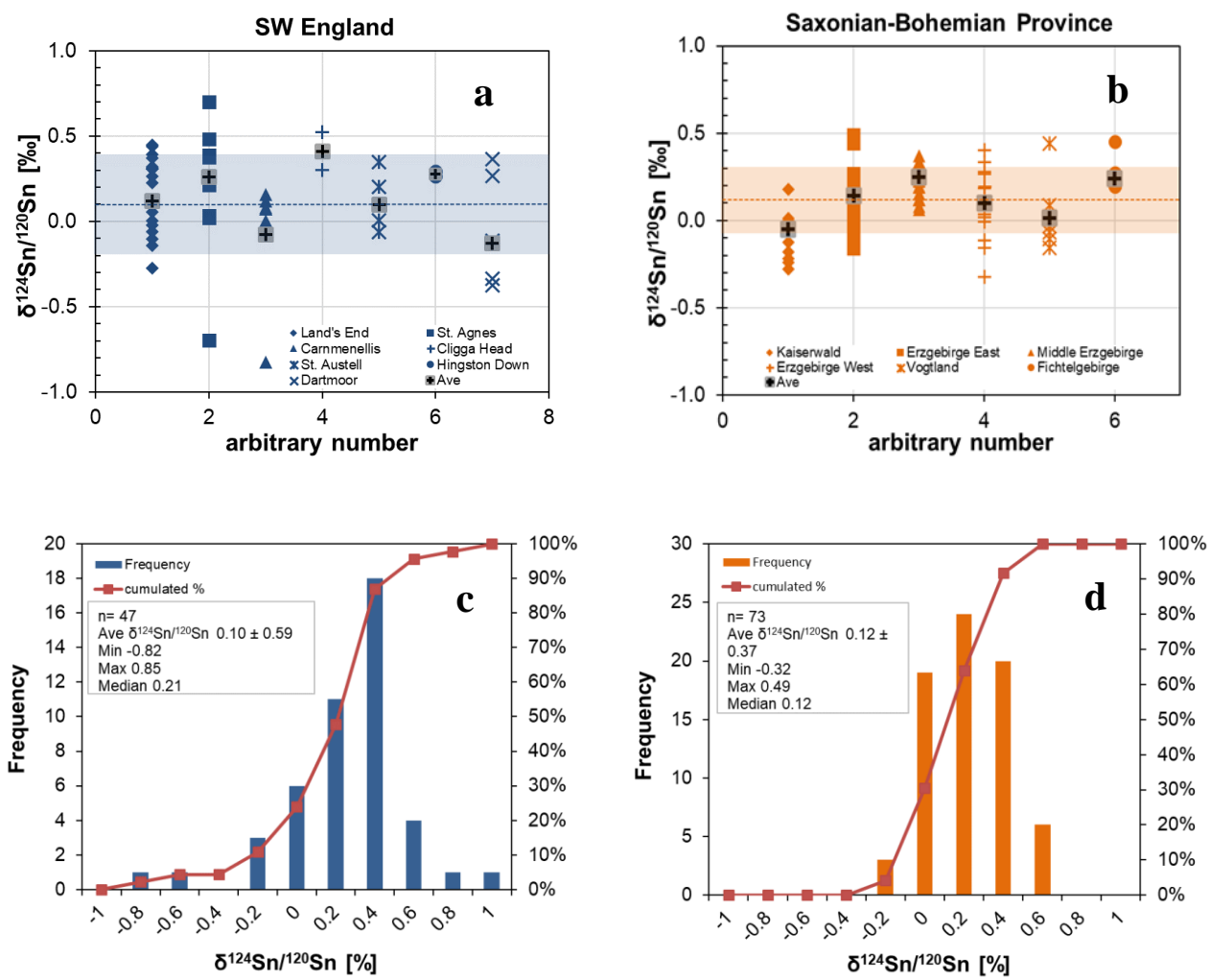


**Figure 6.4:** a and b:  $\delta^{124}\text{Sn}/^{120}\text{Sn}$  vs. an arbitrary number for the isotope ratios of primary cassiterite of the individual mines in SW England and the Saxonian-Bohemian province; c and d: Frequency distribution of SW England and the Saxonian-Bohemian province for primary cassiterite. The averages are calculated based on single mines or mining areas (the 2SD error bars are covered by the symbols).

Table 6.1 and 6.2 summarise the  $\delta^{124}\text{Sn}/^{120}\text{Sn}$  values of primary cassiterites of the individual mines and the average values for the different mining areas or granites. The complete data set in the appendix (Table A1 and A2) links sample labels, types, location, and gives all the isotope ratios calculated during the analysis.

**Table 6.1:** Mean values of the  $^{124}\text{Sn}/^{120}\text{Sn}$  [%] isotope ratios of primary cassiterite from SW England. The data sets are given with 2SD. Individual analytical results are given in the appendix (Table A1).

Granite Area	Deposit	Mineralization	n	$^{124}\text{Sn}/^{120}\text{Sn}$	2SD	$^{124}\text{Sn}/^{120}\text{Sn}$ Median
				Ave		
Land's End	Botallack Mine	Cassiterite	17	0.11	0.51	0.06
	Penzance	Cassiterite powder	8	0.28	0.28	0.29
	St. Just Mine	Cassiterite with quartz	2	-0.05	0.15	
	Wheal Bellan Mine	Cassiterite crystals	1	0.23	0.01	
	North Levant Mine	Cassiterite crystals	1	0.06	0.01	
	Levant Mine	Cassiterite crystals	1	-0.02	0.01	
	Carn Escalls Mine	Cassiterite crystals	1	-0.28	0.01	
	Balleswidden Mine	Cassiterite	1	0.45	0.01	
	St. Ives	Cassiterite powder	1	0.44	0.00	
Carnmenellis	St. Day	Cassiterite crystals	7	-0.04	0.69	0.07
	South Crofty Mine	Cassiterite	1	0.08	0.01	
	Wheal Maid Mine	Cassiterite crystals	1	-0.82	0.02	
	Wheal Pendarves	Cassiterite	1	0.16	0.01	
	Pendarves Mine	Cassiterite with Fe-minerals	1	0.07	0.00	
	Redruth Mine	Cassiterite with quartz	1	0.12	0.05	
	Scorrier Mine	Cassiterite with chlorite	1	0.01	0.03	
St. Austell	Old Beam Mine	Cassiterite in quartz, mica	4	0.12	0.37	0.06
	Goss Moor Mine	Cassiterite graupen	1	0.004	0.003	
	Egloshallen Mine	Cassiterite in quartz	1	0.20	0.01	
	Bunny Mine	Cassiterite in quartz	1	-0.06	0.01	
			1	0.35	0.01	
St. Agnes	St. Agnes Mine	Cassiterite	10	0.30	0.49	0.21
	Wheal Kitty Mine	Cassiterite concentrate	4	0.19	1.30	0.30
	unknown	Cassiterite crystals	2	0.20	0.48	
	Wheal Vottle Mine	Cassiterite crystals	1	0.70	0.03	
	Unknown	Cassiterite crystals	1	0.02	0.01	
	Trevaunance Mine	Cassiterite crystals	1	0.48	0.0001	
		Cassiterite with Fe-minerals	1	0.21	0.002	
Cligga Head	Cligga Head Mine	Cassiterite crystals	2	0.41	0.31	
Hingston Down	Drakewells Mine	Cassiterite crystals	2	0.28	0.05	
Dartmoor	West Vitifer Mine	Cassiterite crystals	5	-0.13	0.63	-0.22
	Hemerdon Mine	Cassiterite crystals	1	-0.34	0.002	
	South Birch Tor Mine	Cassiterite	2	0.32	0.14	
	North Dartmoor	Cassiterite	1	-0.12	0.01	
			1	-0.37	0.01	
SWE		<b>Total</b>	47	0.10	0.59	0.10

**Table 6.2:** Mean values of the  $\delta^{124}\text{Sn}/^{120}\text{Sn}$  [%] isotope ratios of primary cassiterite from the Saxonian-Bohemian province. The data sets are given with 2SD. Individual analytical results are given in the appendix (Table A2).

Area	Deposit	Mineralization	n	$\delta^{124}/^{120}\text{Sn}$	2SD	$\delta^{124}/^{120}\text{Sn}$
				Ave	Median	
Erzgebirge East			19	0.14	0.08	0.14
	Altenberg	Cassiterite	4	0.14	0.25	0.16
	Krupka	Cassiterite	7	0.19	0.50	0.20
Middle Erzgebirge	Cínovez (Zinnwald)	Cassiterite	8	0.11	0.33	0.10
			18	0.25	0.15	0.23
	Ehrenfriedersdorf	Cassiterite with quartz	13	0.20	0.18	0.20
West	Geyer	Cassiterite	4	0.33	0.06	0.32
	Pobershau	Cassiterite	1	0.23	0.01	
	Johanngeorgenstadt	Cassiterite	14	0.10	0.45	0.18
Vogtland	Marienberg	Cassiterite	1	-0.16	0.02	
	Neudorf	Cassiterite	1	0.33	0.01	
	Schwarzenberg	Cassiterite	1	0.18	0.01	
	Pöhla	Cassiterite	1	0.27	0.01	
	Horni Blatná (Platten)	Cassiterite	1	-0.32	0.02	
	Abertamy-Hřebečná	Cassiterite	2	0.25	0.01	
	Přebuz	Cassiterite greisen	3	-0.06	0.15	
	Am Auersberg	Cassiterite with quartz	3	0.24	0.37	0.28
			3	0.17	0.28	0.19
Fichtelgebirge	Mühlleithen	Cassiterite in topaz-greisen	7	-0.001	0.24	0.02
	Gottesberg	Tin ore in granite	4	0.11	0.46	0.03
	Vernéřov	Cassiterite	2	-0.13	0.07	
			1	0.02	0.01	
Kaiserwald	Rudolfstein	Cassiterite	4	0.28	0.23	0.24
	Schönlid	Cassiterite	1	0.27	0.01	
	Weißenhaid	Cassiterite	1	0.21	0.00	
	Seehaus (Tröstau)	Cassiterite	1	0.20	0.01	
			1	0.45	0.01	
SBP	Schönfeld	Cassiterite	11	-0.06	0.12	-0.09
	Schlaggenwald	Cassiterite	3	-0.09	0.22	-0.03
	Sangerberg	Cassiterite	7	-0.10	0.32	-0.13
			1	0.01	0.00	
<b>Total</b>			73	0.12	0.37	0.17

Overall, the  $\delta^{124}\text{Sn}/^{120}\text{Sn}$  values for cassiterites from the primary deposits vary by 1.65 ‰ ranging from -0.82 to 0.85 ‰. This extent of fractionation is observed in the St. Agnes granite and in Carnmenellis in SW England whereas the cassiterites from the Saxonian-Bohemian province indicate smaller fractionation effects ranging from -0.32 to 0.49 ‰ (Fig. 6.4 a and b). However, the average  $\delta^{124}\text{Sn}/^{120}\text{Sn}$  in primary cassiterite of both provinces is very similar. This is true regardless whether the average is calculated based on mining regions or granites (SWE:  $0.15 \pm 0.39$  ‰; SBP:  $0.12 \pm 0.27$  ‰) or based on single mines (SWE:  $0.10 \pm 0.59$  ‰; SBP:  $0.12 \pm 0.37$  ‰). The average for Cornwall (Land's End, Carnmenellis, St. Austell, St. Agnes, Cligga Head, Hingston Down) is  $0.13 \pm 0.33$  for  $\delta^{124}\text{Sn}/^{120}\text{Sn}$  calculated based on mining regions (Table 6.1).

In all cases, the average and median values of  $\delta^{124}\text{Sn}/^{120}\text{Sn}$  are similar thus indicating a normal frequency distribution of the isotope ratios in both tin provinces (Fig. 6.4 c and d).

Figure 6.5 provides a more detailed look at the Land's End Granite, the Eastern Erzgebirge and the Western Erzgebirge. It shows the averages of the samples from the single mines or mining areas within these granite complexes. The grey crosses show the mines or mining areas with one sample per mine. The overall average for the Land's End granite is  $0.11 \pm 0.51\text{‰}$  for  $\delta^{124}\text{Sn}/^{120}\text{Sn}$ , for the Eastern Erzgebirge  $0.14 \pm 0.08\text{‰}$  and  $0.10 \pm 0.45\text{‰}$  for the Western Erzgebirge (Table 6.1 and 6.2). The Land's End granite with a high variation shows several different populations of Sn isotopic compositions, so it is possible to differentiate between the Botallack mine with  $\delta^{124}\text{Sn}/^{120}\text{Sn} 0.28 \pm 0.28\text{‰}$  and Penzance with a lighter isotopic composition of  $-0.05 \pm 0.15\text{‰}$  (Fig. 6.5). The same applies to the Western Erzgebirge where it is possible to identify the tin mining regions of Přebuz and Abertamy-Hřebečná. On the other hand, in the Eastern Erzgebirge it is not possible to distinguish between the three mines of Altenberg, Krupka and Zinnwald in the Erzgebirge East.

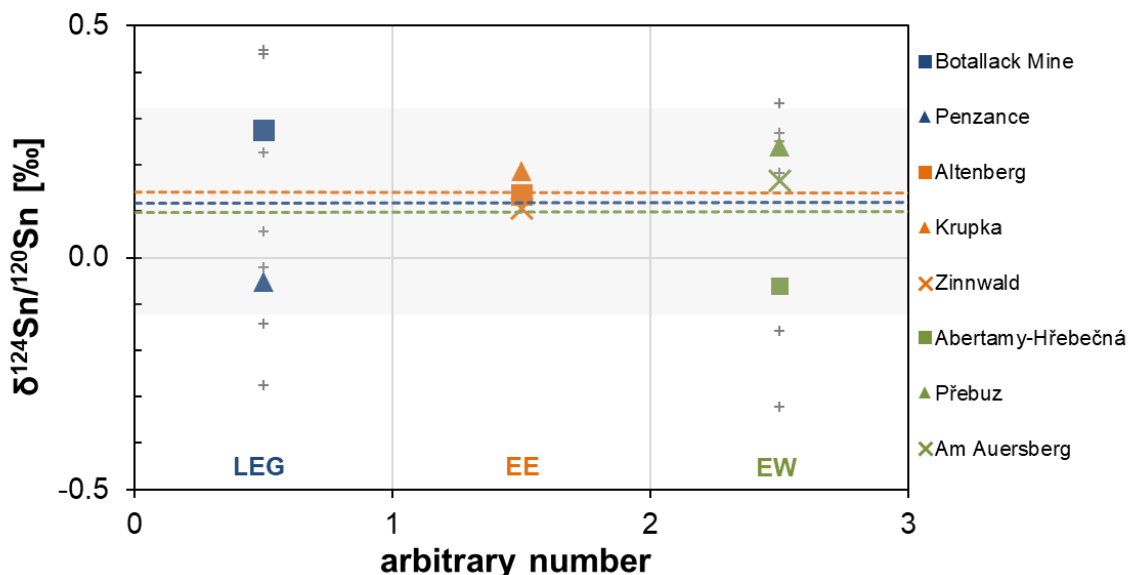


**Figure 6.5:** Land's End granite (LEG), Erzgebirge East (EE) and Erzgebirge West (EW). The grey crosses show other mines or mining areas with only one sample per area. The dotted lines show the average values for the plotted areas and the light grey field is the 2SD for all plotted data (the 2SD error bars are covered by the symbols).

### Iberian Peninsula

From the Iberian Peninsula we analysed 107 samples from primary mineralizations in Portugal and Spain. The minerals were collected from greisen and vein type mineralization. Table 6.3 and 6.4 summarise the  $\delta^{124}\text{Sn}/^{120}\text{Sn}$  values of primary cassiterites of the individual mines and the average values for the different mining areas. The complete data set is given in the appendix (Table A3 and A4).

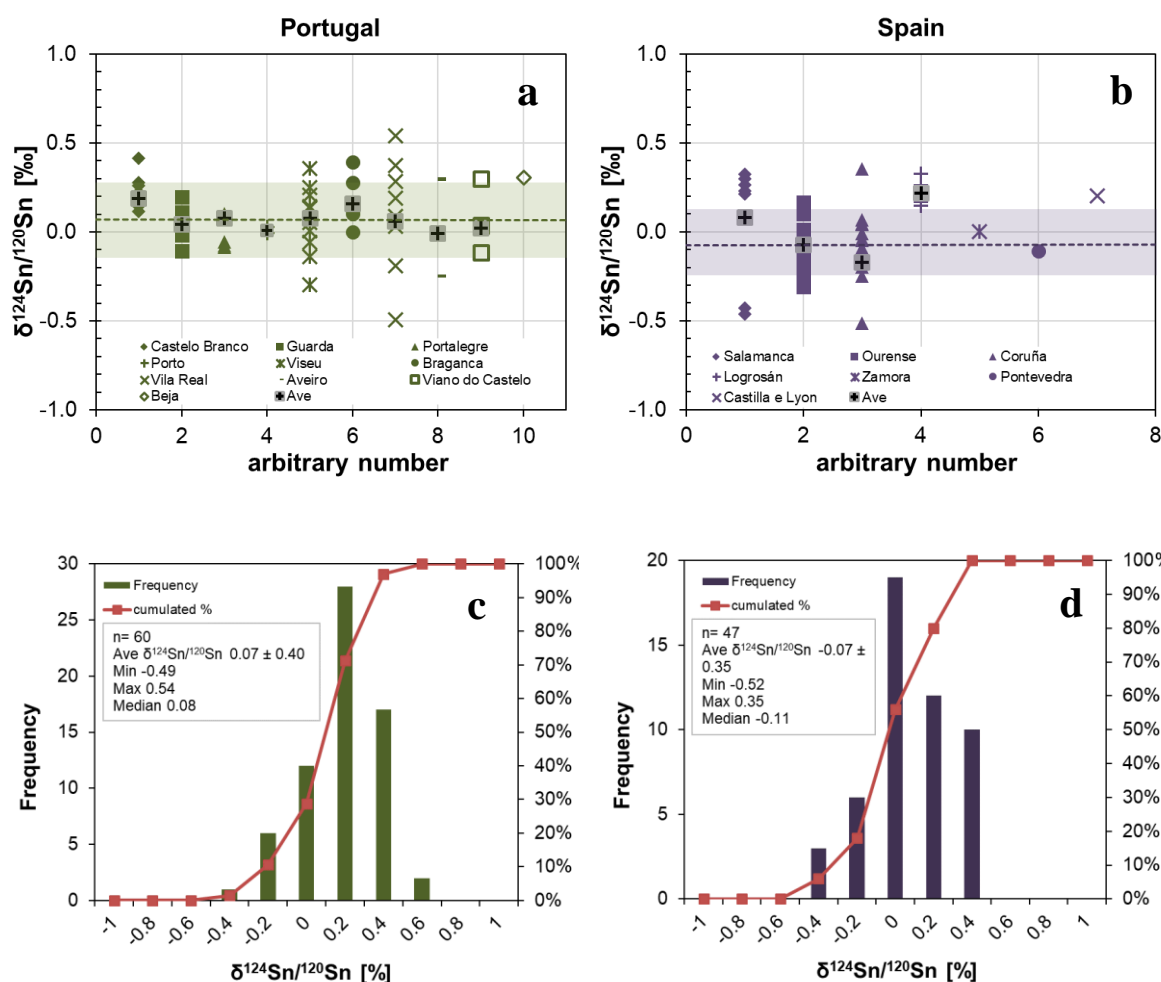


**Figure 6.6:** a and b: Isotope composition in different mining areas of primary cassiterites; c and d: Frequency distribution of primary cassiterite from Portugal and Spain. The average values are calculated on the basis of single mines or mining areas (the 2SD error bars are covered by the symbols).

The average  $\delta^{124}\text{Sn}/^{120}\text{Sn}$  in primary cassiterite of Portugal and Spain differs. This is true regardless whether the average is calculated based on mining regions (Portugal:  $0.08 \pm 0.21 \text{ ‰}$ ; Spain:  $0.02 \pm$

0.31 ‰) or based on single mines (Portugal:  $0.07 \pm 0.40$  ‰; Spain:  $-0.07 \pm 0.35$  ‰), where Spain shows differences in the averages based on mining regions or single mines. Figure 6.6 a and b shows the isotopic composition in the different mining areas or districts of primary cassiterite of the Iberian Peninsula. In Portugal the  $\delta^{124}\text{Sn}/^{120}\text{Sn}$  values for cassiterite vary by 1.03 ‰ ranging from -0.49 to 0.54 ‰. This extent of fractionation is observed only in Vila Real whereas the cassiterite from the other districts indicates smaller fractionation effects.

Except for Viseu, Bragança, Vila Real, Aveiro and Viana do Castelo, the districts lie within the range of 0.40 ‰ (2SD) of the overall Portuguese average. The Spanish cassiterites from primary deposits show smaller fractionation effects varying by 0.87 ‰ ranging from -0.52 to 0.35 ‰ for  $\delta^{124}\text{Sn}/^{120}\text{Sn}$  (Fig. 6.6 b). This extent of fractionation is observed in the Coruña district. The samples from Salamanca have a similar spread. Here in the Iberian Peninsula as well as in SW England and the Saxonian-Bohemian province all cassiterites show a large variation and overlap to a large extent. In Portugal, the average and median values of  $\delta^{124}\text{Sn}/^{120}\text{Sn}$  for the districts are similar thus indicating a normal frequency distribution of the isotope ratios.

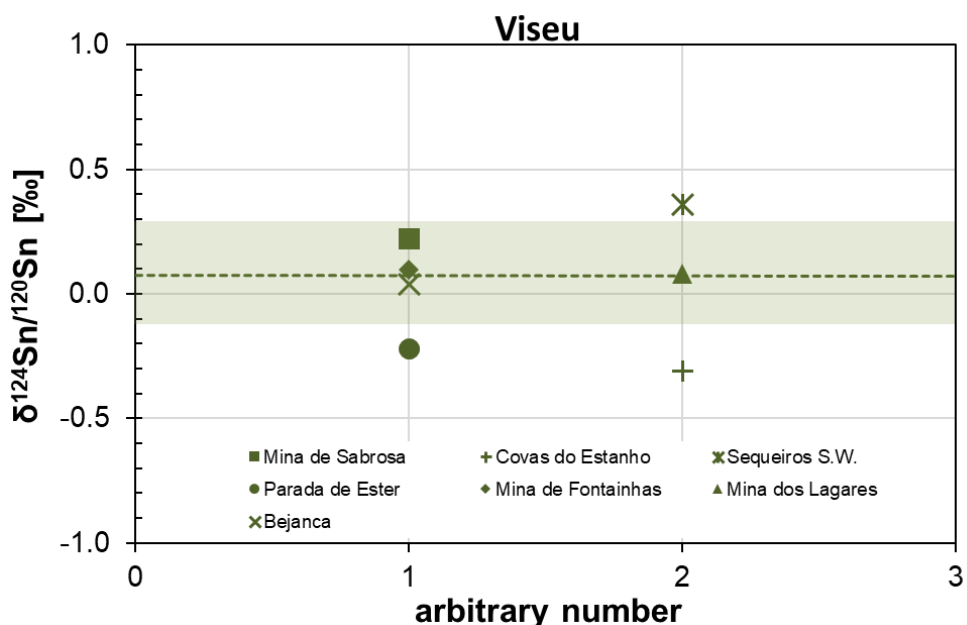


**Figure 6.7:** The tin mines of the Viseu mining district in Portugal (the 2SD error bars are covered by the symbols).

This also applies to the Spanish cassiterites, where the averages of the tin ore districts lie within the whole range of the Spanish average, except for Logrosan, which shows a slightly heavier average (Fig. 6.6 a and b).

As in SWE and in the SBP the results for  $\delta^{124}\text{Sn}/^{120}\text{Sn}$  of one mining area in Portugal are plotted in figure 6.7 in detail. The cassiterites from Spain are not suitable for such a comparison because for most areas we only have samples from one mine (like the Eastern Erzgebirge, Fig. 6.5). The samples from Viseu show the same picture as for the Land's End granite in SW England, where it is possible to distinguish between a few mines. The Covas do Estanho and the Sequeiros mines have different isotopic compositions compared to the other mines and show the lightest ( $-0.31 \pm 0.03 \text{ ‰}$ ) and the heaviest ( $0.36 \pm 0.02 \text{ ‰}$ ) isotopic compositions of this area. However, the Mina de Sabrosa, Mina de Fontainhas and Bejanca show nearly identical  $\delta^{124}\text{Sn}/^{120}\text{Sn}$  values and lie within the 2SD range. Parada de Ester shows similar values for  $\delta^{124}\text{Sn}/^{120}\text{Sn}$  as Covas do Estanho. A clear interpretation could be difficult due to the low number of samples per mine (Table 6.3).

**Table 6.3:** Mean values of the  $\delta^{124}\text{Sn}/^{120}\text{Sn}$  [%] isotope ratios of primary cassiterite from Portugal. The data sets are given with 2SD. Individual analytical results are given in the appendix (Table A3).

Area	Deposit	Mineralization	n	$\delta^{124}\text{Sn}/^{120}\text{Sn}$	2SD	$\delta^{124}\text{Sn}/^{120}\text{Sn}$
				Ave	Median	
Castelo Branco	Mina da Fonte das Galoas	Cassiterite	8	0.18	0.21	0.22
	Gaia	Cassiterite	2	0.24	0.06	
	Panasqueira	Cassiterite	1	0.20	0.02	
Guarda	Mina da Fonte do Seixo	Cassiterite	5	0.23	0.24	
	Quinta do Beja, Rio Torto	Cassiterite	1	0.04	0.21	0.04
	Gonçalo, Belmonte	Cassiterite in pegmatite	1	0.11	0.01	
	Mina da Vela, Belmonte	Cassiterite in pegmatite	1	0.01	0.02	
	Mina das Torrinhas	Cassiterite	1	-0.02	0.02	
	Freixo de Numão	Cassiterite	1	-0.11	0.004	
Portalegre	Baldio do Conde, Elvas	Cassiterite	5	0.06	0.01	
	Santa Eulália	Cassiterite in quartz vein	2	-0.03	0.03	-0.06
			3	0.01	0.27	
Porto	Mina da Reberdosa	Cassiterite	2	-0.01	0.05	
	Friande	Cassiterite	1	0.03	0.01	
			1	-0.01	0.03	
Viseu	Mina de Sabrosa	Cassiterite in quartz vein	14	0.05	0.44	0.09
	Covas do Estanho	Cassiterite	2	0.23	0.06	
	Sequeiros S.W.	Cassiterite	2	-0.31	0.03	
	Parada de Ester	Cassiterite with quartz	1	0.36	0.02	
	Mina das Fontainhas	Cassiterite in pegmatite	2	-0.22	0.23	
	Mina dos Lagares	Cassiterite	2	0.10	0.12	
	Bejanca	Cassiterite	2	0.08	0.21	
	Lagares	Cassiterite	1	0.04	0.27	
			1	0.13	0.02	
Braganca	Unknown	Cassiterite in mica	6	0.17	0.34	0.11
	unknown	Cassiterite in quartz	1	0.10	0.01	
	Mina da Ribeira	Cassiterite in quartz	1	0.00	0.02	
	Mina do Portelo	Cassiterite in greisen	1	0.39	0.01	
Vila Real	Mina da Serrinha da Cascalheira	Cassiterite	3	0.20	0.29	
	Mina do Pinheiro Manso	Cassiterite	9	0.06	0.58	
	Ribeira de Pena	Cassiterite	2	0.46	0.23	
	Mina Praina dos Torganos	Cassiterite	1	0.12	0.02	
	Jales, Revel.	Cassiterite in pegmatite	1	0.03	0.004	
	Mina de Aveleda	Cassiterite in quartz vein	1	-0.19	0.01	
	Vale das Gatas	Cassiterite in quartz vein	1	0.19	0.01	
		Cassiterite in greisen	1	0.09	0.02	
Aveiro	Bustelo, Castro Daire	Cassiterite	4	0.09	0.68	0.02
	Mina de Regoufe	Cassiterite	2	0.30	0.01	
			2	-0.31	0.18	
Viana do Castelo	Penedo da Poça	Cassiterite	5	0.004	0.40	0.03
	Nogueira Almonde	Placer tin	1	0.29	0.02	
	Gondar	Cassiterite in greisen	1	0.05	0.02	
	Unknown	Cassiterite	1	-0.12	0.01	
	Minas do Fontao	Cassiterite	1	0.03	0.01	
Beja	Neves-Corvo	Cassiterite	1	0.04	0.01	
Portugal	<b>Total</b>		60	0.07	0.40	0.08

**Table 6.4:** Mean values of the  $\delta^{124}\text{Sn}/^{120}\text{Sn}$  [%] isotope ratios of primary cassiterite from Spain. The data sets are given with 2SD. Individual analytical results are given in the appendix (Table A4).

Area	Deposit	Mineralization	n	$\delta^{124}\text{Sn}/^{120}\text{Sn}$	2SD	$\delta^{124}\text{Sn}/^{120}\text{Sn}$
				Ave		
Salamanca	Salamanca	Cassiterite	6	0.03	0.74	
Ourense	Vilar de Cervos	Cassiterite	15	-0.08	0.25	-0.12
	Val de Orras	Cassiterite	3	-0.02	0.52	
	Pentes	Cassiterite	1	-0.11	0.02	
	Penouta	Cassiterite in greisen	5	-0.13	0.04	
	Beariz	Cassiterite with mica	1	0.01	0.003	
	Avión	Cassiterite	2	-0.14	0.34	
	Sarreaus	Cassiterite	1	0.17	0.01	
	Vilameá	Cassiterite	1	-0.25	0.01	
Coruña	Minas de San Finx	Cassiterite in greisen	17	-0.17	0.37	-0.09
	Lousame	Cassiterite	8	0.01	0.31	
	Corta la Barrosa	Cassiterite in pegmatite	4	-0.11	0.24	
	Arzúa	Cassiterite	1	-0.16	0.01	
	Portomouro	Cassiterite	1	-0.27	0.01	
	Mina a Magdalena	Cassiterite	1	0.04	0.02	
	O Cobo, Lampón	Cassiterite	1	-0.19	0.02	
Cáceres	Logrosán	Cassiterite	6	0.22	0.13	0.20
Zamora	Calabor	Cassiterite	1	0.0004	0.03	
Pontevedra	Carboeiro	Cassiterite	1	-0.11	0.01	
Castilla e Lyon	Mari Tere mine	Cassiterite	1	0.23	0.09	
Spain	<b>Total</b>		47	-0.07	0.35	-0.11

### France and Italy

The data set of mineralizations from France and Italy consists of 37 samples. The minerals were collected from greisen and vein type mineralization. Table 6.5 summarises the  $\delta^{124}\text{Sn}/^{120}\text{Sn}$  values of the individual mines and the average values for the different mining areas.

France (n=29) shows on average  $-0.005 \pm 0.31\text{‰}$  for  $\delta^{124}\text{Sn}/^{120}\text{Sn}$  and Italy (n=8) has heavier isotopic compositions with an average of  $0.30 \pm 0.20\text{‰}$  (2SD), calculated based on single mines (Fig. 6.8 a and b). The  $\delta^{124}\text{Sn}/^{120}\text{Sn}$  values for cassiterites from France vary by  $0.53\text{‰}$  ranging from -0.29 to  $0.24\text{‰}$ . They indicate a bigger fractionation effect than those of Italy with a span of  $0.19$  to  $0.43\text{‰}$  for  $\delta^{124}\text{Sn}/^{120}\text{Sn}$  (Fig. 6.8 c and d). Except for two samples from Brittany and the Massif Central (France) all samples lie within the 2SD ranges of the averages.

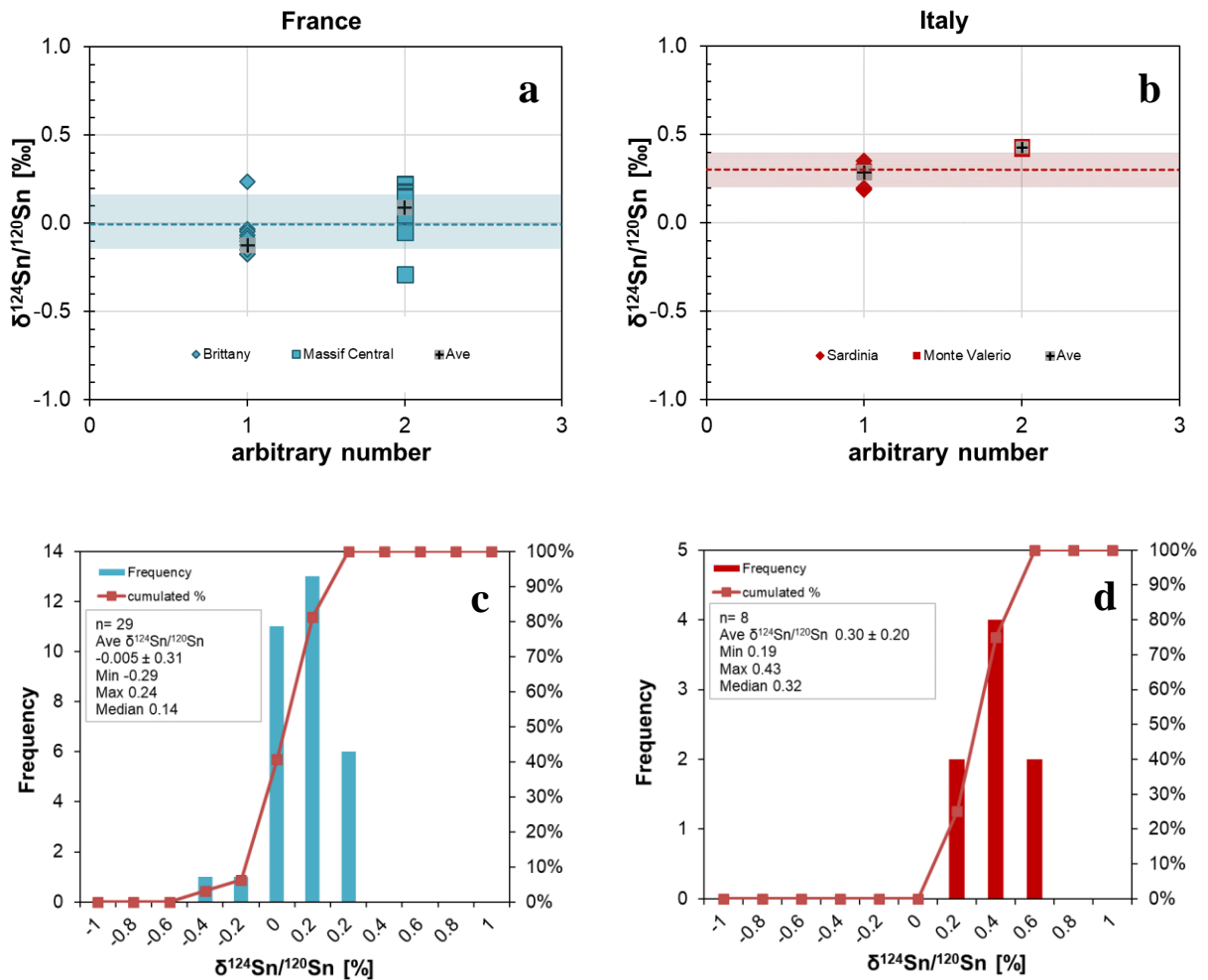


**Table 6.5:** Mean values of the  $\delta^{124}\text{Sn}/^{120}\text{Sn}$  [%] isotope ratios of primary cassiterite from France and Italy. The data sets are given with 2SD. Individual analytical results are given in the appendix (Table A5).

Area	Deposit	Mineralization	n	$\delta^{124}\text{Sn}/^{120}\text{Sn}$	
				Ave	Median
Brittany	Piriac-sur-Mer, Loire Atlantique	Cassiterite	10	-0.06	0.31
	Ruscumunoc, Finistère	Cassiterite	1	-0.18	0.01
	Quily, Dép. Morbihan	Cassiterite	1	0.24	0.02
	Villeder	Cassiterite	3	-0.06	0.07
	Penfeunteun bei Bourg-Blanc, Finistère	Cassiterite	1	-0.17	0.002
	unknown	Cassiterite	1	-0.07	0.007
		Cassiterite	3	-0.12	0.06
Massif Central			19	0.09	0.27
	Montebras Mine	Cassiterite	10	0.18	0.10
	Échassières Mine	Cassiterite	1	0.05	0.003
	Sauvagnac, Dép. Haute-Vienne	Cassiterite	2	-0.17	0.34
	Volondat, Dép. Haute-Vienne	Cassiterite	2	0.18	0.01
	Jouhe (at Vaulry), Dép. Haute-Vienne	Cassiterite	2	0.15	0.02
France	Vaulry, Dép. Haute-Vienne	Cassiterite	2	0.14	0.02
		<b>Total</b>	29	-0.005	0.31
Sardinia					0.14
	Perdu Cara Mine	Cassiterite	6	0.26	0.14
	Villacidro	Cassiterite	2	0.26	0.19
	Canale Serci	Cassiterite	1	0.19	0.01
Monte Valerio	Monte Valerio	Cassiterite	3	0.33	0.04
Italy		<b>Total</b>	2	0.43	0.02
			8	0.30	0.20
					0.32

### *Central Asia and Egypt*

From Egypt and Central Asia, we analysed 9 respectively 57 primary cassiterite samples (cassiterite grains, composite powders) from pegmatite and vein type mineralization. Table 6.6 shows the  $\delta^{124}\text{Sn}/^{120}\text{Sn}$  values of the individual mines and the average values for the different districts. The complete data set is given in table A6 in the the appendix.

Overall, the  $\delta^{124}\text{Sn}/^{120}\text{Sn}$  values for primary cassiterites in Central Asia vary by 1.94 % ranging from -1.27 to 0.67 %. This extent of fractionation is observed in the deposits of Afghanistan and Uzbekistan, whereas the cassiterites from Tajikistan indicate smaller fractionation effects ranging from -0.13 to 0.53 % (Fig. 6.9). The very small number of samples from Uzbekistan (n=1), Kyrgyzstan (n=1) and Kazakhstan (n=2) (Table 7) does not allow clear conclusions about the extent of fractionation in these areas.

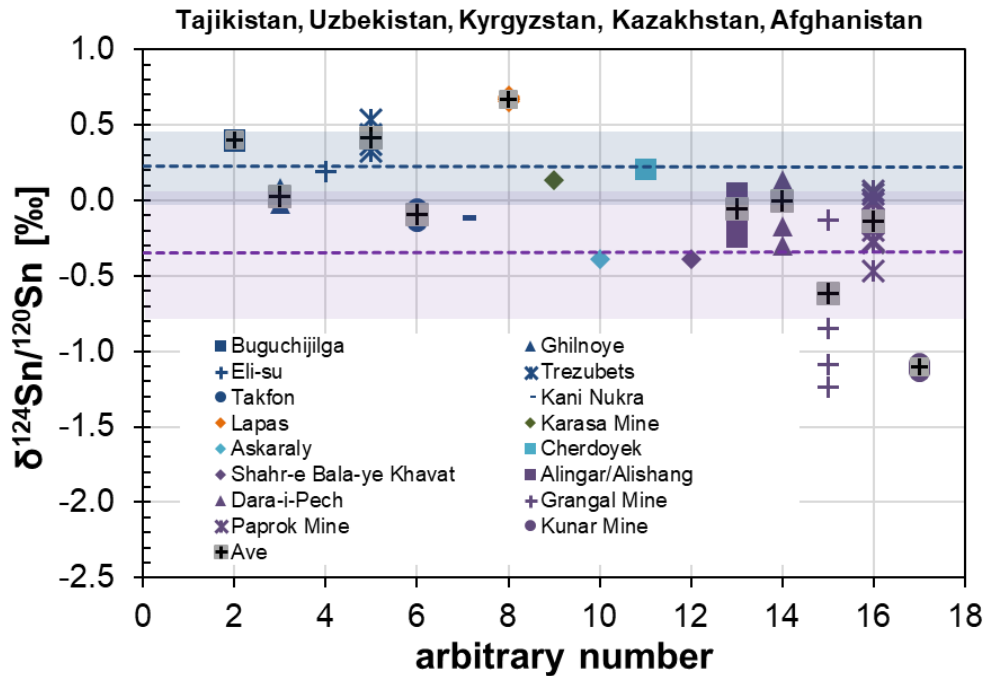


**Figure 6.9:**  $\delta^{124}\text{Sn}/^{120}\text{Sn}$  values versus an arbitrary number for Tajikistan (blue), Uzbekistan (orange), Kyrgyzstan (green), Kazakhstan (aquamarine) and Afghanistan (violet); (the 2SD error bars are covered by the symbols).

However, the averages  $\delta^{124}\text{Sn}/^{120}\text{Sn}$  of primary cassiterite of Tajikistan, Kyrgyzstan and Kazakhstan are slightly different with  $0.19 \pm 0.45 \text{\textperthousand}$ ,  $0.14 \pm 0.02 \text{\textperthousand}$ , and  $-0.09 \pm 0.84 \text{\textperthousand}$  (Fig. 6.9, Table 6.6).

From Lapas (Uzbekistan) we analysed one sample four times with an average of  $0.67 \pm 0.03 \text{\textperthousand}$ . Afghanistan shows the lightest isotopic composition of all observed areas with an average of  $-0.38 \pm 0.84 \text{\textperthousand}$  (Fig. 6.9, violet symbols). The cassiterite samples are all of pegmatitic mineralization type. The  $\delta^{124}\text{Sn}/^{120}\text{Sn}$  values for primary cassiterites in Egypt vary by  $0.36 \text{\textperthousand}$  ranging from  $-0.09$  to  $0.27 \text{\textperthousand}$  (Fig. 6.10), which shows smaller fractionation effects than in Afghanistan. However, the averages  $\delta^{124}\text{Sn}/^{120}\text{Sn}$  in primary cassiterite calculated based on single mines are slightly different with  $-0.05 \pm 0.90 \text{\textperthousand}$  (2SD) for Central Asia and with heavier isotopic compositions of  $0.08 \pm 0.31 \text{\textperthousand}$  (2SD) in Egypt. The average based on mining areas (in this case calculated based on the countries) for Central Asia shows an essential heavier composition of  $0.11 \pm 0.78 \text{\textperthousand}$  (2SD) for  $\delta^{124}\text{Sn}/^{120}\text{Sn}$ .

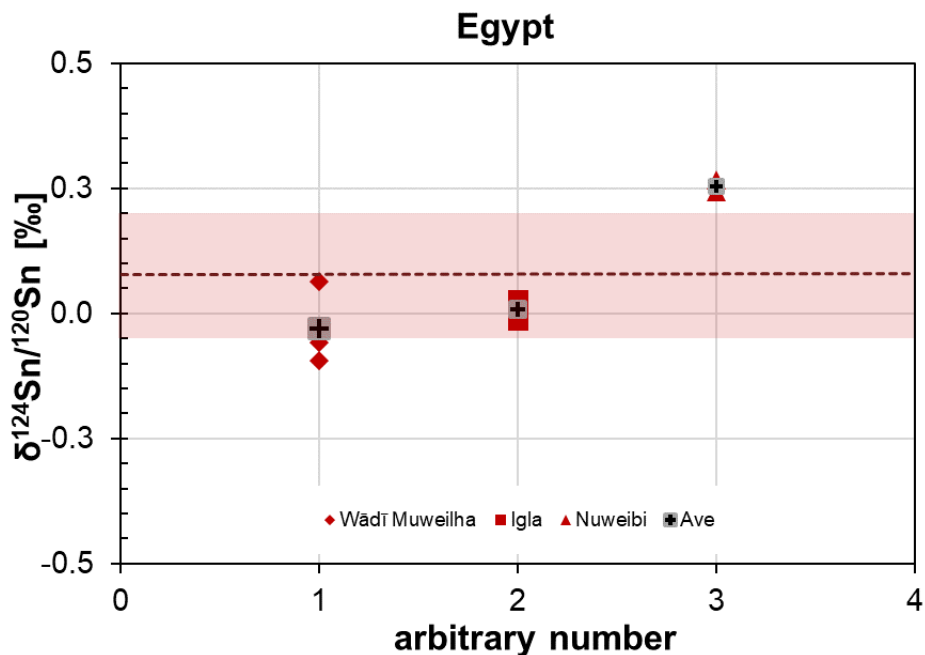


**Figure 6.10:**  $\delta^{124}/^{120}\text{Sn}$  values versus an arbitrary number for Egypt (the 2SD error bars are covered by the symbols).

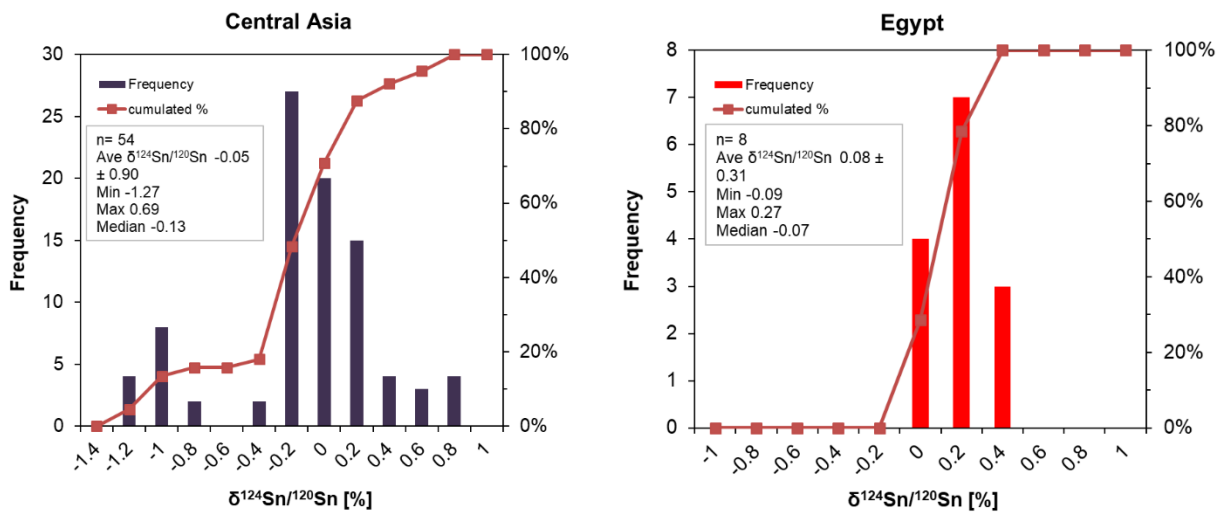


**Figure 6.11:** Frequency distribution for primary cassiterite of Central Asia and Egypt. The average values are calculated on the basis of single mines or mining areas.

**Table 6.6:** Mean values of the  $\delta^{124}\text{Sn}/^{120}\text{Sn}$  [%] isotope ratios of primary cassiterite from Egypt and Central Asia. The data sets are given with 2SD. Individual analytical results are given in the appendix (Table A6).

Area	Deposit	Mineralization	n	$\delta^{124}\text{Sn}/^{120}\text{Sn}$	
				Ave	Median
Egypt	Wādī Muweilha	Cassiterite	7	0.08	0.31
		Cassiterite	3	-0.03	0.17
		Cassiterite	2	0.01	0.06
	Nuweibi	Cassiterite	2	0.25	0.03
Tajikistan	Buguchijilga	Cassiterite	11	0.19	0.45
		Cassiterite	2	0.40	0.01
		Cassiterite	2	0.03	0.15
		Cassiterite	1	0.19	0.01
		Cassiterite	4	0.42	0.18
	Takfon	Cassiterite	2	-0.09	0.12
Uzbekistan	Lapas	Cassiterite	1	0.67	0.03
Kyrgyzstan	Karasa Mine	Cassiterite	1	0.14	0.02
Kazakhstan	Askaraly	Cassiterite	2	-0.09	0.84
		Cassiterite	1	-0.39	0.10
	Cherdoyek	Cassiterite	1	0.21	0.003
Afghanistan	Shahr-e Bala-ye Khavat	Cassiterite	38	-0.38	0.84
		Cassiterite	1	-0.39	0.01
		Cassiterite in pegmatite	6	-0.06	0.22
		Cassiterite in pegmatite	7	-0.001	0.34
		Cassiterite in pegmatite	11	-0.61	1.10
		Cassiterite in pegmatite	10	-0.14	0.36
	Kunar Mine	Cassiterite in pegmatite	4	-1.11	0.05
Central Asia		<b>Total</b>	53	-0.05	0.90
Central Asia & Egypt		<b>Total</b>	60	-0.03	0.82
					0.003

## 6.2.2 Secondary cassiterite

This chapter summarises all  $\delta^{124}\text{Sn}/^{120}\text{Sn}$  data for the secondary cassiterite (Fig. 6.12, Table 8). In figure 6.12 all secondary cassiterite samples are plotted with the corresponding primary cassiterites. Note that from Bukulja (Serbia) and the Mourne Mountains (Ireland) we only have secondary material. All individual analyses of the placer cassiterite data are given in the appendix in table A7.

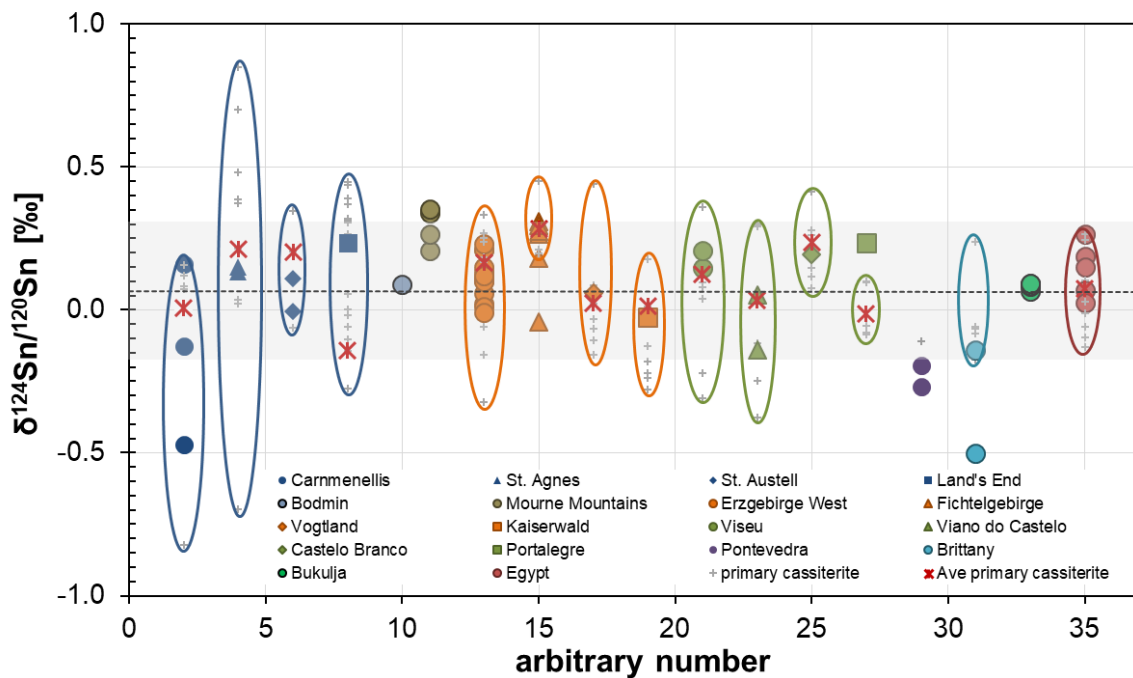


**Figure 6.12:**  $\delta^{124}\text{Sn}/^{120}\text{Sn}$  values versus an arbitrary number for the primary (grey crosses) and secondary cassiterites (colored symbols) from Europe and Egypt. The ellipses show the extension of the primary cassiterites for each region. The dotted line represents the average of all primary and secondary cassiterites from the presented areas of Europe and Egypt, the grey range shows the 2SD (the 2SD error bars are covered by the symbols).

The  $\delta^{124}\text{Sn}/^{120}\text{Sn}$  values for cassiterites from secondary deposits vary by 0.81 ‰ ranging from -0.50 (Brittany) to 0.31 ‰ (Fichtelgebirge; Fig. 6.12). Calculated with all the data presented in table 6.7, the overall  $\delta^{124}\text{Sn}/^{120}\text{Sn}$  averages for primary and secondary cassiterites are nearly the same, with  $0.07 \pm 0.46$  ‰ for the primary samples and  $0.05 \pm 0.39$  ‰ (2SD) for the secondary material. The placer and primary samples taken together have on average  $0.07 \pm 0.44$  ‰ (2SD) for  $\delta^{124}\text{Sn}/^{120}\text{Sn}$ .

The secondary cassiterite from SW England (Carnmenellis, St. Agnes, St. Austell, Land's End) has on average  $\delta^{124}\text{Sn}/^{120}\text{Sn}$   $0.03 \pm 0.43\text{‰}$  (2SD) and is ranging from  $-0.47$  to  $0.23\text{‰}$  (Fig. 6.12). The placer samples from the Saxonian-Bohemian province show a narrower spread with a range of  $-0.04$  to  $0.31\text{‰}$  and are lying within the overall average and the 2SD range. They have on average  $0.15 \pm 0.24\text{‰}$  for  $\delta^{124}\text{Sn}/^{120}\text{Sn}$  (Table 6.7).

**Table 6.7:** Mean values of the  $\delta^{124}\text{Sn}/^{120}\text{Sn}$  [%] isotope ratios of secondary cassiterite from Europe and Egypt. The data sets are given with 2SD. The primary cassiterites presented here are only from the mining areas where we have primary as well as secondary material. The overall averages of primary cassiterites of the different tin mining areas or granites are presented in chapter 6.2.1. Individual analytical results are given in the appendix (Table A7).

Area	Deposit	Mineralization	n	$\delta^{124}\text{Sn}/^{120}\text{Sn}$		$\delta^{124}\text{Sn}/^{120}\text{Sn}$ Median	
				Ave	2SD		
SWE	LEG, CG, SAG, SAUG, BM	Primary cassiterite	37	0.11	0.56	0.08	
		Secondary cassiterite	9	0.03	0.43	0.10	
Ireland	Mourne Mountains	Secondary cassiterite	5	0.30	0.13	0.34	
SBP	KW, EW, VL, FP	Primary cassiterite	36	0.10	0.40	0.17	
		Secondary cassiterite	23	0.15	0.24	0.16	
Portugal	CB, PL, VI, VC	Primary cassiterite	34	0.04	0.43	0.08	
		Secondary cassiterite	6	0.11	0.28	0.10	
Spain	Pontevedra	Primary cassiterite	1	-0.11	0.01		
		Secondary cassiterite	2	-0.23	0.11		
France	Brittany	Primary cassiterite	10	-0.07	0.27	-0.10	
		Secondary cassiterite	2	-0.32	0.51		
Serbia	Bukulja	Secondary cassiterite	2	0.08	0.01	0.09	
Egypt	IG, NU, AD	Primary cassiterite	7	0.07	0.31	0.03	
		Secondary cassiterite	5	0.12	0.16	0.15	
			Primary cassiterite	0.07	0.46	0.06	
			Secondary cassiterite	54	0.05	0.39	
			Total	0.07	0.44	0.08	

The placer cassiterites of Ireland ( $n=5$ ) have the heaviest isotopic composition with  $\delta^{124}\text{Sn}/^{120}\text{Sn}$   $0.30 \pm 0.13\text{‰}$ . The secondary samples from Portugal vary from  $-0.14$  to  $0.24\text{‰}$  ( $n=6$ ) with an average of  $0.11 \pm 0.28\text{‰}$  for  $\delta^{124}\text{Sn}/^{120}\text{Sn}$ . The two placer samples from Spain show lighter isotopic compositions with an average of  $-0.23 \pm 0.11\text{‰}$  for  $\delta^{124}\text{Sn}/^{120}\text{Sn}$  and the two placer samples from Brittany (France) have on average  $-0.32 \pm 0.51\text{‰}$ . The placer samples from Spain and France (Table 6.7) show the lightest isotopic compositions.

Bukulja (Serbia;  $n=2$ ) has on average  $0.08 \pm 0.01\text{‰}$  for  $\delta^{124}\text{Sn}/^{120}\text{Sn}$  (Fig. 6.12) and is therefore almost identical to the total mean value of the secondary cassiterites of all areas. From Bukulja we

have two different samples which were analysed three times each (Table A7). For Egypt the primary and secondary cassiterites fit quite well, with averages of  $0.07 \pm 0.31\text{‰}$  (2SD) and  $0.12 \pm 0.16\text{‰}$  (2SD) for  $\delta^{124}\text{Sn}/^{120}\text{Sn}$ . The placer samples correspond with the primary cassiterite mineralization, although the compositions of the placers are highly variable (Fig. 6.12).

### 6.2.3 Cassiterite versus stannite

The data set of stannite samples consists of 17 samples from SW England, the Saxonian-Bohemian province and Tajikistan (Mushiston, Chachmaniat). Table 6.8 shows the  $\delta^{124}\text{Sn}/^{120}\text{Sn}$  values of the individual mines and the average values for the different districts. In figure 6.13 the stannite samples are plotted with the corresponding cassiterites of the tin mining areas. For the deposit of Mushiston we only have stannite material (primary and secondary), therefore we compare the stannite from Mushiston with primary cassiterite from other tin ore deposits in Tajikistan.

The minerals of cassiterite and stannite show two distinct populations, where the stannite has a systematically lighter  $\delta^{124}\text{Sn}/^{120}\text{Sn}$  composition of  $-0.28 \pm 0.20\text{‰}$  on average than cassiterite from Europe and Central Asia with a far heavier isotopic composition of  $0.21 \pm 0.36\text{ (2SD) ‰}$ , calculated only for the cassiterites plotted in figure 6.13. The stannite samples vary by  $0.31\text{‰}$  ranging from  $-0.45$  to  $-0.14\text{‰}$  (Fig. 6.13, Table 6.8).

The stannite from SW England has on average  $-0.25 \pm 0.28\text{ (2SD) ‰}$  for the Cligga Head samples ( $n=2$ ) and  $-0.35 \pm 0.08\text{ (2SD) ‰}$  for the material from Hingston Down ( $n=2$ ), whereas the stannite from the Saxonian-Bohemian province ( $n=3$ ; Zinnwald) has on average the lightest isotopic compositions with  $-0.42 \pm 0.10\text{‰}$  for  $\delta^{124}\text{Sn}/^{120}\text{Sn}$  and lies outside of the 2SD range of the total stannite (Fig. 6.13). Tajikistan has a similar mean value to SWE with  $-0.21 \pm 0.15\text{ (2SD) ‰}$  for  $\delta^{124}\text{Sn}/^{120}\text{Sn}$ .

The secondary stannite material from Tajikistan is also presented here (Fig. 6.14). The two different sites in Tajikistan show different averages for the secondary stannite samples with  $-0.26 \pm 0.11\text{‰}$  for Mushiston ( $n=15$ ) and  $-0.11 \pm 0.02\text{‰}$  for Kani Nukra ( $n=1$ ) for  $\delta^{124}\text{Sn}/^{120}\text{Sn}$ , which could be due to the different number of samples. The common average for Tajikistan is  $-0.19 \pm 0.22\text{‰}$  for the secondary stannite material from both sites together, which is consistent with the composition of the primary stannites from Mushiston (Fig. 6.14, Table 6.8).

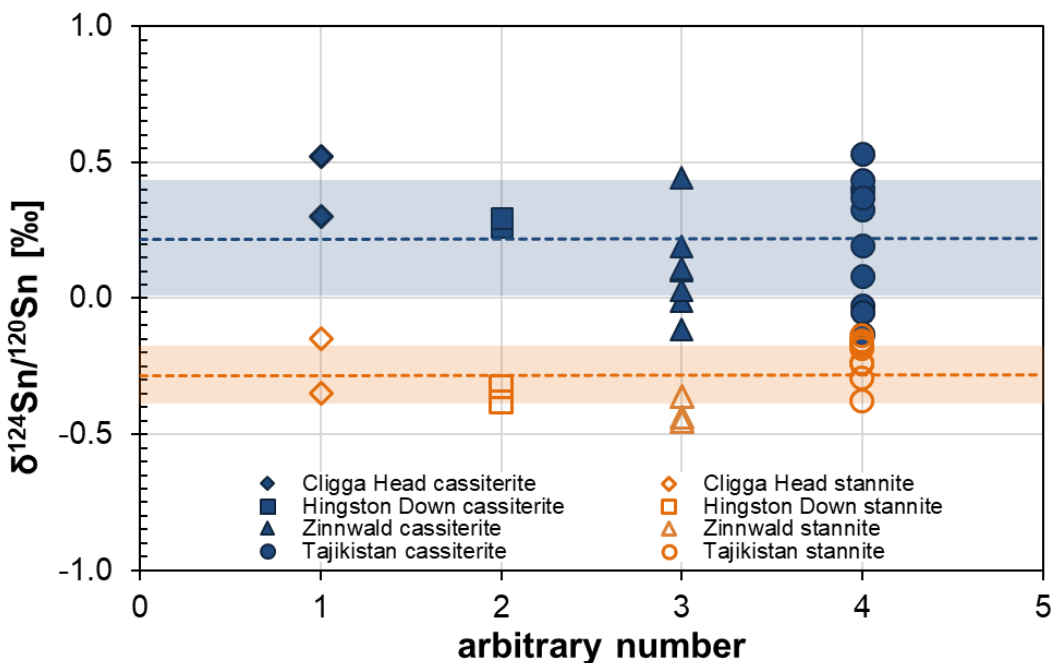


**Figure 6.13:** Primary cassiterite vs. primary stannite of SWE, SBP and Tajikistan. The blue dashed line represents the average for the cassiterite with 2SD (blue area) and the orange dashed line is the average of the stannite with 2SD (orange area); (the 2SD error bars are covered by the symbols).

The mean values of cassiterite and stannite show similar variations across the five deposits in SW England, the Saxonian-Bohemian province and Tajikistan. The  $\delta^{124}\text{Sn}/^{120}\text{Sn}$  range for cassiterite is 0.66‰ and for stannite 0.59‰. However, in each of these deposits, Sn in stannite has lower values for  $\delta^{124}\text{Sn}/^{120}\text{Sn}$  than cassiterite. The reported data are in accord with previous studies of Brügmann et al. (2017b) and Yao et al. (2018). Both found a distinctly lower value for Cornish stannite relative to cassiterite,  $-0.35 \pm 0.02\text{‰}$  ( $2\sigma$ ;  $n=6$ ) for  $\delta^{124}\text{Sn}/^{120}\text{Sn}$  and  $-0.19 \pm 0.04\text{‰}/\text{amu}$  ( $1\sigma$ ;  $n=5$ ), respectively. The studies used different preparation methods, for this work the method of Brügmann

et al. (2017b) was used, and the reproducibility shows that different preparation methods provide consistent analytical results for cassiterite and stannite.

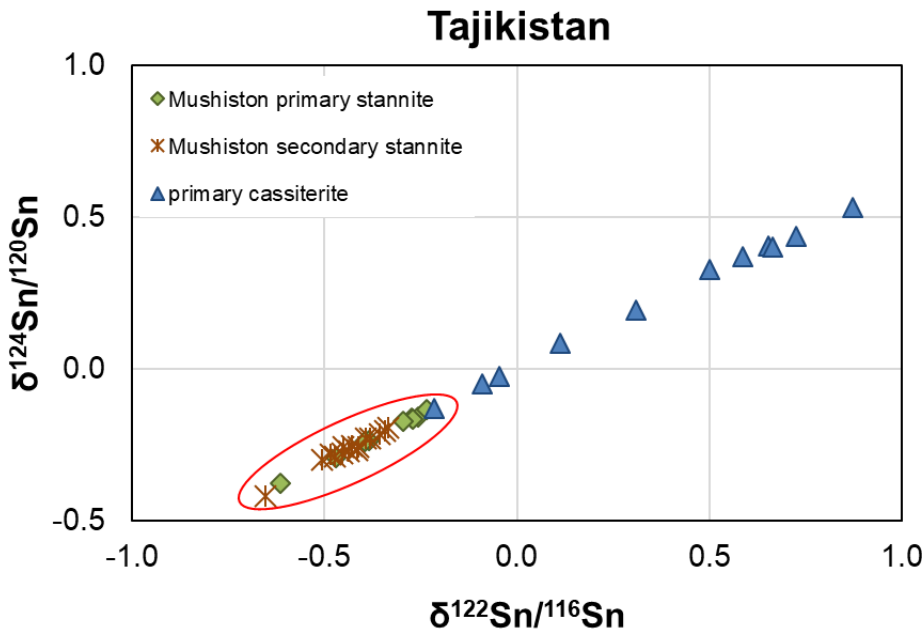


**Figure 6.14:** Primary vs. secondary stannite from Mushiston, Tajikistan (the 2SD error bars are covered by the symbols).

**Table 6.8:** Mean values of the  $\delta^{124}\text{Sn}/^{120}\text{Sn}$  [%] isotope ratios of the stannite samples. The data sets are given with 2SD. Individual analytical results are given in the appendix (Table A7). The Ave cassiterite is calculated only for the tin ore areas presented here with the corresponding stannite samples.

Area	Deposit	n	$\delta^{124}\text{Sn}/^{120}\text{Sn}$	2SD	$\delta^{124}\text{Sn}/^{120}\text{Sn}$
			Ave	Median	
SWE		4	-0.30	0.15	-0.34
	Cligga Head	Primary stannite	2	-0.35	0.08
	Higston Down	Primary stannite	2	-0.25	0.28
SBP	Zinnwald	Primary stannite	3	-0.42	0.10
Tajikistan	Chachmaniat	Primary stannite	1	-0.18	0.004
	Mushiston	Primary stannite	9	-0.22	0.16
	Mushiston	Secondary stannite	15	-0.26	0.11
	Kami Nukra	Secondary stannite	1	-0.11	0.02
Europe		Primary stannite	7	-0.34	0.17
Tajikistan		Primary stannite	10	-0.21	0.15
<b>Total</b>		Primary cassiterite	23	0.21	0.36
		Primary Stannite	17	-0.28	0.20
					-0.24

#### 6.2.4 Types of mineralization

To get an idea of how the mineralization types differ a distinction attempt was made based on the tables and information about the samples. Most of the samples are in the form of powder or cassiterite crystals, so an assignment to a mineralization type is complicated or not possible due to a lack of information about the host rocks. The samples with information about the mineralization type are plotted in figure 6.15.

Europe mainly has cassiterite in quartz and greisen veins (hydrothermal cassiterite), whereas Central Asia (Afghanistan) shows cassiterite in pegmatites. The pegmatite samples plotted for this chapter are from Afghanistan ( $n=38$ ), Spain and Portugal ( $n=3$ ). The greisen and quartz vein samples are mainly from the Iberian Peninsula, the Saxonian-Bohemian province, France, Italy and one sample from SW England ( $n=44$ ). The  $\delta^{124}\text{Sn}/^{120}\text{Sn}$  values for cassiterites from pegmatite mineralizations vary by 1.4 ‰ ranging from -1.27 to 0.13 ‰. The cassiterite from greisen and quartz vein type mineralizations indicates smaller fractionation effects ranging from -0.52 to 0.40 ‰ and from -0.29 to 0.43 ‰ for  $\delta^{124}\text{Sn}/^{120}\text{Sn}$  (Fig. 6.15).

The pegmatites are high temperature ( $>500^\circ\text{C}$ ) crystallisation products with a complex ore mineralogy often containing Nb-Ta-Ti oxides and cassiterite ( $\text{SnO}_2$ ), which is the most common tin mineral (Chesley et al. 1993). They tend to have lighter isotopic compositions (Fig. 6.15) with an average of  $-0.32 \pm 0.92$  ‰ (2SD) for  $\delta^{124}\text{Sn}/^{120}\text{Sn}$  than the hydrothermal greisen and quartz vein type deposits (low T) with  $-0.03 \pm 0.51$  (2SD) ‰ and  $0.14 \pm 0.37$  (2SD) ‰ for  $\delta^{124}\text{Sn}/^{120}\text{Sn}$ , respectively. The vein type deposits are related to granitic rocks (Štemprok 1987; Hall 1990; Štemprok 1995; Romer and Kroner 2016) and precipitated from hydrothermal fluids at temperatures  $< 400^\circ\text{C}$  (Chesley et al. 1993). With decreasing crystallisation temperature, the isotopic composition becomes heavier (Fig. 6.15 a).

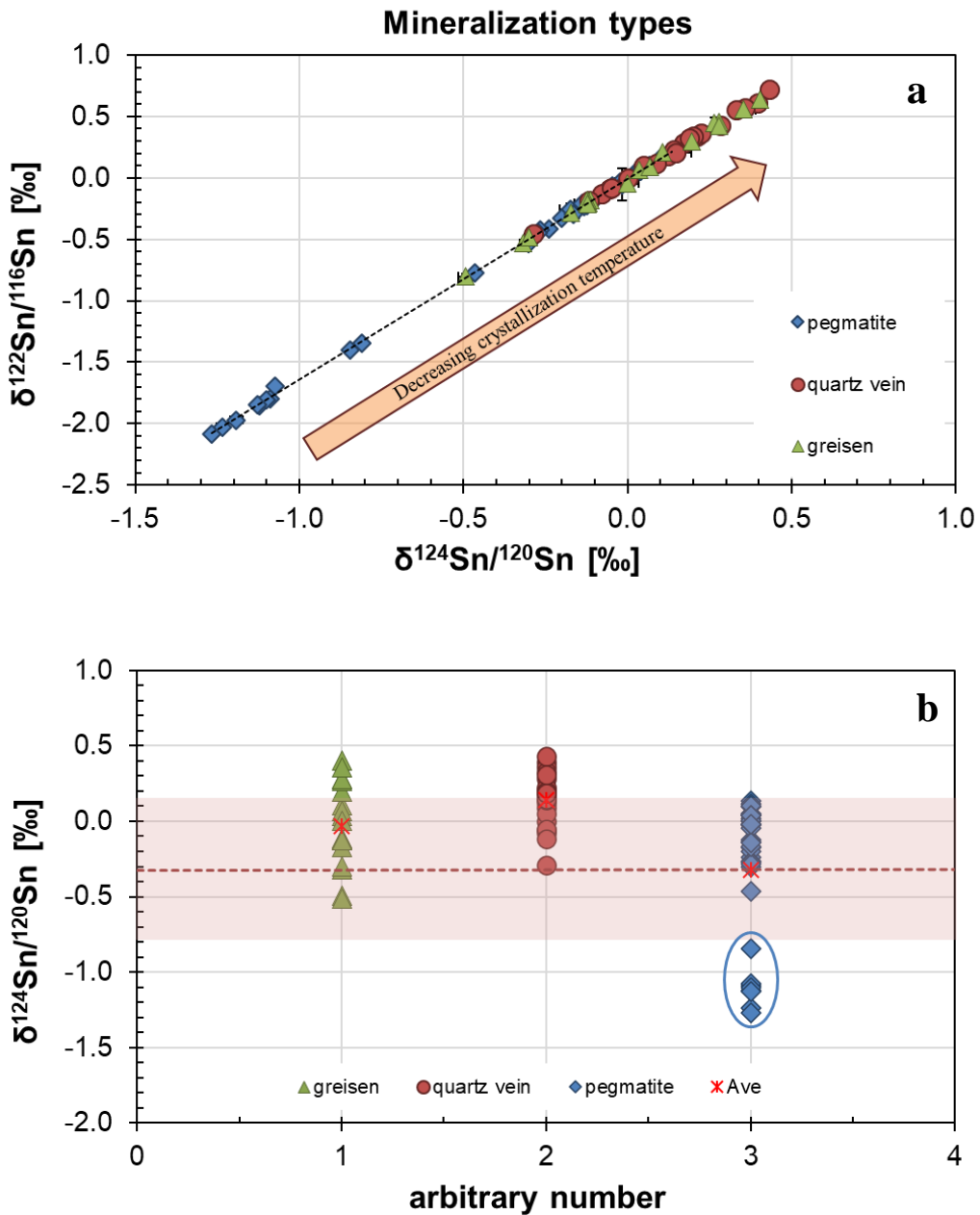


**Figure 6.15:** Differentiation of the various mineralization types (greisen, quartz vein and pegmatite). The blue framed pegmatites are from the Kunar region in Afghanistan. With decreasing crystallisation temperature the isotopic composition becomes heavier, with increasing temperature the composition becomes lighter (the 2SD error bars are covered by the symbols).

Considering the pegmatite samples from Afghanistan and Europe separately, the pegmatites from Afghanistan have on average lighter isotopic compositions with  $-0.34 \pm 0.95$  (2SD) ‰ for  $\delta^{124}\text{Sn}/^{120}\text{Sn}$  and the European pegmatites ( $n=3$ ) have  $-0.11 \pm 0.16$  (2SD) for  $\delta^{124}\text{Sn}/^{120}\text{Sn}$  (Fig. 6.15 b). Within Afghanistan the various tin mining areas have different averages, too. The Kunar mining

region shows the lightest isotopic composition with  $-1.11 \pm 0.05 \text{ ‰}$  for  $\delta^{124}\text{Sn}/^{120}\text{Sn}$  (Fig. 6.15 blue framed data), whereas the Dara-i-Pech region has the heaviest composition with  $-0.001 \pm 0.34 \text{ ‰}$  (Table 6.6).

### 6.2.5 Comparison with previous studies

Due to the advanced mass spectrometer technology, it was expected that the isotopic composition can be measured more precisely relative to previous techniques (NeptunePlus versus VG Axiom MC-ICP-MS, Haustein et al. 2010; Brügmann et al. 2017b). We repeated the analyses of several cassiterite samples from SW England and the Saxonian-Bohemian province. The results for the individual measurements are presented in table A9 in the appendix.

Figure 6.16 shows the  $\delta^{122}\text{Sn}/^{116}\text{Sn}$  vs  $\delta^{117}\text{Sn}/^{119}\text{Sn}$  data of the samples, which were analysed by Haustein et al. (2010) and the ERC project. The previously published data by Haustein et al. (2010) indicate a smaller range of values for  $\delta^{117}\text{Sn}/^{119}\text{Sn}$  with a range from  $-0.49$  to  $0.04 \text{ ‰}$  in contrast to the ERC data with a range from  $-0.47$  to  $0.35 \text{ ‰}$ , which is due to the two outlier samples from SW England. For  $\delta^{122}\text{Sn}/^{116}\text{Sn}$  the ERC data ( $-1.08$  to  $1.37 \text{ ‰}$ ) have a smaller range than the Haustein et al. (2010) data ( $-0.23$  to  $1.46 \text{ ‰}$ ; Fig. 6.16).

Comparing the two data sets it is evident that the new data follow the theoretically expected mass fractionation line very well and the scatter along this line is much smaller. Moreover, the individual analyses have smaller analytical uncertainties, which can be attributed to the more precise technical and chemical process. The combined uncertainty for  $\delta^{124}\text{Sn}/^{120}\text{Sn}$  is better than the  $0.03 \text{ ‰}$  for the tin standard solutions given by Brügmann et al. (2017b; Thermo Scientific Neptune Plus MC-ICP-MS equipped with nine Faraday cups). This represents an upgrade of 25 % of the data quality in contrast to studies by Balliani et al. (2013; quadrupole-based ICP-MS instrument, Thermo X-Series II,

Bremen, Germany) and Yamazaki et al. (2013; MC-ICP-MS, IsoProbe, Micromass, with nine Faraday cups).

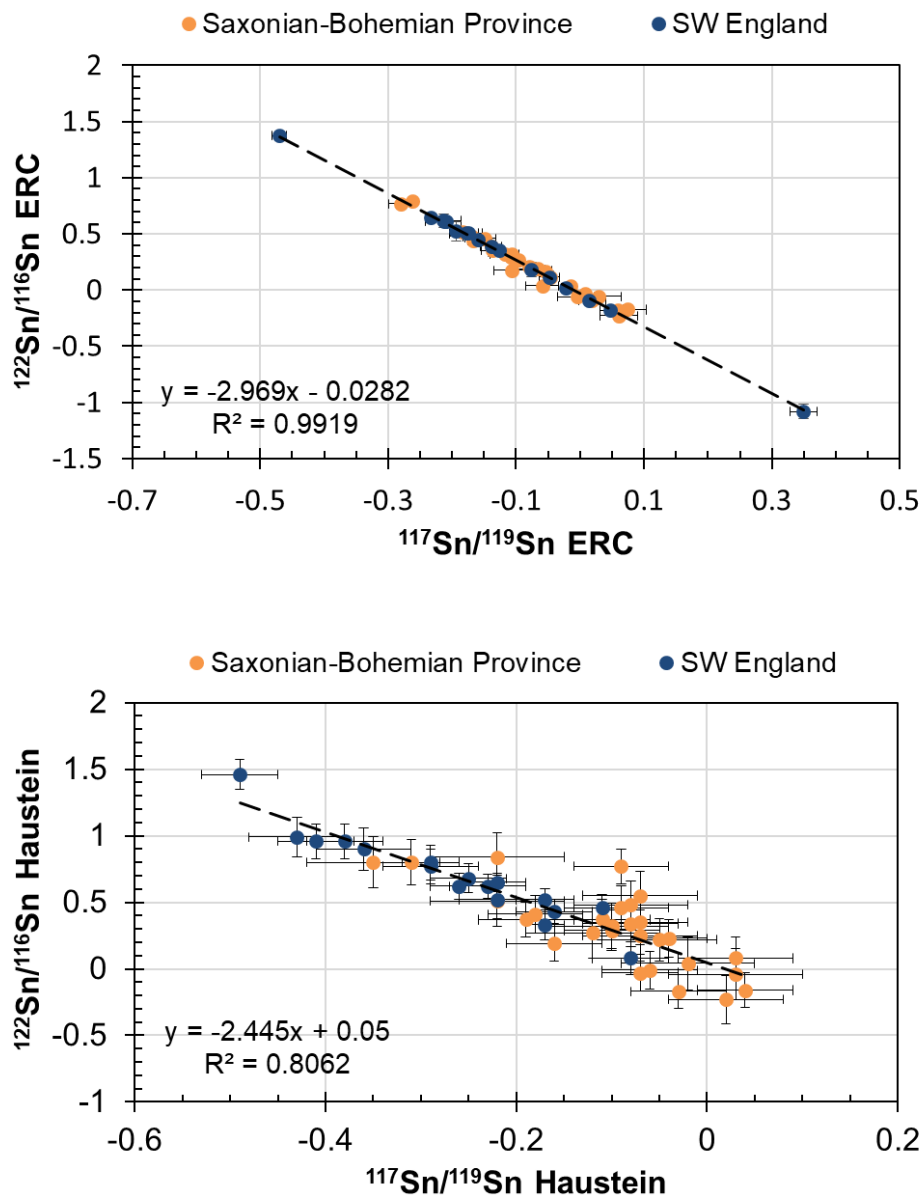


**Figure 6.16:** Comparison of the duplicate measurements of samples from the ERC project and Haustein et al. (2010).

## 7. SYNTHESIS AND CONCLUSIONS

The aim of this subproject from the ERC “Bronze Age Tin” project was to investigate the tin isotopic compositions of tin ore provinces, which could have been of importance in the Old World, like tin deposits in SW England, the Iberian Peninsula and the Erzgebirge of Germany and Czech Republic but also deposits in Central Asia and Egypt. During the work the following questions came up which needed to be answered:

- The stable isotopic composition of Sn in cassiterite could be a key petrological tracer monitoring the evolution of tin-bearing magmatic-hydrothermal fluid systems.
- Thus, the isotopic composition of cassiterite might also be used as a fingerprint discriminating ore deposits or provinces.
- What causes the isotopic variation in the tin ores (fractionation)?
- Is it possible to differentiate between the types of mineralization?
- Is it possible to distinguish primary and secondary cassiterite from each other?
- Which isotopic composition can be observed for stannite?

In this chapter an attempt will be made to answer the central questions. The primary and secondary cassiterite and stannite isotopic compositions are summarised in table 7.1 and the results are discussed below.

### 7.1 What do the results mean?

#### 7.1.1 Primary cassiterite

The primary cassiterites of the investigated areas form three clusters for  $\delta^{124}\text{Sn}/^{120}\text{Sn}$  (Table 7.1): (i) Spain ( $-0.07 \pm 0.22\text{ ‰}$ ), France ( $-0.005 \pm 0.15\text{ ‰}$ ) and Central Asia ( $-0.05 \pm 0.45\text{ ‰}$ ) with the lightest

isotopic compositions; (ii) SW England ( $0.10 \pm 0.29 \text{ ‰}$ ), the Saxonian-Bohemian province ( $0.12 \pm 0.18 \text{ ‰}$ ), Portugal ( $0.07 \pm 0.40 \text{ ‰}$ ), and Egypt ( $0.08 \pm 0.15 \text{ ‰}$ ) with intermediate isotopic compositions and (iii) Italy ( $0.30 \pm 0.10 \text{ ‰}$ ) with the heaviest isotopic composition.

**Table 7.1:** Summary of the cassiterite and stannite  $\delta^{124}\text{Sn}/^{120}\text{Sn}$  [%] averages of all investigated areas. The results are described in chapter 6.2 in detail. All individual data are given in the appendix (Table A1-A9; \*Secondary stannite of Tajikistan, Central Asia).

Area	Primary		Secondary		Stannite	
	cassiterite		cassiterite			
	$\delta^{124}\text{Sn}/^{120}\text{Sn}$	2SD	$\delta^{124}\text{Sn}/^{120}\text{Sn}$	2SD	$\delta^{124}\text{Sn}/^{120}\text{Sn}$	2SD
	Ave		Ave		Ave	
SWE	0.10	0.59	0.03	0.43	-0.30	0.15
Ireland	-	-	0.30	0.13	-	-
SBP	0.12	0.37	0.15	0.24	-0.42	0.10
Portugal	0.07	0.40	0.11	0.28	-	-
Spain	-0.07	0.35	-0.23	0.11	-	-
France	-0.005	0.31	-0.32	0.51	-	-
Italy	0.30	0.20	-	-	-	-
Serbia	-	-	0.08	0.01	-	-
Central Asia	-0.05	0.90	-0.26*	0.13*	-0.21	0.15
Egypt	0.08	0.31	0.12	0.16	-	-

Already Ballèvre et al. (2009) studied possible correlations within the Variscan fold belt (Fig. 4.2). They also investigated a correlation between Spain and France (group i) and SW England and the Saxonian-Bohemian province (group ii).

The two tin provinces of SW England and the Saxonian-Bohemian province show different ranges in the various mines but nearly the same averages with  $0.10 \pm 0.29 \text{ ‰}$  and  $0.12 \pm 0.18 \text{ ‰}$  for  $\delta^{124}\text{Sn}/^{120}\text{Sn}$  calculated based on single mines (Chapter 6.2.1). Comparing the isotopic compositions of cassiterites from SW England and the Saxonian-Bohemian province, it is obvious that these provinces are not distinguishable. The range of variation which is defined by the Saxonian-Bohemian samples lies in the core area of the SW England samples (Fig. 6.4 a and b). But it is possible to distinguish the provinces in detail examining each granite intrusion or tin province individually (Chapter 6.2.1 and Table 6.1 and 6.2). The granite bodies in every province can be divided into three

groups as well. The averages of SW England show three groups with (i) Carnmenellis (n=7) with  $-0.04 \pm 0.69 \text{ ‰}$  and Dartmoor (n=5) with  $-0.13 \pm 0.63 \text{ ‰}$  showing the lightest compositions of all granite intrusions, (ii) Land's End (n=17)  $0.11 \pm 0.51 \text{ ‰}$  and St. Austell (n=4)  $0.12 \pm 0.37 \text{ ‰}$ ; and (iii) St. Agnes (n=10)  $0.30 \pm 0.49 \text{ ‰}$ , Cligga Head (n=2)  $0.41 \pm 0.31 \text{ ‰}$  and Hingston Down (n=2)  $0.28 \pm 0.05 \text{ ‰}$  for  $\delta^{124}\text{Sn}/^{120}\text{Sn}$  with the heaviest isotopic compositions (Fig. 7.1). Hingston Down and Cligga Head show tendencies towards heavy isotopic compositions, but with only two samples per area this statement is not certain.

Between these three groups no spatial correlation can be made (Fig. 4.4, Chapter 4.2). All granitic bodies are of S-type and the samples and their information do not allow a more precise specification.

The averages of the different granite bodies in the Saxonian-Bohemian province (Fig. 7.1) show three groups as well: (i) Kaiserwald (n=11)  $-0.06 \pm 0.12 \text{ ‰}$  and the Vogtland (n=7)  $-0.001 \pm 0.24 \text{ ‰}$ ; (ii) Erzgebirge West (n=14)  $0.10 \pm 0.45 \text{ ‰}$  and Erzgebirge East (n=19)  $0.14 \pm 0.08 \text{ ‰}$  and (iii) Middle Erzgebirge (n=18)  $0.25 \pm 0.15 \text{ ‰}$  and the Fichtelgebirge (n=4)  $0.28 \pm 0.23 \text{ ‰}$  for  $\delta^{124}\text{Sn}/^{120}\text{Sn}$  with the heaviest isotopic compositions of the Saxonian-Bohemian province. A correlation between the granite types is difficult or even impossible. The Vogtland and the Fichtelgebirge for example have different isotopic compositions but are both composed of two-mica S-type granites. The Kaiserwald, which shows a similar composition like the Vogtland is of biotite S-type granite composition.

The mineralization in the Eastern, Middle and Western pluton of the Erzgebirge is primarily associated with greisen and vein systems (Powell et al. 2019). Tectonic movement in the Erzgebirge resulted in larger and more deeply eroded S-type plutons in the southwest, and smaller A-Type plutons in the northeast, which are more volcanic-associated (Breiter 2012). According to Powell et al. (2019) such variations in the geological setting are expected to be associated with different Sn isotope compositions among plutons. And although there is a huge overlap between the different tin ore regions, there is also a variation in mean and range, which was also shown by Powell et al. (2019). They found out, that the deeper level ores of the Western Erzgebirge tend to have lower  $\delta^{124}\text{Sn}/^{120}\text{Sn}$

values and the Eastern Erzgebirge tends to have higher values for  $\delta^{124}\text{Sn}$ , which is consistent with the data obtained in this work (Erzgebirge West  $0.10 \pm 0.45\text{‰}$  and Erzgebirge East  $0.14 \pm 0.08\text{‰}$  for  $\delta^{124}\text{Sn}/^{120}\text{Sn}$ ). The isotopic composition of the Eastern Erzgebirge and Cornwall ( $0.13 \pm 0.33\text{‰}$ ) are almost identical, however, Powell et al. (2019) show that Cornwall tends toward slightly higher values.

Within one granite it is possible to distinguish several mines or mining areas with Sn isotopy, like the Botallack mine ( $n=8$ ) and Penzance ( $n=2$ ) in the Land's End granite (Fig. 6.5). In the Western Erzgebirge it is possible to differentiate between the tin mining regions of Přebuz ( $n=3$ ) and Abertamy-Hřebečná ( $n=2$ ). Due to the few available samples per mine this should be considered a tendency only. On the other hand, it is not possible to distinguish between the three mines of Altenberg, Krupka and Zinnwald in the Erzgebirge East (Fig. 6.5).

The data within one tin mineralised area or granite form two groups or clusters in some extent, for example Dartmoor and the Vogtland (Fig. 6.4 a and b).

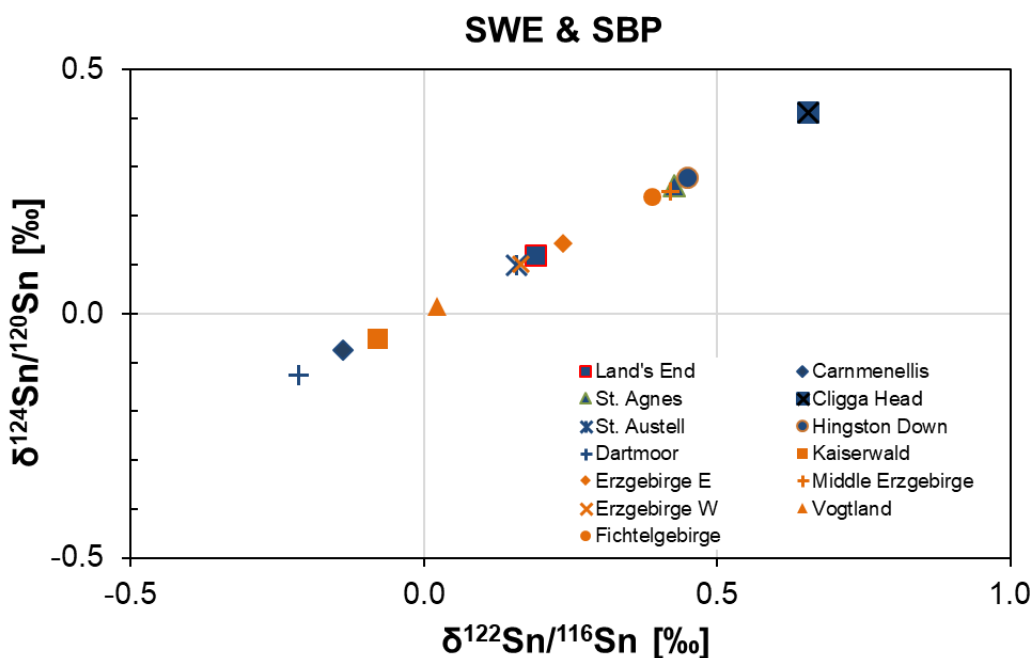


**Figure 7.1:** Averages of the granites respectively tin mining areas in SW England and the Saxonian-Bohemian province (the 2SD error bars are covered by the symbols).

To obtain a better picture more detailed studies of each single mining area would be required, but maybe this is related to the two main processes which lead to the formation of hydrothermal ore bodies, namely the separation of fluids directly from the crystallising magma and the later induction of external fluids. Or the full range is not yet covered due to the limited number of samples from these areas, and the gap could be closed with a more detailed study per area. The two samples in St. Agnes and Carnmenellis with the lightest isotopic compositions investigated in SWE (Fig. 6.4 a) could give a hint that our data set does not yet show the full spread of tin isotopic compositions of the granite. It is also possible that they are outliers in the measurement, but the large spread of all data speaks for the former argument.

Compared to SW England and the Saxonian-Bohemian province the samples from the Iberian Peninsula offer a slightly different picture. The cassiterite from Spain tends to have lighter isotopic compositions (Table 7.1) than the cassiterite from Portugal or SWE and the SBP and therefore the Spanish samples are well distinguishable from the Portuguese cassiterite samples. Within Portugal and Spain, the tin mining areas can also be grouped. In Portugal Castelo Branco and Bragança (E Portugal;  $0.18 \pm 0.21$  and  $0.17 \pm 0.34$  ‰ for  $\delta^{124}\text{Sn}/\delta^{120}\text{Sn}$ ) have intermediate tin isotopic compositions and Beja (S Portugal;  $0.31 \pm 0.02$  ‰ for  $\delta^{124}\text{Sn}/\delta^{120}\text{Sn}$ ) shows the heaviest isotopic composition. However, the full range of Sn isotope composition of cassiterite from Beja cannot be determined from only a single analysis. The other tin ore districts within Portugal have lighter isotopic compositions (Guarda, Portalegre, Porto, Viseu, Vila Real, Aveiro, Viana do Castelo; W/NW Portugal; Fig. 7.2). The samples of these groups can be allocated to the different geological zones described in chapter 4.5 due to their places of recovery. The lightest isotopic composition can accordingly be found in the Central Iberian Zone, the Galicia Tras os Montes Zone shows intermediate  $\delta^{124}\text{Sn}/\delta^{120}\text{Sn}$  values and the South Portuguese Zone (one sample from Beja) has the heaviest isotopic composition indicating a different tin isotopy in these geological zones.

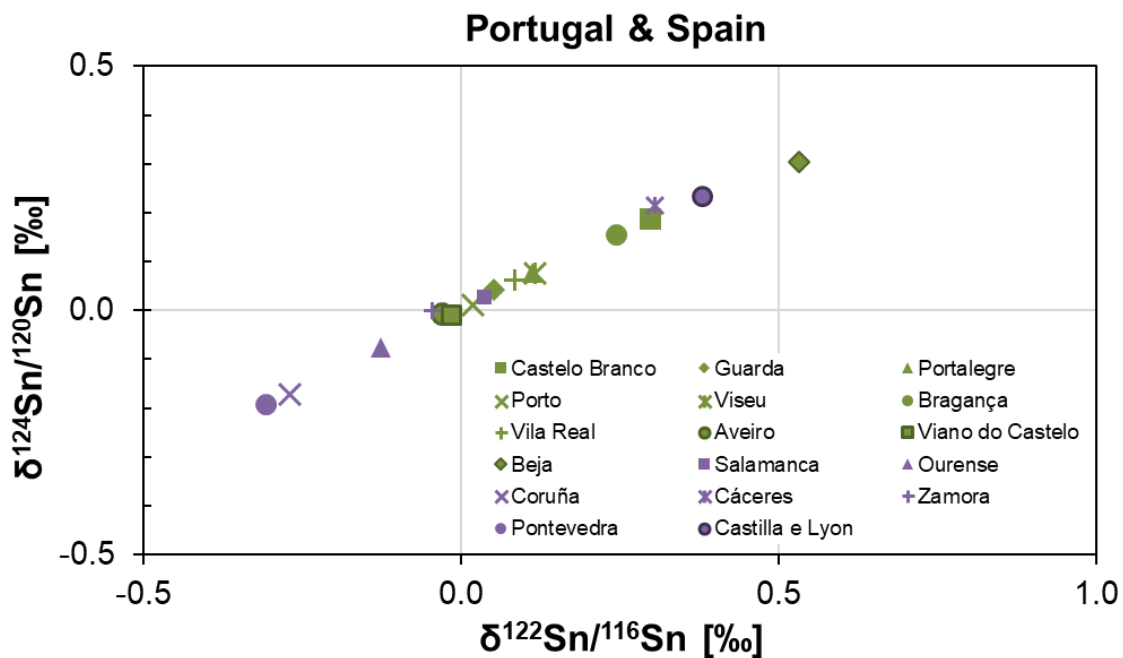


**Figure 7.2:** Averages of the granites respectively tin mining areas in Portugal (green) and Spain (purple; the 2SD error bars are covered by the symbols).

The districts of Spain can be divided into two groups, with Cáceres and Castilla e Lyon with heavier isotopic compositions for  $\delta^{124}\text{Sn}/^{120}\text{Sn}$  than Salamanca, Ourense, Coruña, Zamora and Pontevedra with lighter compositions (Fig. 7.2). All of the Spanish tin ore deposits belong to the Central Iberian Zone, except for Coruña, which lies in the Galicia Tras os Montes Zone (Fig. 4.7). Here the Central Iberian Zone has two different tin isotopic clusters, so there could be a gradient within this one zone. On the basis of this grouping in the Iberian Peninsula it is possible to spatially allocate the tin based on its isotopy to some extent.

Within one tin ore district it is partly possible to distinguish between different mines. The Covas do Estanho ( $n=2$ ) and the Sequeiros ( $n=1$ ) mines show the lightest ( $-0.31 \pm 0.03 \text{\%}$ ) and the heaviest ( $0.36 \pm 0.02 \text{\%}$ ) isotopic compositions of the Viseu district (Chapter 6.2.1). But the full range of Sn isotope composition of cassiterite from these two mines cannot be determined from one or two samples, the number of samples is not significant enough to make a clear distinction. It needs more

---

detailed studies on the single mines and their building conditions and more sample material from each single mine to make a reliable statement.

France with  $-0.005 \pm 0.15 \text{ ‰}$  belongs to the group with intermediate isotopic compositions, whereas Italy with  $0.30 \pm 0.10 \text{ ‰}$  for  $\delta^{124}\text{Sn}/^{120}\text{Sn}$  has the heaviest isotopic composition of all investigated areas (Table 7.1). Within France the two investigated areas of Brittany and Massif Central can be well distinguished on the basis of their tin isotopic compositions (Chapter 6.2.1). Italy with the heaviest isotopic composition of all investigated areas in Europe and Central Asia is a speciality. Details on the kind of material of the samples are not known. We only have the information that they are primary cassiterite, but no data about the mineralization type or the exact place of discovery is available, which is a problem for a detailed geological investigation and conclusions about the petrographical composition of a sample. But nevertheless, the two areas of Sardinia ( $0.26 \pm 0.14 \text{ ‰}$ , n=6) and Monte Valerio ( $0.43 \pm 0.02 \text{ ‰}$ , n=2) can be distinguished based on their different tin isotopic compositions.

Central Asia has the largest variation in all observed areas with  $1.94 \text{ ‰}$  ranging from  $-1.27$  to  $0.67 \text{ ‰}$  for  $\delta^{124}\text{Sn}/^{120}\text{Sn}$ . This extent of fractionation is observed in Afghanistan (n=39) and Uzbekistan (n=1). Afghanistan has the lightest isotopic composition of all investigated areas with  $-0.38 \pm 0.84 \text{ (2SD) ‰}$  for  $\delta^{124}\text{Sn}/^{120}\text{Sn}$  (Table 6.6). The samples are all of pegmatite type, so maybe pegmatite has lighter isotopic compositions than other mineralization types. In any case, Afghanistan is a special case. Tajikistan with  $0.19 \pm 0.45 \text{ ‰}$  (n=11) and Kyrgyzstan (n=1) with  $0.14 \pm 0.02 \text{ ‰}$  for  $\delta^{124}\text{Sn}/^{120}\text{Sn}$  build the intermediate group within Central Asia. Uzbekistan (n=1) shows the heaviest tin isotopic composition with  $0.67 \pm 0.03 \text{ ‰}$  of all areas in Central Asia. The one sample from the Lapas region in Uzbekistan was analysed 4 times, the same applies to Kyrgyzstan, where we only have one analysis from one sample ( $0.14 \pm 0.02$ ). These two regions will therefore not be subject of discussion. Also, Kazakhstan with only 2 samples will not be discussed. A clear statement is not possible due to the small number of samples.

Egypt with on average  $0.08 \pm 0.31 \text{ ‰}$  for  $\delta^{124}\text{Sn}/^{120}\text{Sn}$  for primary cassiterites belongs to the group with intermediate tin isotopic compositions (Table 7.1). Within Egypt Nuweibi has heavier isotopic compositions than the other two investigated areas and is therefore well distinguishable from those two (Table 6.10). An allocation to a specific granite type is not possible in this case because we only have cassiterite grains and thus no information about the mineralization type and the host rock.

Prospectively it could be possible to assign specific samples to the large European tin provinces with tin isotopy, but the overall averages overlap to a large extent. The results show that small local differences in the isotope composition of tin do exist. The Saxonian-Bohemian province as well as the SW England tin province comprise many tin deposits, which can be spatially separated from one another and can be related to specific granite intrusions but have great similarities in their tin isotopic composition. The reason for this similar variation is the fact that the deposits in both provinces are similar in terms of time and petrology, and therefore the processes leading to the isotope fractionation are the same. The same applies to all European tin ore deposits which were formed during the Variscan orogeny. The more or less same averages for some granites indicate the same source. On the other hand, the samples from the European as well as the Central Asian tin provinces show a very large range of isotopic compositions. This wide range shows that the source material of the granitic melt must be heterogeneous with different degrees of anatexis and fractional crystallisation (Brügmann et al. 2017a), like in Portugal, where the different geological zones like the CIZ, GTMZ and SPZ seem to have different tin isotopic compositions, thus a different origin and geology.

Summarized it is possible to discern mining areas on a more detailed scale with Sn isotopy, whereas the overall averages from the tin provinces are more or less the same. The consideration of the isotopic compositions on smaller levels or scales could be a helpful tool to get a detailed fingerprint of single mines or mining areas and for the assignment of tin bronze artefacts to certain tin ore mining areas. Together with archaeological methods, such as determination of origin by association with a particular production method or style of the artefacts within a distribution area, tin in artefacts could

---

be associated with a deposit or at least a tin isotopic group like with light, intermediate or heavy tin isotope compositions. This could at least narrow down the origin of the tin.

The granites must be examined in even more detail. A clear statement about many samples is in some cases difficult because with cassiterite crystals we do not have exact information about the provenance (like exact GPS coordinates) or what type of mineralization they are. Clear statements about tin ore areas with small amounts of samples are not very meaningful and can give only tendencies about the tin isotopic compositions.

### **7.1.2 Secondary cassiterite**

All secondary cassiterite samples fit with the associated primary occurrences (Fig. 6.12). This means that the single deposits in this province are homogeneous and that there is no significant difference between the primary tin ores and the placer deposits as already established by Haustein et al. (2010). For Bodmin Moor and the Mourne Mountains we only have secondary cassiterite material so a comparison with primary material is not possible.

The secondary cassiterite samples from Brittany show a lighter isotopic composition than the primary cassiterite sample of the associated area (Fig. 6.12). When the mean values of the placers do not fit the mean values of the primary ores it points to different mineralization types, respectively different provenances of the placers. All placer samples from SW England fit very well to their origin except one sample from the Carnmenellis granite (FG-011126) with -0.49 ‰ for  $\delta^{124}\text{Sn}/^{120}\text{Sn}$  (Appendix Table A7). This sample has a lighter isotope composition relative to the other secondary samples from Carnmenellis, which means that it could be an outlier sample (Fig. 6.12) or that it has another provenance and does not represent the tin isotopic composition of the Carnmenellis granite. But the Carnmenellis granite has another sample of primary cassiterite with a lighter isotopic composition, which could mean that we have not covered the whole area with our samples set yet as another

explanation besides the different types of mineralization. In the Carnmenellis Granite (SWE), the Fichtelgebirge (SBP), Pontevedra (Portugal) and Brittany (France) the entire range for their granites or tin mining areas is not covered yet with the samples sets because the placer samples constitute more populations and show for example lighter isotopic compositions than the primary cassiterites (Fig. 6.12). The placers represent the composition of the whole granite or tin area so the areas in between still have to be covered.

### **7.1.3 Stannite**

The stannite minerals of Europe and Central Asia have on average lighter  $\delta^{124}\text{Sn}/^{120}\text{Sn}$  compositions of  $-0.28 \pm 0.20\text{ ‰}$  (Chapter 6.2.3) than the cassiterite with a heavier isotopic composition of  $0.21 \pm 0.36\text{ ‰}$ , which shows a large Sn isotopic variation between cassiterite and stannite. This has been observed by the most recent studies too, although different methods for processing the samples were used (Brügmann et al. 2017b; Yao et al. 2018). This reproducibility shows that different preparation methods yield consistent analytical results for cassiterite and stannite. The observed shift is attributable to the oxidation of  $\text{Sn}^{2+}$  in the hydrothermal fluids, according to the mechanism which depend on oxidation for cassiterite precipitation (Heinrich 1990) and the results of the synchrotron experiments of Polyakov et al. (2005).

During mineralization in hydrothermal fluids Sn passes a redox reaction and therefore it is probable that the electron transfer required to form cassiterite or soluble  $\text{Sn}^{4+}$ - complexes favors the heavier isotopes of tin (Yao et al. 2018). The precipitation of cassiterite enriched with heavy Sn leads to residual dissolved Sn with lighter isotopic compositions (Yao et al. 2018). Tin in stannite forms later than cassiterite in the paragenetic sequence (Sugaki et al. 1981; Lehmann 1987; Chicharro et al. 2016; Yao et al. 2018). Therefore, the oxidation-driven precipitation of cassiterite left the hydrothermal solution enriched in tin of lighter isotopic composition, so the oxidation of the residual  $\text{Sn}^{2+}$  resulted in the precipitation of stannite with negative  $\delta^{124}\text{Sn}/^{120}\text{Sn}$  values. The  $\text{Sn}^{4+}$  is less

compatible compared to Sn<sup>2+</sup> during partial melting and is enriched in the silicate melt with heavier isotopes, whereas the Sn<sup>2+</sup> is enriched with lighter isotopes in the residue (Wang et al. 2018). That means for an ore deposit that the isotopic shift can be recorded in the Sn isotope composition of the paragenetically earlier cassiterite (heavy isotope enriched) and of the late-stage stannite (light isotope enriched; Yao et al. 2018). In hydrothermal systems the early formation of cassiterite and the late formation of stannite is well established by detailed ore microscopy work on tin provinces like Cornwall (Jackson et al. 1982) and Spain (Chicharro et al. 2016).

#### **7.1.4 Types of mineralization**

The types of mineralization described in chapter 6.2.4 overlap to a large extent. A clear distinction between high-T (pegmatite) and low-T (quartz vein, greisen) mineralizations is possible with the pegmatites from the Kunar region in Afghanistan. This could be a hint for possibly different sedimentary sources for the granites in Afghanistan (n=38) in contrast to Europe (n=3). The different composition of the source material results in different tin isotopic compositions. Figure 7.3 shows the isotopic composition of cassiterite in pegmatites from Afghanistan compared to primary and secondary cassiterite in Central Asia (mineralization types unknown). The samples marked as cassiterite and secondary cassiterite are not specified in more detail in the tables, but their isotopic composition fits to low-T mineralizations (Fig. 6.15, Chapter 6.2.4). All these samples marked as pegmatite material are from the Gangral mine, Paprok mine, Dari-i-Pech, Alingar and Kunar region in Afghanistan and have the lightest averages of all samples ( $-0.34 \pm 0.95 \text{ ‰}$  for  $\delta^{124}\text{Sn}/^{120}\text{Sn}$ ). The Kunar mining region has the lightest isotopic composition (Fig. 7.3 blue marked data).

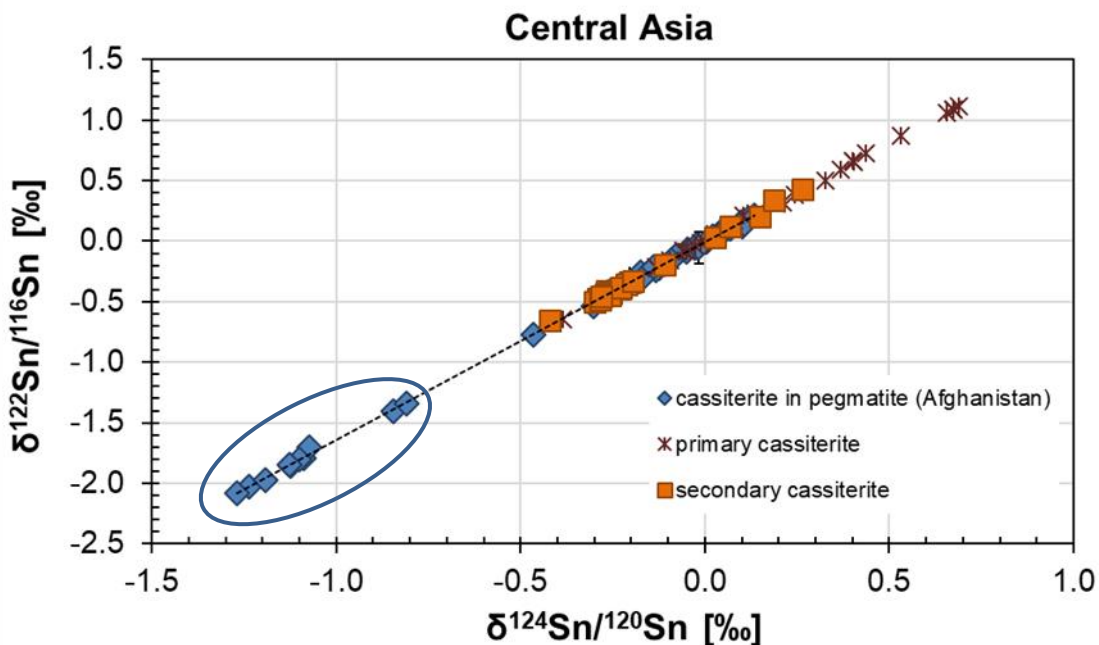


**Figure 7.3:** Pegmatites from Afghanistan vs. primary and secondary cassiterite from Central Asia (the 2SD error bars are covered by the symbols).

The pegmatites from Afghanistan have even lighter isotopic composition than the stannites from Tajikistan ( $-0.21 \pm 0.15 \text{ ‰}$  for  $\delta^{124}\text{Sn}/^{120}\text{Sn}$ ), although its stannite shows the lightest isotopic compositions compared to the cassiterite from the same region (Chapter 6.2.3).

The chronology of the crystallisation provides information about the genesis of the different mineralization types (Fig. 7.4). Pegmatites emerge as plutonic rocks from the slow cooling of granitoid residual melts. The residual melt is enriched with REEs and other elements which, due to the size of the ionic radius, do not fit into the lattice structure of already crystallising minerals.

The simultaneous presence of water lowers the individual mineral melting point, which is why the slow cooling of the rock melt promotes crystal growth. In addition, due to their high mobility, the residual melts can penetrate into existing rock fissures or cavities and solidify there (Okrusch and Matthes 2005). After that the greisen and quartz veins crystallise. If all mineralization types of one deposit originate from one source, they do not differ either (Fig. 7.4).

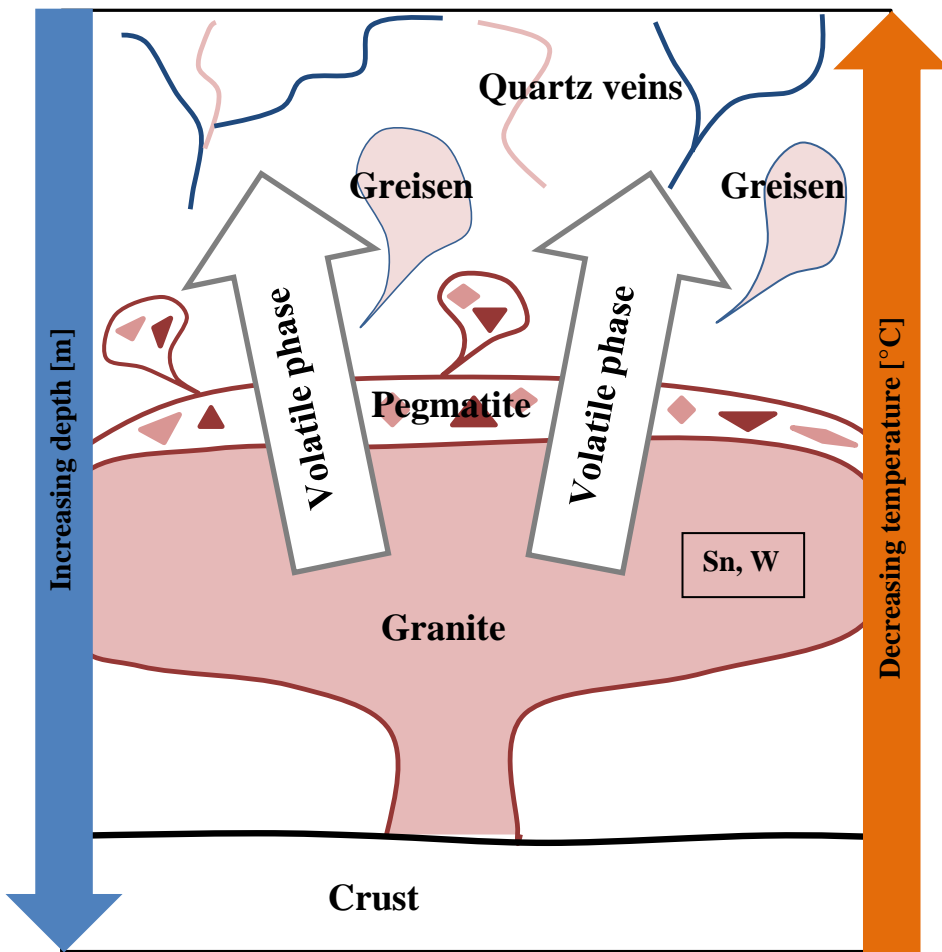


**Figure 7.4:** Simplified schematic illustration of the stratigraphy of the mineralization of pegmatite, greisen and quartz veins.

The pegmatites from Afghanistan, at least from the Kunar region, should have another source compared to the other mineralization types there, but this can not be verified because we do not have enough pegmatitic material from Europe for a comparison with the other European mineralization types. Afghanistan represents a special occurrence which needs more detailed studies.

Cassiterite did not crystallise in one stage (e.g., greisenisation) and was deposited in various generations, which is shown by the systematic compositional change of the cassiterite (Haapala 1997). Experiments show that the solubility of cassiterite in granitic melts decreases with decreasing temperature and increasing  $f(O_2)$  as well as with decreasing  $(Na+K)/Al$  and  $Na/K$  of the melt. Tin as

$\text{Sn}^{2+}$  is a highly incompatible element under reducing conditions in granitic systems and it fractionates in the residual melt and thus, the content of Sn in feldspar and quartz-rich granites is lower than in the melt from where it crystallised (Linnen et al. 1992; Wang et al. 2018). The mean values of the cassiterite from the various deposits are different and this can indicate that the initial Sn isotope composition in the early formed cassiterite relates to variations in the source or magmatic processes. Therefore, tin isotope compositions have the capability to give information on petrological sources or processes and redox geochemical reactions (Yao et al. 2018).

On the basis of our data, it is not possible to distinguish between the different mineralization types because the samples are mostly available in powder form only and there is no exact indication in the tables, since they are from an older collection. The samples which can be clearly distinguished in greisen and quartz veins do not show any great differences in the tin isotope composition (Fig. 6.15 b) except for the Kunar region in Afghanistan (Fig. 7.3).

The large overlap respectively variation within tin ore areas but also within individual deposits points out that the development of fluids in pegmatite and hydrothermal systems is mainly controlled by mixing processes, temperature gradients and fractional crystallisation of cassiterite (Černý et al. 2005).

## 7.2 Possible causes of fractionation in tin ores

In order to distinguish different types of mineralization (Chapter 6.2.4 and 7.1.4) and their petrogenesis one has to answer the question what causes the isotopic variation in the tin ores.

After Haustein et al. (2010) the cause of tin isotope fractionation in natural minerals and metal artefacts is still unknown. Their data provide no petrological information on the evolution of tin-bearing magmatic-hydrothermal fluid systems. Badullovich et al. (2017) have presented evidence for a mechanism that induces isotopic variation of tin-partitioning of  $\text{Sn}^{4+}$  between magma and ilmenite

during fractional crystallisation of basalt. The chemical behavior of Sn changes as a function of oxygen fugacity. During crystallisation of silicates the Sn isotopes are unfractionated, but during the precipitation of ilmenite they reduce to lighter values (Badullovich et al. 2017). According to Yao et al. (2018) high-temperature geological processes fractionate tin isotopes and lead to the variation measured in these materials. They make the fractionation associated with oxidation responsible for the observed isotopic variations in their sample material. Because tin passes a redox reaction in hydrothermal fluids during mineralization, it is probable that the electron transfer, which is necessary for cassiterite formation, favours the heavier isotopes of tin (Yao et al. 2018). In hydrothermal systems the fractionation of Sn isotopes may be related to several variables: formation of various Sn compounds in solution, electron transfer, temperature, pressure, liquid-vapor partitioning, competing bonding environments, and equilibrium processes, which are responsible for the division of Sn into different phases (Yao et al. 2018). In hydrothermal fluids tin is transported in the reduced state ( $\text{Sn}^{2+}$ ), but the formation of cassiterite and stannite needs an oxidative transformation to  $\text{Sn}^{4+}$  (Yao et al. 2018). It has been demonstrated multiple times that the oxidation of multivalent metals gives a significant isotopic fractionation favoring the heavy isotopes (Dauphas et al. 2009; Dauphas et al. 2014; Domagal-Goldman and Kubicki 2008; Sherman 2013; Badullovich et al. 2017; Yao et al. 2018). After Polyakov et al. (2005) the oxidation state has a large effect on fractionation of Sn, based on INRXS and Mössbauer spectroscopy experiments. Yao et al. (2018) established a possible fractionation due to high-temperature redox changes because low-temperature processes or partitioning between co-precipitating minerals complicate the hydrothermal Sn isotopic system examined in their experiments.

The average Sn isotope composition of a mining region probably corresponds to the source rock from which the tin granite was formed and the distribution of Sn between the magma and the residual rock. Therefore, isotope variations of deposits could originate from the fractionation during ore genesis (Powell et al. 2019).

Since precipitation of cassiterite requires the oxidation of tin from  $\text{Sn}^{2+}$  to  $\text{Sn}^{4+}$ , the stronger bonding environment associated with oxidized tin benefits the heavier isotopes (Yao et al. 2018; Wang et al. 2019), and the enrichment of lighter isotopes over time occurs (Yao et al. 2018). According to Powell et al. (2019) small and fast formed ores should have more homogenous isotope compositions while larger deposits should show more heterogenous and zoned isotope signatures, because the reaction front was advanced with time. In addition, the formation of vapor during ore formation triggers the fractionation of tin isotopes, which leads to the accumulation of heavier isotopes in the vapor and lower  $\delta^{114}\text{Sn}$  values in the residual liquids (Wang et al. 2019; Powell et al. 2019). These could lead to specific fingerprints of tin ore areas or bodies which could be merged with those of their derived metals (Powell et al. 2019).

### 7.3 Further studies

Tin could be fractionated by the equilibrium fractionation between co-existing Sn-oxide and Sn-sulphide or by kinetic fractionation during dissolution or precipitation of Sn into or from a fluid or melt (McNaughton and Loss 1990). The equilibrium fractionation represents the difference between Sn-oxides (cassiterite) and Sn-sulphides (stannite), whereas the kinetic fractionation is the difference between high-T (pegmatite) and low-T (vein type mineralization) cassiterites. A differentiation between these mineralization types is almost impossible based on our data with the pegmatites from Afghanistan representing the only particularity. More detailed studies on the mineralization types are needed to be able to draw clear conclusions. This requires samples of the host rock rather than just tin minerals or powder samples.

The question of the cause of the mass-dependent fractionation, which was found in the cassiterites from the various deposits, cannot be answered within this work and our analysis. The tin behavior during the tin ore formation, from the partial melting in the source, the fractional crystallisation of the granitic melt to precipitation in the hydrothermal fluid needs more research. Which processes

have finally led to the fractionation within the deposits is not conclusively clarified, since the granites or deposits have not been investigated in detail. This work gives an overview about the important tin provinces and enlarges the database. More studies about the fractionation and detailed studies about special deposits could be of importance, for example trace element studies of the tin ores and whole rock analyses to get an idea about the composition of the host rocks of the tin ores. After Haapala (1997) the electron microprobe analyses of the major elements show that the  $\text{Nb}_2\text{O}_5+\text{Ta}_2\text{O}_5$  and FeO contents in cassiterite decrease from granite through pegmatite to greisen in order of decreasing crystallisation temperature. This kind of analysis could be of importance in identifying the types of mineralization.

The provinces that form two clusters also need more detailed studies (e.g., Fig. 6.4 St. Agnes, Carnmenellis and Dartmoor) in order to find out whether the individual samples are outliers in the measurements or if the areas have such wide spreads. Furthermore, a closer look at the different tin isotope data of the Iberian Peninsula could be interesting because the different geological units seem to have different tin isotope compositions (Chapter 6.2.1). Each unit should be examined for its tin isotopy with even larger data sets which can be compared to its geology, host rock composition and genesis. More detailed studies could clarify even more questions such as the existence of the three tin isotopic groups which were found in the averages of the tin provinces (Chapter 7.1.1).

## 7.4 Significance for archaeology

In archaeology, it was unclear for a long time that in the third millennium BCE a material appeared that gave its name to an entire cultural epoch, namely the alloy of copper and tin called bronze. Copper deposits are relatively widespread, but very few tin deposits are known in the Old World (Europe, the Mediterranean region and southwest Asia). Since the late 19th century, archaeologists have debated the question of the origin of the tin which was used to produce the earliest bronzes,

without finding a clear answer. The question has even grown in recent decades, as the earliest bronzes have been found to appear in a wide area from the Aegean to the Persian Gulf that is geologically devoid of any tin deposits. Tin is widespread in Western and Central Europe and also in Central Asia (Pernicka 1998). Thus, tin or bronze seems to have been traded over long distances, but it is unknown in which direction.

With the new method of tin isotope analysis, it has become possible to trace ancient tin via tin isotope signatures. First results were obtained by Gale (1997), Begemann et al. (1999), Gillis et al. (2003) and especially Haustein et al. (2010).

In 2013 a large-scale project on the application of tin isotope analysis applied to the provenance of tin in the Bronze of Eurasia began with the support of the European Research Council (Advanced Grant no. 323861). Until then, the Nebra Sky Disk and some Iron Age and Roman finds from Spain were the only artefacts that had been investigated in terms of tin isotopes, but they did not provide clear evidence of the origin of tin in the earliest bronzes of the Near East and the eastern Mediterranean (Berger et al. 2014). Since then, a number of tin artefacts and tin deposits have been investigated by Berger et al. (2014, 2018, 2019), Brügmann et al. (2017a, b), Marahrens et al. (2016), and Nessel et al. (2018, 2019), for example the investigation of 27 tin ingots from Late Bronze Age sites in the eastern Mediterranean Sea (Mochlos, Uluburun, Hishuley Carmel, Kfar Samir south, Haifa; Berger et al. 2019). Together with the lead isotope composition and in combination with trace element studies the Cornish tin ores (potentially from Carnmenellis) are the most probable sources for the tin, because there is also some archaeological evidence for trading contacts between SWE and the central Mediterranean area via the lands between them (Muhly 1973, 1985). However, other European tin provinces should not automatically be disregarded (Berger et al. 2019). This example shows that more research on the isotope and chemical composition of tin ores and artefacts together with trace element studies during smelting is necessary to consolidate conclusions like that. Although there is no new archaeological evidence, the analytical results of Berger et al. (2019) could contribute to answering the old question about the sources of tin.

Berger et al. (2018) also investigated the tin ore smelting procedure under prehistoric conditions by smelting experiments that were carried out in the laboratory and in the field. They found out that the experimental smelting of cassiterite in a bowl furnace unveiled significant fractionation of stable tin isotopes during the conversion of tin oxide to metallic tin. The open designed furnace during the field experiments favoured the formation of flue gas and thus increased loss of tin with a total tin recovery of maximum 30 % in the field experiments, whereas the laboratory experiments yielded significantly higher recovery rates due to ideal reducing conditions. The fractionation of metallic tin relative to the original ore was comparable and rather low ( $\Delta^{124}\text{Sn} = 0.09$  to  $0.18 \text{ ‰}$ ; Berger et al. 2018), although different conditions and tin yields prevailed in the laboratory and field experiments. Berger et al. (2019) propose to include a fractionation factor of  $0.25 \text{ ‰}$  when trying to trace back the tin in metal artefacts to its deposit. Since metallic tin is usually isotopically heavier than the corresponding cassiterite, it can always be assumed that the original composition of the tin ore is isotopically lighter than the resulting tin-bearing artefact (Berger et al. 2018). The variation in the tin isotopic ratios of cassiterite from tin ore provinces like SW England ( $\delta^{124}\text{Sn} = -0.82$  to  $0.85 \text{ ‰}$ ), the Saxonian-Bohemian province ( $\delta^{124}\text{Sn} = -0.32$  to  $0.49 \text{ ‰}$ ) or the Iberian Peninsula ( $\delta^{124}\text{Sn} = -0.52$  to  $0.54 \text{ ‰}$ ) are much greater than the fractionation resulting from the smelting process (Haustein et al. 2010; Berger et al. 2018).

For the determination of the provenance of tin in bronze or tin metal artefacts data of the single granites or mining areas should be used as opposed to the overall averages of a country or district with their large overlap. Because the areas in detail are partially distinguishable from each other it could be possible to assign an artefact to its tin ore sources. The analysed reference alloys of BAM 211 (10.6 wt% Sn, 87.7 wt% Cu, < 1 wt% Zn and Pb) and IARM-91D (6.4 wt% Sn, 81.9 wt% Cu, 7.8 wt% P and 3.2 wt% Zn; Brügmann et al. 2017b) make a good basis for the comparison of future data sets and their quality. With the tin isotopy in combination with other methods like lead isotopy and chemical investigations like trace element studies it could be possible to approximate the origin

of the tin in the artefacts (Berger et al. 2019). They also postulate that the radiogenic lead in the artefacts could give indications about the geological model ages of the parental tin ores.

Tin deposits in SW England and the Saxonian-Bohemian province are potentially important tin sources for Bronze Age objects in Central Europe. Overall, the isotopic composition in cassiterite in these provinces varies by more than 1 ‰ for  $\delta^{124}\text{Sn}/^{120}\text{Sn}$ . However, the isotopic composition from both provinces and also from the other investigated areas in Europe and Central Asia overlap to a large extent. This observation makes distinct assignments of bronze artefacts to a specific province very difficult. Exceptions are bronze objects having extreme heavy or light tin isotope compositions, where an assignment to a specific ore district or deposit might be possible.

In the establishment and spread of tin bronze in Central Europe at the beginning of the 2<sup>nd</sup> century BC the Únětice culture played a significant role (Berger et al. 2014). The artefacts from the Únětice culture with tin bronzes > 3 wt% Sn from several large hoards show a fairly small isotopic variation of  $\delta^{124}\text{Sn}/^{120}\text{Sn}$  of  $0.25 \pm 0.03 \text{ ‰}$  (Brügmann et al. 2017a; Berger et al. 2018; Nessel et al. 2018). Approximately 30 % of the primary cassiterite samples from the Saxonian-Bohemian province have these heavy tin isotopic compositions (Fig. 6.4 b). Berger et al. (2018) assume that the fractionation is mainly due to complete tin smelting with 20 to 30 % recovery. Thus, the original ores used to produce the bronze artefacts should have had  $\delta^{124}\text{Sn}$  values in the range of -0.04 to 0.21 ‰ with average values of 0.15 ‰ (30 %) and 0.06 ‰ (20 %), respectively. Such tin ore compositions can be found in the Erzgebirge East ( $0.14 \pm 0.08 \text{ ‰}$  (2SD)) and Erzgebirge West ( $0.10 \pm 0.45 \text{ ‰}$  (2SD); s. Chapter 6.2.1), whereas the Kaiserwald ( $-0.06 \pm 0.12 \text{ ‰}$  (2SD)) and the Vogtland ( $-0.001 \pm 0.24 \text{ ‰}$  (2SD)) are less likely to be a tin source because of their low tin isotope compositions. The  $\delta^{124}\text{Sn}/^{120}\text{Sn}$  of the Middle Erzgebirge ( $0.25 \pm 0.15 \text{ ‰}$  (2SD)) and the Fichtelgebirge ( $0.28 \pm 0.23 \text{ ‰}$  (2SD)) would not be expected to be processed to tin metal because of their heavier isotope compositions, so they are less likely to be a tin source for the Únětice bronzes too (Berger et al. 2018). These comparisons can be made for any other tin-bearing metal object, since the fractionation

during tin smelting is always about 0.1 - 0.2 ‰ (Berger et al. 2018) or rather 0.25 ‰ (fractionation factor presented by Berger et al. 2019).

Powell et al. (2019) also studied four tin sources (Cornwall, Erzgebirge East, Middle and West) and compared the tin isotope data with those of several Bohemian hoards (Habří, Kroclov, Kučeř, Slavč, Veselíčko). They characterized the isotope composition of these regions and of several tin-bearing artefacts to investigate indications that the tin ores of the Erzgebirge were already mined in the Bronze Age. They found a difference in the isotopy of older and younger ingots, namely the older ingots have a modal peak of  $\delta^{124}\text{Sn}$  0.65 ‰ whereas the younger artefacts show a  $\delta^{124}\text{Sn}$  modal peak of 0.4 ‰. This could point to a change of the tin ore sources from the Early-Middle Bronze Age to the Middle and Late Bronze Age. Including the 0.25 ‰ per amu correction factor for smelting induced fractionation presented by Berger et al. (2019), it is 99.8% likely that the tin ore comes from the Middle Erzgebirge, whereas it is 98.7% possible that the tin was of British origin without including the factor (Powell et al. 2019). The Middle Pluton of the Erzgebirge seems to be the more probable origin for the tin, because there is no archaeological evidence that there was a trading connection between SWE and the SBP in the Early Bronze Age. Powell et al. (2019) support the experimental finding of Berger et al. (2019) and recommend the use of the correction factor for future Sn provenance studies. This is a good example of how tin isotope analysis can support and consolidate archaeological questions and the data presented here may be useful for further investigations of Bronze Age tin artefacts and the trading of tin.

The Balkan region is also mentioned as an important tin source for a large number of Bronze Age artefacts. The idea of the Balkans as a possible tin source for bronze artefacts from these territories appears for the first time in the early 20<sup>th</sup> century, at the same time when an interest for origin of tin in prehistoric bronzes increases (Mladenović 2017). In the Balkans and Eastern Mediterranean a large number of bronze artefacts were recorded and this raises the question of available deposits, exploitation and distribution of tin in this area (Mladenović 2017). Studies of tin sources (Charles 1975; Muhly 1985; Maddin et al. 1977; Gillis et al. 2003) usually do not mention tin ores from the

Balkans, instead Cornwall, the Iberian Peninsula or Central Europe, and less frequently Brittany, Sardinia and Tuscany are mentioned. These latter sources were probably not used during the Bronze Age (Muhly 1985; Penhallurick 1986; Niederschlag et al. 2003) and researchers tend to overlook the Balkans when it comes to possible trade and exchange routes of tin, copper and bronze between Central and Southeastern Europe (Mladenović 2017). After McGeehan-Liritzis and Taylor (1987) Western Serbia is the closest tin-rich area to the Aegean and the tin for the bronze production could have been supplied from there. The existence of tin ores in West Serbia and a possible connection between these ores and the Bronze Age cultures in South Serbia were presented in a major work by Durman (1997). The presence of several copper sources in West Serbia makes the tin from Cer and Bukulja even more valuable (Durman 1997). It is possible that bronze was alloyed direct on site or that the tin was transported as a finished product (e.g., ingots), which is evident from Bronze Age shipwreck finds (Hauptmann 2010). For the tin source of Bukulja there is no archaeological evidence for tin mining in prehistory (Powell et al. 2020) and no clear correlation between the tin isotope composition of these ores and local artefacts, even when the 0.25 ‰ correction is taken into account (Berger et al. 2019; Powell et al. 2019; Mason et al. 2020). It can be concluded that Bukulja was not mined in the Late Bronze Age or made a minor contribution to the tin economy of Serbia compared to Mt. Cer and the Erzgebirge at that time (Powell et al. 2020). From the tin ore sources identified by Durman (1997) only Cer, Bukulja and Motajica appear to have an adequate cassiterite concentration for potential placer tin exploitation, but Cer is the only site that appears to have contributed significantly to the tin economy of the region, based on the isotope composition of these source (Powell et al. 2020).

Questions also arose about the origin of the tin bronze artefacts from Mesopotamia and the ancient Orient, since there are neither copper nor tin deposits in Mesopotamia, so the majority of scientists concluded that the tin must come from deposits in Central Asia (Garner 2015). In Central Asia, large copper and tin deposits can be found with traces of mining dating back to the Middle and Late Bronze Age and tin production during the Early Bronze Age is also probable, based on tin bronze finds (Garner 2015). In the Zeravshan valley huge tin deposits occur and several Bronze Age tin mining

areas (Alimov et al. 1998; Alimov et al. 1999; Parzinger and Boroffka 2003) were excavated: Karnab and Lapas, Čangali, which were dated to the Middle 2<sup>nd</sup> millennium BC and Mushiston, which started at the end of the 3<sup>rd</sup> millennium BC until the Late Bronze Age (Garner 2015). Mushiston was not located in the direct catchment area of the main ancient traffic routes along the Zeravshan river compared to Karnab, Lapas and Čangali with a more favorable infrastructure, but had a much larger and maybe a higher output of tin than these deposits (Garner 2015).

The growth of analytical techniques to measure tin isotopic composition in the last years is considered to be a promising tool for the determination of tin ore and thus for the comparison of mining practices and the related prehistoric production of tin bronze (Berger et al. 2014, 2018, 2019; Brügmann et al. 2017a, b; Nessel et al. 2018, 2019). Many recent studies work on the correlation of tin isotope data from tin ores and tin artefacts from Central Europe and the Mediterranean and they suggest that many tin sources across Europe were used in the Late Bronze Age, especially those of Cornwall and the Saxonian-Bohemian province (Berger et al. 2019; Nessel et al. 2019). A reliable assignment of the ore provenance is considered difficult, as the composition of the metal-bearing regions largely overlaps and the geological processes which are responsible for the strong fractionation are not known (Marahrens et al. 2016; Brügmann et al. 2017a, b; Powell et al. 2019). But the tin isotopy in combination with archaeological investigations and further methods like the using of trace elements and lead isotopes could be a suitable tool to assign the tin of artefacts to a specific deposit.

## 8. OUTLOOK

The selection of 413 tin samples of different mineralization types was mainly based on their origin to get a comprehensive collection of ore data from all tin ore deposits in Europe and Central Asia that were of importance in ancient times and of current economically mineable deposits.

Within this work we found a variation of about 2 ‰ for  $\delta^{124}\text{Sn}/^{120}\text{Sn}$  in Europe and Central Asia, which is more than expected. In contrast to e.g., McNaughton and Rosman (1991) our investigated natural Sn isotope fractionation is relatively high. The isotopic ratios in cassiterites are highly variable and overlap to a large extent in the Variscan and Central Asian fold belts, which means that the same processes lead to the formation of tin. SW England, the Saxonian-Bohemian province and Portugal are, based on their  $\delta^{124}\text{Sn}/^{120}\text{Sn}$  averages over all areas, indistinguishable. The same applies for Spain and France as one group. Here more detailed studies are necessary to determine the isotopic composition of a single granite or area.

For the cassiterites from the investigated areas regional differences in ores could be found. For example, a distinction could be made between the deposits of the Botallack mine and Penzance in SW England (Fig. 6.5). However, this was not possible for all deposits. Because in some cases we only have one sample per mine, more detailed studies must also be carried out here, but our results show tendencies to certain tin isotopic compositions. The data overlap to a very large extent, so that the different tin provinces cannot be distinguished on a larger scale on the basis of their tin isotopic data. A distinction on a smaller scale like different mines within one tin ore area is possible. So the analysis of Sn isotopes could be of importance for the provenance of tin bronze artefacts.

The derivation of findings on a possible connection between the genesis and isotopy of the ores was only possible to a very limited extent. The high-T pegmatites have on average lighter isotopic compositions than the hydrothermal mineralizations, but this applies only to the pegmatites from Afghanistan. Otherwise, the pegmatic and hydrothermal mineralizations cannot be discriminated

---

because the range of tin isotope ratios is similar in both ore types. A discrimination between the hydrothermal types (greisen, quartz vein) is difficult, too.

The cassiterites from placers are consistent with the primary mineralization and the stannite samples have significantly lighter isotope compositions than the associated cassiterite. The similar isotope variation throughout provinces or mining areas and the large variation within single deposits suggest that the evolution of the fluids in the pegmatitic and hydrothermal systems are essentially controlled by mixing processes, temperature gradients and fractional crystallisation of cassiterite (Černý et al. 2005).

In summary we have demonstrated that:

- The isotopic compositions in cassiterites are highly variable and overlap to a large extent in the Variscan and Asian fold belts.
- On a more detailed scale it is possible to discern mines or mining areas within one area.
- Cassiterite from placers are consistent with the primary mineralization.
- Stannite samples have significantly lighter isotopic compositions than the associated cassiterites. A possible explanation could be the crystallisation from hydrothermal solutions after the cassiterite.
- Pegmatitic and hydrothermal mineralizations can be discriminated partially but this topic needs more analysis.

The question of fractionation cannot be clarified on the basis of our data. The study of Yao et al. (2018) has proven that oxidation of Sn at high temperatures causes predictable fractionation of the Sn isotopes. The fractionation of the Sn isotope system may offer a better control of high-temperature redox reactions than those systems where such signatures could be covered by isotopic partitioning between coexisting phases (e.g., Fe; Yao et al. 2018). In addition, the stability of cassiterite towards processes like weathering preserves its isotope signature. Besides that, the tin isotopy has great potential as a wide-ranging applicable analytical tool to give insights into the processes that are

related to the granite mineralization and to support provenance studies of bronze and tin artefacts. This study can generate new discussions and provide a good basis for future studies on the origin and trading of tin.

## REFERENCES

- Abdalla H.M., Matseuda H., Obeid M.A., Takahashi R. (2008): Chemistry of cassiterite in rare metal granitoids and the associated rocks in the Eastern Desert, Egypt. *Journal of Mineralogical and Petrological Sciences* 103, 318-326
- Abdalla H.M., Helba H., Matsueda H. (2009): Chemistry of zircon in rare metal granitoids and associated rocks, Eastern Desert, Egypt. *Resour. Geol.* 59 (1), 51-68
- Abrajevitch A., Van der Voo R., Bazhenov M.L., Levashova N.M., McCausland P.J.A. (2008): The role of the Kazakhstan orocline in the late Paleozoic amalgamation of Eurasia. *Tectonophysics* 455, 61-76
- Agricola G. (1556): *De re metallica libri XII*. 708 pp. Basel. Translated by Herbert Clark Hoover. 676 pp. Kessinger Publishing (2003)
- Alderton D.H.M., Harmons R.S. (1991): Fluid inclusion and stable isotope evidence for the origin of mineralizing fluids in south-west England. *Mineral. Mag.* 55, 605-611
- Alderton D.H.M. (1993): Mineralization associated with the Cornubian Granite Batholith. In: Patrick R.A.D., Polya D.A. (Eds.): *Mineralization in the British Isles*. Chapman and Hall, London, 270-354
- Alexeiev D.V., Cook H.E., Buvtyshkin V.M., Golub L.Y. (2009): Structural evolution of the Ural-Tien Shan junction: a view from Karatau ridge, South Kazakhstan. *Comptes Rendus Geosciences* 341, 287-297
- Alexeiev D.V., Ryazantsev A.V., Kröner A., Tretyakov A.A., Xia X., Liu D.Y. (2010): Geochemical data and zircon ages from rocks in a high-pressure belt of Chu-Yili Mountains, southern Kazakhstan: implications for the earliest stages of accretion in Kazakhstan and the Tianshan. *Journal of Asian Earth Sciences* 42, 805-820
- Alimov K., Boroffka N., Burjakov J., Cierny J., Lutz J., Parzinger H., Pernicka E., Ruzanov V., Shirinov T., Weisgerber G. (1998): Prähistorischer Zinnbergbau in Mittelasien. *Vorbericht der Kampagne 1997. Eurasia Antiqua* 4, 137-199
- Alimov K., Boroffka N., Burjakov J., Cierny J., Lutz J., Parzinger H., Pernicka E., Ruzanov V., Shirinov T., Weisgerber G. (1999): Research at Karnab, Uzbekistan. Preliminary Notes from the 1997 Campaign. Pod red. T. Š. Širinova, *Istorija materialnoj Uzbekistana* 30, 80-87
- Anderson H., Walsh J.J., Cooper M.R. (2016): Faults, intrusions and flood basalts: the Cenozoic structure of the north of Ireland. In: Young M.E. (Ed.), *Unearthed: Impacts of the Tellus Surveys of the North of Ireland*. Royal Irish Academy, Dublin, 179-189
- Anderson H., Walsh J.J., Cooper M.R. (2018): The development of a regional-scale intraplate strike-slip fault system; Alpine deformation in the north of Ireland. *Journal of Structural Geology* 116, 47-63
- Arenas R., Fernández R.D., Rubio Pascual F.J., Sánchez Martínez S., Martín Parra L.M., Matas J., González del Tánago J., Jiménez-Díaz A., Fuenlabrada J.M., Andonaegui P., García-Casco A. (2016): The Galicia-Ossa-Morena Zone: Proposal for a new zone of the Iberian Massif. Variscan implications. *Tectonophysics* 681, 135-143

- Arndt N., Ganino C. (2012): Metals and Society. An Introduction to Economic Geology. Springer Heidelberg
- Azevedo M.R., Valle Aguado B. (2006): Origem e instalação de granítoides variscos na Zona Centro-Ibérica. Departamento de Geociências, Universidade de Aveiro, Portugal.
- Badham J.P.N. (1980): Late igneous phenomena in the Cornish batholith-useful field guides fort in mineralization. Proceedings of the Ussher Society 5, 44-53
- Badullovivh N., Moynier F., Creech J., Teng F., Sossi P. (2017): Tin isotope fractionation during igneous differentiation and Earth's mantle deposition. Geochemical Perspectives Letters 5, 24-28
- Ballèvre M., Bosse V., Ducassou C., Pitra P. (2009): Palaeozoic history of the Armorican Massif: Models for the tectonic evolution of the suture zones. C.R. Geoscience 341, 174-201
- Ballèvre M., Fourcade S., Capdevila R., Peucat J.-J., Cocherie A., Fanning C.M. (2012): Geochronology and geochemistry of Ordovician felsic volcanism in the Southern Armorican Massif (Variscan belt, France): Implications for the breakup of Gondwana. Gondwana Research 21, 1019-1036
- Balliani E., Aramendía M., Resano M., Barbante C., Vanhaecke F. (2013): Copper and tin isotopic analysis of ancient bronzes for archaeological investigation: development and validation of a suitable analytical methodology. Analytical and Bioanalytical Chemistry 405, 2973-2986
- Bankoff A., Bulatović A., Mitrović S., Filipović V., Boger R., Powell W., Huska A., Kulkarni C. (2013): New Archaeological Research in the Jadarska region of West Serbia, 2010 and 2011. In: Filipović V., Arsic R., Antonović D. (Eds.), The results of new archaeological research in northwestern Serbia and adjacent territories (Rezultati novih arheoloških istraživanja u severozapadnoj Srbiji i susednim teritorijama), Serbian Archaeological Society, Belgrade, Institute for Protection of Cultural Monuments of Valjevo, 57-75
- Barrera J.L., Farias P., González F., Marquínez J., Martín L.M., Martínez J.R., Del Olmo A., De Pablo J.G. (1989): Mapa Geológico 1: 200,000 de Ourense/Verín. Memoria explicativa, Publicación del Instituto Technológico Geominero de España, Madrid
- Bartelheim M., & Niederschlag E. (1998): Untersuchungen zur Buntmetallurgie, insbesondere des Kupfers und Zinns, im sächsisch-böhmischem Erzgebirge und dessen Umland. Arbeits- und Forschungsberichte zur sächsischen Bodendenkmalpflege 40, 8–87
- Baxter D.C., Rodushkin I., Engstrom E., Malinovsky D. (2006): Revised exponential model for mass bias correction using an internal standard for isotope abundance ratio measurements by multi-collector inductively coupled plasma mass spectrometry. Journal of Analytical Atomic Spectrometry 21 (4), 427-430
- Begemann F., Kallas K., Schmitt-Strecker S., Pernicka E. (1999): Tracing ancient tin via isotope analysis. In: Hauptmann A., Pernicka E., Rehren T., Yalcin Ü. (Eds.), The beginnings of metallurgy, Der Anschnitt, Beiheft 9, 277-284
- Berger D., Pernicka E., Nessel B., Brügmann G., Frank C., Lockhoff N. (2014): Neue Wege zur Herkunftsbestimmung des bronzezeitlichen Zinns. Blickpunkt Archäologie (4), 76–82
- Berger D., Figueiredo E., Brügmann G., Pernicka E. (2018): Tin isotope fractionation during experimental cassiterite smelting and its implications for tracing the tin sources of prehistoric metal artefacts. Journal of Archaeological Science 92, 73-86
- Berger D., Soles J.S., Guimilia-Mair A.R., Brügmann G., Galili E., Lockhoff N., Pernicka E. (2019): Isotope systematics and chemical composition of tin ingots from Mochlos (Crete) and other Late

Bronze Age sites in the eastern Mediterranean Sea: An ultimate key to tin provenance? PLoS One 14 (6), doi: 10.1371/journal.pone.0218326

Biske Y.S. (1996): Paleozoiskaya Struktura I Istorya Uznoego Tyan-Shanya (Paleouoic Structure and History of the South Tein Shan). St. Petersburg University Press, 192 pp. (in Russian)

Biske Y.S., Seltmann R. (2010): Paleozoic Tian-Shan as a transitional region between the Rheic and Urals-Turkestan oceans. Gondwana Research 17, 602-613

Blevin P.L., Chappell B.W. (1995): Chemistry origin, and evolution of mineralized granites in the Lachlan Fold Belt, Australia: the metallogeny of I- and S-Type Granites. Econ Geol 90, 1604-1619

Boni M., Balassone G., Villa I.M. (1999): Age and evolution of granitoids from South West Sardinia: genetic links with hydrothermal ore bodies. Abstracts of the Joint SGA-IAGOD Intern. Meeting, London, August, 1255-1958

Boni M., Parente G., Bechstädt T., De Vivo B., Iannace A. (2000): Hydrothermal dolomites in SW Sardinia (Italy): evidence for a widespread late-Variscan fluid flow event. Sedimentary Geology 131, 181-200

Boni M., Stein H.J., Zimmerman A., Villa I.M. (2003): Re-Os age for molybdenite from SW Sardinia (Italy): a comparison with 40Ar/39Ar dating of Variscan granitoids. In: Eliopoulos D.G. et al. (Eds.): Mineral exploration and sustainable development. Proceedings 7<sup>th</sup> Biennial SGA Meeting, Athens, Millpress, Rotterdam, 247-250

Borisenco A.S., Borovikov A.A., Zhitova L.M., Pavlova G.G. (2006): Composition of magmatogenic fluids, factors of their geochemical spezialization and metal-bearing capacity. Russian Geology and Geophysics 47, 1308-1325

Bouchot V., Milesi J.-P., Ledru P. (2000): Crustal scale hydrothermal palaeofield and related Au, Sb, W orogenic deposits at 310-305 Ma (French Massif Central, Variscan Belt). SGA News 10, 6-12

Bouchot V., Ledru P., Lerouge C., Lescuyer J.-L., Milesi J.-P. (2005): Late Variscan mineralizing systems related to orogenic processes: The French Massif Central. Ore Geology Reviews 27, 169-197

Bouzek J., Koutecký D., Simon K. (1989): Tin and prehistoric mining in the Erzgebirge (ore mountains): some new evidence. Oxford Journal of Archaeology 8 (2), 203-212

Bray C.J., Spooner E.T.C. (1983): Sheeted vein Sn-W mineralization and gresenisation associated with economic kaolinisation, Goonbarrow China Clay Pit, St. Austell, Cornwall, England: geologic relationships and geochronology. Economic Geology 78, 1064-1089

Breiter K., Förster H.J., Seltmann R. (1999): Variscan silicic magmatism and related tin-tungsten mineralization in the Erzgebirge-Slavkovsý les metallogenic province. Mineral. Deposita 34, 505-521

Breiter K. (2012): Nearly contemporaneous evolution of the A- and S-type fractionated granites in the Krušné hory/Erzgebirge Mts., Central Europe. Lithos 151, 105-121

Brügmann G., Berger D., Frank C., Marahrens J., Nessel B., Perkicka E. (2017a): Tin isotope fingerprints of ore deposits and ancient bronze. In: Dartmoor Tinworking Research Group (Eds.), The Tinworking Landscape of Dartmoor in a European Context, Papers presented at a conference in Tavistock, Devon, 103-114

- Brügmann G., Berger D., Pernicka E. (2017b): Determination of the Tin Stable Isotopic Composition in Tin-bearing Metals and Minerals by MC-ICP-MS. *Geostandards and Geoanalytical Research* 41, 437-448
- Brügmann G. (2018): Introduction of the ERC-Project - The determination of the tin isotopic composition. Presentation at the Bronze Age Tin - Geological sources, production, and distribution of tin in Bronze Age Eurasia Workshop 2018, Mannheim, unpublished
- Burg J.P., Matte P. (1978): A cross section through the French Massif Central and the scope of 1st Variscan evolution. *Z Dtsch. Geol. Ges.* 129, 429-440
- Campbell A., Panter K. (1990): Comparison of fluid inclusions in coexisting (cogenetic?) wolframite, cassiterite, and quartz from St. Michael's Mount and Cligga Head, Cornwall, England. *Geochimica et Cosmochimica Acta* 54, 673-681
- Carmignani L., Carosi R., Di Pisa A., Gattiglio M., Musumeci G., Oggiano G., Pertusati P.C. (1994): The Hercynian chain in Sardinia (Italy). *Geodin. Acta* 7, 31-47
- Carvalho D. (1977): Lineament patterns and hypogene mineralization in Portugal. *Estudos Notas e Trab. do S.F.M. (Portugal)* 23, 91-106
- Casini L., Cuccuru S., Puccini A., Oggiano G., Rossi Ph. (2015): Evolution of the Corsica-Sardinia Batholith and late-orogenic shearing of the Variscides. *Tectonophysics* 646, 65-78
- Charles J.A. (1975): Where is the tin? *Antiquity* 49, 19-24
- Černý P. (1991) Rare-element granite pegmatites. Part I: anatomy and internal evolution of pegmatite deposits. Part II: regional to global relationships and petrogenesis. *Geoscience Canada* 18, 49-81
- Černý P., Blevin P.L., Cuney M., London D. (2005): Granite-related Ore Deposits. In: Hedenquist J.W., Thompson J.F.H., Goldfarb R.J., Richards J.P. (Eds.), *Economic Geology 100th Anniversary Volume*. Society of Economic Geologists, 337-370
- Chauris L., Marcoux E. (1994): Metallogeny of the Armorican Massif. In: Chantraine J., Rolet J., Santallier D.S., Pique A., Keppie J.D. (Eds.), *Pre-Mesozoic Geology in France and Related Areas*. Springer, Berlin Heidelberg, 243-264
- Chen C., Lu H., Jia D., Wu S. (1999): Closing history of the Tianshan ocean basin, western China: an oblique collisional orogeny. *Tectonophysics* 302, 23-40
- Chesley J.T., Halliday A.N., Snee L.W., Mezger K., Shepherd T.J., Scrivener R.C. (1993): Thermochronology of the Cornubian Batholith in southwest England: implications for pluton emplacement and protracted hydrothermal mineralisation. *Geochim. Cosmochim. Acta* 57, 1817-1835
- Chicharro E., Villaseca C., Valverde-Vaquero P., Belousova E., López-García J.A. (2014): Zircon U-Pb and Hf isotopic constraints on the genesis of a post-kinematic S-type Variscan tin granite: the Logrosán cupola (Central Iberian Zone). *J. Iber. Geol.* 40, 451-470
- Chicharro E., Boiron M.-C., López-García J.A., Barford D.N., Villaseca C. (2016): Origin, ore forming fluid evolution and timing of the Logrosán Sn-(W) ore deposit (Central Iberian Zone, Spain). *Ore Geol. Rev.* 72, 896-913
- Clayton R., Gillis C., Pernicka E., Gale N. (2002): Further data on the possible use of isotopes in provenance and archaeometallurgical studies. Proceedings of the 33<sup>rd</sup> Int. Symposium on Archaeometry, Amsterdam

- Clemens J.D. (2003): S-type granitic magmas-petrogenetic issues, models and evidence. *Earth-Science Reviews* 61, 1-18
- Cocks L.R.M. (2001): Ordovician and Silurian global geography. *Journal of the Geological Society of London* 158, 197-210
- Cocks L.R.M. and Torsvik T.H. (2002): Earth geography from 500 to 400 million years ago: a faunal and palaeomagnetic review. *Journal of the Geological Society of London* 159, 631-644
- Coleman R.G. (1989): Continental growth of northwest Chino. *Tectonics* 8, 621-635
- Cooper M.R. (2004): Paeogene extrusive igneous rocks. In: *The Geology of Northern Ireland-Our Natural Foundation*. Geological Survey of Northern Ireland, Belfast 167-178
- Cooper M.R., Johnston T.P. (2004): Paleogene intrusive igneous rocks. In: *The Geology of Northern Ireland-Our Natural Foundation*. Geological Survey of Northern Ireland, Belfast, 179-198
- Cooper M.R., Anderson H., Walsh J.J., Van Dam C.L., Young M.E., Earls G., Walker A. (2012): Paleogene Alpine tectonics and Icelandic plume-related magmatism and deformation in Northern Ireland. *J. Geol. Soc.* 169, 29-36
- Csontos L. (1995): Tertiary tectonic evolution of the Intra-Carpathian area: a review. *Acta Vulcan* 7, 1-13
- Cuccuru S., Naitza S., Secchi F., Puccini A., Casini L., Pavanello P., Linnemann U., Hofmann M., Oggiano G. (2016): Structural and metallogenic map of late Variscan Arbus Pluton (SW Sardinia, Italy). *Journal of Maps* 12 (5), 860-865
- Cuney M., Friedrich M., Blumenfeld P., Bourguignon A., Boiron M.-C., Vigneresse J.-L., Poty B. (1990): Metallogenesis in the French part of the Variscan orogen: Part I. Preconcentration in Pre-Variscan and Variscan formations – a comparison with Sn, W and Au. *Tectonophysics* 177, 39-57
- Cuney M., Marignac C., Weisbrod A. (1992): The Beauvoir Topaz-Lepidolite albite granite (Massif Central, France): the disseminated magmatic Sn-Li-Ta-Nb-Be mineralization. *Economic Geology* 87, 1766-1794
- Cuney M., Alexandrov P., Le Chalier de Veslud C., Cheillett A., Raimbault L., Ruffet G., Scaillet S. (2002): The timing of W-Sn rare metals mineral deposit formation in the Western Variscan chain in their orogenic setting: the case of Limousin area (Massif Central, France). In: Blundell D.J., Neubauer F., von Quadt A. (Eds.): *The Timing and Location of Major Ore Deposits in an Evolving Orogen*, Geological Society, London, Special Publications no. 204, 213-228
- Cvetković V., Downes H., Prelević D., Lazarov M., Resimić-Sarić K. (2007a): Geodynamic significance of ultramafic xenoliths from Eastern Serbia: Relics of sub-arc oceanic mantle? *J. Geodyn.* 43, 504-527
- Cvetković V., Poli G., Christofides G., Koroneos A., Pécskay Z., Resimić-Sarić K., Eric V. (2007b): The Miocene granitoid rocks of Mt. Bukulja (central Serbia): evidence for pannonian extension-related granitoid magmatism in the northern Dinarides. *Europ. J. Mineral* 19, 513-532
- Dauphas N., Craddock P.R., Asimow P.D., Bennett V.C., Nutman A.P., Ohnenstetter D. (2009): Iron isotopes may reveal the redox conditions of mantle melting from Archean to Present. *Earth and Planetary Science Letters* 288, 255-267

- Dauphas N., Roskosz M., Alp E., Neuville D., Hu M., Sio C., Tissot F., Zhao J., Tissandier L., Médard E. (2014): Magma redox and structural controls on iron isotope variations in Earth's mantle and crust. *Earth and Planetary Science Letters* 398, 127-140
- De Laeter J.R., Jeffery P.M. (1965): The isotopic composition of terrestrial and meteoritic tin. *J. Geophys. Res.* 70, 2895
- De Laeter J.R., Jeffery P.M. (1967): Tin: Its isotopic and elemental abundance. *Geochimica et Cosmochimica Acta* 31, 969-985
- Devillers C., Lecomte T., Hagemann R. (1983): Absolute isotope abundances of tin. *International Journal of Mass Spectrometry and Ion Processes*, 50, 205-217
- Del Moro A., Di Similico P., Ghezzo C., Rita F., Sabatini G. (1975): Radiometric data and intrusive sequences in the Sardinian batholith. *N. Jb. Geol. Mineral. Abh.* 126, 28-44
- Dias G., Leterrier J., Mendes A., Simoes P., Bertrand J. (1998): U-Pb zircon and monazite geochronology of post-collisional Hercynian granitoids from Central Iberian Zone (northern Portugal). *Lithos* 45, 49-369
- Dias G., Simões P., Ferreira N., Leterrier J. (2002): Mantle and crustal sources in the genesis of late-Hercynian granitoids (NW Portugal): geochemical and Sr-Nd isotopic constraints. *Gondwana Res.* 5, 87-305
- Domagal-Goldman S.D., Kubicki J.D. (2008): Density functional theory predictions of equilibrium isotope fractionation of iron due to redox changes and organic complexation. *Geochimica et Cosmochimica Acta* 72, 5201-5216
- Dominy S.C., Busell M.A., Camm G.S. (1996): Developments of complex, granite-hosted, tin-bearing fracture systems in southwest England: applications of fluid inclusion microfracture studies. *Trans. Instn. Min. Metall B* 105, 139-144
- Duchoslav M., Marks M.A.W., Drost K., McCammon C., Marschall H.R., Wenzel T., Markl G. (2017): Changes in tourmaline composition during magmatic and hydrothermal processes leading to tin-ore deposition: The Cornubian Batholith, SW England. *Ore Geology Reviews* 83, 215-234
- Durman A. (1997): Tin in South-eastern Europe? *Opuscula Archaeologica* 21, 7-14
- Eby G.N. (1992): Chemical subdivision of the A-type granitoids: Petrogenetic and tectonic implications. *Geology* 20, 641-644
- Eibschütz M., Hermon E., Shtrikman S. (1967): Determination of cation valencies in  $\text{Cu}_2^{57}\text{Fe}^{119}\text{SnS}_4$  by Mössbauer effect and magnetic susceptibility measurements. *Journal of Physics and Chemistry of Solids* 28, 1633-1636
- Exley C.S., Stone M. (1982): Hercynian intrusive rocks. In: Sutherland D. S. (Ed.), *The Variscan Fold Belt in the British Isles*. Chichester: John Wiley, 287-311
- Farias P., Gallastegui G., González Lodeiro F., Marquínez J., Mantín Parra L.M., De Pablo Macía J.G., Rodríguez Fernández L.R. (1987): Aportaciones al conocimiento de la litoestratigrafía y estructura de Galicia Central. *Mem Fac Cienc Univ Porto* 1, 411-431
- Farias P., Ordoñez-Casado B., Marcos A., Rubio-Ordoñez A., Fanning C.M. (2014): U-Pb zircon SHRIMP evidence for Cambrian volcanism in the schistose domain within the Galicia-Trás-os-Montes zone (Variscan Orogen, NW Iberian Peninsula). *Geol. Acta* 12, 209-218

- Faure M., Lardeaux J.-M., Ledru P. (2009): A review of the Pre-Permian geology of the Variscan French Massif Central. *C. R. Geoscience* 341, 202-213
- Fernández-Suárez J., Gutiérrez Alonso G., Jenner G.A. (2000): New ideas on the Proterozoic-Early palaeozoic evolution of NW Iberia: insights from U-Pb detrital zircon ages. *Precambrian Res.* 102, 185-206
- Ferreira N., Iglesias M., Noronha F., Pereira E., Ribeiro A., Ribeiro M.L. (1987): Granitóides de Zona Centro Ibérica e seu enquadramento geodinâmico. In: Bea F., Carnicero A., Gonzalo J., Lopez Plaza M., Rodriguez Alonso M. (Eds.), *Geología de los Granitoides y Rocas Asociadas del Macizo Hesperico*. Editorial Rueda, Madrid, Libro de Homenaje a L.C. García de Figuerola, 37-51
- Fox A. (1957): Excavations on Dean Moor in the Avon valley. *Transactions of the Devonshire Association* 86, 21-62
- Förster H.-J. (1999): The chemical composition of uraninite in Variscan granites of the Erzgebirge, Germany. *Mineralogical Magazine* 63, 239-252
- Förster H.-J., Tischendorf G., Trumbull R.B., Gottesmann B. (1999): Late-collisional granites in the Variscan Erzgebirge (Germany). *J. Petrol.* 40, 1613-1645
- Förster H.-J., Romer R.L. (2010): Carboniferous Magmatism. In: Linnemann U., Romer R. L. (Eds.), *Pre-Mesozoic Geology of Saxo-Thuringia: From the Cadomian Active Margin to the Variscan Orogen*. Schweizerbart, 287-308
- Franke W. (2001): The mid-European segment of the Variscides: tectono-stratigraphic units, terranes boundaries and plate tectonic evolution. *J. Geol. Soc. London* 197, 35-61
- Fuertes-Fuente M., Martin-Izard A., Boirin M.C., Mangas J. (2000): Fluid evolution of rare-element and muscovite granitic pegmatites from central Galicia, NW Spain. *Mineralium Deposita* 35, 332-345
- Gaggero L., Oggiano G., Buzzi L., Slejko F.F., Cortesogno L. (2007): Post-variscan mafic dikes from the late orogenic collapse to the Tethyan rift: evidence from Sardinia. *Ophioliti* 32, 15-37
- Gale N.H. (1997): The isotopic composition of tin in some ancient metals and the recycling problem in metal provenancing. *Archaeometry*, 39, 71-82.
- Gamble J.A., Wysoczanski R.J., Meighan I.G. (1999): Constraints on the age of the British Tertiary Volcanic Province from ion microprobe U-Pb (SHRIMP) ages for acid igneous rocks from NE Ireland. *J. Geol. Soc.* 156, 291-299
- Gao J., Long L., Klemd R., Qian Q., Liu D., Xiong X., Su W., Liu W., Wang Y., Yang F. (2009): Tectonic evolution of the South Tianshan orogen and adjacent regions, NW China: geochemical and age constraints of granitoid rocks. *Int J Earth Sci* 98, 1221-1238
- García-Arias M., Díez-Montes A., Villaseca C., Francisco Blanco-Quintero I. (2018): The Cambro-Ordovician Ollo de Sapo magmatism in the Iberian Massif and its Variscan evolution: A review. *Earth-Science Reviews* 176, 345–372
- Garner J. (2013): Das Zinn der Bronzezeit in Mittelasien II. Die montanarchäologischen Forschungen an den Zinnlagerstätten. *Archäologie in Iran und Turan* 12, Veröffentlichungen aus dem Deutschen Bergbau-Museum Bochum, Band 194

- Garner J. (2015): Bronze Age tin mines in central Asia. In: Hauptmann A., Modarressi-Tehrani D. (Eds.), Der Anschnitt, Beiheft 26. Archaeometallurgy in Europe III. Proceedings of the 3rd International Conference Deutsches Bergbau-Museum Bochum, 135-143
- Gil Ibarguchi J.I., Arenas R. (1990): Metamorphic evolution of the aalochthonous complexes from the northwest of Iberian Peninsula. In: Dallmeyer R.D., Martínez Garcia E. (Eds.), Pre-Mesozoic geology of Iberia. Springer, Berlin Heidelberg New York, 237-246
- Gillis C., Clayton R.E., Pernicka E., Gale N.H. (2001): Tin in the Aegean Bronze Age. In: Polinger-Foster K., Laffineur R. (Eds.), Metron, Proceedings of the 9th International Aegean Conference, volume 24. Aegaeum, Yale University (New Haven, USA), 103–110
- Gillis C., Clayton R., Pernicka E., Gale N. (2003): Tin in the Bronze Age. In: Polinger Foster K., Laffineur R. (Eds.), Metron: measuring the Aegean Bronze Age. Vol. 24, 103-110
- Gillis C., Clayton R. (2008): Tin and the Aegean in the Bronze Age. In: Tzachili I. (Ed.), Aegean metallurgy in the Bronze Age. Ta Pragmata Publications (Athens), 133–142
- González-Clavijo E., Díez Balda M.A., Álvarez F. (1993): Structural study of a semiductile strike-slip system in the Central Iberian Zone (Variscan Folt Belt, Spain): structural controls in gold deposits. *Geol. Rundsch.* 82, 448-460
- Greenwood N., Whitfield H. (1968): Mössbauer effect studies on cubanite ( $\text{CuFe}_2\text{S}_3$ ) and related iron sulphides. *Journal of the Chemical Society, A Inorganic Theoretical* 7, 1697-1699
- Groves D.I., Bierlein F.P. (2007): Geodynamic settings of mineral deposit systems. *Journal of the Geological Society, London*, 164, 19-30
- Gumiell P., Arribas A. (1990): Metallogeny. In: Dallmeyer R.D. and Martínez García E. (Eds.), Pre-Mesozoic Geology of Iberia, Chapter: 2 Autochthonous Sequences. 2.5 Metallogeny. Springer Verlag, 212-219
- Haapala I. (1997): Magmatic and Postmagmatic Processes in Tin-mineralized Granites: Topaz-bearing Leucogranite in the Eurajoki Rapakivi Granite Stock, Finland. *Journal of Petrology* 38 (12), 1645-1659
- Hall A. (1990): Geochemistry of the Cornubian tin province. *Mineralium Deposita* 25, 1-6
- Halliday A.N., Lee D.-C., Christensen J.N., Walder A.J., Freedman P.A., Jones C.E., Hall C.M., Yi W., Teagle D. (1995): Recent developments in inductively coupled plasma magnetic sector multiple collector mass spectrometry. *International Journal of Mass Spectrometry and Ion Processes* 146/7, 21-33
- Halter W.E., Williams-Jones A.E., Kontak D.J. (1996): The role of greisenization in cassiterite precipitation at the East Kemptville tin deposit, Yarmouth County, Nova Scotia. *Econ. Geol.* 91, 368-385
- Hamimi Z., El-Kazzaz Y., Fawzy K., Abdelrahman E., El-Shafei M., Elfakharini A. (2014): Geology and Tectonic Setting of the Arabian-Nubian Shield. *The Open Geology Journal* 8, 1-2
- Hauptmann A. (2010): The archaeometallurgy of copper: evidence from Faynan, Jordan. Springer Berlin, Heidelberg, New York
- Haustein M. (2009): Isotopengeochemische Untersuchungen zu möglichen Zinnquellen der Bronzezeit Mitteleuropas. Habilitationsschrift, eingereicht der Geowissenschaftlichen Fakultät der Eberhard-Karls-Universität Tübingen.

- Haustein M., Gillis C., Pernicka E. (2010): Tin isotopy – a new method for solving old questions. *Archaeometry* 52 (5), 816-832
- Heinrich C.A. (1990): The chemistry of hydrothermal tin (-tungsten) ore deposition. *Econ. Geol.* 85, 457-481
- Heinrich C.A., Neubauer F. (2002): Cu-Au-Pb-Zn-Ag metallogenesis of the Alpine-Balkan-Carpathian-Dinaride geodynamic province. *Mineralium Deposita* 37, 533–540
- Helba H., Trumbull R.B., Morteani G., Khalil S.O., Arslan A. (1997): Geochemical and petrographic studies of Ta mineralization in the Nuweibi albite granite complex, Eastern Desert, Egypt. *Miner. Deposita* 32 (2), 164-179
- Hoefs J. (1997): Stable Isotope Geochemistry. 4th, Completely Revised, Updated, and Enlarged Edition. Springer
- Jackson N.J., Halliday A.N., Sheppard S.M.F., Mitchell J.G. (1982): Hydrothermal activity in the St. Just mining district, Cornwall, England. In: Evans A.M. (Ed.), Metallization associated with acid magmatism. John Wiley and Sons Ltd, London, pp 137-179
- Jackson N.J., Willis-Richards J., Manning D.A.C., Sams M.S. (1989): Evolution of the Cornubian ore field, southwestern England: part II. Mineral deposits and ore-forming processes. *Econ. Geol.* 84, 1101-1133
- Jahn B.-M., Wu F.Y., Chen B. (2000a): Granitoids of the Central Asian Orogenic Belt and continental growth in the Phanerozoic. *Transactions of the Royal Society of Edinburgh, Earth Sciences* 91, 181-193
- Jahn B.-M., Wu F.Y., Chen B. (2000b): Massive granitoid generation in Central Asia: Nd isotope evidence and implication for continental growth in the Phanerozoic. *Episodes* 23, 82-92
- Jahn B.-M., Capdevila R., Liu D.Y., Vernon A., Badarch G. (2004): Sources of Phanerozoic granitoids in the transect Bayanhongor-Ulaan Baatar, Mongolia: geochemical and Nd isotopic evidence, and implications for Phanerozoic crustal growth. *Journal of Asian Earth Sciences* 23, 629-653
- Janković S. (1977): The copper deposits and geotectonic setting of the Tethyan Eurasian metallogenic belt. *Mineral Deposita* 12, 37-47
- Janković S. (1997): The Carpatho-Balkanides and adjacent area: a sector of the Tethyan Eurasian metallogenic belt. *Mineral Deposita* 32, 426-433
- Jebrak M. (1997): Hydrothermal breccias in vein-type ore deposits: a review of mechanisms, morphology and size distribution. *Ore Geol. Rev.* 12, 114-134
- Julivert M., Fontboté J.M., Ribeiro A., Nabais Conde L.E. (1972): Mapa Tectónico de la Península Ibérica y Baleares E. 1: 1000000. Inst Geol Min Esp Madr
- Karamata S., Steiger R., Đorđević P., Knežević V. (1990): New data on the origin of granitic rocks from Western Serbia. *Bulletin CVIII de l'Acad. Serbe des Sciences et des Arts, Classe des Sciences naturelles et mathématiques* 32, 1-9
- Karamata S., Delaloye M., Lovrić A., Knežević V. (1992): Two genetic groups of tertiary granitic rocks of Central and Western Serbia. *Ann Géol Péninsule Balkan* 56, 263-283

- Karamata S., Krstić B., Dimitrijević M.D., Knežević V., Dimitrijević M.N., Filipović I. (1994): Terranes between the Adriatic and the Carpatho-Balkan arc. *Bulletin CVIII de l'Acad. Serbe des Sciences et des Arts, Classe des Sciences naturelles et mathématiques* 35, 47-68
- Kerrick R., Goldfarb R., Richards J.P. (2005): Metallogenic provinces in an evolving geodynamic framework. *Economic Geology* 100, 1097-1136
- Khain E.V., Bibikova E.V., Salnikova E.B., Kröner A., Gibsher A.S., Didenko A.N., Degtyarev K.E., Fedotova A.A. (2003): The Palaeo-Asian ocean in the Neoproterozoic and early Paleozoic: new geochronologic data and palaeotectonic reconstructions. *Precambrian Research* 122, 329-358
- Konopelko D., Biske G., Seltmann R., Eklund O., Belyatsky B. (2007): Hercynian post-collisional A-type granites of the Kokshaal range, Southern Tien Shan, Kyrgyzstan. *Lithos* 97, 140-160
- Korges M., Weis P., Lüders V., Laurent O. (2018): Depressurization and boiling of a single magmatic fluid as a mechanism for tin-tungsten deposit formation. *Geology* 46, 75-78
- Koroneos A., Poli G., Cvetković V., Christofides G., Krstić D., Pécsay Z. (2010): Petrogenetic and tectonic inferences from the study of the Mt. Cer pluton (West Serbia). *Geol Mag* doi: 10.1017/S0016756810000476
- Kovalenko V.I., Yarmolyuk V.V., Kovach V.P., Kotov A.B., Kozakov I.K., Salnikova E.B. (1996): Sources of Phanerozoic granitoids in Central Asia: Sm-Nd isotope data. *Geochemistry International* 34, 628-640
- Kröner A., Windley B.F., Badarch G., Tomutogoo O., Hegner E., Jahn B.-M., Gruschka S., Khain E.V., Demoux A., Wingate M.T.D. (2007): Accretionary growth and crust-formation in the Central Asian orogenic belt and comparison with the Arabian-Nubian shield. In: Hatcher R.D., Carlson M.P., McBride J.H., Martínez Catalán J.R. (Eds.), *4-D Framework of Continental Crust*. Geological Society of America Memoirs 200, 181-209
- Kuz'mina E.E. (1991): Die urgeschichtliche Metallurgie der Andronovo-Kultur. *Bergbau, Metallurgie und Metallbearbeitung. Zeitschrift für Archäologie* 25, 29-48
- Küster D. (2009): Granitoid-hosted Ta mineralization in the Arabian-Nubian Shield: ore deposit types, tectono-metallogenic setting and petrogenetic framework. *Ore Geol. Rev.* 35 (1), 68-86
- Lafon J.-M., Respaut J.-P. (1986): Leucogranites et géochronologie U-Pb sur zircons et monazites. Leucogranites and U-Pb geochronology of zircons and monazites. *11ème Réunion Annuelle des Sciences de la Terre* 11, 103
- Ledru P., Lardeaux J.M., Santallier D., Autran A., Quenardel J.M., Floc'h J.P., Lerouge G., Maillet N., Marchand J., Ploquin A. (1989): Où sont les nappes dans le Massif central français? *Bull Soc Géol Fr* 3, 605-618
- Lee D.-C., Halliday A.N. (1995): Precise determinations of the isotopic compositions and atomic weights of molybdenum, tellurium, tin and tungsten using ICP source magnetic sector multiple collector mass spectrometry. *International Journal of Mass Spectrometry and Ion Processes* 146/7, 35-46
- Lehmann B. (1982): Metallogeny of Tin: magmatic differentiation versus geochemical heritage. *Econ. Geol.* 77, 50-59
- Lehmann B. (1987): Tin granites, geochemical heritage, magmatic differentiation. *Geol. Rundsch.* 76, 177-185
- Lehmann B. (1990): Metallogeny of Tin. Lecture notes in earth sciences 32. Springer-Verlag, Berlin

- Lehmann B. (1993): Metallogeny of granite-related rare-metal mineralization. *Resour. Geol.* 15, 385-392
- Lehmann B., Dietrich A., Wallianos A. (2000): From rocks to ore. *Int J Earth Sci* 89, 284-294
- Lindgren W. (1933): Mineral deposits. MacGraw-Hill, New York, 930 pp
- Linnen R., Williams-Jones A.E., Martin R.F. (1992): Evidence of magmatic cassiterite mineralization at the Nong Sua aplite-pegmatite complex, Thailand. *Canadian Mineralogist* 30, 739-761
- Linnen R., Pichavant M., Holtz F., Burgess S. (1995): The effect of  $fO_2$  on the solubility, diffusion, and speciation of tin in haplogranitic melt at 850°C and 2 kbar. *Geochimica et Cosmochimica Acta* 59, 1579-1588
- Linnen R., Pichavant M., Holtz F. (1996): The combined effects of  $fO_2$  and melt composition on  $SnO_2$  solubility and tin diffusivity in haplogranitic melts. *Geochimica et Cosmochimica Acta* 60, 4965-4976
- Llorens González T., García Polonio F., López Moro F.J., Fernández Fernández A., Sanz Contreras J.L., Moro Benito M.C. (2017): Tin-tantalum-niobium mineralization in the Penouta deposit (NW Spain): Textural features and mineral chemistry to unravel the genesis and evolution of cassiterite and columbite group minerals in a peraluminous system. *Ore Geology Reviews* 81 (1), 79-95
- London D. (2005): Granitic pegmatites: an assessment of current concepts and directions for the future. *Lithos* 80, 281-303
- López-Moro F.J., Moro C., Timón S.M., Cembranos M.I., Cózar J. (2013): Constraints regarding gold deposition in episyenites: the Permian episyenites associated with the Villacampo Shear Zone, central western Spain. *Int. J. Earth Sci.* 102, 721-744
- Maddin R., Wheeler T., Muhly J. (1977): Tin in the ancient Near East: Old questions and new finds. *Expedition*, 35-47
- Marahrens J., Berger D., Brügmann G., Pernicka E. (2016): Vergleich der stabilen Zinn-Isotopenzusammensetzung von Kassiteriten aus europäischen Zinn-Lagerstätten. *Archäometrie und Denkmalpflege* 2016, METALLA Sonderheft 8, 190-193
- Markl G., Schumacher J. (1996): Spatial variations in temperature and composition of greisen-forming fluids. An example from the Variscan Triberg Granite Complex, Germany. *Economic Geology* 91, 576-589
- Martínez Catalán J.R., Arenas R., García F.D., Pascual F.J.R., Abati J., Marquínez J. (1996): Variscan exhumation of a subducted Paleozoic continental margin: the basal units of the Ordenes Complex, Galicia, NW Spain. *Tectonic* 15, 106-121
- Martínez Catalán J.R., Martínez Poyatos D., Bea F. (2004): Zona Centroibérica. In: Vera J.A. (Ed.), *Geología de España*. SGE-IGME, 68-133 (Coord.)
- Martínez Catalán J.R., Arenas R., Diaz García F., González Cuadra P., Gómez-Barriero J., Abati J., Castiñeiras P., Fernández-Suárez J., Sánchez Martínez S., Adonaegui P., González Clavijo E., Díez Montes A., Rubio Pascual F.J., Valle Aguado B. (2007): Space and time in the tectonic evolution of the northwestern Iberian Massif: implications for the Variscan belt. In: Hatcher Jr. R.D., Carlosn M.P., McBride J.H., Martínez Catalán J.R. (Eds.), *Framework of continental crust*. *Geol. Soc. Am. Mem.* 200, 403-423

- Martínez Catalán J.R., Aller J., Alonso J.L., Bastida F. (2008): The Iberian Variscan orogen. In: García Cortés Á, Águeda Villar J., Suárez-Valgrande J.P., Salvador González C.I. (Eds.), Contextos geológicos españoles: una aproximación al patrimonio geológico español de relevancia internacional. Instituto Geológico y Minero de España, Madrid, 14-30
- Martínez Catalán (2012): The Central Iberian arc, an orocline centered in the Iberian Massif and some implications for the Variscan belt. *Int J Earth Sci (Geol Rundsch)* 101, 1299–1314
- Martins H.C.B., Sant’Ovaia H., Abreu J., Oliveira M., Noronha F. (2011): Emplacement of the Lavadores granite (NW Portugal): U/Pb and AMS results. *C. R. Geoscience* 343, 387–396
- Mason A., Powell W., Bankoff H., Mathur R., Bulatović A., Filipović V., Ruiz J. (2016): Tin isotope characterization of bronze artifacts of the Central Balkans. *Journal of Archaeological Science* 69, 110-117
- Mason A., Powell W., Bankoff A.H., Mathur R., Price M., Bulatović A., Filipović V. (2020): Provenance of tin in the Late Bronze Age Balkans based on probabilistic and spatial analysis of Sn isotopes. *Journal of Archaeological Science* 122, DOI: 10.1016/j.jas.2020.105181
- Mateus A., Noronha F. (2001): Late-Variscan uplift of the Iberian Terrane as a response to isostatic rebound: implications for the brittle-ductile transition, fluid circulation and metallogenesis. *Mem. Mus. Lab. Mineral. Geol. Univ. Porto* 7, 295-298
- Mateus A., Noronha F. (2010): Sistemas mineralizantes epigenéticos na Zona Centro-Ibérica: expressão da estruturação orogénica meso- a tardivarisca. In: Cotelo Neiva J.M., Ribeiro A., Mendes Victor L., Noronha F., Magalhães Ramalho M. (Eds.), Ciências Geológicas: Ensino, Investigação e sua História. Vol. II, Geologia Aplicada, 47-61
- Matte P. (1986): Tectonics and plate tectonics model for the Variscan belt of Europe. *Tectonophysics* 126, 329-374
- Matte P. (2001): The Variscan collage and orogeny (480-290 Ma) and the tectonic definition of the Armorica microplate: a review. *Terra Nova* 13(2), 122-128
- McGeehan-Liritzis V., Taylor W.J. (1987): Yugoslavian tin deposits and The Early Bronze Age industries of the Aegean Region. *Oxford Journal of Archaeology* 6 (3), 287–300
- McKerrow W.S., Mac Niocaill C., Ahlberg P.E., Clayton G., Cleal C.J., Eagar R.M.C. (2000): The Late Palaeozoic relations between Gondwana and Laurussia. Geological Society, London, Special Publications V. 179, 9-20
- McNaughton N.J., Loss R.D. (1990): Stable isotope variations of tin. In: Herbert H.K., Ho S.E. (Eds.): Stable isotopes and fluid processes in Mineralization. Geol. Dept. & Univ. Ext., Univ. W. Australia Publ. 23, 269-276
- McNaughton N.J., Rosman K.J.R. (1991): Tin isotope fractionation in terrestrial cassiterites. *Geochimica e Cosmochimica Acta* 55, 499-504
- Meert J.G. (2003): A synopsis of events related to the assembly of eastern Gondwana. *Tectonophysics* 362 (1-4), 1-40
- Melcher F., Graupner T., Gäbler H.E., Sitnikova M., Henjes-Kunst F., Oberthür T., Gerdes A., Dewaele S. (2015): Tantalum-(niobium-tin) mineralisation in African pegmatites and rare metal granites: constraints from Ta-Nb oxide mineralogy, geochemistry and U-Pb geochronology. *Ore Geol. Rev.* 64, 667-719

- Mladenović O. (2017): Some Remarks on Tin Ore Deposits in The Balkans. In: Filipović V., Todorović I. (Eds.), Book XXI Ethno-cultural annals for the study of the culture of eastern Serbia and the adjacent areas, 11-20
- Mochnacka K., Banas M., Kramer W., Pošmourný K. (1995): Metallogenesis. Pre-Permian Geology of Central and Eastern Europe. Springer, Berlin, 360-372
- Moghazi A.M., Harbi H.M., Ali K.A. (2011): Geochemistry of the Late Neoproterozoic Hadb adh Dayheen ring complex, Central Arabian Shield: implications for the origin of rare-metal-bearing post-orogenic A-type granites. *J. Asian earth Sci.* 42 (6), 1324-1340
- Muhly J.D. (1973): Tin trade routes of the Bronze Age. *American Scientist* 61, 404–413
- Muhly J.D. (1985): Sources of tin and the beginnings of Bronze metallurgy. *American Journal of Archaeology* 89, 275–291
- Muller A., Seltmann R., Halls C., Siebel W., Dulski P., Jeffries T., Spratt J., Kronz A. (2006): The ingenious evolution of the Lands End pluton, Cornwall, and associated pre-enrichment of metals. *Ore Geology Reviews* 28, 329-367
- Naitza S., Conte A.M., Cuccuru S., Oggiano G., Secchi F., Tecce F. (2017): A late Variscan tin province associated to the ilmenite-series granites of the Sardinian Batholith (Italy): The Sn and Mo mineralisation around the Monte Linas ferroan granite. *Ore Geol Rev* 80, 1259-1278
- Neiva A.M.R. (1984): Geochemistry of tin-bearing granitic rocks. *Chem. Geol.* 43, 241-256
- Neiva A.M.R. (2002): Portuguese granites associated with Sn-W and Au mineralizations. *Bull. Geol. Soc. Finl.* 74, 79-101
- Neiva A.M.R. (2008): Geochemistry of cassiterite and wolframite from tin and tungsten quartz veins in Portugal. *Ore Geology Reviews* 33, 221-238
- Nessel B., Brügmann G., Berger D., Frank C., Marahrens J., Pernicka E. (2018): Bronze production and tin provenance - new thoughts about the spread of metallurgical knowledge. In: Armada X-L., Murillo-Barroso M., Charlton M. (Eds.), Metals, minds and mobility. Integrating scientific data with archaeological theory. Oxford 2018, 67-84
- Nessel B., Brügmann G., Pernicka E. (2019): Tin isotope ratios in Early and Middle Bronze Age bronzes from Central and southeastern Europe. *The Journal of the International Union for Prehistoric and Protohistoric Sciences* 2, 1-11
- Niederschlag E., Pernicka E., Seifert T., Bartelheim M. (2003): The determination of lead isotope ratios by multiple collector ICP-MS: A case study of early Bronze Age artefacts and their possible relation with ore deposits of the Erzgebirge. *Archaeometry* 45, 61–100
- Nowell G., Clayton R., Gale N.H., Stos-Gale Z.A. (2002): Sources of Tin – Is isotopic evidence likely to help? In: Bartelheim M., Pernicka E., Krause R. (Eds.), Die Anfänge der Metallurgie in der Alten Welt, Rahden/Westfalen, 291-302
- Oggiano G., Casini L., Mameli P., Rossi P. (2007): Long lived dextral strike-slip tectonics in the southern Variscan Belt: evidence from two syn-kynematic intrusions in north Sardinia. *Géol. Fr.* 2, 142
- Okrusch M., Matthes S. (2005): Mineralogie. Eine Einführung in die spezielle Mineralogie, Petrologie und Lagerstättenkunde. Springer-Verlag Berlin Heidelberg

- Pamić J. (1993): Eoalpine to Neoalpine magmatic and metamorphic processes in the northwestern Vardar Zone, the easternmost Periadriatic Zone in the southwestern Pannonian Basin. The origin of sedimentary basins; interferences from quantitative modelling and basin analysis. *Tectonophysics* 226, 503-518
- Pamić J., Balen D. (2001): Tertiary magmatism of the Dinarides and the adjoining South Pannonian Basin: an overview. *Acta Vulcanol.* 13, 9-24
- Paquette J.L., Ménot R.-P., Pin C., Orsini J.B. (2003): Episodic and short-lived granitic pulses in a post-collisional setting: evidence from precise U-Pb zircon dating through a crustal cross-section in Corsica. *Chem. Geol.* 198, 1-20
- Parzinger H., Boroffka N. (2003): Das Zinn der Bronzezeit in Mittelasien I. Die siedlungsarchäologischen Forschungen im Umfeld der Zinnlagerstätten. *Archäologie in Iran und Turan* 5
- Penhallurick R. D. (1986): Tin in Antiquity: Its Mining and Trade Throughout the Ancient World with Particular Reference to Cornwall. The Institute of Metals, London.
- Pereira E., Ribeiro A., Meireiles C. (1993): Cisalhamentos hercínios e controlo das mineralizações de Sn-W, Au e U na Zona Centro-Ibérica, em Portugal. *Cuad. Lab. Xeolóx.* Laxe 18, 89-119
- Pernicka E. (1998): Die Ausbreitung der Zinnbronze im 3. Jahrtausend. In: B. Hänsel (Ed.), *Mensch und Umwelt in der Bronzezeit Europas*. Oetker-Voges Verlag Kiel, 135-147
- Pochon A., Beaudoin G., Branquet Y., Boulvais P., Gloaguen E., Gapais D. (2017): Metal mobility during hydrothermal breakdown of Fe-Ti oxides: Insights from Sb-Au mineralizing event (Variscan Armorican Massif, France). *Ore Geology Reviews* 91, 66-99
- Pohl W.L. (2011): Economic Geology: Principles and Practice. Metals, Minerals, Coal and Hydrocarbons – Introduction to Formation and Sustainable Exploitation of Mineral Deposits.
- Pollard P.J. (1995): A special issue devoted to the geology of rare metal deposits: geology of rare metal deposits; an introduction and overview. *Econ. Geol.* 90 (3), 489-494
- Polyakov V., Mineev S., Clayton R., Hu G., Mineev K. (2005): Determination of equilibrium isotope fractionation factors from synchrotron radiation experiments. *Geochimica et Cosmochimica Acta* 69, 5531-5536
- Porter T.M. (2006): The Tien Shan Belt: Golden heart of Central Asia. *The Gangue* 88, 1-5
- Powell W., Mathur R., John J., Price M., Bankoff H.A., Tisucká M., Godfrey L. (2019): Unearthing Europe's Bronze Age Mining Heritage with Tin Isotopes: A Case Study from Central Europe. *European Geologist Journal* 48, 58-62
- Powell W., Mladenović O., Cruse S., Bankoff H.A., Mathur R. (2020): Revisiting "Tin in south-eastern Europe?" *Starinar* 70, 85-94
- Puchkov V.N. (1997): Structure and geodynamics of the Uralian orogen. In: Burg J.P., Ford M. (Eds.): *Orogeny through time*. Geological Society, London, Special Publications 121, 201-236
- Raimbault L. (1998): Composition of complex lepidolite-type pegmatites and of constituent columbite-tantalite, Chédeville, Massif Central, France. *Canadian Mineralogist* 36, 563-583
- Raimbault L., Cuney M., Azencott C., Duthou J.-L., Joron J.-L. (1995): Geochemical evidence for a multistage magmatic genesis of Ta-Sn-Li mineralization in the granite at Beauvoir, French Massif Central. *Economic Geology* 90, 548-576

- Ribeiro A., Quesada C., Dallmeyer R.D. (1990): Geodynamic evolution of the Iberian Massif. In: Dallmeyer R.D., Martínez-Garcia E. (Eds.), Pre-Mesozoic Geology of Iberia. Springer, Berlin, 397–410
- Robb L. (2005): Introduction to ore-forming processes. Blackwell Publishing
- Romer R.L., Kroner U. (2015): Sediment and weathering control on the distribution of Paleozoic magmatic tin-tungsten mineralization. *Mineral. Deposita* 50, 327-338
- Romer R.L., Kroner U. (2016): Phanerozoic tin and tungsten mineralization-Tectonic controls on the distribution of enriched protoliths and heat sources for crustal melting. *Gondwana Research* 31, 60-95
- Romer R.L., Thomas R., Stein H.J, Rhede D. (2007): Dating multiply overprinted Sn-mineralized granites- examples from the Erzgebirge, Germany. *Mineral. Deposita* 42, 337-359
- Rosman K.J.R., Loss R.D., De Laeter J.R. (1984): The isotopic composition of tin. *Int. Journal of Mass Spectrometry and Ion Processes* 56, 281-291
- Rosman K. J. R., McNaughton N. J. (1987): High precision measurement of isotopic fractionation in tin. *International Journal of Mass Spectrometry and Ion Processes* 75, 91-98
- Rossi P., Oggiano G., Cocherie A. (2009): A restored section of the “southern Variscan realm” across the Corsica-Sardinia microcontinent. *Compt. Rendus Geosci.* 341, 224-238
- Ruban D.A., Al-Husseini M.I., Iwasaki Y. (2007): Review of Middle Paleozoic plate tectonics. *GeoArabia* 12, 35-56
- Rudnick R., Gao S. (2003): Composition of the continental crust. *Trestise on Geochemistry* 3, 1-64
- Russel W.A., Papanastassiou D.A., Tombrello T.A. (1978): Ca isotope fractionation on the earth and other solar system materials. *Geochim. Cosmochim. Acta* 42, 1075-1090.
- Rytsk E.Y., Kovach V.P., Yarmolyuk V.V., Kovalenko V.I. (2007): Structure and evolution of the continental crust in the Baikal Fold Region. *Geotectonics* 41, 440-464
- Sánchez-García T., Pereira M.F., Bellido F., Chichorro M., Silva J.B., Valverde-Vaquero P., Pin C., Sola A.R. (2014): Early Cambrian granitoids of North Gondwana margin in the transition from a convergent setting to intra-continental rifting (Ossa-Morena Zone, SW Iberia). *Int J Earth Sci (Geol Rundsch)* 103, 1203–1218
- Sami M., Ntaflos T., Farahat E.S., Mohamed H.A., Ahmed A.F., Hauzenberger C. (2017): Mineralogical, geochemical and Sr-Nd isotopes characteristics of fluoирite-bearing granites in the Northern Arabian-Nubian Shield, Egypt: Constraints on petrogenesis and evolution of their associated rare metal mineralization. *Ore Geology Reviews* 88, 1-22
- Sakura W.M., Buckman S., Nutman A.P., Belousova E.A., Yan Z., Aitchison J.C. (2017): Continental origin of the Gubaoquan eclogite and implications for evolution of the Beishan Orogen, Central Asian Orogenic Belt, NW China. *Lithos* 294-295, 20-38
- Schefer S., Cvetković V., Fügenschuh B., Kounov A., Ovtcharova M., Schaltegger U., Schmid S.M. (2011): Cenozoic granitoids in the Dinarides of southern Serbia: age of intrusion, isotope geochemistry, exhumation history and significance for the geodynamic evolution of the Balkan Peninsula. *Int J Earth Sci* 100, 1181-1206

- Scrivener R.C., Shepherd D.J. (1998): Mineralization. In: Selwood E.B., Durrance E.M., Bristow C.M. (Eds.), *The Geology of Cornwall*. University of Exeter Press, Exeter, 136-157
- Seghedi I., Downes H., Szakacs A., Mason P.R.D.m Thirlwall M.F., Rosu E., Pécskay Z., Marton E., Panaiotu C. (2004): Neogene-Quaternary magmatism and geodynamics in the Carpathian-Pannonian region: a synthesis. *Lithos* 72, 117-146
- Seltmann R., Porter T.M. (2005): The porphyry Cu-Au/Mo deposits of Central Eurasia. 1. Tectonic, Geologic and Metallogenic setting, and significant deposits. In: Porter T.M. (Ed.), *Super porphyry copper and gold deposits: A global perspective*. PGC Publishing 2, Adelaide, 467-512
- Şengör A.M.C., Natal'in B.A. (1996): Paleotectonics of Asia: fragments of a synthesis. In: Yin A., Harrison M. (Eds.), *The tectonic evolution of Asia*. Cambridge University Press. Cambridge, 486-640
- Shaw S.E., Flood R.H. (1992): A compilation of Late Permian and Triassic Biotite Rb-Sr data from the New England Batholith and areas to the southeast. In. Carr P.F. (Ed.), *CIS Research Report 1991-1992*: CSIRO Mineral Research Laboratories, 151-155
- Shaw J., Johnston S.T., Gutiérrez-Alonso G., Weil A.B. (2012): Oroclines of the Variscan orogen of Iberia: Paleocurrent analysis and paleogeographic implications: *Earth and Planetary Science Letters*, v. 329–330, 60–70
- Sherman D.M. (2013): Equilibrium isotopic fractionation of copper during oxidation/reduction, aqueous complexation and ore-forming processes: Predictions from hybrid density functional theory. *Geochimica et Cosmochimica Acta* 118, 85-97
- Smith M., Banks D., Yardley B., Boyce A. (1996): Fluid inclusion and stable isotope constraints on the genesis of the Cligga Head Sn-W deposit, SW England. *European Journal of Mineralogy* 8, 961-974
- Solomon M., Groves D.I. (1994): The geology and origin of Australia's mineral deposits.
- Solomovich L.I., Trifonov B.A. (2002): Postcollisional granites in the South Tien Shan Variscan collisional belt, Kyrgyzstan. *J. Asian Earth Sci.* 21, 7-21
- Solomovich L.I., Trifonov B.A., Sabelnikov S.E. (2012): Geology and mineralization of the Uchkoshkon tin deposit associated with a breccia pipe, Eastern Kyrgyzstan. *Ore Geology Reviews* 44, 59-69
- Stampfli G.M., Borel G.D. (2002): A plate tectonic model for the Paleozoic and Mesozoic constrained by dynamic plate boundaries and restored synthetic oceanic isochrons. *Earth and Planetary Science Letters* 196, 17-33
- Stampfli G.M., Mosar J., Favre P., Pillevuit A., Vanney J.-C. (2001): Permo-Mesozoic evolution of the western Tethys realm: the Neo-Tethys East Mediterranean Basin connection. In: Ziegler P.A., Cavazza W., Robertson A.H.F., Crasquin-Soleau S. (Eds.), *Peri-Tethyan Rift/Wrench Basins and Passive Margins*. Mémoires du Muséum National d'Historie Naturelle Paris 186, 51-108
- Stampfli G.M., von Rauner J., Wilhem C. (2011): The distribution of Gondwana-derived terranes in the Early Palaeozoic. In: Gutiérrez-Marco J.C., Rábano I., García-Bellido D. (Eds.), *Ordovician of the World*. Cuad. Mus. Geomin. 14. Instituto Geológico y Minero de España, Madrid, 567-574
- Stampfli G.M., Hochard C., Vérard C. Wilhem C., von Rauner J. (2013): The formation of Pangea. *Tectonophysics* 593, 1-19

- Stech T., Pigott V.C. (1986): The metals trade in Southwest Asia in the Third Millennium B.C. *Iraq* 48, 39-64
- Štemprok M. (1987): Greisenization (a review). *International Journal of Earth Sciences* 76, 169-175
- Štemprok M. (1995): A comparison of the Krušné hory-Erzgebirge (Czech Republic - Germany) and Cornish (UK) granites and their related mineralisation. *Geoscience in South-West England* 8(4), 347-356
- Štemprok M., Blecha V. (2015): Variscan Sn-W-Mo metallogeny in the gravity picture of the Krušné hory/Erzgebirge granite batholith (Central Europe). *Ore Geol. Rev.* 69 (1), 285-300
- Stone M., Exley C.S. (1985): High heat production granites of southwest England and their associated mineralization: a review. In: *High Heat Production (HHP) Granites, hydrothermal circulation and ore genesis*, The Institution of Mining and Metallurgy, London, 571-593.
- Sugaki A., Ueno H., Shimada M., Kitakaze A., Shima H., Sansines O., Saavedra A. (1981): Geological study on polymetallic hydrothermal deposits in the Oruro District, Bolivia. *Science Reports, Tohoku University, Series 3: Mineralogy, Petrology, and Economic Geology* 15, 1-52
- Sun L., Hu Y., Sun W., Gao Z., Tian M. (2017): Selective recovery of Mushistonite from gravity tailings of copper-tin minerals in Tajikistan. *Minerals* 7 (12), 242-252
- Sverchkov L.M. (2009): A history of research on ancient mining in Uzbekistan. *Archäologische Mitteilungen aus Iran und Turan* 41, 141-164
- Tartèse R., Boulvais P. (2010): Differentiation of peraluminous leucogranites „en route“ to the surface. *Lithos* 114, 353-368
- Taylor R.G. (1979): Geology of tin deposits; Developments in Economic Geology v. 11, Elsevier, 543 p.
- Taylor J.R., Wall V.J. (1993): Cassiterite solubility, tin speciation, and transport in a igneous aqueous phase. *Economic Geology* 88, 437-460
- Tischendorf (1989): Silicic Magmatism and Metallogenesis of the Erzgebirge. *Akademie der Wissenschaften der DDR, Zentralinstitut für Physik der Erde* 107, 1-316
- Tischendorf G., Dill H.G., Förster H.-J. (1995): Metallogenesis of the Saxothuringian Basins. In: Dallmeyer R.D., Franke W., Weber K. (Eds.), *Tectono-Stratigraphic Evolution of the Central and East European Orogens*. Springer, Heidelberg, 266-273
- Tolksdorf J., Schröder F., Petr L., Herbig C., Kaiser K., Kočář P., Füllin, A., Heinrich S., Höning H., Hemker C. (2019): Evidence for Bronze Age and Medieval tin placer mining in the Erzgebirge mountains, Saxony (Germany). *Geoarchaeology*, DOI: 10.1002/gea.21763
- Tomek F., Trubač J., Žák J., Sennewald R., Šešulka V., Krátký O., Štemprok M. (2019): Postmagmatic evolution of the Cínovec/Zinnwald granite cupola (Bohemian Massif): is there a genetic relationship of pluton architecture to brittle structures and greisen vein system? Conference: 17th Meeting of the Central European Tectonic Studies Groups (CETeG), 2019, Rozdrojovice, Czech Republic, DOI: 10.13140/RG.2.2.29602.48320
- Torsvik T.H. (1998): Palaeozoic palaeogeography: a North Atlantic viewpoint. *Geol. Soc. Sweden* 120, 109-118

- Torsvik T.H., Cocks L.R.M. (2004): Earth geography from 400 to 250 Ma: a palaeomagnetic, faunal and facies review. *Journal of the Geological Society of London* 161, 555-572
- Trifonov B.A., Doroshenko N.I., Shkil N.M. (1984): Geologo-osobennosti olovorudnogo mestorozhdeniya Uchkoshkon (Structure geology of the Uchkoshkon tin deposit). *J. Sov. Geol.* 2, 32-40 (in Russian)
- Tylecote R.F., Photos E., Earl B. (1989): The Composition of Tin Slags from the South-West of England. *World Archaeology*, Vol. 20 (3), Archaeometallurgy
- Unrug R., Haranczyk C., Chocyk-Jaminska M. (1999): Easternmost Avalonian and Armorican-Caledonian terranes of Central Europe and Caledonian-Variscan evolution of the polydeformed Krakow mobile belt: geological constraints. *Tectonophysics* 302, 133-157
- Vail J.R. (1985): Pan-African (late Precambrian) tectonic terrains and the reconstruction of the Arabian-Nubian Shield. *Geology* 13 (12), 839-842.
- Vallance J., Boiron M.C., Cathelineau M., Fourcade S., Marignac C. (2000): Fluid migration and alteration in the granite hosting Moulin de Cheni gold mineralization (Saint-Yrieix district). In: Moritz R., Bouchot V. (Eds.), *A Geode-Géo-France 3D Workshop on Orogenic Gold Deposits in Europe with Emphasis on the Variscides; Extended Abstracts. Documents du BRGM* 297, 73-74
- Vallance J., Cathelineau M., Marignac C., Boiron M.-C., Fourcade S., Martineau F., Fabre C. (2001): Microfracturing and fluid mixing in granites: W (Sn) ore deposition at Vaulry (NW French Massif Central). *Tectonophysics* 336, 43-61
- Vernikovsky V.A., Vernikovskaya A.E., PeaseV.L. (2004): Neoproterozoic orogeny along the margins of Siberia. In: Gee D.G. (Ed.), *The Neoproterozoic Timanide Orogen of Eastern Baltica: Geological Society of London, Memories* 30, 233-247
- Villaseca C., Merino E., Oyarzun R., Orejana D., Pérez-Soba C., Chicharro E. (2014): Contrasting chemical and isotopic signatures from Neoproterozoic metasedimentary rocks in the Central Iberian Zone (Spain) of pre-Variscan Europe: implications for terrane analysis and Early Ordovician magmatic belts. *Precambrian Res.* 245, 131-145
- Von Blanckenburg F., Davies J.H. (1995): Slab breakoff: a model for syncollisional magmatism and tectonics in the Alps. *Tectonics* 14, 120-131
- Walder A. J., Freedman P. A. (1992): Isotopic ratio measurement using a double focusing magnetic sector mass analyser with an inductively coupled plasma as an ion source. *J. Anal. Atomic Spect.* 7, 571-575
- Walder A. J., Furunata, N. (1993): High precision lead isotope ratio measurement by inductively coupled plasma multiple collector mass spectrometry. *Anal. Sciences* 9, 675-680
- Wang X., Amet Q., Fitoussi C., Bourdon B. (2018): Tin isotope fractionation during magmatic processes and the isotope composition of the bulk silicate Earth. *Geochimica et Cosmochimica Acta* 28, 320-335
- Wang D., Mathur M., Powell W., Godfrey L., Zheng Y. (2019): Experimental Evidence for Fractionation of Tin Chlorides by Redox and Vapor Mechanisms. *Geochimica et Cosmochimica Acta* 250, 209-218
- Webster J., Thomas R., Förster H.-J., Seltmann R., Tappen C. (2004): Geochemical evolution of halogen-enriched granite magmas and mineralizing fluids of the Zinnwald tin-tungsten mining district, Erzgebirge, Germany. *Mineralium Deposita* 39, 452-472

- Wilde S.A., Wu F.-Y., Zhao G. (2010): The Khanka Block, NE China, and its significance for the evolution of the Central Asian Orogenic Belt and continental accretion. In: Kusky T.M., Zhai M.G., Xiao W. (Eds.), *The Evolving Continents: Understanding Processes of Continental Growth*. Geological Society, London, Special Publication 338, 117-137
- Wilhem C., Windley B.F., Stampfli G.M. (2012): The Altaiids of Central Asia: A tectonic and evolutionary innovative review. *Earth-Science Reviews* 113, 303-341
- Williamson B.J., Spratt J., Adams J.T., Tindle A.G., Stanley C.J. (2000): Geichemical constraints from zoned hydrothermal tourmalines on fluid evolution and Sn mineralization: an example from Fault Breccias at Roche, SW England. *Journal of Petrology* 41, 1439-1453
- Windley B.F., Alexeiev D., Xiao W., Kröner A., Badarch G. (2007): Tectonic models for accretion of the Central Asian orogenic belt. *Journal of the Geological Society of London* 164, 719-737
- Wood S.A., Samson I.M. (1998): Solubility of ore minerals and complexation of ore metals in hydrothermal solutions. *Techniques in hydrothermal ore deposits*. In: Richards J., Larson P. (Eds.), *Reviews in Economic Geology*. Vol. 10, 33-80
- Xiao W., Santosh M. (2014): The western Central Asian Orogenic Belt: A window to accretionary orogenesis and continental growth. *Gondwana Research* 25, 1429-1444
- Yakubchuk A. (2004): Architecture and mineral deposit settings of the Altaiid orogenic collage: a revised model. *Journal of Asian Earth Sciences* 23, 761-779
- Yakubchuk A., Cole A., Seltmann R., Shatov V. (2002): Tectonic setting, characteristics, and regional exploration criteria for Gold mineralization in the Altai Orogenic Collage: The Tien Shan province as a key example. *Society of Economic Geologists Special Publications* 9, 177-201
- Yamazaki E., Nakai S., Yokoyama T., Ishihara S., Tang H. (2013): Tin isotope analysis of cassiterites from Southeastern and Eastern Asia. *Geochemical Journal* 47, 21-35
- Yamazaki E., Nakai S., Sahoo Y., Yokoyama T., Mifune H., Saito T., Chen J., Tagaki N., Hokanishi N., Yasuda A. (2014): Feasibility studies of Sn isotope composition for provenancing ancient bronzes. *Journal of Archaeological Science* 52, 458-467
- Yao J., Mathur R., Powell W., Lehmann B., Tornos F., Wilson M., Ruiz J. (2018): Sn-Isotope fractionation as a record of hydrothermal redox reactions. *American Mineralogist* 103(10), 1591-1598
- Yi W., Halliday A.N., Lee D.-C., Christensen J.N. (1995): Indium and tin in basalts, sulfides, and the mantle. *Geochimica et Cosmochimica Acta*, 59, 5081–5090
- Yi W., Budd P., McGill R.A.R., Young S.M.M., Halliday A.N., Haggerty R., Scaife B., Pollard A.M. (1999): Tin isotope studies of experimental and prehistoric bronzes. In: Hauptmann A., Pernicka E., Rehren Th., Yalçın Ü. (Eds.), *The Beginnings of Metallurgy*, Der Anschnitt, Beiheft 8. Deutsches Bergbaumuseum, Bochum, 285-290
- Žák J., Verner K., Janoušek V., Holub F.V., Kachlík V., Finger F., Hajná J., Tomek F., Vondrovic L., Trubač J. (2014): A plate-kinematic model for the assembly of the Bohemian Massif constrained by structural relationships around granitoid plutons. In: Schulmann K., Martinez Catalán J.R., Lardeaux J.M., Janoušek V., Oggiano G. (Eds.), *The Variscan Orogeny: Extent, Timescale and the Formation of the European Crust*. Geological Society, London, Special Publications 405, 169-196

Zhang R.Q., Lehmann B., Seltmann R., Sun W.D., Li C.Y. (2017): Cassiterite U-Pb geochronology constraints magmatic-hydrothermal evolution in complex evolved granite systems: The classic Erzgebirge tin province (Saxony and Bohemia). *Geology* 45, 1095-1098

## APPENDIX: TIN ISOTOPE DATA

**Table A1:**  $^{124}\text{Sn}/^{120}\text{Sn}$  and  $^{122}\text{Sn}/^{116}\text{Sn}$  isotope ratios of every individual analysis of the primary cassiterites from SW England. The data sets are given with 2SD.

Area	Deposit/Location	Sample number	$^{124}\text{Sn}/^{120}\text{Sn}$ [%]	2SD	$^{122}\text{Sn}/^{116}\text{Sn}$ [%]	2SD
Land's End	Botallack Mine	MA-080513	0.311	0.040	0.506	0.018
	Botallack Mine	MA-080519	0.265	0.001	0.451	0.038
	Botallack Mine	MA-080521	0.309	0.039	0.506	0.009
	Botallack Mine	MA-080522	0.391	0.027	0.648	0.025
	Botallack Mine	MA-080523	0.307	0.036	0.522	0.082
	Botallack Mine	MA-080518	-0.077	0.011	-0.114	0.021
	Botallack Mine	MA-080518	-0.075	0.020	-0.121	0.022
	Botallack Mine	MA-080518	-0.084	0.007	-0.137	0.004
	Botallack Mine	MA-080518	-0.043	0.014	-0.070	0.027
	Botallack Mine	MA-080518	-0.022	0.005	-0.029	0.022
	Botallack Mine	FG-011508	0.318	0.024	0.505	0.062
	Botallack Mine	MA-080520	0.371	0.004	0.615	0.020
	St Just Mine	MA-080509	0.226	0.006	0.389	0.028
	Wheal Bellan Mine	MA-156058	0.057	0.011	0.097	0.015
	North Levant Mine	MA-156063	-0.020	0.007	-0.037	0.010
	Levant Mine	MA-156064	-0.275	0.013	-0.443	0.007
	Carn Escalls Mine	MA-156071	0.449	0.006	0.725	0.026
	Balleswidden Mine	MA-160207	0.438	0.000	0.723	0.000
	Penzance	MA-080870	-0.105	0.017	-0.164	0.012
	Penzance	MA-080869	0.007	0.001	0.015	0.018
	Penzance	MA-080869	-0.001	0.007	-0.001	0.009
	St. Ives	MA-080866	-0.143	0.007	-0.232	0.015
Carnmenellis	St. Day	MA-156062	0.082	0.008	0.137	0.013
	South Crofty Mine, Pool	FG-011139	-0.823	0.020	-1.270	0.040
	Wheal Maid Mine	MA-156060	0.156	0.006	0.262	0.000
	Wheal Pendarves Mine	MA-081297	0.035	0.008	0.050	0.037
	Wheal Pendarves Mine	MA-081297	0.094	0.074	0.154	0.124
	Wheal Pendarves Mine	MA-081297	0.066	0.033	0.106	0.038
	Wheal Pendarves Mine	MA-081297	0.058	0.038	0.086	0.091
	Wheal Pendarves Mine	MA-081297	0.072	0.020	0.113	0.043
	Wheal Pendarves Mine	MA-081297	0.115	0.001	0.178	0.003
	Wheal Pendarves Mine	MA-081297				
St. Agnes	St. Agnes Mine	MA-080510	0.235	0.019	0.385	0.029
	St. Agnes Mine	MA-080510	0.203	0.039	0.323	0.046
	St. Agnes Mine	MA-080511	0.431	0.079	0.689	0.071
	St. Agnes Mine	MA-080511	0.342	0.031	0.546	0.052
	St. Agnes Mine	MA-080508	0.849	0.010	1.375	0.021
	St. Agnes Mine	MA-080508	0.859	0.015	1.388	0.022
	St. Agnes Mine	MA-080507	-0.699	0.038	-1.080	0.068
	Wheal Kitty Mine	FG-011120	0.035	0.033	0.059	0.062
	Wheal Kitty Mine	MA-080874	0.374	0.004	0.612	0.027
	unknown	MA-156061	0.700	0.026	1.135	0.048
	unknown	MA-156061	0.713	0.008	1.137	0.009
	Wheal Vottle Mine	MA-156066	0.021	0.013	0.060	0.010
	unknown	MA-156068	0.482	0.000	0.783	0.022
	Trevaunance Mine	MA-161102	0.214	0.002	0.321	0.005
Cligga Head	Cligga Head Mine	MA-156059	0.300	0.009	0.483	0.012
	Cligga Head Mine	MA-160218	0.522	0.006	0.829	0.006
St. Austell	Old Beam Mine	MA-160222	0.004	0.003	-0.001	0.018

	Goss Moor Mine	MA-160219	0.203	0.010	0.333	0.012
	Egloshellen Mine	MA-160220	-0.063	0.009	-0.111	0.023
	Bunny Mine	MA-160221	0.346	0.008	0.560	0.002
Hingston Down	Drakewells Mine	MA-156057	0.262	0.011	0.425	0.018
	Drakewells Mine	MA-160223	0.296	0.013	0.471	0.005
Dartmoor	West Vitifer Mine	MA-156070	-0.335	0.002	-0.544	0.012
	Hemerdon Mine	MA-160224	0.268	0.007	0.412	0.008
	Hemerdon Mine	MA-162664	0.365	0.010	0.576	0.012
	South Birch Tor Mine	MA-162660	-0.115	0.013	-0.185	0.017
	North Dartmoor	MA-162667	-0.374	0.013	-0.617	0.023

**Table A2:**  $^{124}\text{Sn}/^{120}\text{Sn}$  and  $^{122}\text{Sn}/^{116}\text{Sn}$  isotope ratios of every individual analysis of the primary cassiterites from the Saxonian-Bohemian province. The data sets are given with 2SD.

Area	Deposit/Location	Sample number	$^{124}\text{Sn}/^{120}\text{Sn}$ [%]	2SD	$^{122}\text{Sn}/^{116}\text{Sn}$ [%]	2SD
Kaiserwald	Schönfeld	FG-011052	-0.220	0.012	-0.368	0.013
	Schönfeld	FG-011401	-0.033	0.010	-0.064	0.023
	Schönfeld	FG-050671	-0.021	0.003	-0.033	0.021
	Schlaggenwald	FG-011393	-0.279	0.005	-0.465	0.014
	Schlaggenwald	FG-011406	0.178	0.007	0.297	0.009
	Schlaggenwald	FG-011421	-0.180	0.003	-0.286	0.013
	Schlaggenwald	FG-011424	-0.238	0.007	-0.390	0.007
	Schlaggenwald	FG-011513	-0.035	0.012	-0.050	0.014
	Schlaggenwald	FG-050673	-0.126	0.002	-0.175	0.010
	Schlaggenwald	FG-011003	-0.001	0.007	0.006	0.018
	Sangerberg	FG-011423	0.013	0.003	0.027	0.014
Erzgebirge East	Altenberg	FG-011441	0.135	0.003	0.222	0.002
	Altenberg	FG-050685	-0.035	0.002	-0.059	0.009
	Altenberg	MA-168276	0.268	0.004	0.456	0.025
	Altenberg	FG-011512	0.179	0.004	0.283	0.018
	Krupka	FG-011103	0.352	0.007	0.584	0.019
	Krupka	FG-011425	-0.001	0.003	-0.019	0.003
	Krupka	FG-011420	0.442	0.022	0.721	0.020
	Krupka	FG-011426	-0.019	0.005	-0.027	0.006
	Krupka	FG-011427	0.201	0.001	0.333	0.011
	Krupka	FG-050695	0.488	0.004	0.792	0.005
	Krupka	MA-168281	-0.160	0.007	-0.244	0.020
	Zinnwald	FG-011106	0.444	0.008	0.724	0.008
	Zinnwald	FG-011107	-0.115	0.012	-0.184	0.009
	Zinnwald	FG-011392	0.107	0.005	0.205	0.010
	Zinnwald	FG-011500	0.189	0.020	0.322	0.026
	Zinnwald	FG-050679	-0.010	0.008	-0.022	0.028
	Zinnwald	FG-050680	0.102	0.005	0.169	0.007
	Zinnwald	FG-050682	0.031	0.006	0.037	0.009
	Zinnwald	FG-050683	0.110	0.004	0.175	0.020
Middle Erzgebirge	Ehrenfriedersdorf	FG-011414	0.119	0.008	0.190	0.011
	Ehrenfriedersdorf	FG-011416	0.230	0.013	0.392	0.011
	Ehrenfriedersdorf	FG-011493	0.081	0.006	0.138	0.010
	Ehrenfriedersdorf	FG-011494	0.192	0.002	0.322	0.019
	Ehrenfriedersdorf	FG-011501	0.153	0.011	0.270	0.015
	Ehrenfriedersdorf	FG-011506	0.062	0.005	0.115	0.010
	Ehrenfriedersdorf	FG-050664	0.20	0.072	0.354	0.057
	Ehrenfriedersdorf	FG-050665	0.12	0.002	0.198	0.002
	Ehrenfriedersdorf	FG-050666	0.310	0.002	0.515	0.012
	Ehrenfriedersdorf	FG-050667	0.279	0.004	0.466	0.006

	Ehrenfriedersdorf	FG-050668	0.238	0.016	0.444	0.010
	Ehrenfriedersdorf	FG-050672	0.284	0.006	0.473	0.013
	Ehrenfriedersdorf	FG-050672	0.279	0.015	0.474	0.022
	Ehrenfriedersdorf	MA-156073	0.124	0.005	0.216	0.004
	Geyer	FG-011461	0.307	0.009	0.502	0.020
	Geyer	FG-011460	0.307	0.007	0.513	0.011
	Geyer	FG-011464	0.372	0.018	0.609	0.037
	Geyer	FG-011497	0.336	0.008	0.566	0.006
	Pobershau	FG-011523	0.226	0.009	0.376	0.009
Erzgebirge West	Johanngeorgenstadt	MA-168277	-0.158	0.017	-0.245	0.033
	Marienberg	MA-168278	0.333	0.005	0.535	0.020
	Neudorf	MA-168279	0.183	0.011	0.317	0.017
	Schwarzenberg	MA-168280	0.268	0.007	0.434	0.019
	Pöhla	FG-011505	-0.322	0.015	-0.519	0.014
	Abertamy-Hřebečná	FG-011397	-0.008	0.024	-0.032	0.033
	Abertamy-Hřebečná	FG-011398	-0.113	0.011	-0.180	0.024
	Horní Blatná	FG-011043	0.251	0.006	0.400	0.007
	Přebuz	FG-011396	0.278	0.015	0.457	0.018
	Přebuz	FG-011399	0.036	0.012	0.062	0.015
	Přebuz	FG-011402	0.403	0.015	0.641	0.014
	Am Auersberg	FG-050669	0.194	0.008	0.318	0.016
	Am Auersberg	FG-050674	0.287	0.013	0.460	0.021
	Am Auersberg	FG-050675	0.016	0.011	0.037	0.009
Vogtland	Mühlleithen	FG-050688	-0.045	0.006	-0.076	0.007
	Mühlleithen	FG-050688	-0.073	0.017	-0.100	0.001
	Mühlleithen	FG-050688	-0.074	0.009	-0.090	0.020
	Mühlleithen	FG-050688	-0.078	0.006	-0.095	0.036
	Mühlleithen	FG-050689	0.441	0.002	0.768	0.020
	Mühlleithen	FG-050690	-0.031	0.003	-0.057	0.049
	Mühlleithen	FG-050690	-0.037	0.001	-0.058	0.022
	Mühlleithen	FG-050691	0.086	0.011	0.156	0.016
	Gottesberg	FG-050692	-0.105	0.015	-0.174	0.021
	Gottesberg	FG-050693	-0.158	0.013	-0.228	0.010
	Vernérov	FG-011404	0.023	0.010	0.023	0.012
Fichtelgebirge	Rudolfstein	MA-147429	0.270	0.014	0.460	0.003
	Schönlind	MA-081254	0.211	0.002	0.349	0.016
	Weissenhaid	MA-147430	0.196	0.012	0.296	0.012
	Seehaus	MA-147432	0.451	0.011	0.731	0.010

**Table A3:**  $^{124}\text{Sn}/^{120}\text{Sn}$  and  $^{122}\text{Sn}/^{116}\text{Sn}$  isotope ratios of every individual analysis of the primary cassiterites from Portugal with 2SD.

Area	Deposit/Location	Sample number	$^{124}\text{Sn}/^{120}\text{Sn}$ [%]	2SD	$^{112}\text{Sn}/^{116}\text{Sn}$ [%]	2SD
Castelo Branco	Mina da Fonte das Galoas	MA-170964	0,261	0,011	0,417	0,009
	Mina da Fonte das Galoas	MA-170965	0,223	0,006	0,333	0,016
	Gaia	MA-171006	0,076	0,015	0,128	0,016
	Panasqueira	MA-171037	0,413	0,013	0,674	0,016
	Panasqueira	MA-171038	0,145	0,027	0,222	0,030
	Panasqueira	MA-171039	0,220	0,018	0,326	0,017
	Panasqueira	FG-011152	0,278	0,024	0,440	0,032
	Panasqueira	FG-011153	0,116	0,013	0,164	0,019
Guarda	Mina da Fonte do Seixo	MA-170967	0,196	0,007	0,293	0,005

	Quinta do Beja	MA-170963	0,110	0,009	0,168	0,007
	Gonçalo, Belmonte	MA-170995	0,012	0,023	0,006	0,020
	Mina da Vela, Gonçalo	MA-170997	-0,016	0,021	-0,054	0,017
	Mina das Torrinhas	MA-171014	-0,106	0,004	-0,193	0,010
	Freixo de Numão	MA-171028	0,063	0,011	0,088	0,009
Portalegre	Baldio do Conde, Elvas	MA-170968	-0,088	0,012	-0,143	0,030
	Baldio do Conde, Elvas	MA-170969	0,101	0,016	0,155	0,029
	Santa Eulália	MA-171040	0,096	0,029	0,150	0,023
	Santa Eulália	MA-171041	-0,056	0,014	-0,090	0,029
	Santa Eulália	MA-171042	-0,078	0,007	-0,132	0,009
	Santa Eulália	MA-171043	0,236	0,024	0,354	0,032
Porto	Mina da Rebordosa	MA-170957	0,026	0,013	0,040	0,019
	S. Tomé de Friande	MA-171022	-0,006	0,030	-0,005	0,044
Viseu	Mina de Sabrosa	MA-170976	0,209	0,005	0,302	0,014
	Mina de Sabrosa	MA-170973	0,250	0,006	0,381	0,005
	Covas do Estanho	MA-170983	-0,319	0,009	-0,533	0,007
	Covas do Estanho	MA-170984	-0,298	0,011	-0,474	0,013
	Sequeiros S.W.	MA-170986	0,358	0,022	0,574	0,011
	Parada de Ester, Couto E.	MA-170988	-0,139	0,025	-0,209	0,013
	Parada de Ester, Couto E.	MA-170989	-0,301	0,010	-0,482	0,027
	Mina das Fontainhas	MA-170991	0,141	0,013	0,211	0,031
	Mina das Fontainhas	MA-170992	0,054	0,021	0,064	0,022
	Mina dos Lagares	MA-170993	0,005	0,018	0,005	0,020
	Mina dos Lagares	MA-171030	0,156	0,018	0,250	0,032
	Bejanca	MA-171012	-0,059	0,011	-0,102	0,017
	Bejanca	MA-171024	0,134	0,014	0,214	0,021
	Lagares	MA-170951	0,126	0,019	0,194	0,028
Bragança	unknown	MA-171031	0,103	0,005	0,177	0,011
	unknown	MA-171032	0,000	0,024	-0,005	0,034
	Mina da Ribeira	MA-171033	0,395	0,006	0,610	0,008
	Mina do Portelo	MA-171035	0,278	0,017	0,427	0,030
	Mina do Portelo	MA-171045	0,123	0,009	0,178	0,017
	Mina do Portelo	MA-153250	-0,015	0,023	-0,020	0,034
Vila Real	Borralha	MA-171046	0,539	0,023	0,842	0,025
	Borralha	MA-171047	0,375	0,016	0,555	0,024
	M. da Serrinha da Cascalheira	MA-171019	0,121	0,017	0,181	0,042
	Mina do Pinheiro Manso	MA-171020	0,032	0,004	0,024	0,009
	Ribeira de Pena	MA-171016	-0,189	0,015	-0,262	0,025
	Mina Praina dos Torganos	MA-171025	0,189	0,015	0,280	0,008
	Jales. Revel.	MA-171027	0,089	0,025	0,120	0,018
	Mina de Aveleda	MA-171023	0,284	0,008	0,430	0,017
	Mina de Vinheiros	MA-171036	-0,494	0,023	-0,804	0,021
Aveiro	Bustelo SE (Block A)	MA-170981	0,301	0,039	0,451	0,035
	Bustelo SE	MA-170982	0,293	0,022	0,437	0,033
	Mina de Regoufe, Arouca	MA-171017	-0,377	0,022	-0,606	0,034
	Regoufe, Arouca	MA-171018	-0,247	0,022	-0,400	0,032
Viano do Castelo	Penedo da Poça, Vale garrido	MA-170966	0,299	0,021	0,441	0,006
	Nogueira Almonde	MA-171002	0,053	0,024	0,080	0,024
	Gondar, Caminha	MA-171021	-0,118	0,006	-0,202	0,023
	unknown	MA-153246	-0,141	0,045	-0,235	0,008
	unknown	MA-080885	0,032	0,005	0,053	0,010
	unknown	MA-153246	-0,230	0,001	-0,342	0,011
	Minas do Fontao	FG-011117	0,040	0,012	0,093	0,057
Beja	Neves-Corvo	MA-156049	0,305	0,019	0,532	0,040

**Table A4:**  $^{124}\text{Sn}/^{120}\text{Sn}$  and  $^{122}\text{Sn}/^{116}\text{Sn}$  isotope ratios of every individual analysis of the primary cassiterites from Spain. The data sets are given with 2SD.

Area	Deposit/Location	Sample number	$^{124}\text{Sn}/^{120}\text{Sn}$ [%]	2SD	$^{112}\text{Sn}/^{116}\text{Sn}$ [%]	2SD
Salamanca	unknown	MA-080777	-0,427	0,013	-0,660	0,011
	unknown	MA-080779	-0,464	0,008	-0,722	0,042
	unknown	MA-080783	0,322	0,007	0,494	0,015
	unknown	MA-080784	0,211	0,007	0,317	0,010
	unknown	MA-080785	0,296	0,004	0,450	0,009
	unknown	MA-080786	0,232	0,041	0,330	0,010
	Mari Tere mine	FG-011118	0,266	0,011	0,419	0,003
	Mari Tere mine	FG-011118	0,201	0,006	0,341	0,026
Ourense	Vilar de Cervos	MA-176528	0,162	0,023	0,242	0,035
	Vilar de Cervos	MA-176556	-0,311	0,023	-0,496	0,025
	Vilar de Cervos	MA-176529	0,104	0,022	0,165	0,010
	Val de Orras	MA-176530	-0,114	0,017	-0,184	0,025
	Pentes	MA-176531	-0,134	0,021	-0,233	0,009
	Penouta	MA-176532	-0,125	0,007	-0,198	0,008
	Penouta	MA-176533	-0,121	0,008	-0,177	0,018
	Penouta	MA-176534	-0,125	0,016	-0,185	0,006
	Penouta	MA-176535	-0,173	0,010	-0,280	0,037
	Penouta	MA-176539	-0,123	0,006	-0,211	0,014
	Beariz	MA-176552	0,012	0,003	0,024	0,008
	Avión	MA-176554	-0,257	0,015	-0,441	0,024
	Avión	MA-176555	-0,015	0,027	-0,015	0,015
	Sarreaus	MA-176559	0,166	0,011	0,254	0,005
	Vilameá	MA-176560	-0,249	0,014	-0,412	0,026
Coruña	Minas de San Finx	MA-176536	-0,125	0,007	-0,199	0,017
	Minas de San Finx	MA-176537	-0,008	0,006	-0,021	0,003
	Minas de San Finx	MA-176538	0,044	0,028	0,059	0,014
	Minas de San Finx	MA-176540	-0,116	0,014	-0,185	0,019
	Minas de San Finx	MA-176542	0,355	0,036	0,556	0,026
	Minas de San Finx	MA-176544	-0,090	0,012	-0,169	0,017
	Minas de San Finx	MA-176545	0,069	0,011	0,090	0,011
	Minas de San Finx	MA-176550	-0,047	0,021	-0,089	0,023
	Lousame, Noia	MA-176562	0,017	0,012	0,011	0,011
	Lousame, Noia	MA-176553	-0,038	0,019	-0,060	0,020
	Lousame, Noia	MA-176548	-0,169	0,017	-0,275	0,026
	Lousame, Noia	MA-153249	-0,249	0,030	-0,455	0,050
	Corta la Barrosa	MA-176547	-0,165	0,007	-0,296	0,005
	Arzúa	MA-176557	-0,267	0,008	-0,426	0,023
	Portomouro	MA-176564	0,043	0,019	0,081	0,019
	Mina a Magdalena	MA-176565	-0,197	0,021	-0,276	0,024
	O Cobo, Lampón	MA-176569	-0,515	0,016	-0,784	0,024
Cáceres	Logrosán	MA-176549	0,325	0,010	0,500	0,005
	Logrosán	MA-178298	0,205	0,024	0,286	0,030
	Logrosán	MA-178299	0,145	0,031	0,204	0,025
	Logrosán	MA-178300	0,168	0,028	0,225	0,071
	Logrosán	MA-178301	0,189	0,003	0,259	0,025
	Logrosán	MA-155139	0,260	0,026	0,350	0,045
Zamora	Calabor	MA-176546	0,0004	0,034	-0,046	0,022
Pontevedra	Carboeiro, Silleda	MA-176558	-0,109	0,011	-0,183	0,029

**Table A5:**  $^{124}\text{Sn}/^{120}\text{Sn}$  and  $^{112}\text{Sn}/^{116}\text{Sn}$  isotope ratios of every individual analysis of the primary cassiterites from France and Italy. The data sets are given with 2SD.

Area	Deposit/Location	Sample number	$^{124}\text{Sn}/^{120}\text{Sn}$ [%]	2SD	$^{112}\text{Sn}/^{116}\text{Sn}$ [%]	2SD
Brittany	Piriac-sur-Mer	MA-153247	-0,176	0,014	-0,290	0,003
	Ruscumunoc	MA-153248	0,238	0,018	0,382	0,022
	Quily	MA-156053	-0,034	0,016	-0,063	0,027
	Quily	MA-156054	-0,103	0,015	-0,179	0,019
	Quily	MA-170608	-0,045	0,018	-0,082	0,024
	Villeder	MA-168286	-0,172	0,002	-0,299	0,007
	Penfeunteun	FG-011109	-0,066	0,007	-0,117	0,007
	unknown	MA-080498	-0,084	0,022	-0,169	0,020
	unknown	MA-080499	-0,148	0,017	-0,252	0,029
	unknown	MA-080500	-0,123	0,008	-0,206	0,020
Massif Central	Montebras	MA-160002	0,197	0,032	0,334	0,022
	Montebras	MA-160003	0,121	0,013	0,228	0,007
	Montebras	MA-160004	0,212	0,012	0,342	0,015
	Montebras	MA-160005	0,171	0,005	0,281	0,010
	Montebras	MA-160006	0,224	0,007	0,364	0,019
	Montebras	MA-160007	0,217	0,006	0,368	0,017
	Montebras	MA-160008	0,180	0,055	0,272	0,029
	Montebras	MA-170600	0,209	0,006	0,360	0,008
	Montebras	MA-170601	0,143	0,017	0,245	0,039
	Montebras	MA-080493	0,219	0,021	0,376	0,032
	Montebras	MA-080493	0,076	0,005	0,145	0,019
	Échassières Mine	MA-160009	0,050	0,003	0,101	0,015
	Sauvagnac, Haute-Vienne	MA-170598	-0,287	0,008	-0,455	0,009
	Sauvagnac, Haute-Vienne	MA-170599	-0,049	0,009	-0,081	0,015
	Volondat, Haute-Vienne	MA-170602	0,181	0,019	0,260	0,015
	Volondat, Haute-Vienne	MA-170603	0,171	0,014	0,255	0,024
	Jouhe, Haute-Vienne	MA-170604	0,141	0,010	0,230	0,017
	Jouhe, Haute-Vienne	MA-170605	0,157	0,007	0,245	0,022
	Vaulry, Haute-Vienne	MA-170606	0,131	0,008	0,203	0,018
	Vaulry, Haute-Vienne	MA-170607	0,148	0,046	0,206	0,019
Sardinia	Perdu Cara Mine	MA-061430	0,199	0,010	0,342	0,013
	Perdu Cara Mine	FG-040671	0,331	0,005	0,555	0,010
	Villacidro	FG-993120	0,188	0,009	0,321	0,008
	Canale Serci	MA-175694	0,318	0,006	0,524	0,008
	Canale Serci	MA-175695	0,311	0,009	0,519	0,027
	Canale Serci	MA-175696	0,352	0,011	0,575	0,027
Monte Valerio	unknown	MA-061429	0,431	0,012	0,718	0,015
	unknown	MA-080789	0,420	0,006	0,687	0,038

**Table A6:**  $^{124}\text{Sn}/^{120}\text{Sn}$  and  $^{122}\text{Sn}/^{116}\text{Sn}$  isotope ratios of every individual analysis of the primary cassiterites from Central Asia and Egypt. The data sets are given with 2SD.

Area	Deposit/Location	Sample number	$^{124}\text{Sn}/^{120}\text{Sn}$ [%]	2SD	$^{112}\text{Sn}/^{116}\text{Sn}$ [%]	2SD
Tajikistan	Buguchijilga	FG-001701	0,405	0,019	0,654	0,024
	Buguchijilga	FG-992580	0,400	0,013	0,664	0,028
	Ghilnoye	FG-001705	0,082	0,009	0,112	0,019
	Ghilnoye	FG-992581	-0,026	0,015	-0,045	0,028
	Eli-su	FG-001706	0,194	0,012	0,309	0,024
	Trezubets	FG-001700	0,436	0,016	0,724	0,021
	Trezubets	FG-001703	0,531	0,013	0,874	0,010
	Trezubets	FG-001704	0,326	0,017	0,501	0,027
	Trezubets	FG-992579	0,369	0,001	0,587	0,019
	Takfon	MA-154294	-0,051	0,003	-0,089	0,022
	Takfon	MA-175688	-0,132	0,011	-0,215	0,009
Uzbekistan	Lapas	MA-152426	0,690	0,039	1,111	0,028
	Lapas	MA-152426	0,673	0,021	1,089	0,045
	Lapas	MA-152426	0,656	0,022	1,064	0,030
	Lapas	MA-152426	0,673	0,034	1,088	0,047
Kyrgyzstan	Karasa Mine	MA-175690	0,137	0,016	0,233	0,013
Kazakhstan	Askaraly	MA-151011	-0,385	0,010	-0,645	0,020
	Cherdoyek	MA-175692	0,211	0,003	0,324	0,002
Afghanistan	Shahr-e Bala-ye Khavat	MA-150418	-0,391	0,010	-0,632	0,015
	Alingar/Alishang	MA-161100	-0,023	0,005	-0,048	0,014
	Alingar/Alishang	MA-161101	0,052	0,002	0,073	0,013
	Alingar/Alishang	MA-161098	-0,124	0,018	-0,225	0,032
	Alingar/Alishang	MA-161099	-0,238	0,013	-0,414	0,021
	Alingar/Alishang	MA-161100	-0,048	0,013	-0,068	0,039
	Alingar/Alishang	MA-161101	0,043	0,021	0,080	0,059
	Dara-i-Pech	MA-161760	0,021	0,004	0,042	0,012
	Dara-i-Pech	MA-161764	0,134	0,006	0,213	0,010
	Dara-i-Pech	MA-161763	0,098	0,009	0,154	0,026
	Dara-i-Pech	MA-161756	0,116	0,003	0,181	0,011
	Dara-i-Pech	MA-161757	-0,174	0,031	-0,256	0,048
	Dara-i-Pech	MA-161758	-0,303	0,006	-0,538	0,028
	Dara-i-Pech	MA-161759	0,100	0,014	0,122	0,040
	Grangal Mine	MA-168029	-1,235	0,017	-2,029	0,029
	Grangal Mine	MA-168033	-0,132	0,007	-0,235	0,020
	Grangal Mine	MA-168035	-1,089	0,012	-1,795	0,017
	Grangal Mine	MA-168046	-0,845	0,013	-1,400	0,019
	Grangal Mine	MA-168047	-1,27	0,008	-2,086	0,019
	Grangal Mine	MA-168018	0,041	0,009	0,060	0,022
	Grangal Mine	MA-168024	-0,051	0,012	-0,089	0,016
	Grangal Mine	MA-168029	-1,197	0,019	-1,988	0,028
	Grangal Mine	MA-168029	-1,239	0,013	-2,042	0,016
	Grangal Mine	MA-168029	-1,175	0,011	-1,941	0,014
	Grangal Mine	MA-168029	-1,127	0,008	-1,853	0,023
	Grangal Mine	MA-168029	-1,222	0,012	-2,029	0,014
	Grangal Mine	MA-168034	-0,808	0,004	-1,343	0,024
	Grangal Mine	MA-168039	-0,080	0,017	-0,125	0,022
	Grangal Mine	MA-168048	-0,093	0,012	-0,157	0,008
	Paprok Mine	MA-168011	0,067	0,003	0,100	0,007
	Paprok Mine	MA-168012	-0,201	0,012	-0,328	0,017
	Paprok Mine	MA-168015	0,003	0,014	-0,008	0,015
	Paprok Mine	MA-168014	0,007	0,014	0,002	0,013

Paprok Mine	MA-168017	-0,265	0,013	-0,421	0,021
Paprok Mine	MA-168008	-0,464	0,016	-0,774	0,032
Paprok Mine	MA-168009	-0,273	0,014	-0,448	0,012
Paprok Mine	MA-168010	-0,022	0,006	-0,035	0,024
Paprok Mine	MA-168011	0,041	0,010	0,057	0,007
Paprok Mine	MA-168016	-0,282	0,019	-0,477	0,028
Kunar Mine	MA-172862	-1,123	0,022	-1,852	0,021
Kunar Mine	MA-172863	-1,074	0,006	-1,699	0,131
Kunar Mine	MA-172864	-1,100	0,001	-1,804	0,011
Kunar Mine	MA-172865	-1,127	0,022	-1,850	0,010
Egypt	Wādī Muweilha	FG-001709	-0,095	0,011	-0,159
	Wādī Muweilha	FG-992577	-0,058	0,011	-0,081
	Wādī Muweilha	MA-175687	0,064	0,004	0,117
	Iqla, Morsa Alan	FG-001707	0,028	0,019	0,059
	Iqla, Morsa Alan	MA-153113	-0,011	0,007	-0,012
	Iqla, Morsa Alan	MA-153113	-0,129	0,010	-0,217
	Iqla, Morsa Alan	MA-153113	0,103	0,021	0,216
	Nuweibi	MA-154992	0,244	0,011	0,384
	Nuweibi	FG-992717	0,266	0,007	0,421

**Table A7:**  $^{124}\text{Sn}/^{120}\text{Sn}$  and  $^{122}\text{Sn}/^{116}\text{Sn}$  isotope ratios of every individual analysis of the secondary cassiterites. The data sets are given with 2SD.

Pontevdra	Goián, Tui Pico do Corvo, Forcarei	MA-176561 MA-176563	-0,270 -0,194	0,018 0,015	-0,417 -0,325	0,019 0,018
<b>France</b>						
Brittany	Treguennec, Finistère Saint-Renan, Finistère	MA-153252 MA-156052	-0,141 -0,502	0,011 0,002	-0,219 -0,830	0,028 0,016
<b>Serbia</b>						
	Bukulja	MA-155140	0,064	0,006	0,080	0,010
	Bukulja	MA-155140	0,093	0,010	0,135	0,006
	Bukulja	MA-155140	0,089	0,020	0,115	0,010
	Bukulja	MA-155141	0,081	0,007	0,116	0,001
	Bukulja	MA-155141	0,085	0,012	0,123	0,011
	Bukulja	MA-155141	0,094	0,012	0,140	0,023
<b>Egypt</b>						
	Igla near Morsa Alan	FG-992232	0,026	0,016	0,035	0,017
	Nuweibi	FG-011077	0,149	0,015	0,199	0,032
	Abu Dabbab	FG-992716	0,069	0,012	0,117	0,019
	Abu Dabbab	MA-156047	0,187	0,030	0,341	0,040
	Abu Dabbab	MA-156048	0,265	0,031	0,429	0,072

**Table A8:**  $^{124}\text{Sn}/^{120}\text{Sn}$  and  $^{122}\text{Sn}/^{116}\text{Sn}$  isotope ratios of every individual analysis of the primary and secondary (Tajikistan) stannites. The data sets are given with 2SD.

Area	Deposit/Location	Sample number	$^{124}\text{Sn}/^{120}\text{Sn}$ [%]	2SD	$^{122}\text{Sn}/^{116}\text{Sn}$ [%]	2SD
<b>SWE</b>						
Cligga Head	Cligga Head Mine	MA-082550	-0,349	0,014	-0,571	0,002
	Cligga Head Mine	MA-082569	-0,149	0,017	-0,251	0,021
Hingston Down	Hingston Down Quarry	FG-011142	-0,380	0,028	-0,629	0,059
	Hingston Down Quarry	FG-011143	-0,327	0,011	-0,539	0,018
<b>SBP</b>						
Erzgebirge East	Zinnwald	FG-011481	-0,360	0,009	-0,586	0,016
	Zinnwald	FG-011490	-0,452	0,010	-0,754	0,001
	Zinnwald	FG-011550	-0,439	0,025	-0,739	0,008
<b>Central Asia</b>						
Tajikistan	Kani Nukra	MA-154228	-0,109	0,017	-0,198	0,013
	Mushiston	MA-154217	-0,268	0,013	-0,414	0,004
	Mushiston	MA-154219	-0,256	0,015	-0,413	0,023
	Mushiston	MA-154220	-0,204	0,007	-0,342	0,001
	Mushiston	MA-154221	-0,231	0,020	-0,392	0,011
	Mushiston	MA-154222	-0,290	0,009	-0,472	0,011
	Mushiston	MA-154237	-0,300	0,010	-0,505	0,010
	Mushiston	MA-154238	-0,283	0,016	-0,485	0,006
	Mushiston	MA-154239	-0,254	0,008	-0,428	0,026
	Mushiston	MA-154240	-0,214	0,021	-0,357	0,038
	Mushiston	MA-154244	-0,270	0,005	-0,436	0,021
	Mushiston	MA-154249	-0,258	0,018	-0,450	0,007
	Mushiston	MA-154252	-0,229	0,009	-0,381	0,009
	Mushiston	MA-154273	-0,280	0,022	-0,453	0,015
	Mushiston	MA-154278	-0,422	0,017	-0,655	0,023
	Mushiston	MA-154434	-0,196	0,008	-0,333	0,012

**Table A9:**  $^{122}\text{Sn}/^{116}\text{Sn}$  and  $^{117}\text{Sn}/^{119}\text{Sn}$  isotope ratios of every individual analysis of cassiterite which were analysed by Haustein et al. (2010) and the ERC project. The data sets are given with 2SD.

SBP Sample number	Haustein		ERC						
	$^{122}\text{Sn}/^{116}\text{Sn}$	[‰]	2SD	$^{117}\text{Sn}/^{119}\text{Sn}$	2SD	$^{122}\text{Sn}/^{116}\text{Sn}$	2SD	$^{117}\text{Sn}/^{119}\text{Sn}$	2SD
FG-011414	0,25	0,19	-0,07	0,06	0,19	0,01	-0,07	0,01	
FG-011416	0,37	0,15	-0,11	0,05	0,39	0,01	-0,14	0,00	
FG-011494	0,27	0,19	-0,12	0,07	0,32	0,02	-0,12	0,02	
FG-011501	0,04	0,20	-0,02	0,07	0,27	0,01	-0,10	0,00	
FG-011506	0,08	0,16	0,03	0,06	0,12	0,01	-0,05	0,00	
FG-050664	0,34	0,17	-0,08	0,05	0,35	0,06	-0,14	0,02	
FG-050665	0,23	0,14	-0,04	0,04	0,20	0,00	-0,08	0,00	
FG-050666	0,41	0,14	-0,18	0,05	0,51	0,01	-0,18	0,01	
FG-050667	0,77	0,13	-0,09	0,05	0,47	0,01	-0,17	0,01	
FG-050668	0,35	0,17	-0,07	0,05	0,44	0,01	-0,17	0,01	
FG-050672	0,48	0,18	-0,08	0,06	0,47	0,01	-0,17	0,01	
FG-011406	0,29	0,15	-0,10	0,05	0,30	0,01	-0,11	0,01	
FG-050671	-0,04	0,19	0,03	0,07	-0,03	0,02	0,01	0,00	
FG-050673	-0,16	0,13	0,04	0,05	-0,18	0,01	0,06	0,01	
FG-011392	0,19	0,13	-0,16	0,05	0,21	0,01	-0,08	0,01	
FG-050680	0,22	0,16	-0,05	0,06	0,17	0,01	-0,05	0,01	
FG-050682	0,32	0,17	-0,10	0,06	0,04	0,01	-0,06	0,03	
FG-050683	0,84	0,18	-0,22	0,07	0,18	0,02	-0,11	0,03	
FG-050685	0,46	0,16	-0,09	0,05	-0,06	0,01	0,00	0,03	
FG-050669	0,37	0,13	-0,19	0,05	0,32	0,02	-0,11	0,01	
FG-050674	0,51	0,19	-0,22	0,07	0,46	0,02	-0,15	0,02	
FG-050675	0,55	0,18	-0,07	0,06	0,04	0,01	-0,02	0,00	
FG-050692	-0,17	0,13	-0,03	0,05	-0,17	0,02	0,07	0,03	
FG-050693	-0,23	0,18	0,02	0,06	-0,23	0,01	0,06	0,03	
FG-050688	-0,01	0,14	-0,06	0,05	-0,09	0,02	0,02	0,02	
FG-050689	0,80	0,19	-0,35	0,07	0,77	0,02	-0,28	0,02	
FG-050690	-0,03	0,14	-0,07	0,04	-0,06	0,04	0,03	0,04	
FG-050695	0,80	0,17	-0,31	0,05	0,79	0,00	-0,26	0,00	
SWE Sample number	Haustein		ERC						
	$^{122}\text{Sn}/^{116}\text{Sn}$	2SD	$^{117}\text{Sn}/^{119}\text{Sn}$	2SD	$^{122}\text{Sn}/^{116}\text{Sn}$	2SD	$^{117}\text{Sn}/^{119}\text{Sn}$	2SD	
MA-080513	0,96	0,13	-0,38	0,04	0,51	0,02	-0,18	0,03	
MA-080518	0,08	0,12	-0,08	0,04	-0,09	0,02	0,01	0,01	
MA-080519	0,96	0,13	-0,41	0,04	0,45	0,04	-0,16	0,01	
MA-080520	0,99	0,15	-0,43	0,05	0,61	0,02	-0,21	0,01	
MA-080521	0,52	0,14	-0,22	0,04	0,51	0,01	-0,17	0,01	
MA-080522	0,90	0,16	-0,36	0,05	0,65	0,02	-0,23	0,00	
MA-080523	0,80	0,13	-0,29	0,03	0,52	0,08	-0,19	0,01	
MA-080881	0,33	0,11	-0,17	0,02	-0,18	0,03	0,05	0,02	
MA-080874	0,62	0,09	-0,23	0,04	0,61	0,03	-0,21	0,00	
MA-080504	0,46	0,10	-0,11	0,04	0,18	0,07	-0,08	0,02	
MA-080508	1,46	0,11	-0,49	0,04	1,37	0,02	-0,47	0,01	
MA-080510	0,43	0,09	-0,16	0,04	0,35	0,04	-0,13	0,00	
MA-080511	0,77	0,13	-0,29	0,05	0,62	0,06	-0,21	0,03	
MA-080507	0,65	0,07	-0,22	0,03	-1,08	0,07	0,35	0,02	
MA-081297	0,68	0,11	-0,25	0,04	0,11	0,06	-0,05	0,02	
MA-080878	0,52	0,08	-0,17	0,03	0,02	0,03	-0,02	0,00	
MA-080509	0,62	0,10	-0,26	0,03	0,39	0,03	-0,14	0,02	



## Danksagung

Hier möchte ich allen beteiligten Personen meinen großen Dank aussprechen, die mich bei der Anfertigung meiner Dissertation unterstützt haben:

Herrn Prof. Dr. Ernst Pernicka danke ich für die Möglichkeit in seiner Arbeitgruppe meine Dissertation angefertigt haben zu dürfen und für die Betreuung während der Zeit.

Außerdem möchte ich Herrn Dr. Gerhard Brügmann für die Betreuung und Begleitung während der ganzen Zeit danken.

Dem gesamten Forschungsprojekt *Bronzezeitliches Zinn - Zinnisotope und die Quellen des bronzezeitlichen Zinns in der Alten Welt* spreche ich ebenfalls meinen Dank für die Unterstützung und für die Hilfsbereitschaft aus: Dr. Daniel Berger, Dr. Gerhard Brügmann, Carolin Frank, Dr. Bianka Nessel und Prof. Dr. Ernst Pernicka.

Nicole Lockhoff, Sigrid Klaus, Dr. Michael Brauns und Bernd Höppner danke ich für die Unterstützung im Labor.

Für viele fruchtbare Gespräche und Anregungen danke ich sehr meinen Büronachbarn Nicole Lockhoff, Steffen Kraus und Moritz Numrich.

Für die Durchsicht dieser Arbeit danke ich Prof. Dr. Ernst Pernicka, Dr. Gerhard Brügmann sowie Kadir Nakiboglu.

Für die finanzielle Unterstützung danke ich dem ERC.

Und zum Schluss möchte ich noch einen großen Dank meiner Familie aussprechen und ganz besonders meinem Ehemann Mirco Marahrens, der mich jederzeit unterstützt und meine Launen ertragen hat, und meiner Arbeit viel Verständnis und Geduld entgegenbrachte.



**Eidesstattliche Versicherung gemäß § 8 der Promotionsordnung für die  
Naturwissenschaftlich-Mathematische Gesamtfakultät der Universität Heidelberg /  
Sworn Affidavit according to § 8 of the doctoral degree regulations of the Combined  
Faculty of Natural Sciences and Mathematics**

1. Bei der eingereichten Dissertation zu dem Thema / **The thesis I have submitted entitled**

.....

handelt es sich um meine eigenständig erbrachte Leistung / **is my own work.**

2. Ich habe nur die angegebenen Quellen und Hilfsmittel benutzt und mich keiner unzulässigen Hilfe Dritter bedient. Insbesondere habe ich wörtlich oder sinngemäß aus anderen Werken übernommene Inhalte als solche kenntlich gemacht. / **I have only used the sources indicated and have not made unauthorised use of services of a third party. Where the work of others has been quoted or reproduced, the source is always given.**

3. Die Arbeit oder Teile davon habe ich wie folgt/bislang nicht<sup>1)</sup> an einer Hochschule des In- oder Auslands als Bestandteil einer Prüfungs- oder Qualifikationsleistung vorgelegt. / **I have not yet/have already<sup>1)</sup> presented this thesis or parts thereof to a university as part of an examination or degree.**

Titel der Arbeit / **Title of the thesis:** .....

Hochschule und Jahr / **University and year:** .....

Art der Prüfungs- oder Qualifikationsleistung / **Type of examination or degree:** .....

4. Die Richtigkeit der vorstehenden Erklärungen bestätige ich. / **I confirm that the declarations made above are correct.**

5. Die Bedeutung der eidesstattlichen Versicherung und die strafrechtlichen Folgen einer unrichtigen oder unvollständigen eidesstattlichen Versicherung sind mir bekannt. / **I am aware of the importance of a sworn affidavit and the criminal prosecution in case of a false or incomplete affidavit.**

Ich versichere an Eides statt, dass ich nach bestem Wissen die reine Wahrheit erklärt und nichts verschwiegen habe. / **I affirm that the above is the absolute truth to the best of my knowledge and that I have not concealed anything.**

.....  
Ort und Datum / **Place and date**

.....  
Unterschrift / **Signature**

<sup>1)</sup> Nicht Zutreffendes streichen. Bei Bejahung sind anzugeben: der Titel der andernorts vorgelegten Arbeit, die Hochschule, das Jahr der Vorlage und die Art der Prüfungs- oder Qualifikationsleistung. / **Please cross out what is not applicable. If applicable, please provide: the title of the thesis that was presented elsewhere, the name of the university, the year of presentation and the type of examination or degree.**